Inheritance Across the Scales – Assessing the Relative Importance of Crustal and Lithospheric Structures during Rift Evolution

MALTE FROEMCHEN

Inheritance Across the Scales – Assessing the Relative Importance of Crustal and Lithospheric Structures during Rift Evolution

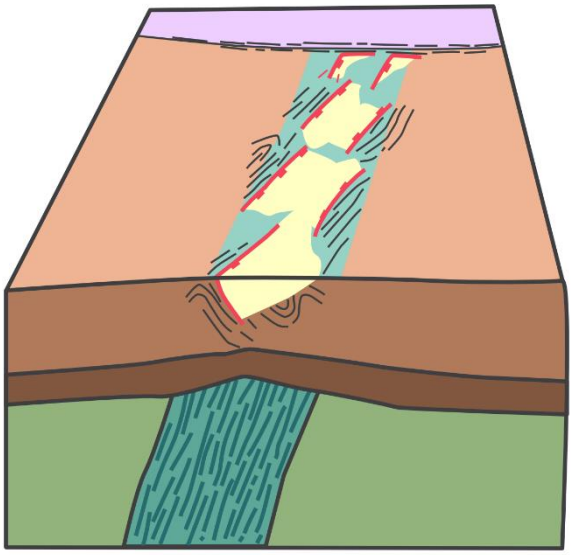

This thesis is submitted in partial fulfilment of the requirements for the degree of Doctor of Philosophy at Durham University.

Department of Earth Sciences

University of Durham

Malte Froemchen

July 2024

Abstract

Continental lithosphere is a heterogeneous assemblage of different units with variable strength, sutured together by a plethora of structures such as faults, shear zones, and other deformation fabrics. When this pre-existing framework of heterogenous lithosphere is broken apart, by extensional forces, these pre-existing structures and strength contrasts will have a considerable impact on the evolution of the resultant rift basins – a process known as inheritance. Inherited structures vary in scale and nature, ranging from broad zones of deformation fabrics in the upper mantle, to discrete faults in the upper crust. Inherited structures are often envisioned to influence rift evolution by reactivation of the inherited structure by a newly formed fault, yet this may not be the only mechanism in which inherited structures influence rifting. The constraint on how the scale and rheology of an inherited structure influence their effect on rift basins and their "reactivation" mechanism is poorly understood. Furthermore, the timing of when different scales of inheritance influence rift evolution is equally poorly constrained.

In this thesis, a multidisciplinary approach is used to understand how different scales of inheritance vary in their influence on continental rift evolution. Quantitative geomorphology of the Shanxi Rift in North China was used to constrain the rift evolution and analyse it under consideration of inherited structures, both in the upper crust and the deeper mantle. 2D geodynamic modelling of the North China Cenozoic rift systems was employed to better understand the impact of upper mantle structures and lithospheric architecture on rifting style, localisation, and migration. And finally, the interpretation of 2D and 3D seismic data of the Great South Basin, offshore New Zealand was carried out to constrain the temporal dimension of inheritance and contrast the impact of two variable terrane boundaries on rift evolution.

Each chapter illuminates a different aspect of the scale dependence of inheritance, in combination the results show that inherited structures do not necessarily need to reactivate to influence rift evolution. They also show that deeper seated structures in the lower crust or upper mantle are most important during the early localisation of rifting and determine the broader rift orientation. Meanwhile, shallow crustal structures segment individual rift faults at a smaller scale. These shallow crustal structures influence rifting most significantly in later stages during linkage and can sustain fault activity for longer along individual faults. These results not only present major implications for how we interpret the evolution of rift basins but also have practical considerations for seismic hazard assessments of active rifts and economic considerations for fluid flow in rift basins.

Contents

Table of Figures

Supplementary Figures

Tables

Acknowledgements

This thesis marks the culmination of nearly four years of research that has led me down unexpected paths and avenues. I would like to thank several individuals who have made this work possible and have helped me along the way.

First and foremost, I would like to thank my brilliant supervisory team for their guidance, patience, and unwavering support throughout the past four years. Starting a PhD in the middle of a global pandemic was certainly not how we initially planned this project. While it took nearly a year until we had our first in-person meeting; from the first Zoom call, everyone was focused on setting me up for a successful project. Ken, you have been a fantastic main supervisor, thanks to your encouragement and motivation throughout the years, I was able to complete this project. You have provided me the freedom to truly make this project my own and have been a great mentor along the way. Thank you for also keeping me focused on finishing in time and stopping me from going down another rabbit hole. Thank you to Mark for encouraging me to work on the geomorphology of the Shanxi Rift, which ended up becoming such a big part of this project. Your enthusiasm for Shanxi and North China led me to work on these fascinating regions. Furthermore, you always provided a critical, yet constructive perspective on each aspect of this project. A big thank you to Jeroen as well who was indispensable to the modelling part of my project. Your guidance eased my way into working with ASPECT and inspired my enthusiasm for geodynamical modelling. Many thanks to Tom as well: Your initial contribution to shaping this project was important and you offered valuable advice during the difficult early phase of my PhD.

Outside of my supervisory team, many others offered advice, constructive feedback, and technical support. Big thanks to Phil, whose enthusiasm for all things modelling and geodynamics is contagious and, has offered valuable advice and ideas on how to set up my ASPECT models. Fernando for offering any and all help with Hamilton-related issues, which made the modelling work possible in the first place. I'd also like to appreciate the help of Yueren Xu, for contributing his wealth of knowledge and experience working on the Shanxi Rift. And of course, the many people who offered constructive feedback and positive comments at various iterations of EGU, TSG or DRT.

I am grateful for the financial support I have received from the IAPETUS2 DTP, which made this project possible in the first place. I am also thankful for the financial support I have received for my placement at the British Geological Survey in Edinburgh through IAPETUS2. Thank you to Dave and his team at the BGS for making me feel so welcome during my three months with you and listening to my contrived ideas about inheritance in the East Irish Sea Basin.

Many thanks to the postgraduate community in Durham, especially Alavya, Bex, Akos, Kilian and Josh, which made the past four years a lot more fun. The pub quizzes at the Elm Tree, happy hours, postgraduate weekend aways, BBQs or just simple lunchtime chats have helped immensely, especially when the PhD seemed to be going nowhere. I am also thankful for the many friends from my time in Aberdeen or Germany whose continued friendship throughout my PhD has provided me with well-needed distractions from the PhD stress. And of course, big thanks to everyone at DUHWS for the much-appreciated weekend getaways to the Lakes, Snowdonia, Cheviots, or the Scottish Highlands.

I would also like to thank my family who have supported me throughout the entire time. Most of all thank you to my father and sister for always being there for me. You have sparked an interest in the natural world within me from an early age and took me on all the holidays to the Austrian and Swiss Alps (I may not have appreciated it initially, but I do now). Big thanks as well to Marion, Niko, Roman and Maren. I cherish the time we spend together as the big patchwork family and coming home from Christmas was always a great way to switch off. I would also like to thank those who are not here with us anymore to see me finish my educational journey: My mother and my paternal grandparents. You have been incredibly important in my life, and it is thanks to you that I am the person I am now.

Lastly, Kathryn, I am eternally grateful to you for always supporting me. I can't put into words how grateful I am to have met you. Thank you for your understanding, patience, time, and attention. Especially in the past weeks, your support has carried me through finishing this thesis and I can't thank you enough for it. I can't wait to see where life leads us next.

Thank you to everyone listed and anyone else I might have forgotten to mention who helped me along this journey!

This thesis is dedicated in loving memory to my mother, Dr Petra Sommer-Frömchen. Thank you for everything, forever in our hearts and minds.

Declaration

I declare that this thesis, submitted for the degree of Doctor of Philosophy at Durham University, is my own work and not substantially the same as any which has been previously submitted at this or any other university. Where appropriate, I have clearly indicated the contributions of colleagues to fully acknowledge all collaborative work.

Malte Froemchen

Durham University

July 2024

Funding

The work that has led to this thesis was supported by the Natural Environment Research Council (NERC) IAPETUS2 Doctoral Training Partnership (DTP) [grant number NE/S007431/1] whose support is gratefully acknowledged.

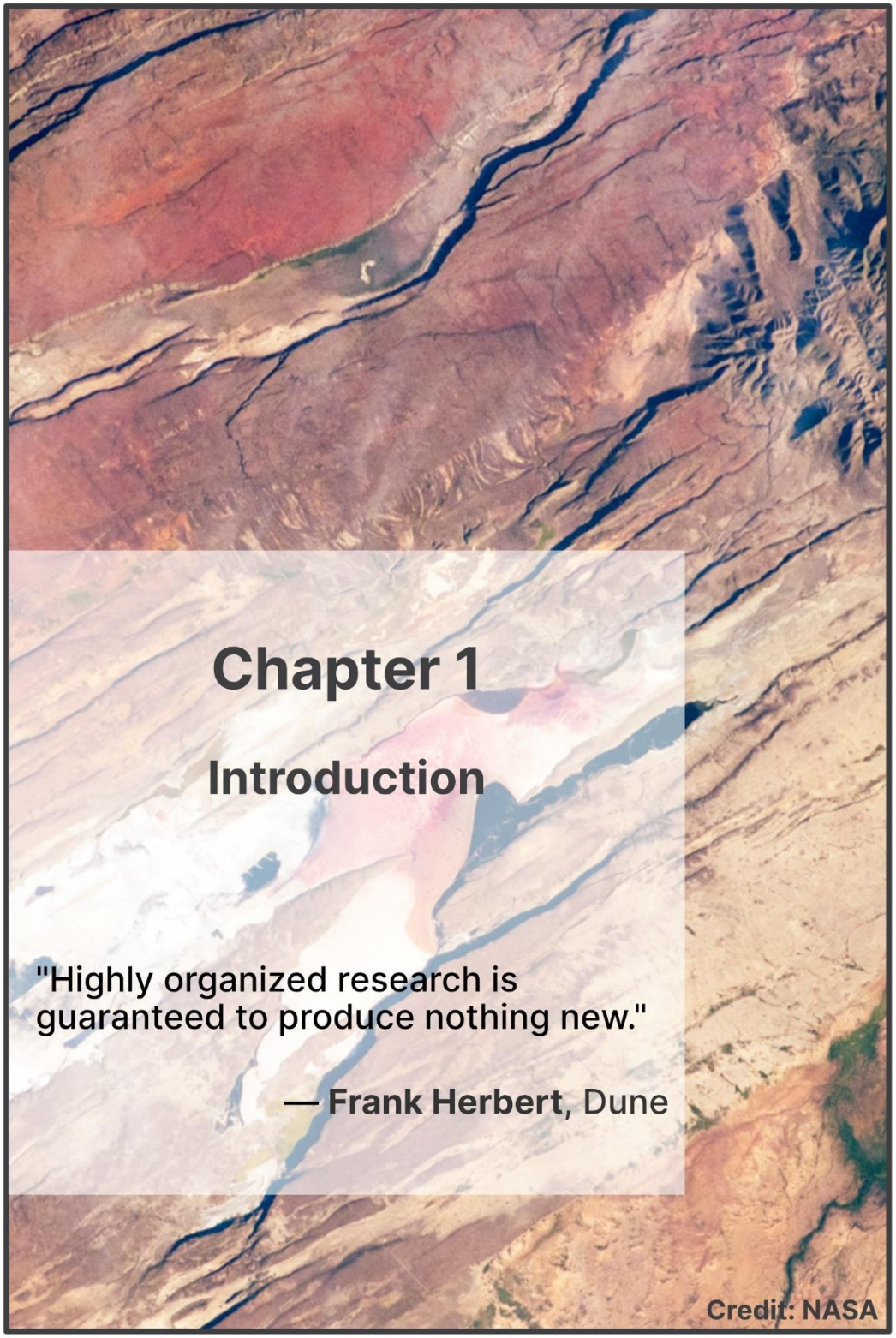
Chapter 1
Introduction
"Highly organized research is guaranteed to produce nothing new."
— Frank Herbert, Dune
Credit: NASA

1. Introduction

1.1 Rationale

1.1.1 Continental Rifting

Continental rifts are the first manifestation of continental lithosphere being pulled apart by geodynamic forces (Brune et al., 2023). They may progress into larger rift systems and ultimately culminate in the break-up of continental lithosphere as, for example, the Atlantic (Whitmarsh et al., 2001) and the relict Alpine Tethys (Lemoine et al., 1986; Manatschal, 2004) or become dormant as is the case for the North Sea (Ziegler, 1992) or the West Antarctic Rift (Jordan et al., 2020). As the principal mechanism in the breakup of continental lithosphere, it is responsible for the breakup of supercontinents such as Gondwana and Pangea, shaping the continental landmasses we know today. Continental rifts vary in size and morphology, they can be thousands of kilometres long and tens to hundreds of kilometres wide, dependent on kinematics and rheology of the lithosphere. They not only pose significant hazards such as earthquakes, landslides, or volcanic activity but are also of economic importance, as they hold considerable reserves of hydrocarbons, mineral resources and potential geothermal energy, hence they have attracted considerable attention by researchers to better understand their evolution.

Continental rifts on a large scale are governed by a balance of between an applied extensional tectonic force and the mechanical resistance of the lithosphere. Generally, rifts form when the applied tectonic force exceeds the resistance of the lithosphere and brings the entire lithosphere to its yield point which results in the formation of brittle failures such as faults and fractures (Brune et al., 2023). The main driving tectonic forces in the case of rifting are subduction-related forces (van Summeren et al., 2012), lithospheric buoyancy forces (Bott, 1992; Coblentz et al., 1994) and mantle convection (Morgan, 1972; Richter and McKenzie, 1977) (Fig. 1.1). Subduction related forces are one of the main driving factors of continental rifting: Slab pull by the

downgoing slab can cause extension in the lower plate (e.g. Red Sea Rift (Bellahasen et al. 2003) or Woodlark Basin (Taylor et al., 1999)), while lateral trench retreat, for example during slab rollback, will cause extension in the upper plate (e.g. marginal basins of East Asia (Karig, 1971; Tatsumi et al., 1989)). Lithospheric buoyancy forces are related to a gradient of the gravity potential energy which may either arise due to differences in topography or lithospheric structure (i.e. different crust – mantle lithosphere ratios, temperature, density) these are common in former orogenic belts, after removal of the compressive deviatoric stresses. In places such as East Africa (Rajaonarison et al., 2021), Basin and Range (Jones et al., 1996) or North China (He et al., 2003), lithospheric buoyancy forces arising from high topography either due to past orogenic history or dynamic topography have contributed to rifting. Mantle convection forces can generate horizontal or vertical traction (resulting in dynamic topography, which in turn may generate lithospheric buoyancy forces), which may be helped by an upwelling mantle plume, however, the effect of these traction forces especially in areas of thick lithosphere is debated (Brune et al., 2023). A combination of these forces may act on the initiation of a rift, yet further away from subduction zones, lithospheric buoyancy forces may become more important (Brune et al., 2023). However, even combining all these forces may not be enough to overcome the resistance of strong, cold lithosphere and form a rift, in those cases, the exploitation of discrete inherited structures that weaken the lithosphere is important to initiate rifting (Dunbar and Sawyer, 1988; Petersen and Schiffer, 2016). After the yield stress of the lithosphere has been overcome and the rifting has been initiated the progression of rifting is governed by different weakening and resisting mechanisms, upwelling asthenosphere can generate heat and weaken the lithosphere (Sengör and Burke, 1978; Huismans et al., 2001) while faulting and brittle failure can further reduce grain size and the mechanical cohesion (Byerlee, 1978) causing the rift to get weaker.

Cooling of the lithosphere during slow rifting (van Wijk and Cloetingh, 2002) or isostatic adjustment due to the negative topography created by rifting may counteract the forces that generate rifting. Changes in the balance of these forces may cause rifting to progress or become dormant. Magmatism associated with rifting is commonly due to asthenosphere upwelling and decompression (McKenzie and Bickle, 1988) and is another major weakening contributor to rifting (Bialas et al., 2010; Havlin et al., 2013), however due to the focus on amagmatic rifts in this study it is not further considered here.

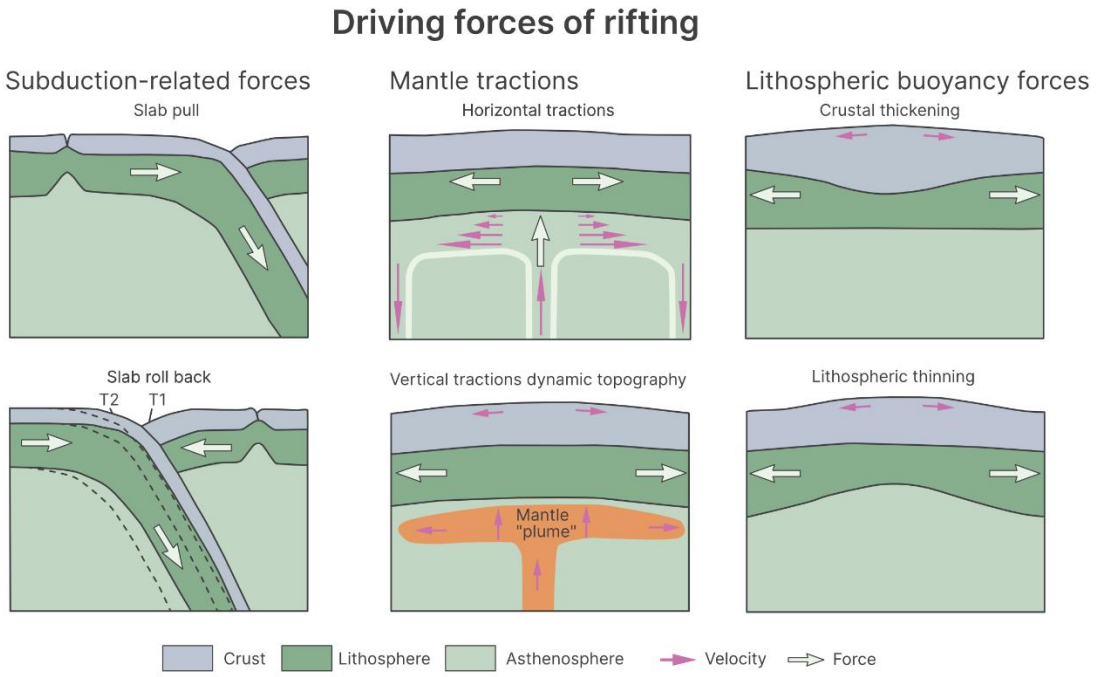

Figure 1.1 Driving Forces of Rifting.

Simplified sketches of the main forces that drive continental rifting (adapted from Brune et al., 2023). Subduction can generate major forces that drive rifting either in the downgoing plate (slab pull) or the overriding plate (Slab rollback). T1 and T2 (in dashed lines) indicate the original position and the later position of the downgoing slab during slab rollback. Mantle tractions either due to horizontal tractions from convection cells or vertical tractions generated by dynamic topography from a

possible mantle plume, can drive rifting in the absence of subduction forces. Heterogeneities in the lithosphere, i.e. the differential thickness of crust and mantle, can generate buoyancy forces that drive rifting.

Rifts and humans have been interlinked since the evolution of the human species in the East African rift valleys (Schrenk et al., 1993; Blumenschine et al., 2003), in fact, the development of the rift lakes of the East African Rift may have been an important contributor to human evolution (Bailey et al., 2000; Trauth et al., 2010; Bailey et al., 2011). Ever since humans have settled close to many rift valleys (Stewart and Piccardi, 2017) across the globe and have been exposed to the significant hazards posed in regions of active rifting, which includes seismicity (de Boer and Sanders, 2004; Ma et al., 2020; Hao, 2023), volcanism (Davies, 2008; Biggs et al., 2021) but also landslides (Dewitte et al., 2021). At present day millions of people live close to active rifts for example in China, Africa, Russia and the USA. While the normal faults of rift systems cannot generate the large magnitude earthquakes of thrust faults or strike-slip systems, they are capable of generating devastating earthquakes, made worse by the proximity of human civilization centres close to rift faults, as demonstrated by recent events such as the L'Aquila earthquake in 2009 (Chiarabba et al., 2009) or devastating historic earthquakes such as 1303 Hongdong earthquake (Xu et al., 2018). But rifts do not only pose a hazard but are also regions of economic opportunities. The discovery of oil and gas reserves in the North Sea, starting with the Groningen field in 1959 (Watson and Swanson, 1975), has transformed the economies of adjacent countries such as the UK or Norway. But in the face of climate change and attempts to be less reliant on fossil fuels, rifts may yet again be significant zones of interest. Rifts have potential for geothermal energy, helium and deposits of metals and critical minerals. The thinned lithosphere arising from rifting results in higher geothermal gradients which are preferential for hydrothermal circulation in rift basins (Faulkner et al., 2010),

this may result in the widespread formation of geothermal reservoirs (Rowland and Sibson, 2004). In fact, in many rifts around the globe such as the Rhine Graben, the Basin and Range and the Kenya Rift, geothermal energy is already being generated (Jolie et al., 2021) and is likely to be a viable resource in many more regions of continental rifting. In various rift settings sedimentary hosted ore deposits are found due to the strong circulation of fluids and the elevated geotherm that benefit the precipitation and upward mobility of minerals (Tosdal et al., 2009; Lawley et al., 2022). However, despite recent advances and new ideas about the formation of ore deposits in rift settings (Hoggard et al., 2020; Dall'Asta et al., 2023), more work is needed to discover further mineral resources which are needed for the energy transition. Furthermore, continental rifting is a major source of CO2 that is being emitted into the atmosphere through degassing from the mantle during rifting (Lee et al., 2016; Brune et al., 2017; Wong et al., 2019). The amount of CO2 emitted from rifts shows drastic variations across the globe (Seward and Kerrick, 1996; Weinlich et al., 1999; Lee et al., 2016) and is possibly influenced by the initial lithospheric state prior to rifting (Foley and Fischer, 2017; Muirhead et al., 2020). Knowledge of the CO2 emissions from rifts is crucial to understanding how rifting is related to climate change across geological timescales. In summary, continental rifts may be as important to our future existence as they have been in the past.

Rifts around the world show considerable variation in their morphology and evolution (Brun et al., 1999), they range from narrow, localised rifts such as Baikal (Petit et al., 1996), Shanxi (Xu and Ma, 1992) and the East African Rift basins (Rosendahl, 1987) to wide distributed rifts stretching over 1000s of kms such as the Basin and Range (Friedmann and Burbank, 1995) or the Bohai Rift (Allen et al., 1997). However, all rifts are the manifestation of the stretching of continental lithosphere and display faults and basins as their main features. The architecture of continental rifts can be complex,

and they are often segmented into different basins. Faults are the result of brittle failure that accommodates the applied extension by localised shear deformation (Scholz, 2019), as faulting progresses, they generate subsidence in the hanging wall and form basins which are in turn infilled by alluvial, lacustrine and marine sediments, study of these sediments may constrain the evolution of rifting (Allen et al., 1997; Gawthorpe and Leeder, 2008; Ford et al., 2013). This generated subsidence also leads to the generation of rift lakes, which are common in continental rifts and are some of the world's largest lakes: Lake Baikal, Lake Tanganyika or Lake Malawi. While subsidence is generated in the hanging wall of rift faults, the footwall is uplifted due to flexural forces (Yielding and Roberts, 1992), this generates considerable topography in the footwalls of rift faults which can be used to deduce their kinematic history through geomorphic (Densmore et al., 2004; Fernández-Blanco et al., 2020; Harkins et al., 2005) or thermochronological approaches (Su et al. 2021; Gavel et al., 2021). The architecture of each rift varies considerably along strike and can be complex, however, most rifts are composed of a series of half-graben (bounded by one principal master fault) and graben structures (bounded by two opposing faults) which form distinct rift segments. During the initial stages of rifting isolated faults form (Fig. 1.2 -T1) and slip rates across the rift are slow. As rifting progresses the strain becomes progressively more localised causing the isolated faults to link up and form larger rift basins, while some of the earlier faults become dormant as strain is localised on larger structures (Cowie et al., 2005). Further rifting leads to the migration of strain towards the centre of rifting and basins further away become dormant. As faults will initially localise as discrete, isolated segments, zones of interaction between these faults will form. These zones as relay structures can occur across many scales and initially experience less deformation than the faults themselves (Fossen and Rotevatn, 2016). Relay zones are commonly referred to as the zone separating two faults in which fault tips interact

(Larsen, 1988; Peacock and Sanderson, 1991; Crider and Pollard, 1998; Fossen and Rotevatn, 2016). At a larger scale when multiple faults and segments are involved these zones are also referred to as accommodation zones or transfer zones (Bosworth, 1985; Morley et al., 1990). Both terms have been used interchangeably (Morley et al., 1990), but most commonly accommodation zones are characterised by overlapping or underlapping fault terminations while transfer zones are defined as discrete zones of strike-slip or oblique-slip deformation that separate two rift basins and often trends parallel to the extension direction (Faulds and Varga, 1998) although a clear distinction between transfer and accommodation zones of the two can be difficult to establish as they characterise zones of complex deformation that will include both dip-slip and strike-slip faulting. More generally these large-scale zones of separation and linkage between rift basins are known as Rift Interaction Zones (RIZ) (Nelson et al., 1992; Zwaan et al., 2016; Kolawole et al., 2021a) where they progressively link across and experience increased amounts of strain during progressive rifting (Fig. 1.2 - T2 and T3). RIZs may include smaller zones of fault interaction that can be classified as transfer zones or accommodation zones (Rosendahl, 1987; Morley et al., 1990; Kolawole et al., 2021a). The geometry of accommodation, transfer and rift interaction zones is governed by a range of factors including initial lateral separation and geometry (Morley et al., 1990; Faulds and Varga, 1998; Kolawole et al, 2021; Kolawole et al., 2024), these parameters and their location within rift systems is possibly related to underlying inherited structures, as shown by various studies based on map-scale patterns (Versfelt and Rosendahl, 1987; Ring, 1994; Faulds and Varga, 1998), analogue modelling (Acocella et al., 1999; Corti, 2012; Zwaan et al., 2016) and field-based studies (Theunissen et al., 1996). These zones are important during rift evolution as they often tend to be zones where strain is concentrated and therefore also see increased seismicity. However, they are also

important for understanding fluid flow (Morley et al., 1990; Rowland and Sibson, 2004; Fossen and Rotevatn, 2016) and syn-rift sedimentation during rifting (Gawthorpe and Leeder, 2000) which can be of economic importance.

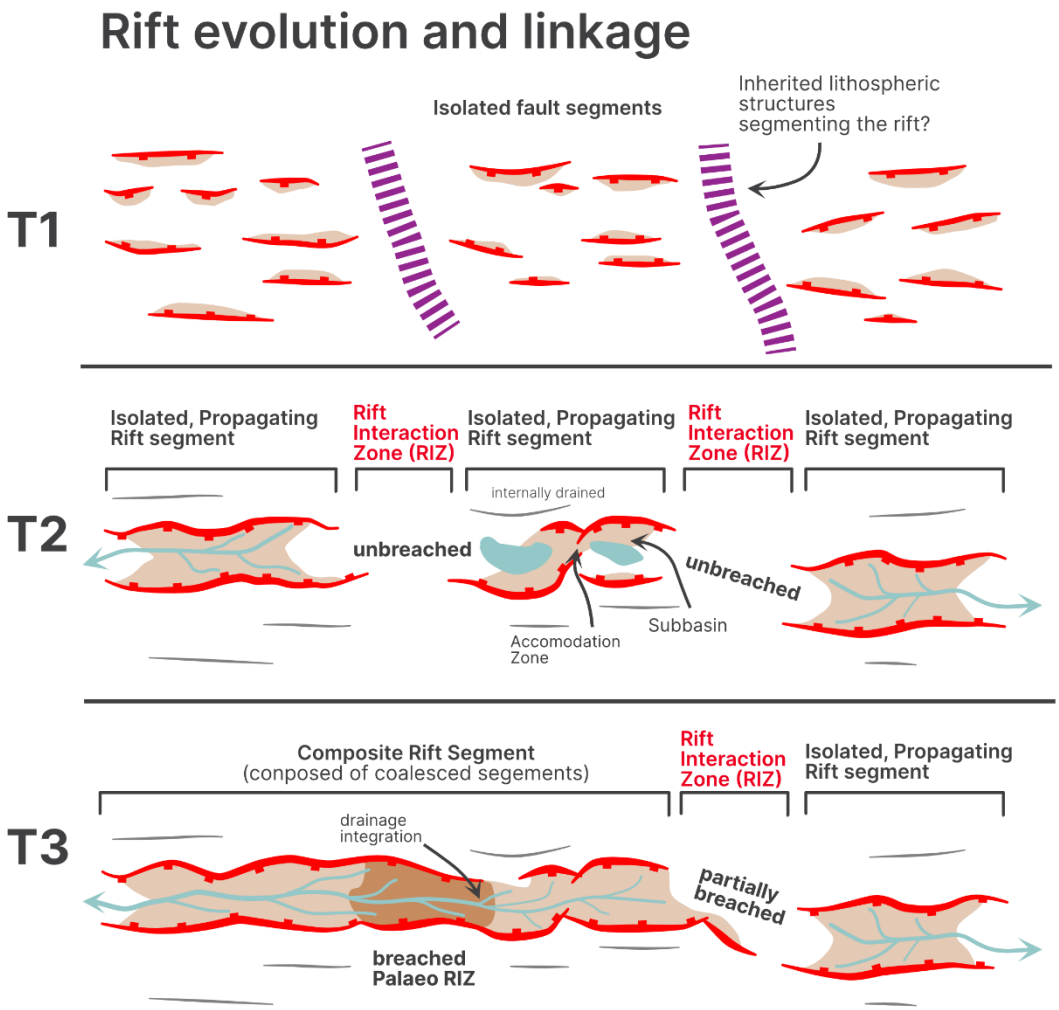

Figure 1.2 Rift Evolution and Linkage

Schematic evolution of a segmented rift basin (adapted from Kolawole et al. 2021a), showing the progressive coalescence of rift basins and linkage across Rift Interaction Zones (RIZs). T1 – Numerous isolated fault segments form as a first response to extension; inherited structures may have a first-order effect where faults localise and segment the rift basins. T2 – Isolated rift faults have started to coalesce into distinct rift basins which are separated by RIZs. Accommodation and

transfer zones form within rift basins and faults further away from the established rift axis become dormant. T3 – Linkage of rift basins continues across the RIZs, breaching fault connecting the different rift basins established and at later stages of linkage the drainage across basins is connected. The initial geometry of RIZs affects the stage of linkage. Oblique RIZ is only partially breached and drainage between basins is not integrated.

Theoretically, rift faults will form sub-perpendicular to the applied extension direction and will form colinear or en-echelon patterns, which may later be linked either as relay or accommodation zones. However, in various rift basins worldwide, faults oriented obliquely to one another or to the suggested extension direction, have been observed (Reeve et al., 2015; Duffy et al., 2015; Williams et al., 2019). The simplest explanation for this observation is that the rift experienced multiple rift phases with different extension directions – while this has been observed in rift systems such as the Gulf of Corinth (Nixon et al., 2016; Gawthorpe et al., 2018) and the North Sea (Bell et al., 2014; Phillips et al., 2019) and multiphase rifting is important in the evolution of a rift to a rifted margin (Naliboff and Buiter, 2015) – this is not always the case. While this explanation has often been invoked to explain the variety of fault orientations in various locations (e.g. East Africa - Bonini et al., 1997; Boccaletti et al., 1998) – similar rift patterns can also develop under a single phase of rifting (Williams et al. 2019; Reeve et al., 2015). This has been shown in analogue experiments (Agostini et al., 2009; Phillipon et al., 2015; Zwaan et al., 2022) and studied in the field (Corti et al., 2013; Smith and Mosley, 1993). As these structures are often oblique to the regional strain field it has been suggested in modelling studies (Agostini et al., 2009) that these faults have oblique slip kinematics. However, both field studies (Delvaux et al., 2012; Xu et al., 2018) and more recent modelling studies (Corti et al., 2013; Phillipon et al., 2015) show that oblique faults have pure dip-slip kinematics which suggests the strain

field has been locally rotated (Morley, 2010). Strain may also be partitioned across a variety of strike-slip, oblique-slip and dip-slip faults, which has been often observed in reactivated rift systems like the Moray Firth (Tamas et al., 2022); the Orcadian Basin (Dichiarante et al., 2016) or the Northumberland basin (de Paola et al., 2005). An alternative to the multiphase rifting explanation is that complex fault patterns may be the result of inherited structures reorientating faults by either direct reactivation or by perturbating the strain field and causing local strain rotations.

1.1.2 Inheritance in Rift Basins

Inheritance in broad terms describes the influence of preexisting heterogeneities in the continental lithosphere on later deformation events such as rifting or collisional tectonics (Butler, 1989; Butler et al., 2006; Mohn et al., 2014). This study is chiefly concerned with the effect of inheritance on the evolution of rift basins. But inheritance has an impact on nearly all continental tectonic processes (Holdsworth, 2001), for example, it is well-studied that Tethyan rift structures influenced later contractional deformation in the Alps (e.g. Butler, 1989; Butler et al., 2006; Mohn et al., 2014) Inheritance in rift basins lowers the mechanical resistance of the lithosphere to deformation and therefore may favour the initiation and propagation of rifts. There are different types of inheritance (Manatschal et al., 2015): Thermal, compositional and structural, which may be co-dependent and influence the style, architecture and evolution of continental rifts. Thermal inheritance is the effect of the pre-rift thermal state of the lithosphere on rifting i.e. the difference between the young, hot and thin lithosphere of a recently deformed region and the strong, old and cold lithosphere of an undeformed craton. While the strength of the lithosphere may vary with its thermal state and evolution, this study is chiefly concerned with equilibrated lithosphere with a strong mantle lithosphere, a strong upper crust and a weak mid-lower crust (often

termed the jelly sandwich; Burov and Watts, 2006). Other studies have questioned the assumption that the lithosphere is strong and hypothesise that while the upper crust is strong, the lower crust and mantle lithosphere are weak, based on observations that most earthquakes occur in the upper crust (Jackson et al., 2002). However, it is debated how stable this would be for a wide range of tectonic settings (Burov, 2010) while the "Crème Brulee" model may apply to certain regions (Liu et al., 2020), the bulk of the mantle lithosphere most likely is strong, especially in stable continental interiors. This is tightly interlinked with compositional inheritance which is concerned with the influence of a compositionally heterogeneous lithosphere on rifting, i.e. the different rheological response of heterogeneous lithologies such as intrusions, high-pressure metamorphic rocks or sedimentary rocks as well as different mantle compositions (fertile or depleted mantle). Structural inheritance on the other hand mainly deals with discrete inherited structures from previous deformation events such as shear zones or pre-existing faults. This study is chiefly concerned with the effect of structural inheritance and focusses on the influence of pre-existing basement fabrics, faults, terrane boundaries and shear zones on the evolution of the rift system. However, as mentioned above these can be hard to separate at times as composition and thermal effects, especially at larger scales (as seen in Chapter 3), work together with

structures to segment rift basins.

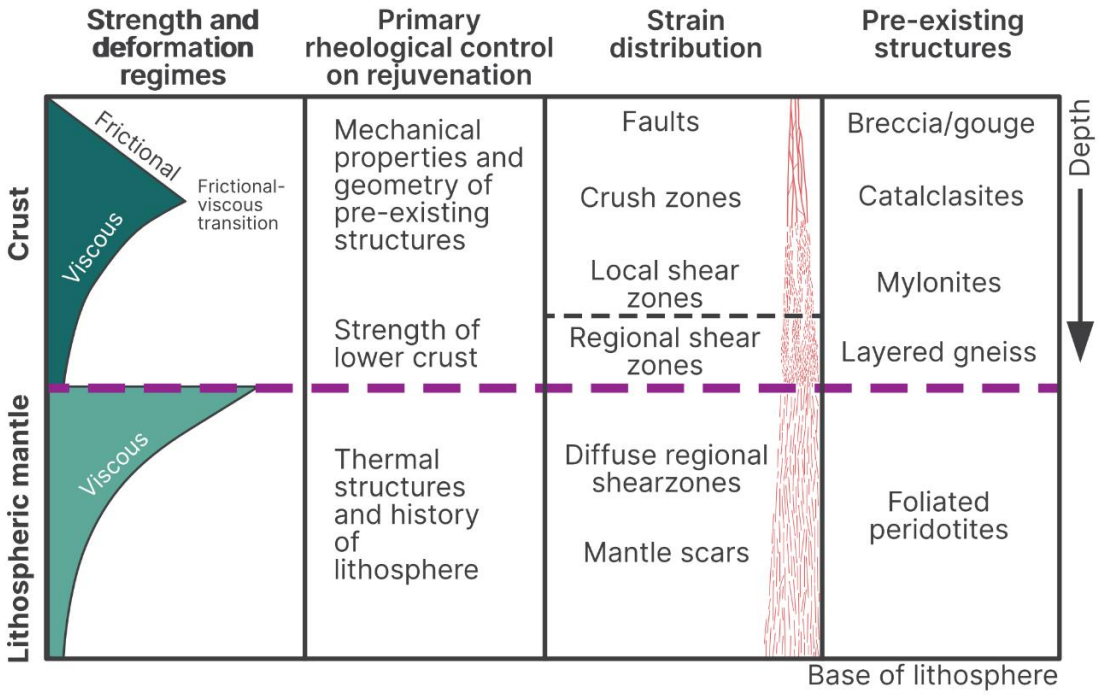

Figure 1.3 Strength of the Lithosphere

(adapted from Sibson, 1977; Holdsworth et al., 2001a and Holdsworth et al. 2001b) – Schematic diagram of the strength of the lithosphere and the deformation regimes acting in different parts of the lithosphere, as well as the primary rheological control on rejuvenation (or inheritance), strain distribution and the pre-existing structures present at that depth.

Inheritance influences rifts at different scales from larger lithospheric structures to small-scale faults (Corti et al., 2022). At different scales different mechanisms of inheritance operate (Fig. 1.3): While inheritance in the upper crust is mostly controlled by mechanical properties of pre-existing structures, deeper in the mantle where viscous creep is the predominant deformation mechanism the thermal structure of the lithosphere is an important control (Holdsworth et al., 1997; Holdsworth et al., 2001a; Samsu et al., 2023). There are a multitude of structures in the upper crust that may

influence deformation. These vary in scale and their rheological behaviour and therefore may have different effects on rifting. Pervasive basement fabrics (e.g. orogenic or metamorphic fabrics) or shear zone fabrics (Morley et al., 2004; Reeve et al., 2015; Phillips et al., 2016; Fazlikhani et al., 2017; Osagiede et al., 2020; Vasconcelos et al., 2020) can reach tens of kilometres in scale, while individual faults may influence deformation at the outcrop scale over just a few meters. During a multiphase rift history, such as that observed in the North Sea, faults and rift fabrics formed during previous rifting can influence the nucleation and orientation of faults formed in subsequent extension events (Henza et al., 2011; Henstra et al., 2015). Magmatic intrusions can influence deformation in multiple ways dependent on their scale and rheology: Large granitic batholiths are more resistant to deformation, causing faults to splay and rift basins to form at their edges (Fraser and Gawthorpe, 1990; Phillips and McCaffrey, 2019), while meter scale dyke-host rock margin may be preferential sites of reactivation at the outcrop scale (Wedmore et al., 2020; Holdsworth et al., 2020). Most upper crustal structures do not exceed 10s of km of scale and their impact on rift evolution has been intensely studied through a combination of field-based studies and interpretation of seismic reflection data. Lithospheric scale inherited structures often exceed tens to hundreds of kilometres in scale and are often best recognised on the regional map scale (>100 km). Lithospheric inheritance includes orogenic belts, suture zones, terrane boundaries and pre-existing rift systems. A close relationship between pre-existing orogenic belts and rift basins has been postulated from early 1960s for the Atlantic margins (Wilson, 1966; Vauchez et al., 1997), Baikal Rift (Petit et al., 1996) or East African Rift (Rosendahl, 1987; Daly et al., 1989; Ring, 1994) (Fig. 1.4). However, while many orogenic belts present weakzones that facilitate later rifting and break-up, not all orogenic belts do, as for example the Ural Mountains (Krabbendam, 2001; Krabbendam and Barr, 2000), which

have an anomalously high lithospheric strength, and are stronger than the surrounding lithosphere. Orogenic belts contain a plethora of structures such as thrust faults, shear zones and deformation fabrics in the upper crust but more significantly they may represent major mechanical weaknesses of lithospheric scale. As these are possibly relatively weaker than the surrounding lithosphere, they preferentially accommodate strain at the large scale and aid the nucleation of rift systems. This mechanical weakness of orogens is amplified when adjacent to cratonic blocks, for example, continental rifts such as East Africa (Daly et al., 1989; Rosendahl, 1987) or Baikal (Petit et al., 1996; Petit and Déverchère, 2006) (Fig. 1.4). This large-scale type of inheritance is also referred to as tectonic inheritance (Şengör et al., 2019; Sengör and Burke, 1978). Inherited structures do not exist in isolation and may be superimposed within orogens for example a major lithospheric weakness exists alongside regional kilometre-scale shear zones and metamorphic fabrics. Inherited structures in the upper crust have been more intensely studied due to the widespread availability of seismic data sets that image the upper crust (Phillips et al., 2016; Fazlikhani et al. 2017; Deng et al., 2020) and direct observational field datasets for continental crust (Hodge et al., 2018; Dawson et al., 2018; Wedmore et al., 2020; Kolawole et al. 2022). However numerical (Heron et al., 2019) and analogue modelling (Molnar et al., 2020; Zwaan et al. 2022) as well as map scale observations (Tomassi and Vauchez, 2001) suggest that structures in the upper mantle may have a significant large-scale effect on rifting and may aid the nucleation and large-scale segmentation of rift basins. This has been suggested to be either the presence of discrete structures in the upper mantle (known as mantle scars (Heron et al., 2016)) that preferentially localise strain or through an upper mantle fabric with a crystalline preferred orientation which guides the strain (Tomassi and Vauchez, 2001). These structures are the result of large-scale tectonic events such as major orogenies and collision zones and are either

representative of subducted slabs remanent in the upper mantle or mylonitic fabrics. While these different types of inherited structures and their scales have been observed and documented the relative impact and their interaction of lithospheric and crustal inheritance have, apart from recent modelling advances by Molnar et al. (2020) and Zwaan et al., (2022), rarely been assessed.

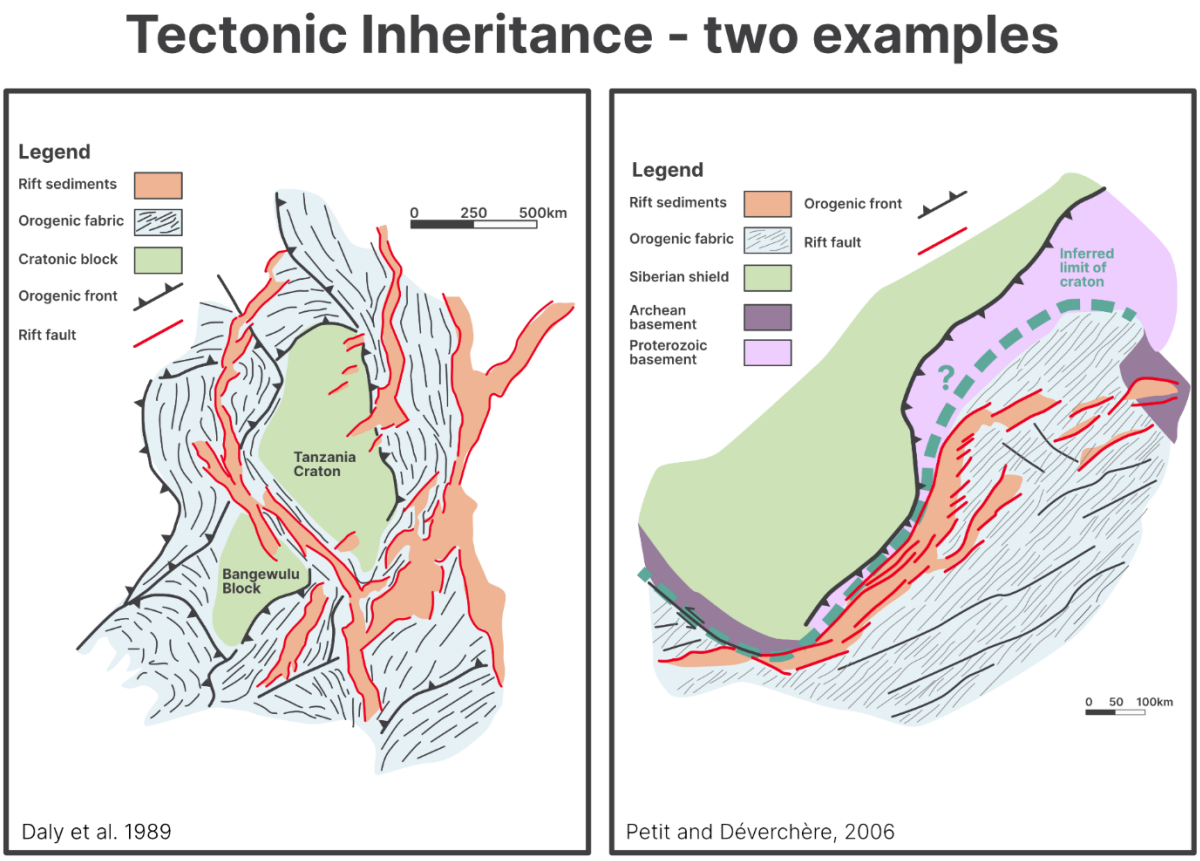

Figure 1.4 Tectonic Inheritance Examples from East Africa and Baikal

Schematic sketches of two examples of rift basins forming within a pre-existing orogenic fabric from the East African Rift (modified from Daly et al., 1989) and Baikal (modified from Petit and Déverchère, 2006). In both cases the orogenic belts are adjacent to stronger cratonic blocks which resist deformation, hence the mobile

belt acts as a mechanically weaker region and accommodates most of the deformation.

Inheritance can play a role throughout the entire life cycle of a rift from initiation to necking when it forms into a hyperextended rifted margin (Manatschal et al., 2015). However, the duration that inheritance plays a role remains poorly constrained. Many studies highlight the importance of inheritance in nucleation of rifting during the earliest phase (Daly et al., 1989; Vauchez et al., 1997) – especially large-scale structures such as orogenic belts, suture zones and pervasive upper mantle fabrics seem to be important in the nucleation of rifting. Apart from controlling the location of rift basins, during the early stage of rifting, inheritance also may cause rift basins to be orientated obliquely to the imposed extension direction (Phillipon et al., 2015). Other studies show the importance of inheritance during the linkage of established rift basins during progressive rifting, this has been shown in conceptual analogue models (Zwaan and Schreus, 2017) but also in nature for example for the East African Rift (Heilman et al., 2019). The influence of inheritance may be important during the formation of later intrarift faults as they may also follow the trend of inherited basement fabrics and strike oblique to the extension direction (Muirhead and Katternhorn, 2018). Inheritance may not only play a part once in rift evolution but may be an influence during multiple stages of the rift evolution (Vasconcelos et al., 2019). Furthermore, in rift systems that have evolved towards breakup and the rifted margin stage, recent studies show the importance of inherited structures and composition on the development of necking faults (Muñoz-Barrera et al., 2020). Examples from the North Sea, however, show the declining effect of inherited structures on rift evolution (Bell et al., 2014; Claringbould et al., 2017; Phillips et al., 2019) due to an increased thermal weakening of the lithosphere during rifting. Here, after the necking stage, the fluids and magmatic processes are more important for the continuation of margin

formation and inheritance has little to no effect as rifting-induced processes govern the further breakup. In summary, whilst the influence of inheritance has been documented during a major part of the lifecycle of a rift, there remains little comprehensive understanding of defining a sequence of events that might form when inheritance shapes a rift and what controls which pre-existing structures are active in the reorganization process at any stage.

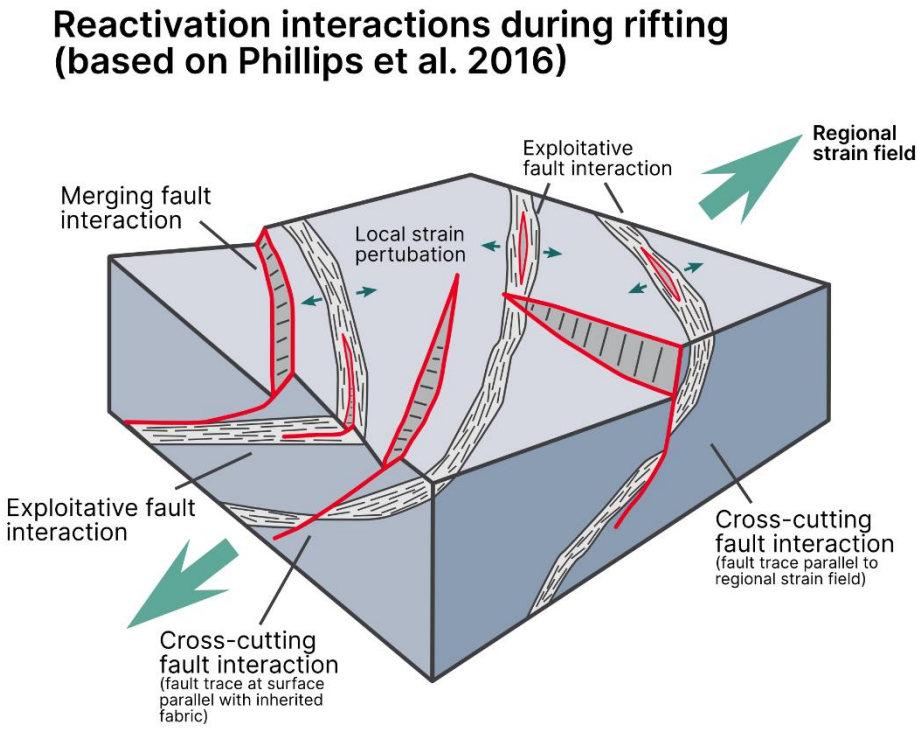

Figure 1.5 Reactivation Interactions during Rifting

Examples of reactivation interactions during rift basin formation (modified from Phillips et al., 2016). Some rift faults exploit the inherited structures (in this case shear zones) and will nucleate within the inherited fabric, this causes the rift fault to strike oblique to the imposed extension direction. Rift faults can also nucleate above the inherited fabric and connect at depth through merging interaction or crosscut the structure – in both cases, they may strike oblique to the regional strain field due to strain perturbation by the heterogeneous basement.

While all these studies show evidence that inheritance probably influenced deformation there is much less clarity on the mechanisms behind the control of inheritance on rifting. Early studies on inheritance chiefly focused on direct brittle reactivation of inherited structures (Holdsworth et al., 1997; Holdsworth et al., 2001b). Frictional reactivation of inherited structures is a feature observed in many regions around the world (North Sea (Phillips et al., 2016; Fazlikhani et al., 2017), East Africa (Laó-Dávila et al., 2015; Kolawole et al., 2018; Wedmore et al., 2020). From seismic data, we observed that the reactivation of inherited structures may occur as an exploitative, merging or cross-cutting relationship (Phillips et al., 2016). The exploitative relationship is the classic reactivation of an inherited structure such as a shear zone (Morley et al., 2004; Fazlikhani et al., 2017), in which faults form directly within the weakened pre-existing fabric and propagate upwards into the overlying cover sequence. Merging and crosscutting relationships differ in the fact that they do not directly re-activate the structure but serve to re-orientate the stress (Fig. 1.5). In both cases faults form above an inherited structure and inherit the geometric orientation of the structure but they do not directly reactivate the structure, merging relationships will propagate downdip and eventually merge with the structure at depth, while cross-cutting structures propagate downdip and offset the inherited structure. Even though reactivation is a direct and perhaps common way in which inherited structures influence rift basins it is not the only viable mechanism. Due to the main focus being on direct reactivation, the terms reactivation and inheritance are sometimes used interchangeably, yet this limits the way we understand the possible influence of inheritance on rifting since not all inherited structures are frictionally reactivated. Recently there has been a growing body of studies that show a more subtle influence of inherited structures in which coeval normal faults form with various orientations (Morley, 2010; Wilson et al., 2010; Reeve et al., 2015; Osagiede et al.,

2020) or fault form that are both oblique to the regional extension direction but also oblique to inherited structures beneath them (Agostini et al. 2009; Phillipon et al., 2015; Hodge et al. 2018; Samsu et al., 2019; Samsu et al., 2021) instead the inherited structures below appear to reorientate the strain field causing contemporaneously formed faults to strike in variable directions. This opens a mechanism in which inherited structures can influence the evolution of a rift basin without an inherent hard link between these. Soft-linked inheritance at shallow depth between different fault populations is recognised in various locations such as the NW shelf of Australia (Phillips et al., 2022) or the Taranaki Basin, NZ (Giba et al., 2012; Collanega et al., 2019), where often a more mechanical incompetent unit decouples the extension. Other examples of strain orientation (Fig. 1.6) include the formation of en-echelon rift basins along a deeper-seated weak zone (Agostini et al. 2009), splaying of faults as they approach stronger more competent units such as batholiths (Phillips and McCaffrey, 2019; Phillips et al., 2023) and the segmentation of rift systems by basement structures leading to the development of accommodation zones and RIZs (Rowland and Sibson, 2004; Fossen et al., 2016). The apparent lack of direct linkage and geometric similarity between inherited structure and rift fault makes this mechanism harder to recognise, however, it may explain the presence of faults with variable geometries which are oblique to both inherited structures and the principal extension direction. Reorientation in rift basins has most likely been underappreciated by previous research due to its elusive nature, therefore a better understanding and novel ways to unravel its impact on rifting are needed.

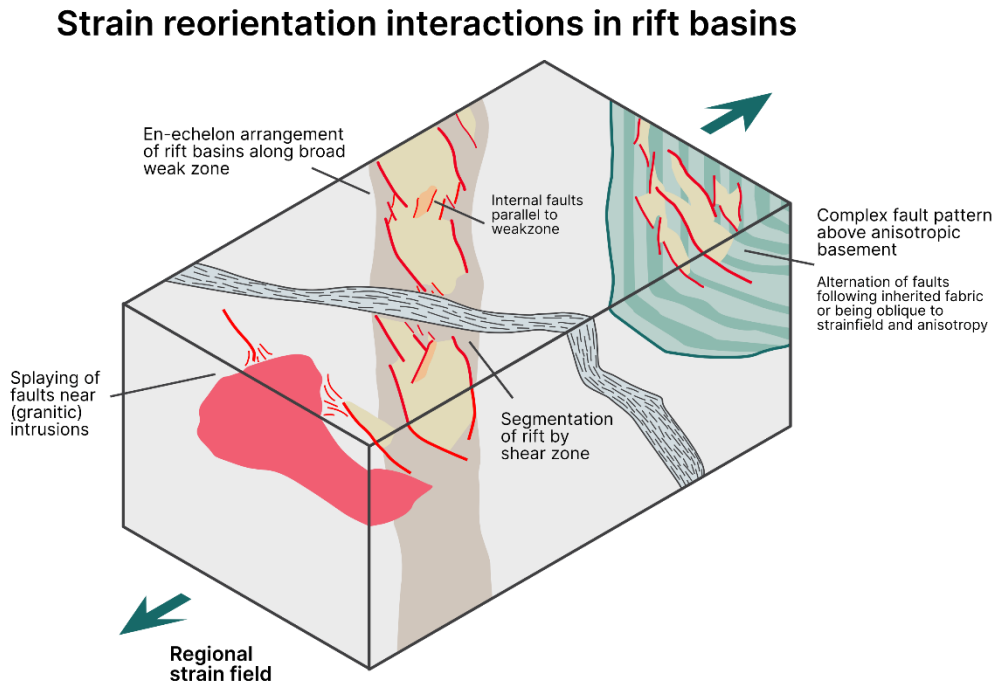

Figure 1.6 Strain Reorientation Interactions during Rifting

Schematic examples of strain reorientation interactions in rift basins – in these cases the pre-existing structures and heterogeneities are not directly reactivated but still influence the observed deformation and rifting through reorientation of the strain field. Deeper seated viscous weak zones (active in the ductile regime of the lower crust or mantle) may reorientate the rift faults that they form in an en-echelon pattern and strike oblique to both the weak zone and the imposed regional strain field. Lithospheric structures can segment the rift basins and form accommodation zones or RIZs. Large igneous intrusions such as batholiths can cause faults to splay in their vicinity. Complex fault patterns can form above an anisotropic basement – the anisotropic basement causes strain field reorientation which causes faults to strike oblique to both the inherited fabric and the regional strain field, the fault pattern may also be complicated by faults striking in multiple directions as they alternate between exploiting the pre-existing fabric or forming perpendicular to the reorientated strain field.

1.2 Thesis Aims

The study of structural Inheritance in rift systems is a rapidly evolving field over the last 10 years with many new discoveries that have been made to move from basic map-scale interpretations of inheritance to a more thorough understanding of the mechanisms behind inheritance. An increasing number of studies have complied a large catalogue of different structures that influence rift evolution in one way or another. In many cases, different levels of inheritance are present as the previous deformation history of the lithosphere has been complex and multiphase or the deformation has manifested in different ways in the crust and mantle lithosphere. Previous studies have highlighted both the role of upper crustal and upper mantle structures in the initiation, segmentation and evolution of rift basins. The main aim of this thesis is to investigate the relative influence of how the upper crust and mantle combine to structure a rift. With this comes a series of larger questions that I try to address:

- How do lithospheric and crustal inherited structures affect rift architecture?
- Which type of inheritance is most important during rift formation?
- Does the importance of lithospheric and crustal inheritance vary over time?
- How can we assess the role of deeper-seated structures on the reorientation of faults during rifting?

1.3 Outline of thesis:

The influence of inheritance is inherently scale-dependent (Samsu et al. 2021; Corti et al. 2022) and most likely different scales of inheritance influence rifting in different ways. Therefore, this study is setup to use different techniques to study inheritance at a variety of scales to gain a bigger picture overview of the variety of ways in which inheritance acts. The thesis is organised as three journal papers that serve as the main chapters, while each of these is standalone, they all are concerned with a common

theme of inheritance in rift basins. The order of the chapters represents an evolving understanding of how different scales of inheritance may influence rifting. Chapter 2 underpins the hypothesis that perhaps structures in the upper mantle as well as the upper crust may have influenced rifting in the Shanxi Rift, which then leads to Chapter 3 which attempts to model how this proposed upper mantle structure may influence wider rift patterns in North China. Finally, Chapter 4 compares how inherited upper crustal and deeper lithospheric structures may express themselves differently during rifting using data from offshore New Zealand. The results from all studies are finally compared and discussed in chapter 5 to bring together into a more generic model.

1.3.1 Chapter 2

In Chapter 2, I take a regional view to study the influence of inheritance on an entire rift zone and how we might be able to detect the influence of different scales of inheritance in active rift zones using topography and geomorphic observations. We chose the Shanxi Rift in North China as the study region, which has been speculated to be influenced by inheritance, but little comprehensive work on the influence of inherited structures on the evolution of this segmented rift has been undertaken. I combine an analysis of the published structural data of the pre-existing structures with a geomorphic analysis of the active present-day faults and their topographic expression using geomorphic indices.

This chapter has been published in a slightly modified form in Solid Earth and is freely accessible online:

Froemchen, M., McCaffrey, K.J.W., Allen, M.B., van Hunen, J., Phillips, T.B., Xu, Y., 2024. Geomorphic expressions of active rifting reflect the role of structural inheritance: a new model for the evolution of the Shanxi Rift, northern China. Solid Earth 15, 1203–1231. https://doi.org/10.5194/se-15-1203-2024

1.3.2 Chapter 3

This chapter is concerned with the larger-scale picture of rifting in North China. The Shanxi Rift from the previous chapter is part of a variety of rift systems contained in the former North China Craton. These rift systems have been separated in time and space and their exact origin and geodynamic drivers remain debated. The effect of the pre-rift lithospheric architecture and discrete inherited structures in the lithosphere on the rift migration pattern observed in North China was investigated in a series of 2D geodynamical models.

1.3.3 Chapter 4

In the previous two chapters, I investigated the relative importance of crustal and deeper lithospheric inherited structures on rifting. In this chapter, I use 3D seismic data collected in a different rift system that is influenced by both shallow crustal structures and deeper lithospheric ones. The Great South Basin, offshore New Zealand formed in the Cretaceous over a mosaic of different basement terranes. I look at three basement terranes and their boundaries in particular which are distinct in scale and nature and have a distinct influence on the rift architecture.

1.3.4 Chapter 5

While all the chapters are self-contained and vary in their methodology and study region, they all serve to reveal more about how inheritance influences continental rifting. Specifically, they all work together to better understand the interaction between deeper-seated lithospheric inheritance and shallow crustal fabrics, and how these different structures manifest themselves during rifting. In the final discussion chapter, I draw on the learnings of the previous chapters to show how they fit in with existing literature and contribute new knowledge to the rapidly evolving field of inheritance. I also consider the practical implications of using geomorphology to study the impact of inheritance on rift basins. Finally, I examine how the findings of this thesis might impact seismic hazard evaluation.

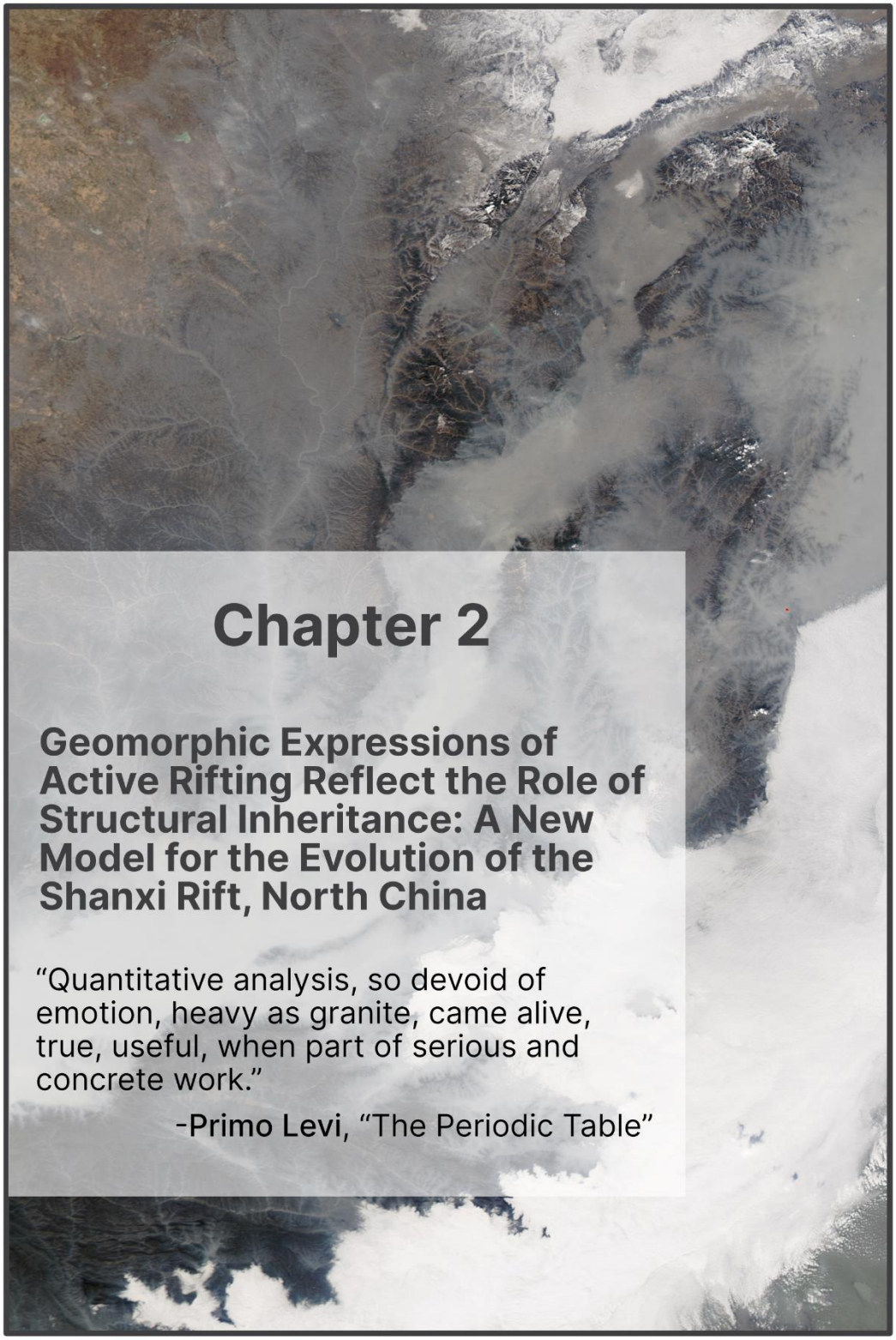

Chapter 2

Geomorphic Expressions of Active Rifting Reflect the Role of Structural Inheritance: A New Model for the Evolution of the Shanxi Rift, North China

"Quantitative analysis, so devoid of emotion, heavy as granite, came alive, true, useful, when part of serious and concrete work."

-**Primo Levi**, "The Periodic Table"

2. Geomorphic Expressions of Active Rifting Reflect the Role of Structural Inheritance: A New Model for the Evolution of the Shanxi Rift, North China

Abstract - Many rifts are influenced by pre-existing structures and heterogeneities during their evolution, a process known as structural inheritance. During rift evolution, these heterogeneities may aid rift nucleation, growth, and segmentation of faults, encourage linkage of various segments, or even inhibit the formation of faults. Understanding how structural inheritance influences early rift evolution could be vital for evaluating seismic risk in tectonically active areas. The Shanxi Rift in the north of China is an active rift system believed to have formed along the trend of the Proterozoic Trans North China Orogen, however, the influence of these pre-existing structures on the present-day rift architecture is poorly known. Here we use tectonic geomorphological techniques, e.g., hypsometric integral (HI), channel steepness (k_{sn}) and local relief to study the evolution of the Shanxi Rift and identify areas of higher tectonic activity. We found that HI was less sensitive to lithology and more valuable in evaluating the tectonic signal and found that activity is concentrated in two rift interaction zones (RIZ) formed between the Xinding, Taiyuan, and Linfen basins. We then evaluated the relationship between the active faults and mapped pre-existing structures and found that many faults formed parallel to inherited structures but faults in the RIZs often crosscut these structures. Based on these observations we propose a new model for the evolution of the Shanxi Rift where inherited structures play an important part in the initial segmentation of the rift which in turn controls the development of the RIZ structures.

2.1 Introduction

Many continental rifts exploit ancient orogenic belts to accommodate extensional strain. Examples include the East African Rift (Rosendahl, 1987; Morley, 1988; Ring, 1994), the Baikal Rift (Petit et al., 1996), and the Rhine Graben (Schuhmacher, 2002). Research has focused on understanding the relationship between old pre-rift structures and how they control the development of younger structures. Pre-existing orogenic belts influence the accommodation of subsequent episodes of extensional strain, due to the presence of discrete and mechanically weak structures, such as shear zones and associated metamorphic fabrics (McCaffrey, 1997; Phillips et al., 2016, Fazlikhani et al., 2017; Kolawole et al., 2018; Peace et al., 2018; Heilman et al., 2019), pre-existing fault networks (Holdsworth et al., 2001b) or lithological contacts (Wedmore et al., 2020; Phillips and McCaffrey, 2019). These mechanical strength contrasts are particularly significant where orogenic belts are adjacent to cratons (Dunbar and Sawyer, 1988; Ziegler and Cloethingh, 2004; Corti et al. 2013) as is the case for the Baikal Rift (Petit et al. 1996), the East African Rift (Versfelt and Rosendahl, 1989) and the Circum-Ordos rifts in North China (Xu and Ma, 1992; Su et al., 2021), because cratonic lithosphere is more resistant to deformation than younger orogenic belts.

Studies of the interaction between rift-related normal faults and inherited structures in offshore basins and margins use high-resolution 2D and 3D seismic reflection data to analyse the influence of inheritance on spatio-temporal patterns of rift evolution (Morley et al., 2004; Phillips et al., 2016; Peace et al., 2018, Mulaya et al., 2022). Detailed field studies, on the other hand, can resolve the kinematic response of faults and infer strainfield directions and interactions (e.g., East Africa, Hodge et al., 2018b; Wedmore et al., 2020; Heilman et al., 2019; Kolawole et al., 2018). Inherited structures and heterogeneities can influence the location, morphology, segmentation, and

orientation of an entire rift zone (Wilson et al., 1966; Tommasi and Vauchez, 2001; Şengör et al., 2019; Heron et al., 2019; Schiffer et al., 2020; Kolawole et al. 2022). They can also influence the geometry and kinematics of individual faults (Wedmore et al., 2020; Samsu et al., 2020; Wilson et al., 2010). Inherited structures can influence the development of rifts and their associated basins by controlling the linkage of fault segments (Brune et al., 2017; Heilman et al., 2019). Pre-existing structures have also been shown to act as barriers to rift faults if they form structures or regions of strengthened crust that are harder to deform than surrounding areas (Krabbendam and Barr, 2000; Phillips and McCaffrey, 2019).

Many rifts that show a strong influence of inheritance are very segmented and exhibit numerous faults and basins that vary in orientation and morphology (Morley et al., 2004; Reeve et al., 2015; Heron et al., 2019; Osagiede et al., 2020). Between individual basins of a rift zone, a complex deformation zone known as a Rift Interaction Zone (RIZ) may develop (Nelson et al., 1992; Koehn et al., 2008; Aanyu and Koehn, 2011; Sachau et al., 2016; Kolawole et al., 2021a). The morphology of these zones is principally controlled by the separation distance between fault segments, the polarity of the respective faults and the amount of overlap between them (Morley et al., 1990; Faulds and Varga, 1998; Zwaan and Schreurs, 2017, Zwaan et al., 2016). RIZs are classified on their geometrical organisation (rift segment faults are underlapping or overlapping, parallel, oblique, or orthogonal). Commonly, these zones are topographically distinct from the rest of the rift. RIZs may form topographic highs in their early evolution, forming as a drainage divide between depocenters (Ebinger et al., 1987; Lambiase and Bosworth, 1995; Gawthrope & Hurst, 1993) and therefore acting as a source of sediment (Gawthrope and Hurst, 1993; Scholz, 1995). As RIZs evolve, they can become breached and eventually link up the rift basins (Kolawole et al., 2021a). RIZs can also be classified on their evolution stage (Kolawole et al., 2021a), i.e.

whether the RIZ is unbreached, partially breached, recently breached, or breached. This is assessed based on two observations: 1) the presence of a breaching fault that extends from one rift segment to the other segment, and 2) the presence of an established physical linkage of depositional environments of both rift segments (i.e., drainage connection between both segments). Recently breached and breached RIZs have an established breaching fault and connect the drainage of two different rift segments, but breached RIZs show less topography due to increased subsidence during the longer time period since the RIZ was breached. Unbreached RIZs show no apparent structural connection and no drainage connection, while partially breached RIZs may have a breaching fault partially connecting the rift basins but the drainage integration has not occurred yet. RIZs may also show a perturbated local strain field due to the influence of the adjacent, bounding rift faults (Crider and Pollard, 1998; Kattenhorn et al., 2000; Maerten, 2000; Kolawole et al., 2024). Development of these zones may be aided by basement fabrics that strike oblique to the main extension direction (Fossen and Rotevatn, 2016); however, basement fabrics may also influence linkage across these zones (Morley et al., 2004; Heilman et al., 2019; Kolawole et al., 2021a). RIZs are important structural domains along rift systems, and inheritance may be key to understanding their geometry and evolution.

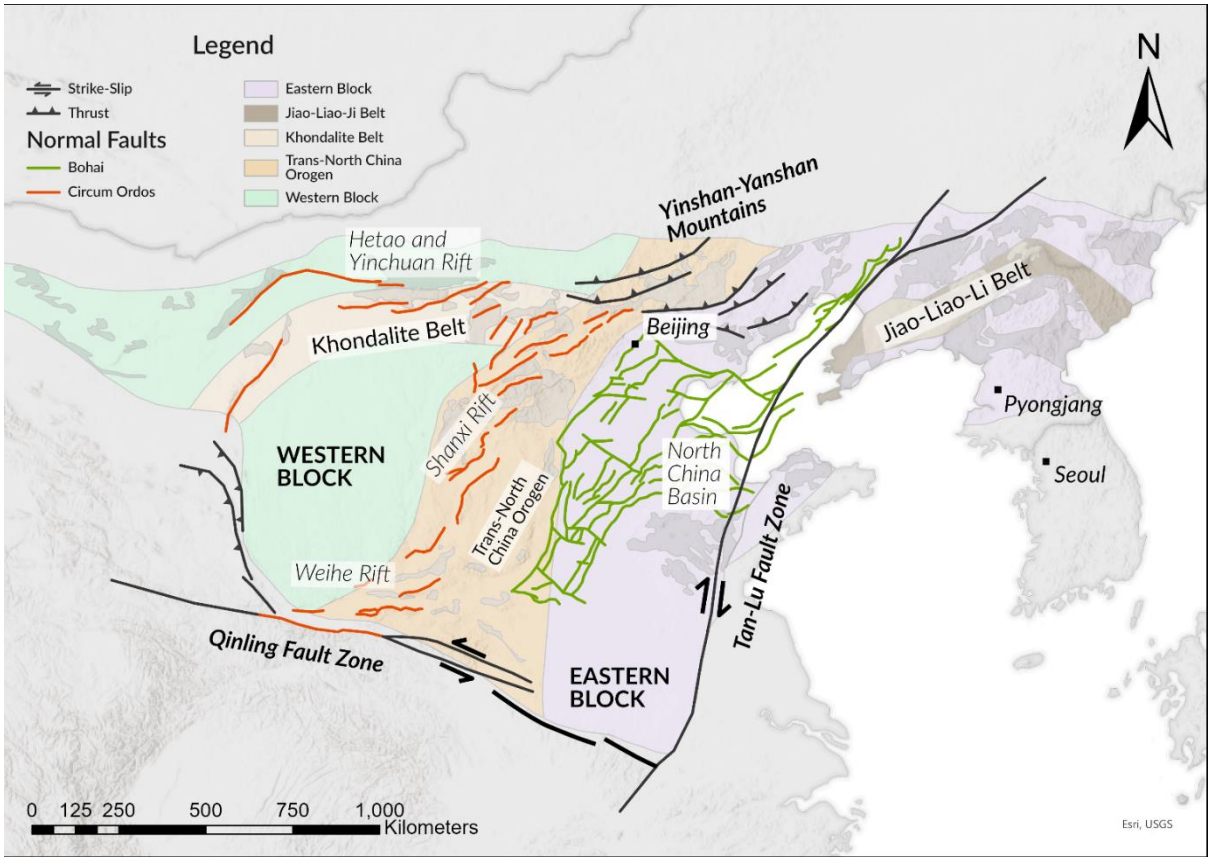

Figure 2.1 Map of the North China Craton

An overview map of the North China Craton (NCC) with boundaries of the different blocks and orogenic belts that make up the NCC shaded in colour. Boundaries after Zhao et al., (2005). Also indicated are the two major rift systems that formed superimposed on the NCC: The Paleogene North China Basin (in green, modified from Qi and Yang, 2010) and the Neogene circum-Ordos Rifts (in red, modified from Zhang et al., 2003; Deng et al., 2007). Bold black lines indicate the major strike-slip fault zones that affect present-day deformation.

The Shanxi Rift is part of a Cenozoic rift system which is known as the Circum-Ordos rifts, which surrounds the Western Block of the North China Craton (NCC) (Fig.1). Due to the strong lithosphere of the cratonic western block of the NCC, deformation was localised in two rift systems along it: The Weihe-Shanxi Rift system in the southeast and the Yinchuan-Hetao rift system in the northwest (Zhang et al., 2003). Timing of

the initiation of these rifts is debated with some authors arguing for the Oligocene-Eocene initiation of the Weihe, Hetao and Yinchuan rifts, with the Shanxi Rift being younger (Zhang et al., 2003; Shi et al., 2020), while other authors argue for a late Miocene initiation for all rifts (Yin, 2000). The Shanxi Rift in North China contains faults with a variety of trends which formed in the Late Miocene to the present day (Su et al., 2023) (Fig.1). The origin of these trends is unclear but the currently accepted model postulates multiple changes in stress axes orientation during transtensional evolution of the Shanxi Rift since the late Miocene, with strain being partitioned into dip-slip and strike-slip fault systems during transtension (Shi et al., 2015a). There has been little focus on the influence of structural inheritance on the wider evolution of North China, with a few exceptions that show active normal faults often following the trends of inherited structures (Su et al., 2021) and possibly detaching into low-angle shear zones at depth (Pavlides et al., 1999). Major faults in the Shanxi Rift commonly expose basement massifs of the Trans North China Orogen (TNCO) in their footwalls. The TNCO formed during the collision of the eastern block and western block of the NCC in the Paleoproterozoic. These basement massifs have been intensively studied to unravel the exact timing and kinematics of the Proterozoic collision (Kusky and Li, 2003; Zhao et al., 2005; Trap et al., 2007, Trap et al., 2008; Faure et al., 2007; Trap et al., 2009a; Trap et al., 2009b; Zhai et al., 2010; Zhai and Santosh, 2011), their impact on the late Cenozoic rifting in the Shanxi Rift has not been considered in detail.

There is limited seismic reflection data available for the Shanxi Rift (Xu et al., 1993; Ai et al., 2019). However, the degree of tectonic activity and subaerial exposure makes it possible to use geomorphology to study the structural evolution. In active rifts geomorphology and surface expression of faults have been commonly used to study the tectonic evolution of a rift and successfully employed in regions such as the Basin and Range (Jackson and Leeder, 1994; Densmore et al., 2003; Densmore et al., 2004),

the Apennines (Whittaker et al., 2008; Geurts et al., 2020; Fisher et al., 2022), the Gulf of Corinth (Leeder and Jackson, 1993; Goldsworthy and Jackson, 2000; Gallen et al., 2021) or the East African Rift (Erbello et al., 2022; Dulanya et al., 2022). These geomorphic approaches are varied and include studying the drainage evolution, the topographic response to faulting or using rivers to track the transient uplift rate. Landscapes are primarily formed by two competing forces: tectonics and erosion (Whittaker, 2012). Geomorphic indices have been used to quantify landscape response to tectonics (Bull and McFadden, 1980; Cox et al., 1994; Hamdouni et al., 2008; Gao et al., 2016; Markrai et al., 2022). This study uses three indices, hypsometric integral, channel steepness and local relief, to evaluate the landscape response to faulting in the Shanxi Rift.

By using geomorphic analysis to evaluate the tectonic evolution of the Shanxi Rift, highlighting areas of increased tectonic activity, and comparing these with the distribution of inherited structures, we provide new insights into the influence of inheritance on the evolution of the Shanxi Rift. Specifically, our results question the need for rapid changes in the Neogene strain field orientation to explain the varying fault orientations and fault evolution in the Shanxi Rift. Instead, we show a novel, simpler model whereby inheritance under a constant strain field creates a segmented rift system and creates RIZs where strain and earthquake activity are focused. More generally, our work shows how geomorphic indicators can be used to identify the most active (and potentially hazardous) faults in an active extensional system.

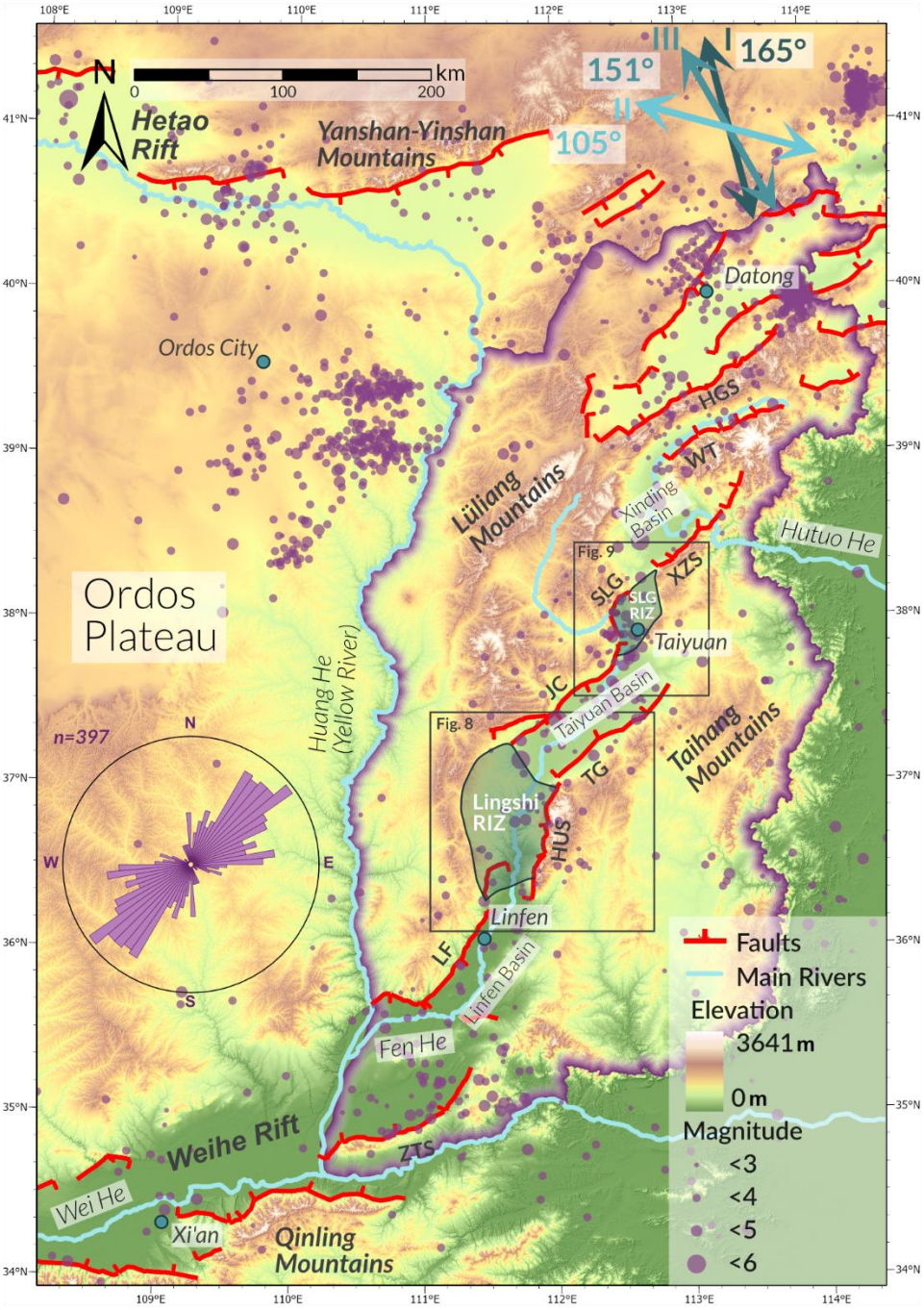

Figure 2.2 Topographic Map of the Shanxi Rift

Detailed map of the circum-Ordos Rifts and the main rivers. Extension directions shown are from: I - Zhang et al. (1998) II - Shen et al. (2000) III - Middleton et al. (2017). Rose plot shows the mean orientation of major rift faults in the Shanxi Rift (defined here as the regions that lie within the purple bounding line). Faults were split into individual segments according to their orientation. Purple dots represent

earthquakes from the ISC catalogue (Storchak et al., 2013; 2015; Di Giacomo et al., 2018) and are weighted by magnitude. (Abbreviations: HGS-Hengshan; WT-Wutai; XZS-Xizhoushan; SLG-Shilingguan; JC-Jiaocheng; TG-Taigu; HUS-Huoshan; LF-Linfen; ZTS-Zhongtiaoshan)

2.2 Geological Setting

The Shanxi Rift system in North China is an active continental rift system that is superimposed on the 1.8 Ga TNCO (Fig. 2.1) when the collision of the Eastern and Western Blocks formed the NCC. The exact timing and kinematics of this collision remain uncertain (Zhao et al., 2005; Kusky et al., 2007; Zhai and Santosh, 2011). Since the Proterozoic, the NCC has been a stable cratonic block with a lithospheric thickness of 200 km, evidenced by Palaeozoic kimberlites (Menzies et al. 1993; Griffin et al., 1998; Menzies et al., 2007). The Paleoproterozoic and Archean basement rocks are unconformably overlain by the greenschist facies metasedimentary rocks (Faure et al., 2007) of the Paleoproterozoic Hutuo Group, which was deposited in a foreland basin during the TNCO Orogeny (Li et al., 2010). The lower Palaeozoic cover consists of Cambrian continental siliclastic successions, followed by shallow marine carbonates and Ordovician platform carbonates. Carboniferous and Permian rocks were deposited in changing shallow marine to fluvio-deltaic conditions and contain coal measures. These are topped by Mesozoic continental clastics, grading into cross-bedded aeolian sequences in the Jurassic (SBGMR, 1989). This evolution led to a clear division of lithologies in the Shanxi Rift, the Paleoproterozoic rocks, which include all the rocks that made up the TNCO, including Archean Tonalite-trondhjemite-granodiorite complexes, high-grade metamorphic rocks such as greenstone belts and orthogneisses as well as post-orogenic granites. These rocks are referred to as Paleoproterozoic crystalline rocks in this study (dark brown in Fig.3) and are very resistant to erosion. The second group comprises the cover sequence of these rocks

and is principally composed of low-grade metamorphic rocks such as clastic metasediments and carbonates of Mesozoic and Palaeozoic age, which are referred to as low-grade metasediments in this study (blues and greens in Fig. 2.3).

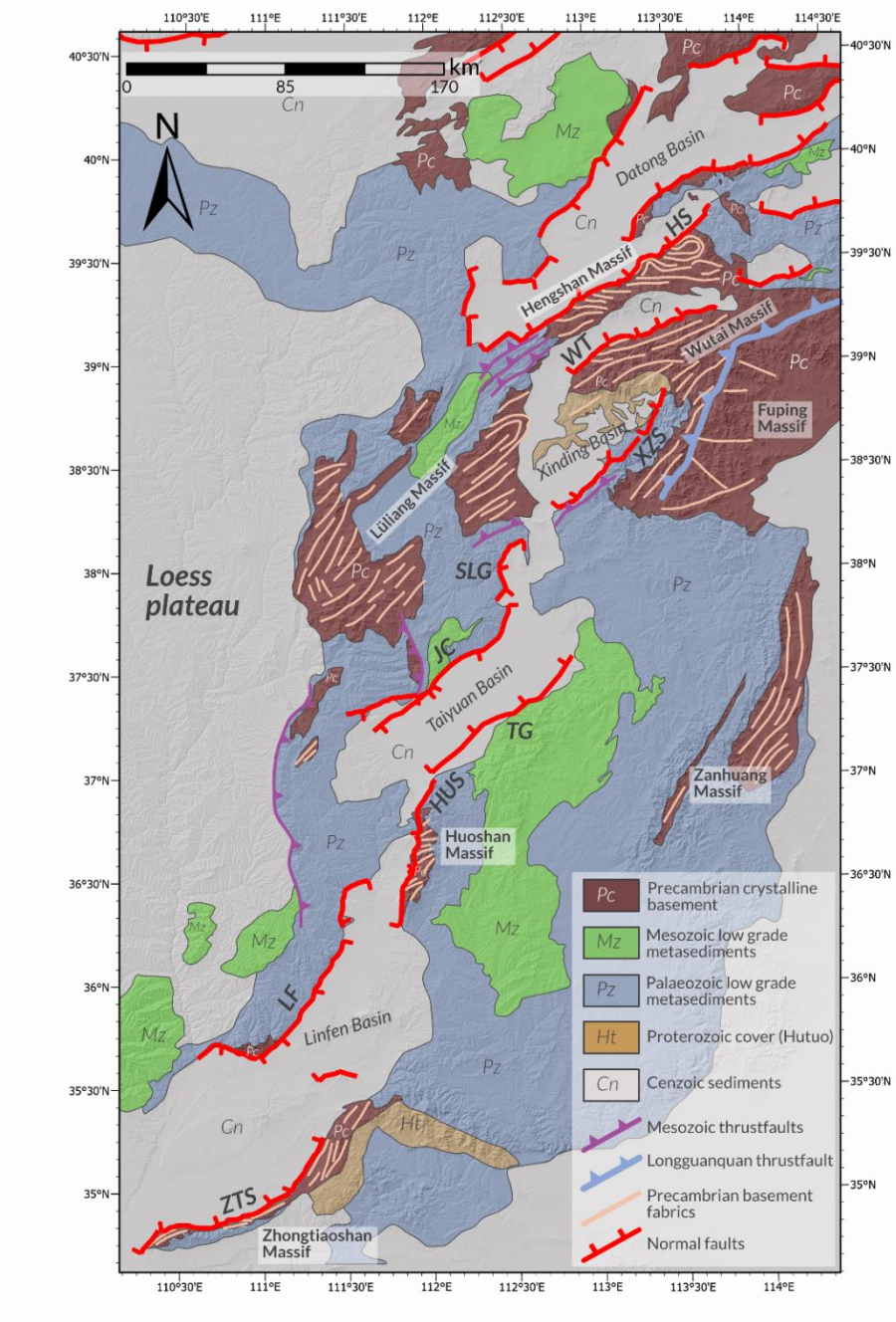

Figure 2.3 Geological Map of the Shanxi Rift

A simplified geological map of the Shanxi Rift (modified from SBGMR, 1989 and Clinkscales et al., 2021) showing the main pre-existing structures of the study area

(Faure et al., 2007, Trap et al., 2007, Trap et al., 2009, Zhang et al., 2011; Clinkscales and Kapp, 2019). Main metamorphic fabrics are indicated in light brown lines which are predominantly orientated NE-SW.

(Abbreviations: HGS-Hengshan; WT-Wutai; XZS-Xizhoushan; SLG-Shilingguan; JC-Jiaocheng; TG-Taigu; HUS-Huoshan; LF-Linfen; ZTS-Zhongtiaoshan)

Since the Mesozoic, parts of the NCC have been removed by thermal erosion (Griffin et al., 1998; Menzies and Xu, 1998) and/or partial delamination (Gao et al., 2002; Gao et al., 2004), which is likely to be connected to the subduction of the palaeo-Pacific underneath East Asia (Menzies et al., 2007; Zhu et al., 2012). The eastern and western parts of the NCC underwent a different evolution during the Mesozoic. The eastern part experienced compressive deformation from the Jurassic to Early Cretaceous (Davis et al., 2001), also regionally known as the Yanshanian Movement (Wong, 1927, Dong et al., 2015), which was less pronounced within the Western Block. However, Paleoproterozoic orogenic belts like the TNCO also recorded this widespread compressional event (Zhang et al., 2008; Zhang et al., 2011; Clinkscales and Kapp, 2019). Since the Early Cretaceous, the eastern NCC experienced extension, resulting in structures such as pull-apart basins, core complexes and associated voluminous magmatism (Zhu et al., 2012). Destruction of the cratonic lithosphere was limited to the eastern NCC, which resulted in Mesozoic magmatism almost exclusively affecting the eastern NCC (Zhu et al., 2012). Here, the North China Basin formed in the Eocene-Oligocene (Allen et al., 1997). This basin shows transtensional kinematics, which gives it a resemblance to a giant pull-apart (Chen and Nabelek, 1988; Farangitakis et al., 2020). During the Paleogene, the western NCC experienced limited extension. The Shanxi Rift is one of a series of Neogene, narrow rifts which follow the trend of Precambrian orogenic belts within the NCC, developing around the Ordos Block (Shi et al., 2020).

The Shanxi Rift is a NE-SW trending rift system that consists of a series of left-stepping en-echelon basins (Zhang et al., 2003) (Fig. 2). The system is ~1000 km long and ~300 km wide and is bound to the north by the Yinshan-Yanshan Range and to the south by the Qinling Range (Fig.1). It is commonly believed to have initiated in the Late Miocene based on the oldest sediments found in the rift grabens - the Kouzhai Formation (Xu et al., 1993). The crust beneath the Shanxi Rift is ~32-39 km thick and is thinner in the basinal regions than adjacent to the Lüliang and Taihangshan highlands, which flank the rift to the west and east (Chen, 1987, Tang et al., 2010). The Shanxi Rift is characterized by a series of distinct rift basins that have either half-graben or graben geometries (Fig. S2.1), separated by two topographically higher elevated areas, which have previously been called push-up swells but are referred to here as RIZs (Fig. 2) (Xu and Ma, 1992; Xu et al., 1993). The Linfen Basin to the south is separated by the Lingshi RIZ from the Taiyuan Basin, which is in turn separated from the Xinding Basin in the North by the Shilingguan RIZ. There are two main rivers that drain the Linfen-Taiyuan-Xinding basin system of the Shanxi Rift: The Hutuo River towards the east across the Xizhoushan Fault into the North China plain while the Fen River is diverted to the South where it drains into the Yellow River (Fig. 2), while the main drainage divide between the Fen and Hutuo River, is represented by the Shilingguan RIZ. The syn-rift thickness across the Shanxi Rift varies. While the Taiyuan basins have the thickest syn-rift sediment thickness of up to 3800 m (Xu et al. 1993), the Xinding only contains up to 1800 m (Xu et al. 1993) and the Linfen basin contains up to 2200 m of syn-rift fill (Su et al., 2023). For more details on the syn-rift fill based on well-data see the supplementary material (Fig. S2.1). The Shanxi Rift shows widespread seismicity of M_w = 3-5 events on USGS and ISC records (Fig. 2), but the rift has produced infrequent but devastating earthquakes in historical times. The AD 1303 Hongdong Earthquake is believed to have been an MW ~7.5 event (Xu et al.,

2018) and is well-documented in Chinese historical writings. Shanxi Province itself is densely populated with 36.5 million inhabitants. Large cities like Taiyuan (5 million inhabitants), Linfen (4 million inhabitants) and Datong (3 million inhabitants) are close to active faults (Fig. 2)

Constraining the exact extension direction and rate along extensional faults is difficult due to the Shanxi Rift's low extensional strain rate. Conducted research has been based on field-based fault slip measurements, GPS-derived velocities and/or earthquake focal mechanisms to constrain the extension direction. Studies by Shen et al. (2000), He et al. (2003) and Middleton et al. (2017) constrain the extension direction in the Shanxi Rift to ~105°-165° and extension rate to ~ 0 - 6mm/year (Fig. 2). Examples of GPS derived strain measurements and focal mechanisms of the Shanxi Rift can be seen in the supplementary material (Fig. S2.2). Other studies using field-based measurements (Shi et al., 2015a; Assie et al., 2022) propose a complex evolving strain field that has changed throughout the Cenozoic. According to these studies, NW-SE extension in the Mio-Pliocene initiated the rifting in Shanxi and was followed by NE-SW extension in the early Quaternary, leading to further subsidence. These authors (Shi et al., 2015a; Assie et al., 2022) suggest that the onset of the current NNW-SSE extension strain field started at 0.11 Ma and marked a shift from NW-SE extension to right lateral deformation in the Shanxi Rift, dated using faulted basalts in the Datong Basin (Shi et al., 2015a). Shi et al. (2015b) and Shi et al. (2015a) relate these changes in the strain field to the growth of the Tibetan Plateau.

2.3 Methods

2.3.1 Pre-Rift Architecture and Structural Mapping

I compiled a map of the structures in the Shanxi Rift (Fig. 2.3) by digitising Precambrian basement fabrics, Mesozoic and Precambrian thrust faults as well as Cenozoic active faults from published maps in ArcGIS Pro™. Additionally, I compiled

published structural data from the Paleoproterozoic basement complexes to plot on stereonets (Fig. 2.5). In this study, we primarily focus on the influence of inherited structures in the Palaeoproterozoic basement on the evolution of the Shanxi Rift, therefore, if not specified otherwise, we refer to Palaeoproterozoic structures when discussing basement or inherited fabrics. To map the active fault structures, we identified linear breaks in the landscape on SRTM topographic data with 90 m resolution (https://lpdaac.usgs.gov/products/srtmgl3v003/) aided by slope and curvature attributes. This resolution is appropriate for the larger regional scale of this study and helped keep computing power demands manageable. We define active faults as linear, steep scarps (>20-30°) that offset Quaternary sediments, similar to the approach by Wedmore et al. (2022). Furthermore, we used topographic profiles across faults and geomorphological features such as steepened river channels and triangular facets along the fault scarp as features guiding our identification of active normal faults.

2.3.2 Geomorphic Indices

We used geomorphic indices to quantify the landscape response of the Shanxi Rift to tectonic drivers. We analysed the morphometric indices from 10873 1st-order drainage basins located in the Shanxi Rift, extracted from the SRTM dataset using Topotoolbox2 Matlab scripts (Schwanghart and Scherler, 2014). The same geomorphic indices calculated for 3rd-order drainage basins are shown in Figure S2.3 for comparison. We focused in this study on three geomorphic indices, 1) local relief (R_l), 2) the normalised channel steepness (k_{sn}) 3) the Hypsometric Integral (HI), as these proved to be the most helpful and discerning when evaluating the tectonic signals (Pérez-Peña et al., 2009; Gao et al., 2016; Obaid and Allen, 2019; Groves et al., 2020; Erbello et al., 2022). Using the programming language R, we also generated violin plots that visualise the distribution of values for each geomorphic index (Fig. 2.7). The shape of the “violins”

represents the distribution of values as the violin will be thicker the more data points sit at that range. Using these violin plots, we can also assess the impact of lithology on the geomorphic indices that enable us to compare the distribution of values per fault to the dominant footwall geology of the fault and assess if lithology is the principal factor determining the distribution.

Local Relief (R_l)

Local relief is a commonly used measurement of the variation of topography over an area to analyse spatiotemporal tectonic trends (Ahnert, 1970; Schmidt and Montgomery, 1995; DiBiase et al., 2010). The relief R_l was calculated as the maximum difference in elevation E over; 1) a delineated drainage basin (Fig. S2.4) or 2) within a circular moving window with a 1 km radius:

$$R_l = E_{max} - E_{min} \quad (2.1)$$

where R_l is the local relief and E refers to elevation. High relief landscapes therefore show a higher variation of elevation over an area, which may indicate faster uplift rates. However, local relief is also influenced by lithology, high relief landscapes can also be the result of resistant lithologies with low erodibility (Ahnert, 1970).

Hypsometric Integral (HI)

The Hypsometric Integral (HI) was first used as a geomorphic index by Strahler (1952, 1957). It is a measurement of the distribution of elevation within an area. HI is derived as the integral of the hypsometric curve, which plots normalised elevation over normalised drainage area for each drainage basin. Figure 2.4 illustrates the theory behind HI. The interpretation of the hypsometric curve assumes that topographically more youthful basins will have a convex-up shaped curve while more mature ones will have a more concave-up shape. If uplift outpaces erosion, there will be a greater range

of elevation over an area which results in a convex-up shaped curve and a high HI. Therefore, high HI values should coincide with rapidly uplifting areas (e.g., footwalls of active normal faults) (Hamdouni et al., 2008; Perez-Pena et al., 2009; Obaid and Allen, 2019; Groves et al., 2020; Erbello et al., 2022). HI may be influenced by other factors than tectonic uplift such as climate, lithology and basin shape and area. Lifton and Chase (1992) propose that at larger scale analysis (>1000 km) tectonics will have a larger effect than lithology, while at smaller scales lithology can have a considerable impact. Masek et al. (1994) suggest that climate can influence the hypsometry of an area. Several studies proposed that basin shape and area influence the HI of a basin (Lifton and Chase, 1992; Masek et al. 1994; Hurtrez et al., 1999; Chen et al., 2003), however, Walcott and Summerfield (2008) analysed the basins of southern Africa and could find no impact of basin scale on HI. High HI regions may often be indicative of fast uplift rates but could also be related to other factors therefore when analysing the tectonic implications of HI, it is important to be aware of these limitations. To mitigate the effect of lithology on our tectonic analysis we also compare the HI distribution per fault with the predominant lithology of the fault's footwall using violin plots generated with R.

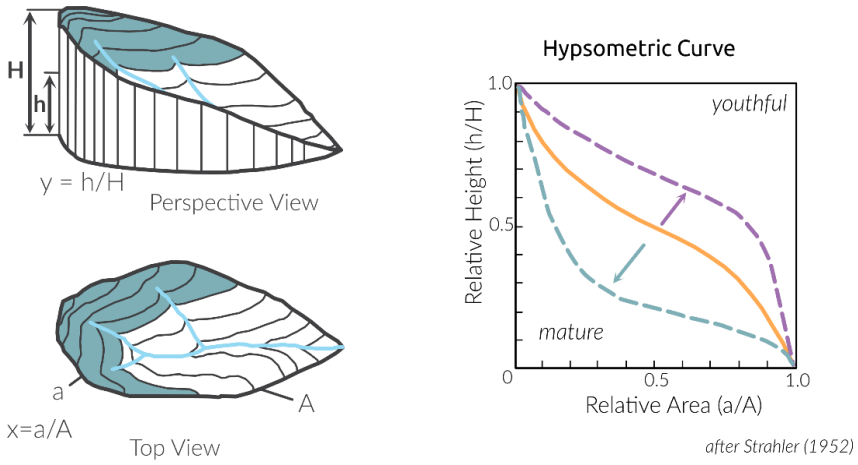

Figure 2.4 Hypsometric Integral Explanation

Schematic diagram explaining the concept of the Hypsometric Integral (after Strahler, 1952) Every drainage basin is dissected into elevation bands to determine a ratio of relative height over relative area. Concave curves indicate more youthful topography while convex-shaped ones indicate more mature topography.

In this study, we calculated the HI per drainage basin (Obaid and Allen, 2019; Groves et al., 2020). The shape and size of drainage basins are controlled by tectonic and geological features; therefore, they are more natural boundaries for comparing areas of variable uplift and erosion rates than calculating HI with an arbitrary moving window. We calculated the hypsometric curves using QGIS 3.16 and derived the integral for each curve through an R script (Supplementary material X1).

Normalised Channel Steepness (k_{sn})

Normalised channel steepness (k_{sn}) is a frequently used topographic metric in tectonic geomorphology (DiBiase et al., 2010; Whittaker and Walker, 2015). For steady-state landscapes, meaning rock uplift rates and river incision rates are at equilibrium, the channel slope S is defined as a power law function (Hack, 1957; Flint, 1974):

$$S = k_s A^{-\theta} \tag{2.2}$$

where A is the drainage area. The parameter k_s is the channel steepness index, and θ denotes the channel concavity index (Snyder et al. 2000). The assumption that the Shanxi Rift topography is in steady-state, i.e. that erosion rates are equal across the region and the landscape adjusts to ensure these equal erosion rates. This makes it possible to calculate k_{sn} using this method, however, while this assumption is often made it is noted that it is debated if landscapes can ever be in steady state (Roberts and Wani, 2024). In natural landscapes, it's well known that variations in the best fit for concavity index (θ) have a significant impact on estimates of k_s. To circumnavigate the problem, we used a reference concavity index of 0.45 (Wobus et al. 2006). Using this

reference concavity index results in a dimensionless “normalised” channel steepness k_{sn}. Variations in k_{sn} along channel segments may be related to changes in the uplift rate of that region (Snyder et al., 2000; Whipple, 2004) with higher k_{sn} values often indicating higher uplift rates.

We used the TopoToolbox2 Matlab scripts (Schwanghart and Scherler, 2014) to extract the river profiles and calculate the normalised channel steepness from smoothed river profiles. This approach is built upon the method developed by Perron and Royden (2013) to analyse river profiles. We extracted streams with a drainage area of above 1 km^2 to avoid hillslope areas. Normalised channel steepness (k_{sn}) is commonly applied to stream networks to visualise knickpoints (variations in the slope of river channels) in rivers. In this study we used Topotoolbox2 to calculate the basin averaged k_{sn} values. This is achieved by calculating the mean of all k_{sn} values in each drainage basin. This makes it easier to compare the k_{sn} values to those for local relief and HI. The k_{sn} stream network map is available in the supplementary material (Fig S2.5).

Shanxi Rift Fault Characteristics

Fault	Trend (in degrees)	Footwall lithology	Mean R_l	Mean HI	Mean k_{sn}	Geomorphic response	Orientation of inherited structures
Hengshan	57	Crystalline Basement	234	0.33	68	medium	ENE-WSW
Wutai	65	Crystalline Basement	367	0.37	79	high	NNE-SSW
Xizhoushan	50	Crystalline Basement	320	0.36	72	high	NE-SW
Shilingguan	5	Low-grade metasediments	217	0.4	57	high	NE-SW
Jiaocheng	48	Low-grade metasediments	193	0.32	39	low	NE-SW
Taigu	49	Low-grade metasediments	168	0.29	33	low	NE-SW

Huoshan	12	Crystalline Basement	301	0.36	68	high	NE-SW
Linfen	38	Low-grade metasediments + Crystalline basement	219	0.38	47	medium	E-W
Zhongtiaoshan	72	Crystalline Basement	208	0.31	43	medium	NNE-SSW

Table 1 – Shanxi Rift Fault Characteristics

Summarising the Fault and their geomorphological response as well as their lithology and the orientation of the inherited fabrics in the vicinity of the fault.

2.4 Results

2.4.1 Pre-Rift Structural Architecture

The northern part of the Shanxi Rift is dominated by uplifted Paleoproterozoic basement massifs. The Hengshan, Lüliang, Wutai and Fuping massifs are exposed in the footwalls of major basin bounding faults (Figs. 2.3, 2.5). In the south, the footwalls are more commonly dominated by Mesozoic and Palaeozoic sedimentary rocks, with notable exceptions being the Huoshan and Zhongtiaoshan faults, which also expose Paleoproterozoic metamorphic basement at the surface.

The general trend of most Paleoproterozoic structures is broadly NE-SW, which is sub-parallel to the active rift faults. In the northern basement massifs (Hengshan and Wutai), there is a subtle change to WNW-ESE-trends (Figs. 2.3, 5). The dip of these structures is variable due to the folded nature of these rocks (Trap et al., 2007; Trap et al., 2009a; Clinkscales and Kapp, 2019). The dip of the fabrics changes from dipping towards and away from the faults along the strike and the dip of the fabrics ranges from 25-85° (Trap et al., 2007; Trap et al., 2009a). The orientations also show plunging fold geometries in the basement massifs of the Hengshan and the Lüliangshan mountains (Stereonets Hengshan and Lüliang, Fig. 2.5). The Fuping Massif displays a

considerable spread of basement fabric trends that can be split into two groups: fabrics trending NE-SW in the NW and fabrics with an NNW-SSE trend in the SE (Stereonets Fuping-West and Fuping-East, Fig. 2.5). These two regions are separated by the NE-SW trending Longguangquan thrust fault (marked as a blue thrust fault on Figs. 2.3 and 2.5), which most likely originated as a shallow-dipping thrust fault in the Paleoproterozoic (Trap et al., 2008). The basement fabrics in the NW-part and the Longguangquan thrust fault are parallel to the Xizhoushan Fault (Fig. 2.5 – stereonet Fuping-West). Further north, the Paleoproterozoic basement fabrics of the Wutai complex are orientated ENE-WSW, which is mirrored by the active normal Wutai Fault.

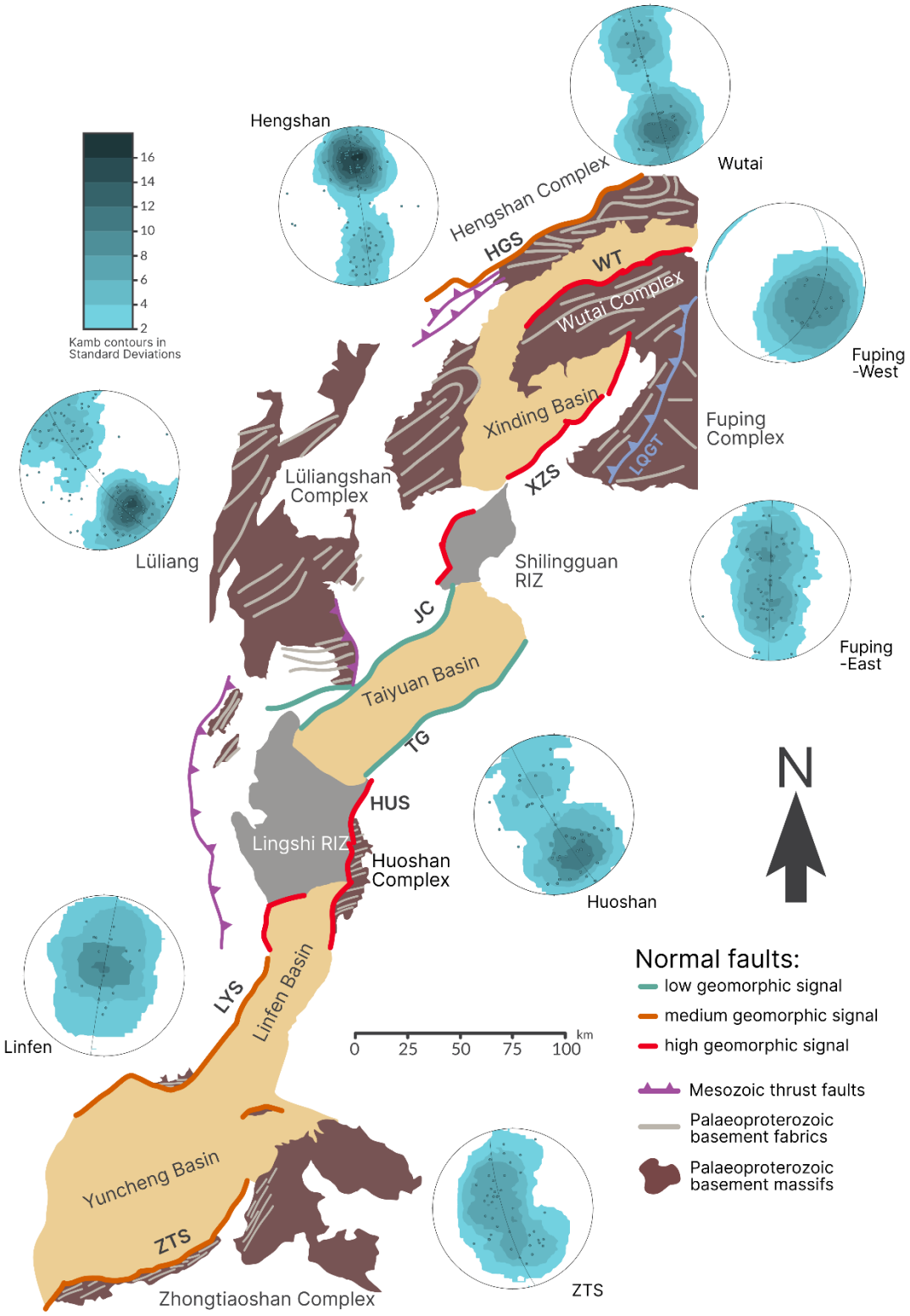

Figure 2.5 Fault Map of the Shanxi Rift with Stereonets of the Basement Fabrics

Schematic fault map of the Shanxi Rift with faults colour-coded according to their geomorphic signal – compare with Table 1. The exposed basement of the TNCO is brown with the main structural trends highlighted in light grey. Stereonets of poles to planes (data from Trap et al., 2007; Trap et al., 2009a) show the structural grain of the main basement complexes. Most basement complexes show an NE-SW orientated grain, but it is more ENE-WSW in the north of the Shanxi Rift (Wutai/Hengshan).

2.4.2 Local Relief (Rl)

The local relief (Fig. 2.6a) closely follows the overall topography of the region but emphasises certain features to make them easier to identify. Two areas of high local relief can be identified in the north and south of the Shanxi Rift.

In the northern region around the Wutai and the Xizhoushan faults, the footwalls of the prominent bounding faults are highly elevated (2500-3000 m) and show local relief values exceeding 1000 m. In the southern part of the Shanxi Rift, the Huoshan Fault to the south also shows high local relief (>1000 m) in the footwall close to the bounding fault. These high relief faults in Shanxi show consistently high local relief values along their fault traces whereas the Zhongtiaoshan Fault has high local relief (>1000 m) along the western end of the fault but lower values towards the east.

The Shilingguan RIZ is characterised by shorter fault segments, and this region shows an elevated local relief of around 500 m. In some examples, in footwalls close to the main fault, the local relief exceeds 1000 m. This is seen where a broadly N-S trending fault and a broadly NE-SW trending fault intersect and link up. Further into the footwall of this fault, there are pockets of high (>1000 m) local relief, which are along the sides of the narrow gorge of the Fen River. Compared to faults in the North and South of the Shanxi Rift such as Huoshan, Zhongtiaoshan or Wutaishan, the elevation in this area is lower (~1500 m) but the local relief remains comparatively high (up to 1000 m). The

two longest faults in the central region of the Shanxi Rift, which bound the Taiyuan Basin (Taigu and Jiaocheng faults), show a lower local relief response rarely exceeding 450 m, with elevation lying between 1500 and 2000 m. There are regions of medium-high values of local relief (450-750 m) away from active structures, for example in the Taihangshan mountains or to the west of the Lingshi RIZ.

The per-fault distribution of relief values (Fig. 2.7a) shows a clear divide between faults. The faults which have Proterozoic basement rocks in the footwall (Huoshan, Xizhoushan, Zhongtiaoshan, Hengshan and Wutai) have a greater range of values often exceeding 400 m. This is especially pronounced for the Wutai and Xizhoushan faults. The Hengshan Fault is slightly different as its distribution of relief values is closer to the faults with Palaeozoic-Mesozoic sedimentary rocks in the footwall, having most of its values between 200-300 m. The Zhongtiaoshan has a maximum at around 200 m and therefore lower relief than the other faults but still has some values in the higher ranges, with maximum values of 600 m. The faults with Palaeozoic and Mesozoic sedimentary rocks in the footwall (Shilingguan, Taigu, Jiaocheng and Linfen) have overall lower values and a smaller range of values. Most of their values lie between 200-300 m but their minimum values are below 100 m. Shilingguan as the RIZ fault shows a similar maximum at 200-300 m but is missing the low minimum values, resulting in a more compact distribution.

2.4.3 Normalised Channel Steepness (k_{sn})

Four regions show high basin averaged k_{sn} values (Fig. 2.6b): The Huoshan Fault, the Xizhoushan Fault (especially its northeastern part), the Wutai Fault and the Zhongtiaoshan Fault. These are the same regions that show high local relief (Fig. 2.6a and Section 4.2). Low values of < 50 are rarely associated with obvious faults with a surface trace. The Jiaocheng and the Taigu faults footwalls have drainage basins with

ksn values between 50-85, which reflects the local relief response of these faults (Fig. 2.6a). The footwall of the fault bounding the Shilingguan RIZ shows elevated values. Notably the area where the broadly N-S and NE-SW trending faults link up shows basins with ksn > 100. The ksn value distribution (Fig. 2.7b) of the different faults shows a similar trend to the Relief as there is a separation between faults with different basement lithologies. The faults with Proterozoic basement footwalls show much higher values reaching values of 200 while the faults with Palaeozoic-Mesozoic basement show narrower distributions rarely > 100 and most values < 50. The notable outliers here are found along the Hengshan Fault whose distribution again is more similar to the Palaeozoic-Mesozoic basement faults. Here the Shilingguan RIZ records higher values (> 100) than the other faults with Palaeozoic-Mesozoic basement footwalls and has a distribution more similar to the faults with Proterozoic basement footwalls like Wutai or Xizhoushan.

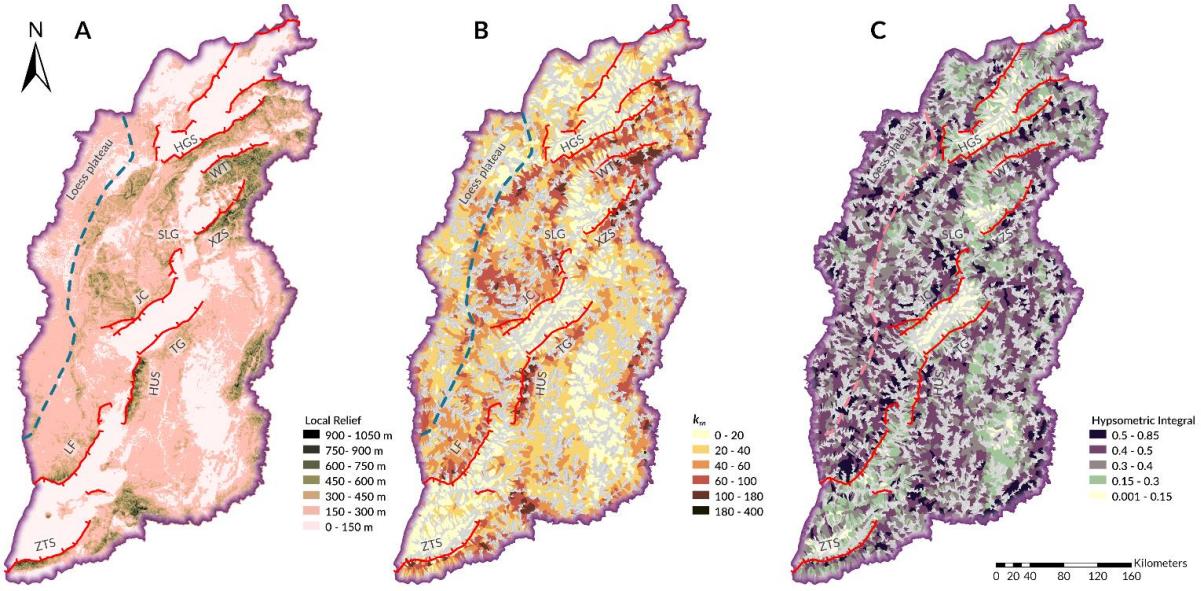

Figure 2.6 Maps of the three geomorphic indices (Relief, k_{sn}, HI)

Geomorphic indices map of the Shanxi Rift. Major extensional faults shown in red, boundary of the Loess plateau indicated by dashed line A) Local relief map. Darker colours indicate higher relief regions. Local relief was calculated within a 1km circular radius. High relief is found especially in the northern Shanxi Rift in the footwalls of the Wutai and Xizhoushan faults as well as further south along the Huoshan and Zhongtiaoshan faults. Noticeably lower local relief values occur along the central Jiaocheng and Taigu faults. B) Mean normalised channel steepness (ksn) calculated for 1st Strahler order basins. High values are commonly located in the footwalls of active faults, especially the Wutai, Xizhoushan and Huoshan faults. Low values are found in the lower-lying basin regions. Central faults (Taigu and Jiaocheng) show noticeably less high ksn basins than other faults. C) Hypsometric Integral (HI) calculated for 1st Strahler order basins. High values are commonly located in the footwalls of active faults, especially the Wutai, Linfen, Shilingguan and Huoshan faults. Low values are found in the lower-lying basin regions.

(Abbreviations: HGS-Hengshan; WT-Wutai; XZS-Xizhoushan; SLG-Shilingguan; JC-Jiaocheng; TG-Taigu; HUS-Huoshan; LF-Linfen; ZTS-Zhongtiaoshan)

2.4.4 Hypsometric Integral (HI)

While the local relief and the channel steepness show broadly similar distributions, the HI differs slightly and shows a more distributed pattern of high (>0.5) HI basins (Fig. 2.5c). The footwall blocks to the Wutai, Xizhoushan and Zhongtiaoshan faults show elevated responses but in contrast to the previously described geomorphic parameters they do not show the highest values. In the footwalls of these faults, HI values mostly range between 0.3-0.5 and only isolated regions show values > 0.5. The bounding fault of the Shilingguan RIZ has among the highest HI responses, with values often > 0.5 and rarely < 0.4. The Lingshi RIZ that is bounded by the Huoshan Fault also shows elevated values compared to the surrounding basins, due to its overall higher

elevation and dissected topography. These high HI values match spatially with the high local relief and ksn values. Therefore, the Shilingguan RIZ and Huoshan Fault have consistently higher values compared to the Wutai, Zhongtiaoshan or Xizhoushan footwalls. The Luoyunshan fault adjacent to the Lingshi RIZ also shows elevated HI basins (>0.5), especially towards the southern end where it shows a distinct fault bend, however, these high HI values are not matched to the same degree by local relief and ksn (Section 4.2/3). The Taigu fault has lower HI values (< 0.4), matching the low values for channel steepness and local relief. The Jiaocheng fault has a greater spread with low values basins (0.2 – 0.4) but also higher HI value basins (0.5 – 0.85), especially towards the northeast of the fault as it approaches the Shilingguan RIZ.

High-value HI basins (> 0.5) are also found in regions away from the active normal faults that showed no recent tectonic activity. High values are observed to the west of the Shanxi Rift in the Loess Plateau on the western edge of the HI map. (Fig. 2.5c). Similar to the relief and the channel steepness, high values are also observed in high-elevation regions further away from mapped active faults. These commonly correspond to known thrust faults or other contractional structures (Fig. 2.3) (SBRGM, 1989) which were last active in the Mesozoic and created relict topography.

The HI value distribution (Fig. 2.7c) differs from the previous two geomorphic indices significantly as a clear separation based on lithology/footwall age is not obvious anymore and the patterns are more dispersed. The general trend still appears that faults with Proterozoic basements have slightly higher values (~0.5), however the Zhongtiaoshan Fault while reaching very high HI values has most values sitting at 0.4, which is below the other faults with Proterozoic footwalls and closer to faults with Palaeozoic-Mesozoic sedimentary rocks in the footwall. Amongst these faults, the

Luoyunshan and Shilingguan faults show higher values than the Taigu and Jiaocheng faults. Overall, the Shilingguan and Huoshan faults within the RIZs record the highest values but they are not significantly elevated over for example the Wutai or Luoyunshan faults.

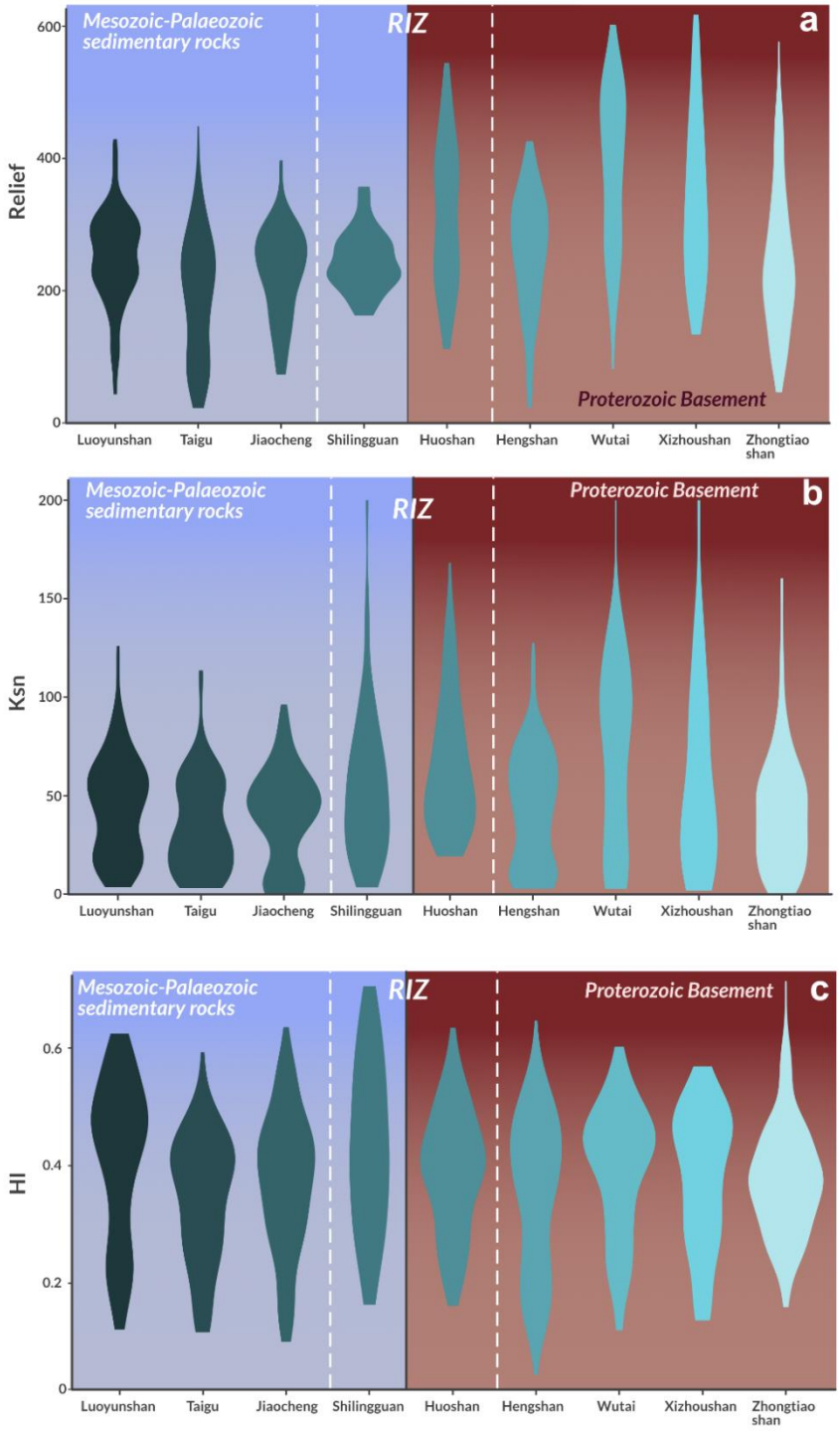

Figure 2.7 Violin Plots of the Geomorphic Indices

Violin plots showing the distribution of geomorphic values for each fault. The background shows the dominant footwall composition of the faults with RIZ faults plotted in the middle. a) Relief. Clear separation of faults with high values all having Proterozoic basement-dominated footwalls. b) k_{sn} values show a similar separation to the mean relief. c) HI values show more distributed values. RIZ tend to have high geomorphic values (see main text for more discussion on this)

2.5 Discussion

The quantitative analysis of the geomorphic response of the main rift faults has shown that the Wutai, Xizhoushan, Shilingguan and Huoshan faults show the highest geomorphic response (Fig. 2.7; Table 1), they are classified by high HI (mean HI > 0.35), k_{sn} (mean k_{sn} >60) and R_l values (mean R_l > 250). Of those the Shilingguan and Huoshan faults are located within the RIZs and exhibit N-S as well as NE-SW trending fault segments. The Taigu and Jiaocheng faults have the lowest geomorphic responses and show low values for all three geomorphic indices (mean HI < 0.3; mean k_{sn} *< 40;* mean R_l < 200). In between these two groups are the Hengshan, Zhongtiaoshan and Luoyunshan faults, described as faults with medium geomorphic response in Table 1. In the following, we will discuss the significance of these results and discuss the possible influence of the pre-existing structures described in section 4.1.

2.5.1 Lithology Dependence of Geomorphic Indices

The distribution of geomorphic indices for each fault shows significant differences (Fig. 2.7). Geomorphic response may be influenced by climate, lithology, and tectonics. The climate across Shanxi is continental and shows broadly little variation in precipitation (Fig. S2.7; Fick and Hijmans, 2017) across the study region, which makes

the differences in geomorphology between faults unlikely to be controlled by the climate. The lithology in Shanxi is more variable, as seen in Figure 3. The various lithologies can be divided into two main groups that differ in rock strength and erodibility. There are Precambrian crystalline rocks, which include Archean Tonalite–trondhjemite–granodiorite complexes, high-grade metamorphic rocks, and post-orogenic granites, which are all part of the TNCO (Trap et al., 2012), and the low-grade metasediments units, which include low-grade clastic metasediments and carbonates from the Palaeozoic-Mesozoic (SBRGM, 1989). Here, we evaluate how these differences in lithology may have impacted the geomorphic response.

Local relief and ksn (Figs. 2.6a, b) show the highest values where crystalline basement lithologies are exposed in the fault footwall. Faults with high mean local relief values (>300 m) have “strong” crystalline basement in their footwalls (e.g., Huoshan, Wutai, and Zhongtiaoshan faults) or are directly adjacent to these (e.g., Xizhoushan Fault), while low values (~<200 m) are found in the faults with Palaeozoic-Mesozoic rocks in their footwalls (e.g., Taigu and Jiaocheng faults). HI (Fig. 2.6c) does not show the same bimodal distribution between faults with different footwall lithologies. The highest HI values correspond to faults with both Proterozoic basement footwall rocks (e.g., Huoshan, Wutai, and Xizhoushan faults) and Palaeozoic-Mesozoic footwall rocks (e.g., Shilingguan, Luoyunshan faults). Meanwhile, low HI values are also found for footwalls of both lithologies (e.g., Hengshan, Taigu, Jiaocheng, and Zhongtiaoshan faults). We can infer that the differences in HI values between these fault blocks are not likely to be caused by lithology but rather by their tectonic history. This suggests that HI may be a more robust geomorphic index for analysing tectonic activity than relief or ksn because it is less influenced by lithology. Our finding that HI is not primarily influenced by lithology agrees with previous studies (Obaid and Allen, 2019; Groves et al. 2020). High HI values are often correlated with high uplift rates,

especially in regions with variable uplift rates, higher HI values are found in regions of higher uplift (Hurtrez et al. 1999). Therefore, the high HI values found in the footwalls of the Huoshan, Wutai, Xizhoushan and Shilingguan faults indicate that these footwalls have been uplifted the most rapidly.

To the western edge of the Shanxi Rift is a region of medium-high HI basins that do not correlate with mapped active faults. This is likely due to the landscape that typifies the Loess Plateau west of the Shanxi Rift. The Loess Plateau is unconsolidated wind-blown sediment that is prone to dramatic erosion, creating deep gullies and ridges, which can lead to high HI values. The Loess Plateau formed in the Pleistocene and its linear ridges and gullies have been carved out by aeolian and fluvial forces (Kapp et al. 2015), therefore the high response of the Loess Plateau is related to young landscapes sculpted by surface processes rather than tectonic forces. This does not detract from the main statement that HI is less influenced by lithology, as the Loess Plateau is an extreme case of unconsolidated sediment, as opposed to the main groups of low-grade metasediments and Palaeoproterozoic crystalline rocks. However, it does highlight that the HI response is sensitive to the presence of Loess. When using HI to evaluate the tectonic response of an area partially covered by Loess, it must be considered that Loess-covered areas may show anomalously high HI values.

The dependence of some geomorphic indices on lithology is observed in many other areas worldwide and highlights the importance of considering the local geology for interpreting the relevance of geomorphic indices (Wobus et al. 2006; Kirby and Whipple, 2012). However, by comparing different faults with similar basement geology, the lithological impact can be reduced as theoretically they should have a similar rock strength and erodibility. This enables us to compare the landscape response of these footwall uplifts to tectonics. In the Shanxi Rift, the footwall of the Huoshan Fault on average has higher values for geomorphic indices than other faults with

Paleoproterozoic crystalline rocks in the footwall (Fig. 2.7). Comparing the response of faults with footwall exposures of low-grade metasediments rocks, it becomes evident that the main bounding fault of the Shilingguan fault has a higher geomorphic response than the Jiaocheng, Luoyunshan and Taigu faults. The difference in geomorphic response between the Shilingguan fault and the other faults with low-grade metasediments in their footwalls is even more pronounced than among faults with Paleoproterozoic crystalline rocks in the basement. For example, the difference between the Huoshan and Hengshan faults is less stark than the difference between the Shilingguan Fault and the Jiaocheng Fault. It must also be noted that the Shilingguan fault shows higher HI and k_{sn} values than faults with "stronger" Paleoproterozoic crystalline rocks in their footwalls (Hengshan and Zhongtiaoshan). By comparing faults with similar footwall lithology, we can show that the difference in geomorphic response is not solely down to lithology and most likely has a tectonic origin.

2.5.2 Implications for Rift Evolution, Linkage and Seismic Hazard

Two significant zones in the evolution of the Shanxi Rift are the Shilingguan and Lingshi, which form between the major basins. Both zones are generally more elevated than the surrounding basins, making them potential sediment sources (Gawthorpe and Leeder, 2000), also shown by their patchy thin sediment fill compared to the major basins (Xu and Ma, 1992). The two RIZs differ in this geometrical organisation. The Shilingguan RIZ can be described as an underlapping parallel divergent RIZ, while the Lingshi RIZ is an underlapping oblique convergent RIZ (compare with Fig.3 in Kolawole et al., 2021a). A potential third RIZ, the Hengshan RIZ, which separates the Datong and Xinding basins can be proposed (Fig. 2.2). As an overlapping divergent RIZ is completely unbreached and therefore it will not be discussed at length in the following. The different RIZ stages come with distinct morphological responses and

have relevance to the seismic hazard so in the following we classify the two RIZs in the Shanxi Rift based on the Kolawole et al. (2021a) classification scheme and assess the response of the geomorphic indices.

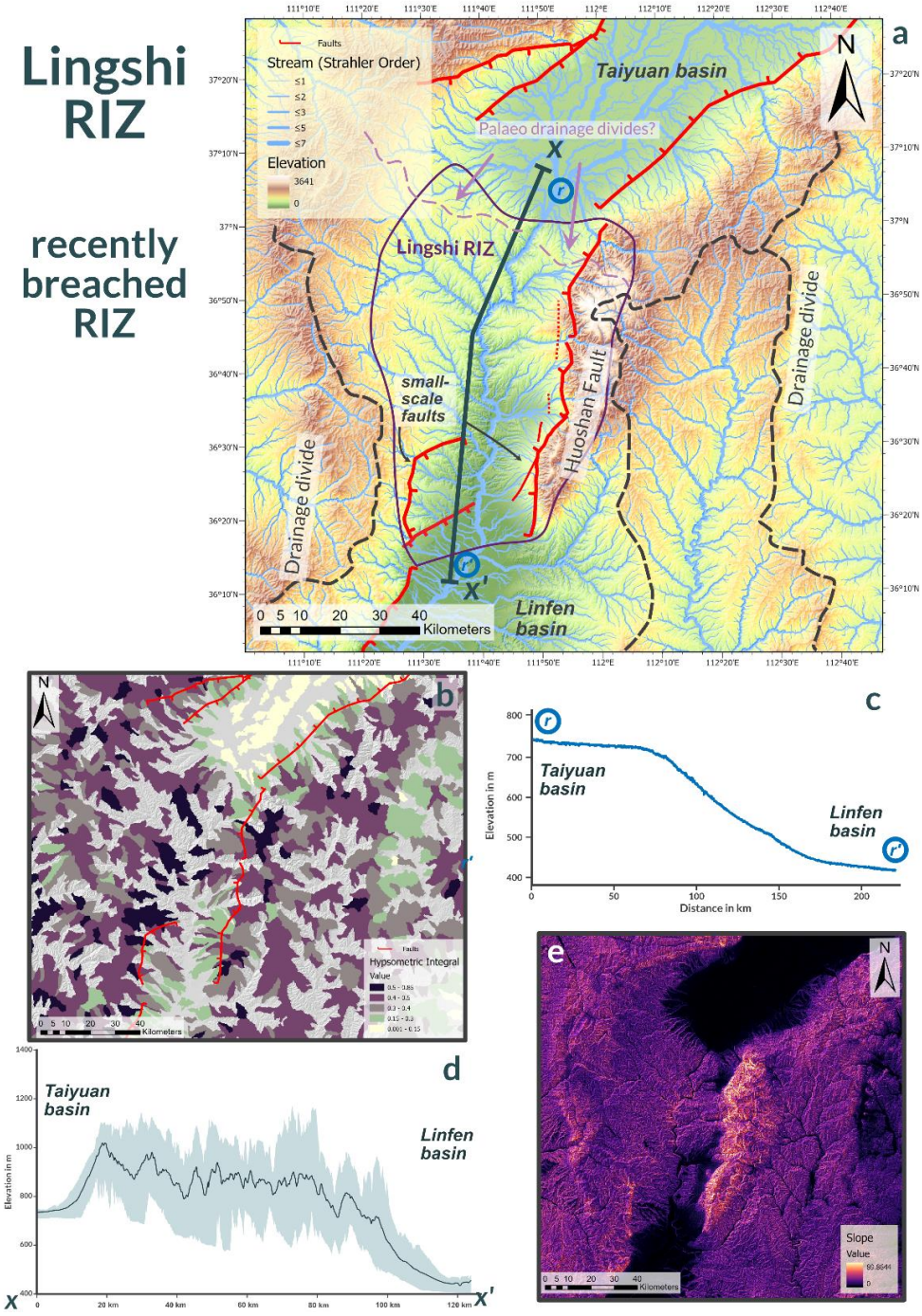

Figure 2.8 Detailed Map of the Lingshi RIZ

a) Topographic map with drainage (weighted by stream order) showing the drainage divide and reorganisation happening at the Lingshi RIZ. b) HI map of the Lingshi RIZ, showing high values in the footwall of the Huoshan Fault but also in the hangingwall. c) Longitudinal river profile of the Upper Fen River showing the characteristic "down stepping" shape of river profiles across recently breached RIZs. d) Swath profile of the Lingshi RIZ, shaded area indicates maximum and minimum elevation in a 5km corridor along the line of section– line of section shown on 7a). e) Slope map of the Lingshi RIZ that shows very high values along the main border fault (Huoshan) but also clear distinct breaks in the SW.

The Lingshi RIZ (Fig. 2.8) is the uplifted region between the Taiyuan and Linfen basins. The breaching fault, which in this case is the Huoshan Fault, is well-developed and has established a physical connection between the Taiyuan and Linfen basins. The Huoshan Fault and other small-scale faults within the Lingshi RIZ are shorter, more segmented, and variably orientated compared to the faults of the major subbasins. These small-scale faults are more visible in the slope map (Fig. 2.8c), as sharp linear breaks. The footwall of the Huoshan fault shows high values of HI > 0.5 (Fig. 2.8b). However, the whole RIZ shows high values of HI, which are sometimes connected to smaller-scale faults, highlighting the complexity and distribution of faulting in the RIZ. As noted in 2.5.1., the Loess Plateau can have a significant impact on the HI response of a region, therefore the high HI response in the Lingshi RIZ may in part be related to the degree of Loess coverage. However, the Loess is constrained to the hanging wall of the Huoshan Fault and therefore the high HI response in the Huoshan Fault footwall is not influenced by Loess. The drainage of the Taiyuan and Linfen basins is connected across the Lingshi RIZ as the Fen River is flowing across it. The drainage was previously not connected as there are possible palaeo-drainage divides (in purple – Fig. 2.8a), where tributaries of streams flow in separate directions. Li et al. (1998)

proposed that during the early evolution of the Shanxi Rift in the Miocene and Pliocene, the basins were filled by isolated lakes and later, during the mid-Pleistocene, a fluvial connection was established. Hu et al. (2005) identified three lake terraces in the Taiyuan and Linfen basins, with the latest regression occurring at 0.13 Ma. Based on this, the integration and breaching across the Lingshi RIZ likely occurred in the Middle-Late Pleistocene. The swath profile of the RIZ and the longitudinal river profile (Figs. 2.8d, e) show the down-stepping morphology that is commonly associated with recently breached RIZs may be a relic of the lake terraces prior to the fluvial connection being established. The Huoshan breaching fault (Huoshan) is well developed and has established a physical connection between the depositional systems of both basins, as the characteristic morphology of the Lingshi RIZ, we classify it as a recently breached RIZ.

The Shilingguan RIZ (Fig. 2.9) separates the Xinding Basin to the north and the Taiyuan Basin to the south. The breaching fault (Shilingguan Fault) is physically connected to the Jiaocheng fault but not to the Xizhoushan fault. The Shilingguan Fault itself appears to be segmented as seen by the various orientations of the fault segments (Fig. 2.9c). The topographic swath profile of the RIZ shows an outstanding topographic high (Fig. 2.9d). The footwall of the Shilingguan fault exhibits very high (>0.5) HI values and the Fen River in its footwall is highly sinuous but has high topography, relief, and steep slopes on either side, also known as an entrenched meander (Gardner, 1975; Harden, 1990). Combining all these observations indicates that this area of the Shanxi Rift has experienced recent uplift. The Shilingguan RIZ represents a drainage divide, with the Hutuo River, north of the RIZ being deflected eastwards and draining across the Xizhoushan fault through the Taihang mountains into the North China Plain (Fig. 2.2). In contrast, the Fen River flows from the NW and crosses the main breaching fault before draining towards the south into the Taiyuan

basin. Windgaps (Fig. 2.9a) in the footwall of the Xizhoushan Fault to the east show that possibly the drainage of the Upper Fen River once occurred across this RIZ from west to east before the initiation of the Shilingguan Fault and uplift of its footwall caused the diversion of the river to the south. As the depositional systems of the Xinding and Taiyuan basins are not connected across the RIZ, and the breaching fault has not established a full physical link, this RIZ represents a partially breached RIZ.

The different breaching stages of the Lingshi and Shilingguan RIZs may be related to their previously mentioned geometrical arrangement (Lingshi RIZ = underlapping oblique convergent RIZ; Shilingguan RIZ = underlapping parallel divergent RIZ), which led to the earlier breaching of the Lingshi RIZ. The influence of initial geometry was shown by Kolawole et al. (2024) in a numerical model of the southern Malawi Rift, where the tip-to-tip arrangement of the Nsanje RIZ favoured rift coalescence compared to the overlapping divergent geometry of the Middle Shire RIZ. The convergent RIZ geometry of the Lingshi RIZ was beneficial for strain localisation and deformation concentration at the fault tips of the surrounding basin bounding faults (Jiaocheng and Linfen), while the divergent geometry of the Shilingguan RIZ stalled rift coalescence. This in turn may also explain why the Hengshan RIZ is unbreached as it has an overlapping divergent geometry, which is unfavourable to concentrating strain and deformation around the RIZ and rift coalescence. The breaching status of the RIZs increases towards the south, which may be controlled by the different RIZ geometries.

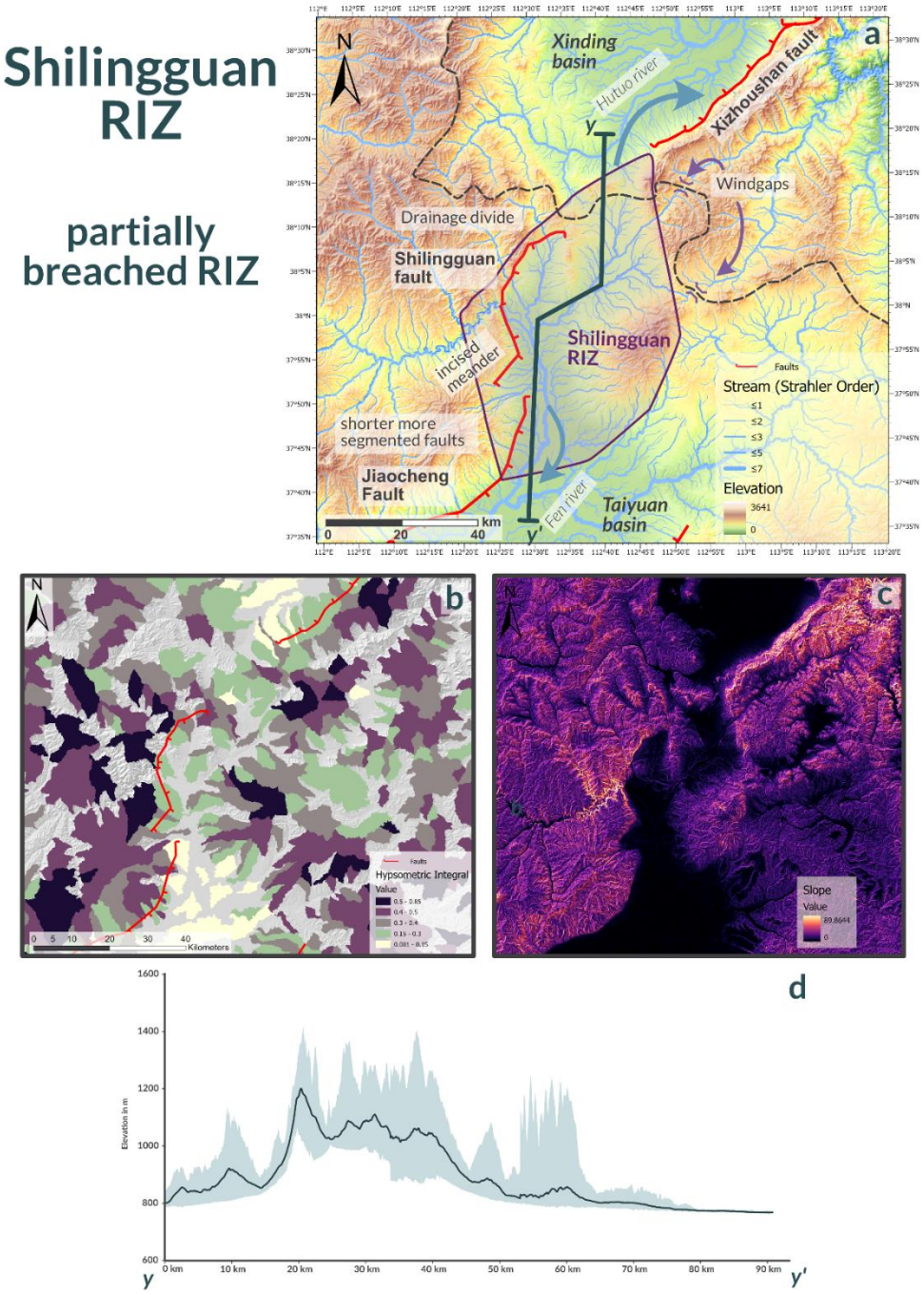

Figure 2.9 Detailed Map of the Shilingguan RIZ

a) Topographic map with streams (weighted by stream order) showing the drainage divide and reorganisation happening at the Shilingguan RIZ. b) HI map of the Shilingguan RIZ, showing the high values in the footwall of the main faults, especially in the Shilingguan fault footwall where the high slope values are found. c) Slope map of the Shilingguan RIZ. High slope values are closely associated with the

main faults but can also be seen along the steep sides of the meandering rivers in both the footwall of the Xizhoushan Fault and the Shilingguan Fault. d) Swath profile of the Shilingguan RIZ, the shaded area indicates maximum and minimum elevation in a 5km corridor along the line of section – line of the section shown in 8a)

Geomorphic evidence shows that the RIZ are currently the most active regions of faulting and reorganisation, as breaching faults of the RIZs (Huoshan and Shilingguan faults) show consistently high geomorphic values (Table 2.1; Fig. 2.7). They also show major changes in fault strike compared to the NE-SW trending basins (Figs. 2.8 and 2.9). Most faults in the RIZs do not strike NE-SW but show more distributed patterns of N-S and NE-SW striking faults. Commonly an overall "zig-zag pattern" forms, with fault segments of variable direction. Faults oblique to the general extension direction commonly form at the intersection points between major faults (Figs. 2.2, 2.8 and 2.9). Hodge et al. (2018a) show in models that Coulomb stress changes along the tips of established faults lead to the formation of new off-axis trending faults, with the geometry of these dependent on the lateral separation and amount of under- or overlap of the interacting faults. This process is common in other rift basins across the world (Maerten, 2000; Morley, 2010) and is similar to observations of faults in the RIZs of Shanxi. The N-S striking fault segments in the RIZs show overall higher geomorphic index values compared to the NE-SW trending faults of the sub-basins, suggesting they are more tectonically active as the active deformation is focused along zones of active linkage. The morphology of the N-S faults in the RIZs suggests that they are younger faults, which are still early in the reorganisation phase, as they are shorter, more segmented, and often show lower topographic offset (Fig. 2.8, 2.9). Morphologically more mature NE-SW striking basin bounding faults have lower geomorphic index values than the faults in the RIZs, but can also show high values,

especially in the case of the Wutai and Xizhoushan faults (Figs. 2.5 and 2.7). In the Shanxi Rift, faults of all orientations may show high activity levels, however, faults in the RIZs show the highest activity. This activity pattern is consistent with an overall stable extension direction (Middleton et al. 2017), where all faults remain possibly active, but activity is concentrated in the linkage zones.

RIZs often experience high seismic activity due to increased strain along the tips of established basin-bounding faults that progressively link across the RIZs. This was observed at the tips of the Rukwa Rift and the Rukwa-Tanganyika RIZ by Kolawole et al. (2021) and Kolawole et al. (2024), as well as for the Turkana Rift (Musila et al., 2023). The breaching faults in the RIZ could have a buffering effect on the NE-SW trending faults of the main sub-basins, as the overall strain accommodated across the Shanxi Rift is concentrated on the breaching faults in the RIZs, therefore the longer NE-SW trending faults accommodate overall less strain. Increased strain rate on faults post linkage has been shown to occur both in a theoretical framework (Cowie et al., 2005) and in natural examples such as the Whakatane Graben, NZ (Taylor, 2004). The heightened activity at these RIZs is not only shown by geomorphology but also by seismicity: Chen et al. (2021) processed receiver function data that show clusters of earthquakes at or near the Lingshi and Shilingguan RIZs, while events in the individual subbasins are more distributed. The ISC catalogue (Storchak et al., 2013; 2015; Di Giacomo et al., 2018) covering earthquakes occurring between 1907 and 2022 (Fig. 2.2) shows similar clusters around the RIZs, although the cluster around the Shilingguan RIZ is more pronounced. The faults in the Shilingguan RIZ are comparatively short and segmented (10-20 km), this might limit the occurrence of large-magnitude earthquakes along their trace. However, the Huoshan Fault, the breaching fault of the Lingshi RIZ, is equally segmented (Fig. 2.7a) with segments 20-

30 km in length and has been shown to be the site of major historic earthquakes. The historic Hongdong Earthquake (Mw 7.2-7.6) in 1303 CE was caused by slip on the Huoshan Fault (Xu et al. 2018) and had an estimated rupture length of 98 km, which shows that multiple segments can link up during seismic slip to generate larger magnitude events. The Shanxi Rift is a low-strain rate region, meaning major earthquakes are infrequent but potentially devastating as evidenced by the Hongdong 1303 event (Xu et al. 2018). Overall, the NE-SW trending faults, which are longer but potentially less active might be capable of generating larger but less frequent events (Scholz et al. 1982; Leonard, 2010), while the more segmented faults in the RIZs could produce more frequent yet smaller magnitude earthquakes.

2.5.3 The Role of Inheritance in the Shanxi Rift – Crust or Mantle Control?

Most continental rifts are influenced by inherited structures that are either reactivated (Daly et al., 1989; Wheeler and Karson et al., 1989; Holdsworth et al., 2001b; Kinabo et al., 2008; Phillips et al., 2016; Wedmore et al., 2020; Kolawole et al., 2021b) or reorientate the rift scale strain field in local areas (Morley, 2010; Philippon et al. 2015; Kolawole et al., 2018; Samsu et al., 2023). The Shanxi Rift exploited rheological weaknesses during its formation at the rift scale (TNCO) and on smaller individual fault scales. At first order, the spatial relationship between the Shanxi Rift and the TNCO is obvious (Fig. 2.1). The Shanxi Rift is directly superimposed on the Paleoproterozoic orogen (Xu et al., 1993). The TNCO acted as a rheological weakness in comparison to the adjacent stronger Western Block of the NCC and therefore the TNCO was exploited by the Shanxi Rift. Orogenic belts behaving as weak zones for nucleating rifts is a common feature (i.e. East Africa (Rosendahl, 1987; Morley, 1988; Daly et al., 1989; Ring, 1994), and Baikal (Petit et al., 1996)). In the Shanxi Rift, faults often define the edges of Paleoproterozoic basement complexes and expose these at the surface by footwall uplift (e.g., Wutai, Hengshan, Xizhoushan, Zhongtiaoshan). Some of the rift

faults do not contain Precambrian crystalline rocks in the footwall, but for example the Jiaocheng and Taigu faults in the direct vicinity of the crystalline Lüliangshan and Taihangshan massifs (~ 50 km distance). Basement complexes, such as the Huoshan, Fuping or Lüliangshan, are also cored by Precambrian granitic plutons, which formed as late orogenic intrusions during the TNCO development. These stronger more buoyant granitic blocks may have been more resistant to deformation hence the rift faults preferentially formed along the pluton margins and are uplifted within the fault footwall. This is similar to observations from offshore New Zealand (Phillips and McCaffrey, 2019; Phillips et al. 2023) or the Carboniferous rift systems of the United Kingdom (Fraser and Gawthorpe, 1990; Howell et al., 2020).

The similar trends of ancient pre-existing structures and active extensional faults show that the Paleoproterozoic fabrics of the TNCO potentially influence the orientation of the active faults of the Shanxi Graben. Major NE-SW trending basin bounding faults in the Shanxi Rift (Wutai, Xizhoushan, Taigu, Jiaocheng, and Zhongtiaoshan faults) are generally parallel to inherited NE-SW (45-55°) trending Paleoproterozoic basement fabrics (Fig. 2.5). The Wutai and Zhongtiaoshan faults all strike ENE-WSW (60-70°), matching the trend of the inherited structures in the footwall (Fig. 2.5). Therefore, it is likely that crustal structures influenced the orientation of these faults. The Hengshan fault locally trends parallel to the basement fabrics but often strikes obliquely and cuts across some of the shallow basement fabrics observed at surface (Fig. 2.5). It is possible that it locally exploits the shallow basement fabrics while following the trend of a deeper-seated weakness that is oblique to the shallow basement fabrics observed at surface, similar to the Bilila-Mtakataka Fault (Hodge et al. 2018b) in Malawi. The Xizhoushan fault follows the trend of the fabrics in the western part of the Fuping complex. There is a major crustal boundary running through the Fuping

complex, which is known as the Longquanguang thrust (LGQT), a gently dipping thrust fault, according to Trap et al. (2012). To the southeast of the LGQT, there is a major change in the trend of the Palaeoproterozoic fabrics to a generally NW-SE/E-W direction (compare stereonets of Fuping-West and Fuping-East in Fig. 2.5). The crustal structures of the eastern Fuping Block have no influence on the Xizhoushan fault (or any other fault in the Shanxi Rift), possibly because the LGQT represents a mechanical barrier. Based on their proximity and matching orientation, we speculate that the Xizhoushan fault may merge with the LQGT at depth. Merging of faults on shallower dipping structures has been observed by Phillips et al. (2016) in the North Sea.
The >50 km long basin bounding faults of the Shanxi Rift nucleated along preferentially orientated inherited fabrics of the Palaeoproterozoic basement complexes, which may have aided with early fault nucleation similar to observations in other global rift systems (Phillips et al., 2016; Rotevatn et al., 2018; Heilman et al. 2019; Collanega et al., 2019; Vasconcelos et al., 2019; Ramos et al., 2022)

Faults in the RIZs show a more disconnected pattern (Figs. 2.8, 2.9), vary more in orientation (N-S and NE-SW), and are shorter (10-30 km) than the large NE-SW trending basin bounding faults (up to 100 km). Individual fault segments in the RIZs follow the broadly NE-SW trending crustal inherited fabric or cut across the fabric and strike N-S or NNE-SSW. As RIZ faults mature, segments link up and grow into one throughgoing a “zig-zag” structure that cuts across pre-existing fabrics. This is especially visible in the plan view of the Huoshan Fault (Fig. 2.8). These “zig-zag” patterns in faults have been observed in offshore West Greenland (Peace et al., 2018, Schiffer et al., 2020), the North Sea (Henza et al. 2011; Henstra et al., 2015) and the main Ethiopian Rift (Moore and Davidson, 1978; Vetel and Le Gall, 2006; Corti et al., 2022; Lezzar et al., 2002; Corti, 2009; Hodge et al., 2018b). In the case of Greenland

and Ethiopia, rifting was oblique to major basement shear zones, which led to the formation of two sets of faults with some of them parallel to the extension direction and others parallel to the inherited structures. In the Shanxi Rift, the regional NW-SE extensional vector (Middleton et al. 2017) is likely perturbed around the RIZs due to interactions of the fault tips of the adjacent basin-bounding faults. Resulting in a strain field that would be oblique to the inherited structures. This leads to the formation of N-S trending faults that are perpendicular to the perturbed strain field and cut across the inherited basement fabrics, as well as NE-SW trending faults that follow the trend of pre-existing Proterozoic structures. Therefore, as the faults grow and coalesce across the RIZs, they will both cut across or locally exploit the inherited fabrics (Heilman et al., 2019; Kolawole et al. 2021b), resulting in the observed zig-zag fault pattern. Fault geometry may also be controlled by multiple levels of inheritance as observed by Wedmore et al. (2020) for the Thyolo Fault in Malawi and Hodge et al. (2018b) for the Bilila-Mtakataka Fault, where shallow-level structures control the surface geometry of the fault, but a deeper-seated weakness guides the overall orientation, which is oblique to the overall strain field. We consider that the NE-SW trending faults in the RIZs formed parallel to inherited fabrics at early stages and were linked up by N-S trending segments later. This behaviour is observed on the Norwegian Margin of the North Sea by Henstra et al. (2015) where rift faults from an early phase of rifting influenced the location and morphology of younger rift faults during a subsequent oblique phase of rifting. However, we did not find major morphological or geomorphological value differences between the N-S and NE-SW trending faults that would suggest a polyphase fault development, therefore it is possible that they are co-eval.

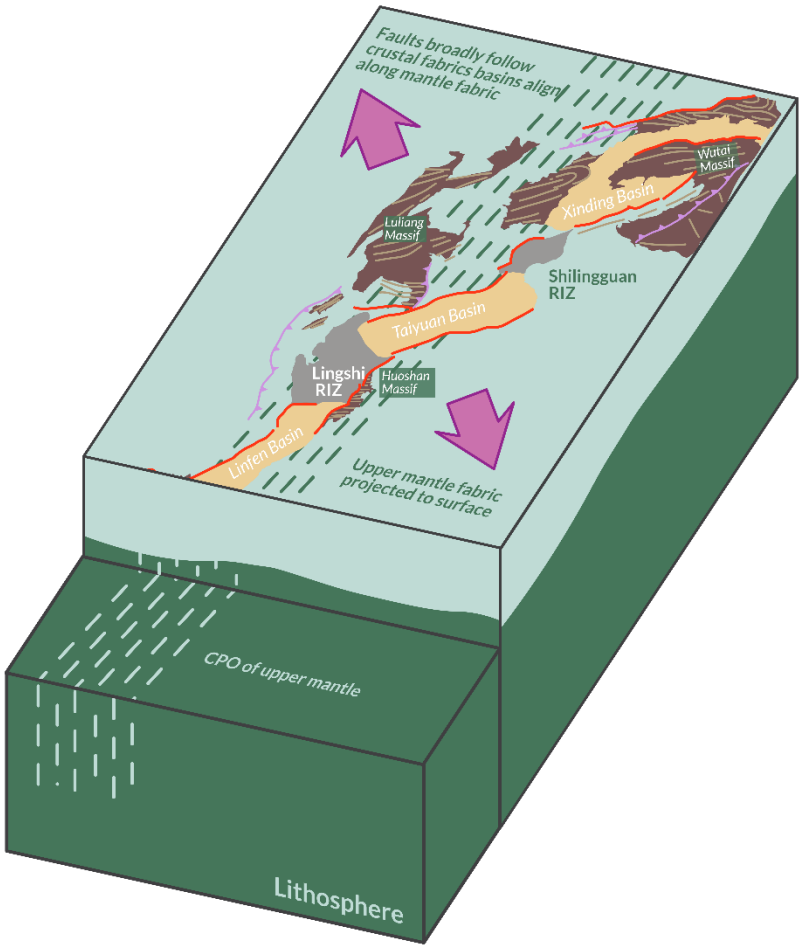

Figure 2.10 3D Diagram of the Crust and Mantle Inheritance Interactions in the Shanxi Rift

Schematic 3D diagram of the Shanxi Rift showing the proposed obliquity between mantle anisotropy and crustal inherited fabrics. Mantle anisotropy is defined by the suggested crystal preferred orientation (evidenced by shear wave splitting data (Zhao and Zheng, 2005)) in the upper mantle, which broadly trends N-S, while the crustal fabrics trend NE-SW. The Shanxi Rift basins are collated with a zone of aligned mantle fabric which is oblique to the principal extension direction (indicated as purple arrows). Individual basins and their bounding faults formed parallel to inherited crustal fabrics. This creates the characteristic en-echelon pattern of the Shanxi Rift.

The N-S and NE-SW trending faults in the RIZs can also be observed at the scale of the entire Shanxi Rift. The Shanxi Rift is an S-shaped en-echelon rift that follows a broad N-S trend with individual basins and their bounding faults orientated NE-SW. While the TNCO broadly trends N-S/NNE-SSW (Fig. 2.1; Zhao et al., 2005), the individual crustal structures, such as major shear zones, thrust faults or fabrics, broadly trend NE-SW (Fig. 2.10). A broadly NNE-SSW to N-S trending anisotropy (0-15°) in the upper mantle of the Central Zone of the North China Craton is shown by shear wave splitting data from the upper mantle (Chen, 2010, Zhao and Zheng, 2005). The apparent obliquity between the trend of crustal structures and the upper mantle fabric shows that crustal inheritance and lithospheric inheritance may not share a common orientation, which is a common feature of many rift zones (Vauchez et al., 1997; Tomassi and Vauchez, 2001). Recent analogue modelling of oblique crustal and mantle fabrics by Zwaan et al. (2022) show similar patterns to those observed in the Shanxi Rift. Analogue models by Molnar et al. (2020) show that lithospheric weaknesses influence the rift trend, while oblique crustal structures segment the rift at a local scale. The difference in lithospheric and crustal structural trends could have occurred during transpressional accretion of the TNCO, as proposed by Li et al. (2010) where subduction initially occurred along an N-S trend with later collision forming NE-SW trending structures. Alternatively, the polyorogenic event that formed the TNCO may have formed the obliquity between crustal and mantle structures, as the initial N-S trending TNCO was partially reworked by a collision of the Columbia supercontinent in the Palaeoproterozoic (Kusky & Li, 2003; Kusky et al. 2007; Santosh, 2010). However, the evolutionary history of the TNCO is debated and the resolution of the exact timing of events is beyond the scope of this paper. Mesozoic compression across North China, commonly known as the Yanshanian orogeny (Zhang et al., 2008; Zhang et al., 2011; Clinkscales and Kapp, 2019) has also affected the Shanxi region

and may have also caused further reworking of the TNCO and rotated the crustal fabrics to the present-day orientation. Solving the apparent obliquity between crustal and lithospheric trends of the TNCO is not resolvable in this study and would require further work on the kinematic evolution of the TNCO. The principal extension direction determined by Middleton et al. (2017) of 151° for the Shanxi Rift is roughly perpendicular to the inherited crustal structures but oblique to the proposed broad upper mantle anisotropy, which resulted in the early rift basins exploiting the favourably orientated crustal fabrics, while the general trend of the rift is oblique to the extension direction along an upper mantle fabric that created a rheological weakness. This en-echelon arrangement of rift basins above a broad oblique deep-seated weak zone has been shown in analogue models by Agostini et al., (2009), showing similar geometries as exhibited by the Shanxi Rift. However, we acknowledge that the observed mantle anisotropy may not be an inherited mantle fabric and could have formed during rifting (Gao et al., 1997; Kendall et al. 2006) and is aligned obliquely to the rift (Tepp et al., 2018; Ebinger et al., 2024). Thus, the mantle fabric underlying Shanxi may be Cenozoic in age and has been formed during the extensional deformation of North China as has been proposed previously (Chang et al., 2012). We emphasise that our interpretation that the architecture of the Shanxi Rift is influenced by crustal and mantle fabrics of the TNCO that are oblique to each other is speculative as the origin of the mantle anisotropy beneath the Shanxi Rift is unresolved. Yet, the apparent N-S trend of the TNCO, a roughly N-S trending mantle anisotropy and the NE-SW trending crustal fabrics may support the hypothesis that crust and mantle fabrics beneath the Shanxi Rift are oblique.

Based on our geomorphic results, we propose a new model for the evolution of the Shanxi Rift that incorporates a heterogenous basement with inherited structures (Fig. 2.11), that can explain the evolution of the Shanxi Rift under a constant and simpler

strain field, than a more variable strain field (Shi et al., 2015a; Shi et al., 2020; Assie et al., 2022). In our model, the extensional strain field trends NW-SE, which is consistent with previous estimations of the present-day extensional strain field using GPS or seismicity data (Middleton et al., 2017; Shen et al., 2000). However, locally the strain is reorientated either by inherited structures (i.e., Wutai and Zhongtiaoshan (Figs. 2.5, 2.8)) or interactions between basin-bounding faults that rotate the local strain field in the RIZs between them (Shilingguan and Lingshi) (Fig. 2.11). This means that there is no specific set of faults that is favoured by changes of strain fields. Therefore, potentially all faults remain active, yet there are certain faults that are more active due to ongoing reorganisation and linkage in the RIZs. Faults were established during early evolutionary stages along preferentially aligned NE-SW trending inherited structures and formed the major en-echelon Taiyuan, Xinding and Linfen basins along an N-S trending upper mantle structure (Fig. 2.10 and 2.11). As the faults and basins grew, they interacted and linked across almost unfaulted topographical high stands - the RIZs. These RIZs had a more complex faulting pattern as the interacting faults created a locally rotated strain field, which is oblique to the crustal structures and the regional strain field. This creates a “zig-zag geometry” as the shorter fault segments grow and coalesce. As linkage progresses, these RIZs link basins and establish physical and sedimentary system links. This linkage is currently ongoing, as represented by the only partially breached RIZ of Shilingguan.

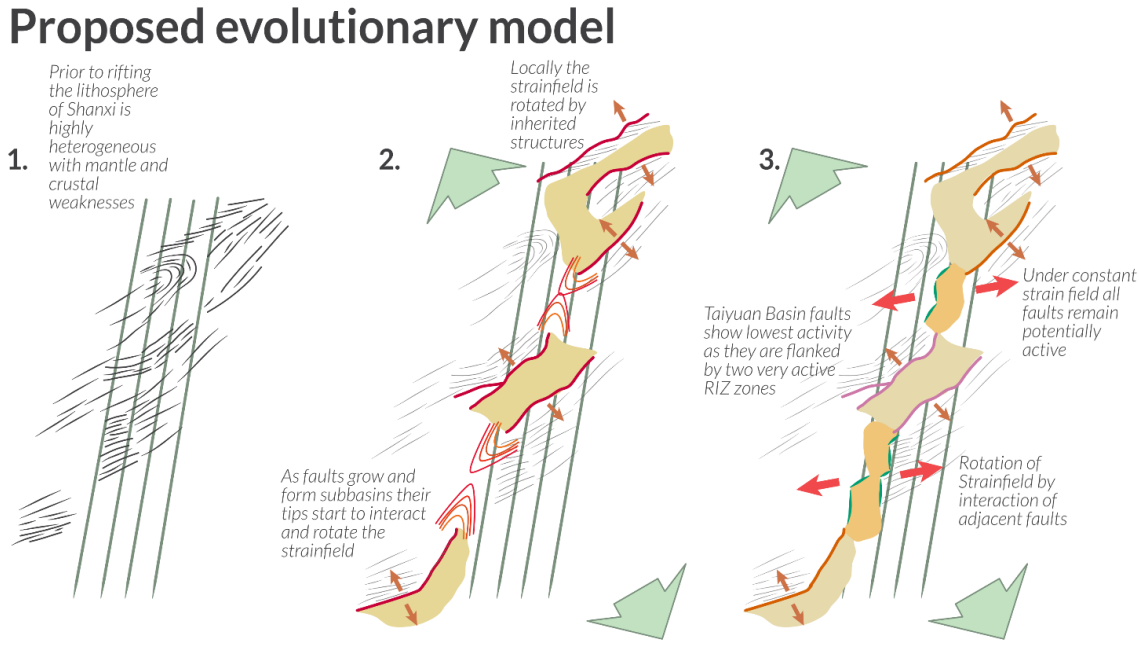

Figure 2.11 Summary Evolutionary Diagram of the Shanxi Rift

The new proposed evolutionary model under a constant strain field shows the linkage of rift basins influenced by two levels of inheritance – crustal and mantle inheritance which result in oblique rifting and the creation of an en-echelon array of basins. 1. Proposed pre-rift framework of NNE-SSW trending mantle fabric and NE-SW trending crustal fabrics. 2. Major basins form en-echelon along the NNE-SSW trending mantle fabric but form perpendicular to the extension direction (large green arrows) and along inherited crustal structures that locally reorientate the strain (smaller orange arrows). RIZs are created and major basin bounding faults start to reorientate the local strain field. 3. The RIZs are being breached and form smaller more segmented fault segments that are influenced by the locally reorientated strain field (red arrows) and inherited crustal structures.

2.6 Conclusions

We applied three different geomorphic indices (R_l, k_{sn} and HI) to analyse the fault distribution and the geometry and occurrence of rift interaction zones (RIZs) along the Shanxi Rift to discuss the distribution of tectonic activity and understand the role

structural inheritance has played in its evolution and the seismic hazard posed by active faults within it. Based on our results we conclude the following:

1. Geomorphic indices are a powerful tool to evaluate the fault evolution and activity and the segmentation of the Shanxi Rift.

2. Our study shows that lithology has a strong influence on the overall geomorphic signal of faults, as those with Paleoproterozoic crystalline basement in their footwalls have overall higher geomorphic values compared to faults with Palaeozoic-Mesozoic metasediments in the footwalls. However, comparing faults with similar basement geology can circumvent this problem. We found that overall HI is less sensitive to these variations of lithology compared to Relief and k_{sn}. Therefore, HI may be more suited to evaluating the tectonic influence on landscapes.

3. Within the Shanxi Rift, the RIZs that link the well-developed large Xinding, Linfen and Taiyuan basins, are the most active zones and show the most signs of active drainage reorganisation. This has major implications for seismic hazard assessments as it hints towards zones which show more complex and more active patterns of faulting due to the strain concentration in the RIZs, experiencing increased seismicity. Linkage of the basins seems to be progressing towards the north, as shown by the increasing breaching status of the RIZs towards the south, which is possibly controlled by their initial geometry.

4. Structural inheritance has played a key role in the evolution and segmentation of the Shanxi Rift. The collision of the two blocks of the NCC created a lithospheric scale weak zone, the Trans-North China Orogen (TNCO), which preferentially accommodates strain. The individual sub-basins of the Shanxi Rift

form en-echelon aligned along a broad N-S trend which coincides with an upper mantle anisotropy fabric – a lithospheric manifestation of the TNCO. The mantle anisotropy is oblique to the NW-SE extension direction, while the NE-SW trending crustal fabrics are perpendicular to the extension direction. Early rift faults nucleated along NE-SW-orientated basement fabrics, establishing basins arranged along the inherited N-S trend. As the boundary faults grew, they began to interact and form RIZs. Within these RIZs, the crustal basement inheritance further influenced and segmented the breaching faults and aided linkage across the basins. The faults within the RIZs both follow and crosscut pre-existing fabrics in the crust, creating a "zig-zag pattern" of small, segmented faults that eventually link up into singular throughgoing fault zones. Therefore, structural inheritance of pre-existing Precambrian basement fabrics and a locally rotated stress field resulted in the complex pattern of faulting observed in the RIZs.

5. Our geomorphic study supports a constant strain field during the formation of the Shanxi Rift with minor changes in the extensional vector. We propose that the Shanxi Rift is a type-example of an oblique rift, with an observed pattern of faulting influenced by a postulated upper mantle anisotropy, crustal basement fabrics, as well as pre-existing faults.

2.7 Supplementary Material

Data availability - A geopackage of the GIS project with the associated raster files of the geomorphic indices is available on the Zenodo repository associated with this publication, it also includes an Excel table with the raw data used for the generation of the violin plots (Fig. 2.7): https://doi.org/10.5281/zenodo.12701306. They can be

opened with QGIS. The R code for calculating the Hypsometric integral is available on GitHub: https://github.com/MFroemchen/R_Hypsometry

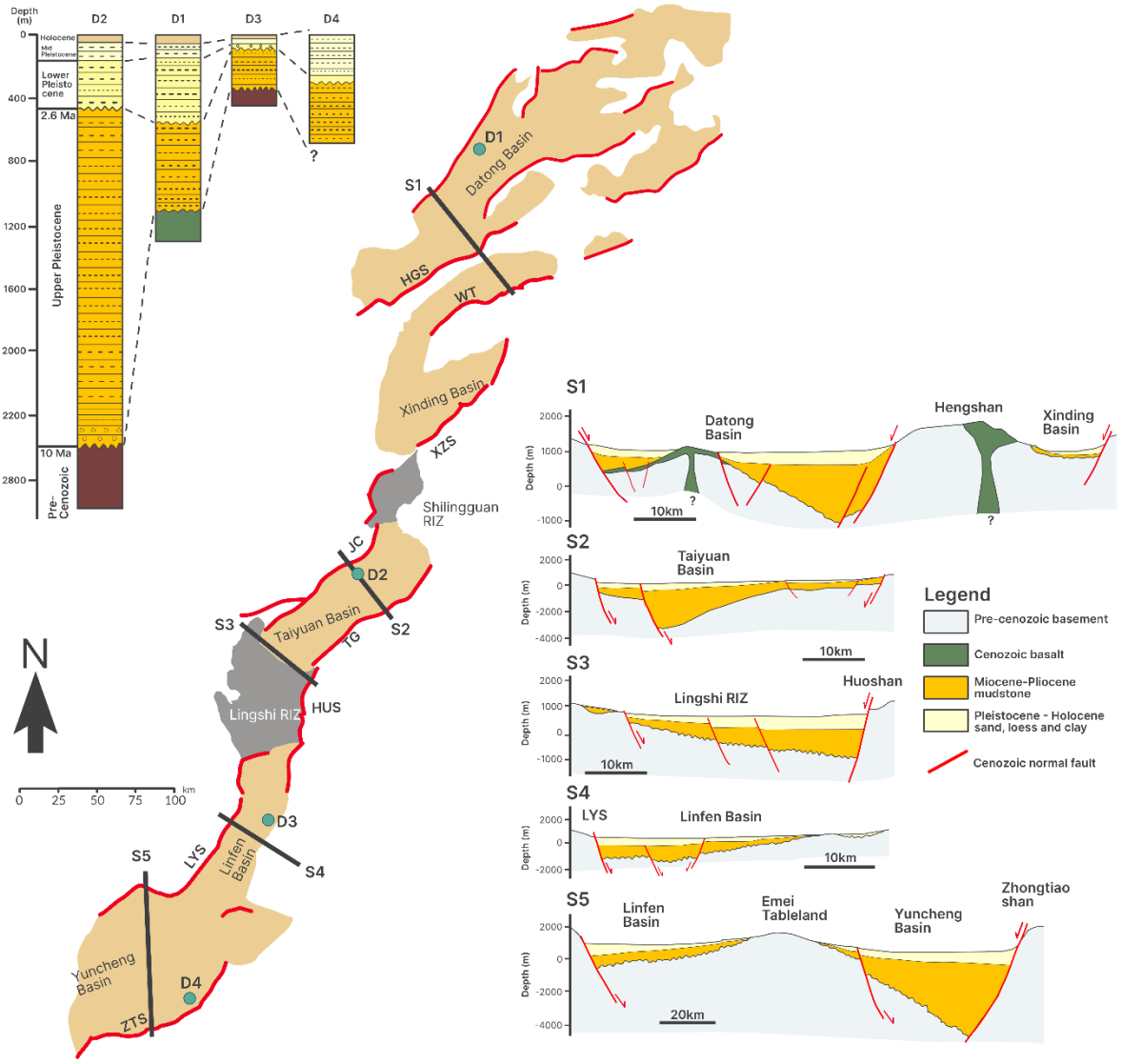

Supplementary Figure S 2.1 Stratigraphy of Shanxi (modified from Shi et al., 2015a)

Sketch map showing the major basins of Shanxi with positions of the four wells that penetrate the stratigraphy of these (D1-D4). S1-S5 show sketches of the basin fill geometries interpreted from seismic data. Cross sections S1 and S5 modified from

GSBSX (2002, 2007); S2, S3 and S4 after Xu et al. (1993). Wells D1, D2 from Xu et al. (1993), D3 from GSBSX (2008), and D4 from Wang et al. (2002).

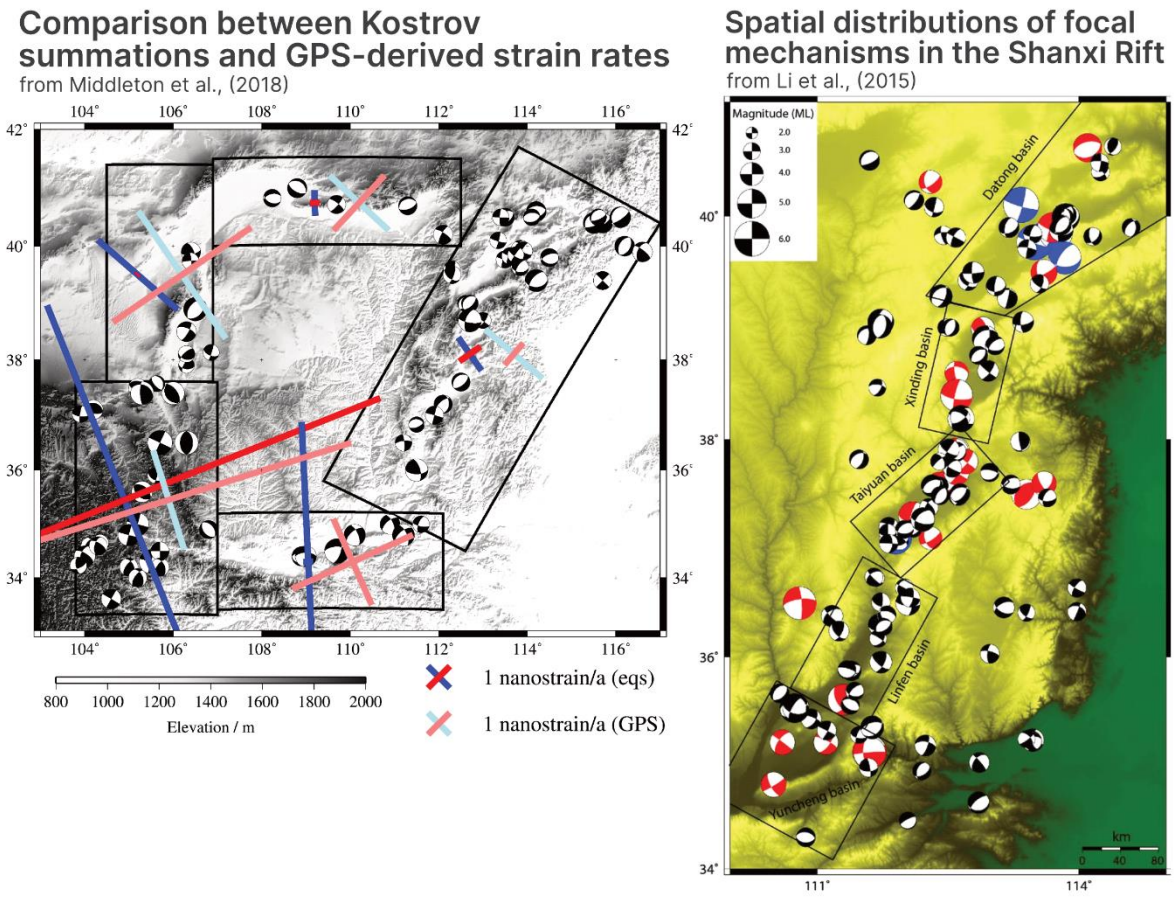

Supplementary Figure S 2.2 Focal mechanism and geodetic observations from Shanxi

a) comparison of Kostrov summation and geodetic derived strain rates by Middleton et al. (2018). Both show a similar orientation and magnitude, with geodetic derived strain rate being slightly higher. b) (from Li et al., 2015) Focal mechanism solution of 143 earthquakes in the Shanxi Rift (solutions (black – from this study; red – from Liu et al.1993, 1995; blue – from Global CMT) – showing considerable complexity of normal and strike-slip earthquakes

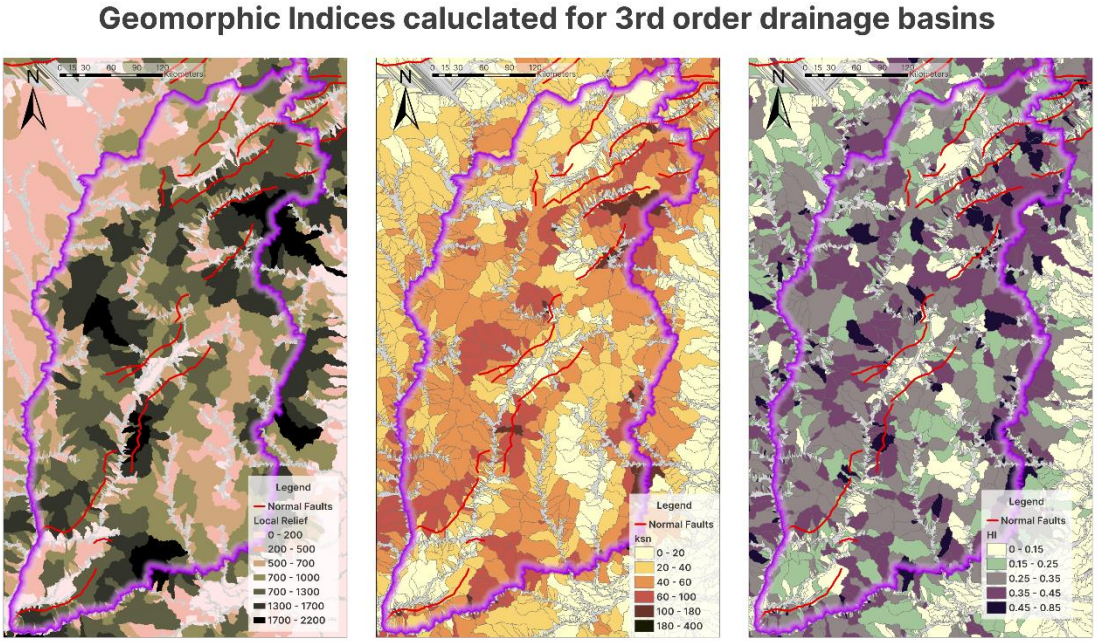

Supplementary Figure S 2.3 - Geomorphic Indices calculated for 3rd Order Drainage Basins

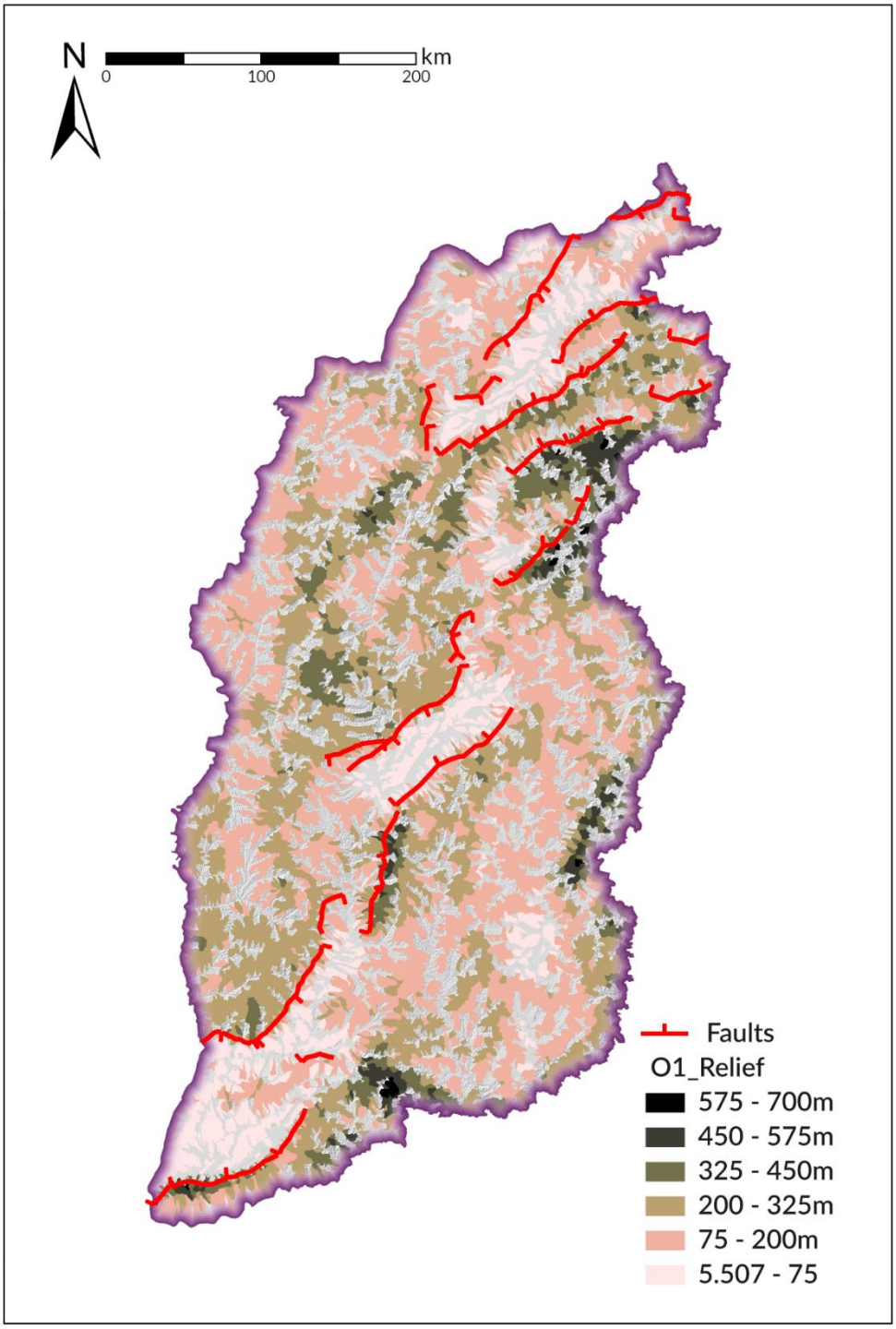

Supplementary Figure S 2.4 - Averaged Local Relief (R_l) per 1st Order Drainage Basin.

Averaged local relief calculated per first-order drainage basin rather than in a moving window (compare with Fig. 2.6a which shows R_l for a moving window).

These values were used to calculate the violin plots of Figure 7 and compare the values for RI with the ksn and HI values.

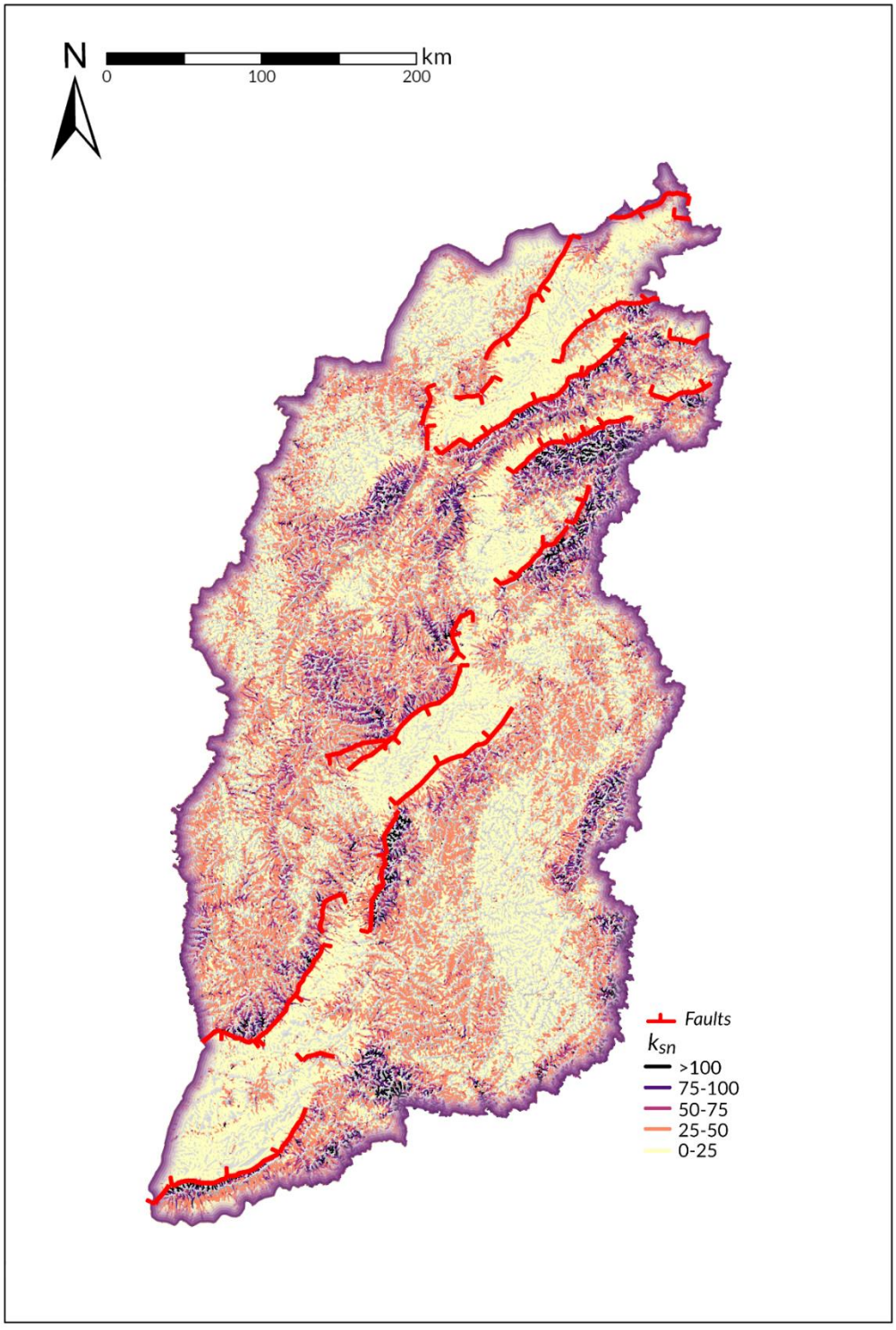

Supplementary Figure S 2.5 - k_{sn} Stream Network of the Shanxi Rift

Stream network map of the normalised channel steepness of the Shanxi Rift calculated using Topotoolbox2 (Schwanghart and Scherler, 2014). See Fig. 2.6b of the main manuscript to compare with the basin averaged ksn distribution.

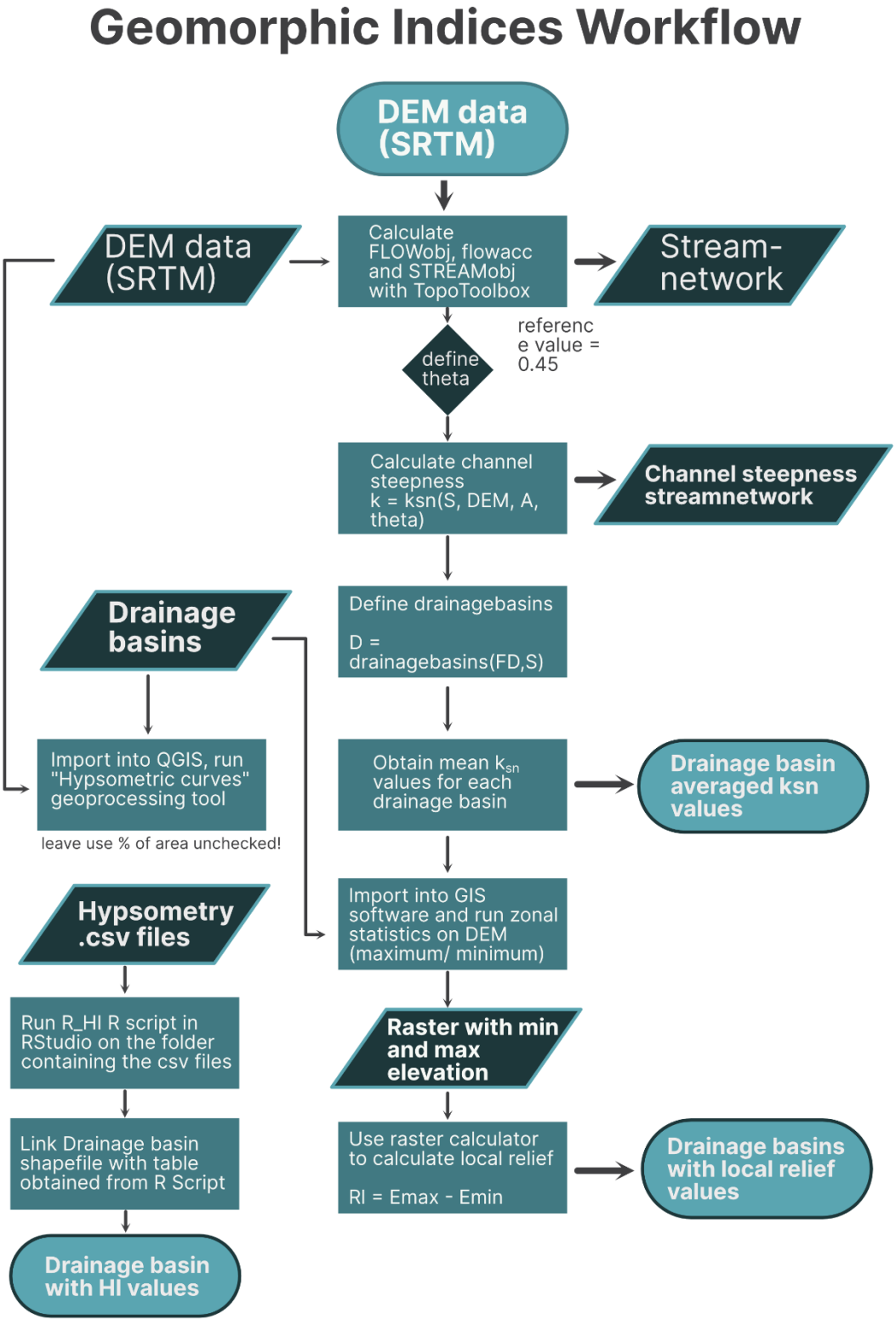

Supplementary Figure S 2.6 - Geomorphic Indices Workflow

Workflow for generating the geomorphic indices using Matlab, R and QGIS/ArcGIS

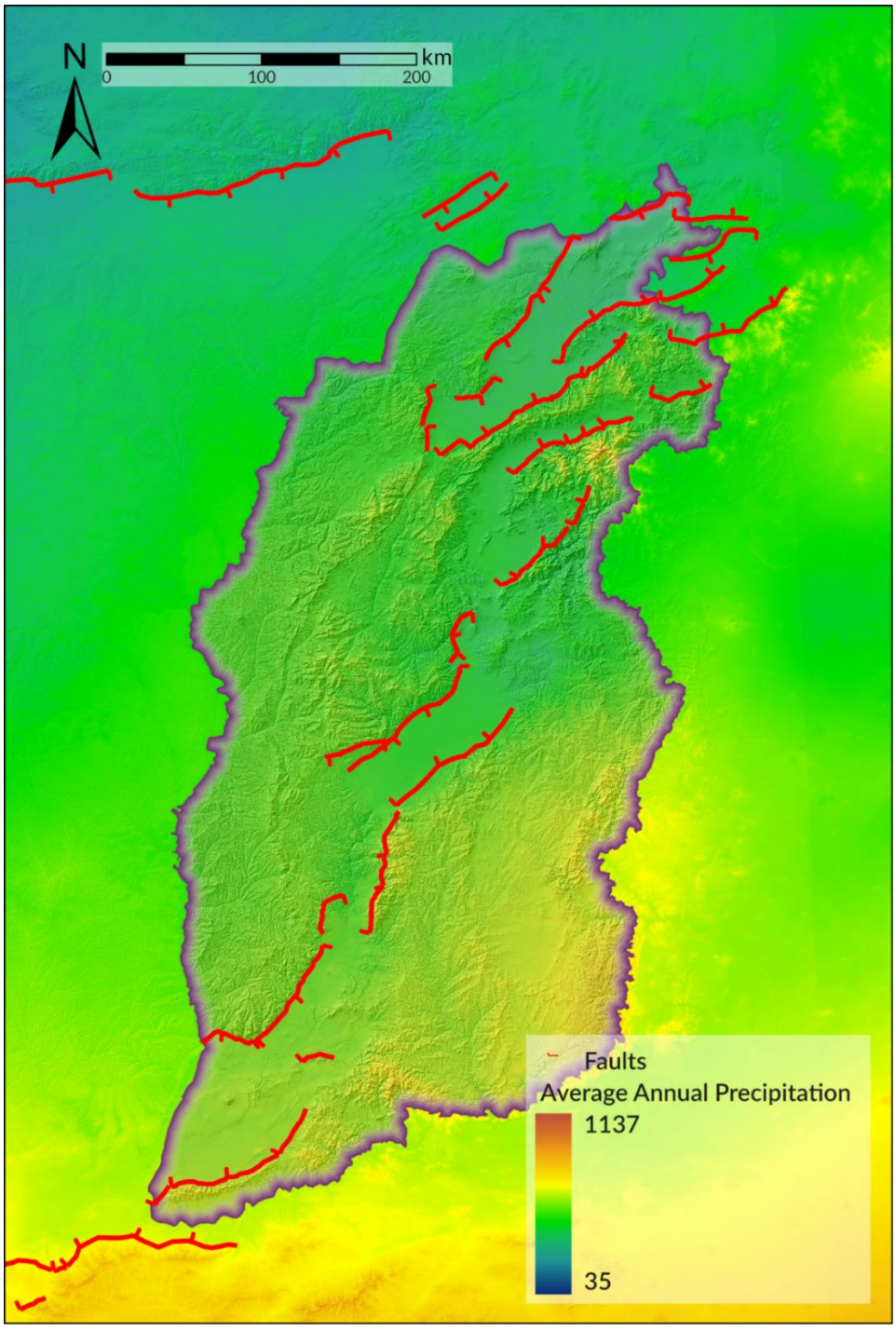

Supplementary Figure S 2.7 - Precipitation Map of the Shanxi Rift

The average annual precipitation of the Shanxi Rift shows little variation in precipitation across the Shanxi Rift. Data from WoldClim2 (Fick and Hijmans, 2017)

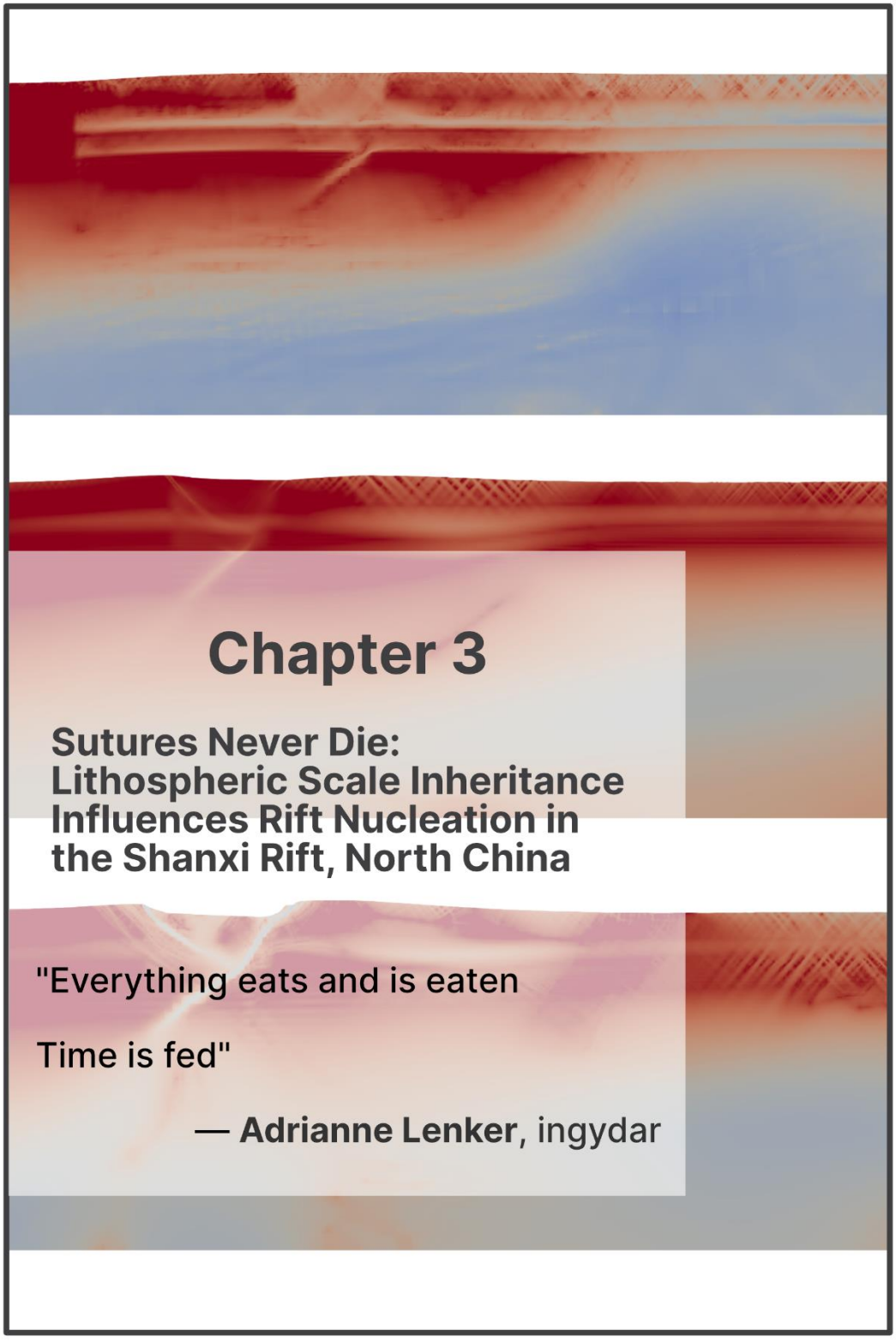

Chapter 3

Sutures Never Die: Lithospheric Scale Inheritance Influences Rift Nucleation in the Shanxi Rift, North China

"Everything eats and is eaten

Time is fed"

— **Adrianne Lenker**, ingydar

3. Sutures Never Die: Lithospheric Scale Inheritance Influences Rift Nucleation in the Shanxi Rift, North China

Abstract - The North China Craton formed during the Palaeoproterozoic when two Archean blocks collided and formed the Trans North China Orogen. Due to its unique evolution and recent geological destruction, the North China Craton shows two different modes of Cenozoic extension that are spatially and temporally separated. In the Paleogene the Bohai Basin exhibited distributed rifting with abundant magmatism while in the Neogene rifting migrated to the circum-Ordos rifts becoming narrower and more focused. The exact mechanism that led to the development of these very different rift systems remains debated, with models commonly invoking Pacific subduction as the driver for the earlier rifting and the India-Asia collision as the cause of the younger deformation. In this study, we perform 2D thermo-mechanical modelling to examine the role of variable lithospheric strength and inherited lithospheric weaknesses in the development of two rift systems separated in time. We found that distributed rifting occurs initially in the weaker non-cratonic lithosphere, while the adjacent cold thick cratonic lithosphere accommodates almost no strain. A period of quiescence between the two rift episodes subsequently strengthened the thinned eastern block and triggered rift migration to the west. An inherited lithospheric weakness, remanent from the collision that formed the TNCO, focussed rifting in the otherwise strong cratonic western block. Our results show how lithospheric thickness and strength variations as well as associated discrete zones of lithospheric weaknesses can influence the style of rifting and facilitate its initiation in an ancient craton. These results are widely applicable to many other continental rifts in the world that have formed around cratons such as the West Antarctic Rift System, that show similar behaviour. The work also shows there is no need for different tectonic regimes

to explain contrasting Cenozoic basin evolution in the North China Craton manifest as the narrow circum-Ordos Rifts and the wide rifts in the Bohai Basin.

3.1 Introduction

Early models of rift basin formation invoked a nearly homogenous “layer-cake” lithospheric architecture where rift basin formation was mostly dependent on extension rate and layer thickness (McKenzie, 1978). Many studies using field and remote sensing data show that pre-existing structures have a strong effect on nucleation (Dunbar and Sawyer, 1988; Schiffer et al., 2020; Tommasi and Vauchez, 2001; Vauchez et al., 1997; Wilson, 1966), segmentation (Corti et al., 2022; Heron et al., 2019; Hodge et al., 2018; Kolawole et al., 2018; Peace et al., 2018; Phillips et al., 2016) and linkage (Brune et al., 2017; Heilman et al., 2019) of rift basins. Modern computing resources enable us to model more of the inherent complexities and pre-existing structures of the lithosphere that influence rift basin formation. To date, crustal inheritance, meaning pre-existing structures and heterogeneities, mainly in the upper crust, has received significantly more attention than structures in the upper mantle inheritance due to the crust being better exposed at the surface or imaged in seismic reflection profiles (Fazlikhani et al., 2017; Kolawole et al., 2018; Mulaya et al., 2022; Phillips et al., 2016). Recent studies show that lithospheric weaknesses and inheritance are significant factors in the nucleation and early segmentation of rift basins and may “overprint” crustal inheritance on a larger scale (Heron et al., 2019; Molnar et al., 2020; Zwaan et al., 2022). Structures such as mantle scars may be relict sutures or subduction zones which can have a significant impact on intraplate tectonics (Heron et al., 2016) and the localisation of rifting (Heron et al., 2019). These mantle scars have been proposed in numerous locations based on geophysical data around the world such as the North Atlantic (Schiffer et al., 2015), the British Isles (Flack and Warner, 1990; Steer et al., 1998) or Canada (Calvert et al., 1995). However,

inheritance may not only occur as discrete structures but also as distributed areas of influence that show variations in the bulk pre-rift rheology, composition and thermal state (Manatschal et al., 2015). The upper mantle is a significant contributor to the overall strength of the lithosphere, especially in old and cold lithosphere (e.g. cratons) (Burov and Watts, 2006; Burov, 2011). Therefore, discrete heterogeneities in the upper mantle may have a significant effect on the overall strength of the lithosphere, which has major implications for the timing and location of rifting.

Large rift systems rarely form during a single phase of rifting (Bell et al., 2014; Naliboff and Buiter, 2015; Tett and Sawyer, 1996; van Wijk and Cloetingh, 2002). Rifting may slow down, speed up or be episodic. Slow extension or a deformation hiatus can lead to strengthening along the rift axis and induce rift migration rather than breakup. In principle, conductive cooling of the lithosphere, the removal of heat-producing elements and a lower ratio of crust-to-mantle thickness will increase the brittle strength of a rift over time during thermal re-equilibration. Rift migration will occur when the integrated strength of the unstretched lithosphere becomes smaller than the integrated lithospheric strength of the rift locus (Naliboff and Buiter, 2015). Several factors influence the occurrence of rift migration: The length of the initial rifting period and the length of the cooling period. (Naliboff and Buiter, 2015). However, there are only a few studies that show how inherited features may influence this migration pattern.

The complex time-protracted rifting history of North China serves as inspiration for this study. The North China Craton was assembled in the Paleoproterozoic, approximately 1.8 billion years ago as the Eastern and Western Block collided (Zhao et al., 2001; Kusky and Li, 2003; Faure et al., 2007; Kusky et al., 2007; Trap et al., 2012). This collision formed orogenic belts such as the Trans-North China Orogen (TNCO) (Fig. 3.1a). The formation of the TNCO was the result of a large-scale continent-

continent collision formed during the assemblage of the supercontinent Columbia, which formed a suture zone within a wide region of Palaeoproterozoic and Archean rocks that are exposed at the surface in Shanxi (Kusky et al., 2007; Trap et al., 2012). This collision most likely involved the lithosphere and has left a mantle scar within the NCC which can be seen on seismic data (Chen et al., 2008; Zheng et al., 2009; Santosh, 2010 – see Fig. S3.1 for examples) possibly representing underplated crustal material and a relic subducted slab from this collision event. The NCC remained relatively stable throughout the Palaeozoic but since the Late Mesozoic has been partially destroyed. The Eastern part has experienced significant destruction (Zhu et al., 2012) possibly due to delamination (Gao et al., 2004, 2002) or thermal erosion (Griffin et al., 1998; Menzies et al., 1993; Menzies and Xu, 1998) triggered by flat slab subduction. This period of destruction is evidenced by voluminous magmatism across the region (Wu et al., 2005; Wu et al., 2019; Lin et al., 2024). This left a thinned and modified craton in the East and a relatively intact craton in the West (Fig. 3.1b).

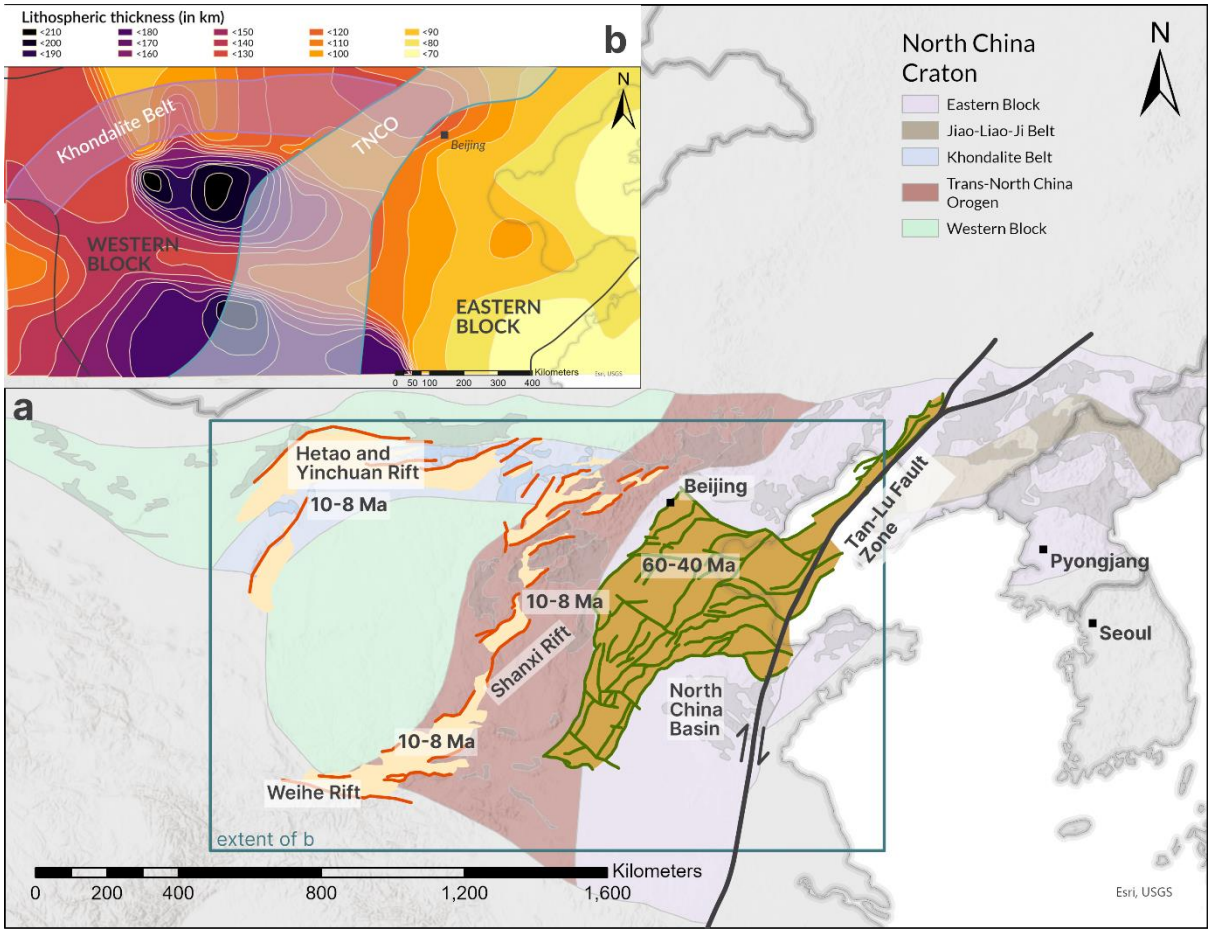

Figure 3.1 Overview Map of the North China Craton and the Cenozoic Rift Systems

Overview of the North China Cenozoic rifts – a) outline of the main structural elements of the North China Craton (NCC). The different parts of the NCC are indicated in different colours (modified from Zhao et al., 2005) with the Trans-North China Orogen (TNCO) and the Khondalite Belt representing major Proterozoic orogens that formed during the assembly of the NCC. The major Cenozoic rift systems are indicated in different colours according to their age. Green lines and orange basin outlines denote Paleogene rift systems, while red lines and yellow basin outlines denote Neogene rift systems. (modified from Zhang et al., 2003; Deng et al., 2007; Qi and Yang, 2010; Zhang et al. 2019) b) Lithospheric thickness map (modified from Shi et al. 2020) of the North China Craton region, darker colours indicate thicker lithosphere. Blue and purple outlines denote the positions of the

main Proterozoic orogens: the TNCO and the Khondalite Belt. See Figure S3.2 in the supplementary material for comparison of lithospheric thickness maps obtained through different geophysical methods (seismic tomography and receiver function data).

The Cenozoic rift systems in North China, notably the Bohai Basin and the Circum Ordos rifts (Shanxi, Weihe, Yinchuan and Hetao) formed (Ye et al., 1987; Yin, 2010) within the North China Craton. In the Eocene, the Bohai Basin started to rift above the previously thinned and modified craton in the East. The Bohai Basin is a “wide” rift with a series of graben and horst blocks which may be attributed to pre-rift rheology (Brun, 1999) or a transtensional strain that formed the North China Basin (Allen et al., 1997; Farangitakis et al., 2020), or, most likely, a combination of both factors. During this period little rifting was recorded in the Western Block, even though several workers documented late Eocene or Oligocene syn-rift sediments in the Yuncheng, Hetao and Weihe Graben these may be pre-rift in nature (Yin, 2010). After the onset of rifting in the Bohai Basin, a period of roughly 20-30 Myrs of tectonic quiescence followed and rifting in the Eastern Block was interrupted. This quiescent period was followed by an extension period that started about 10 Ma, in the Late Miocene. However, this time, deformation was not accommodated in the previously rifted Bohai Basin but instead formed new rift basins such as the Shanxi Rift. This late rifting period is evidenced by the earliest syn-rift sediments in boreholes from the Shanxi Rift dated at 10 Ma (Shi et al., 2015; Su et al., 2023; Xu et al., 1993). Therefore, rifting migrated north-westwards between the Eocene and the Late Miocene in the North China Craton.

The mechanics and underlying tectonics for this behaviour have most commonly been attributed to a change in geodynamic drivers, with the rifting of the Eastern NCC in the Mesozoic attributed to the rollback of the Pacific plate (Northrup et al., 1995; Schellart and Lister, 2005) during subduction, and the opening of the Shanxi Graben attributed

to far-field effects of the Asia-India collision to the South (Shi et al., 2020; Zhang et al., 2003). However recent results by Schellart et al. (2019), have called into question the impact of the India-Asia collision on the formation of continental rift basins in North China. Therefore, here we explore a different reason that may explain the rift history in North China: tectonic inheritance.

In this paper, we conduct a 2D thermo-mechanical modelling study to constrain the parameters consistent with this geological history. The results apply to other rift basins and emphasise the role of tectonic inheritance in controlling rift basin formation, up to at least 2 billion years after the original events.

3.2 Methodology

The role of a lithospheric scale suture in the localisation of a rift in cratonic lithosphere adjacent to non-cratonic lithosphere is investigated using a numerical approach. The models are solved using the ASPECT code version 2.3.0 (Bangerth et al., 2018; Glerum et al., 2018; Heister et al., 2017; Kronbichler et al., 2012; Rose et al., 2017) which uses the finite element method to solve a set of equations describing the movement of highly viscous fluid driven by differences in gravitational force due to density that depends on temperature. The model uses a visco-plastic material model which can model both brittle (plastic) and non-linear viscous deformation.

3.2.1 Governing Equations

We solved the equations of conservation of momentum, mass and energy after assuming an incompressible medium with an infinite Prandtl number,

$$-\nabla \cdot \left(2\mu \dot{\boldsymbol{\epsilon}}(\boldsymbol{u})\right) + \nabla P = \rho \boldsymbol{g} \tag{3.1}$$

$$\nabla \cdot \boldsymbol{u} = 0 \tag{3.2}$$

$$\rho C_P \left(\frac{\partial T}{\partial t} + \boldsymbol{u} \cdot \nabla T\right) - \nabla \cdot k \nabla T = \rho H \tag{3.3}$$

Where μ is the dynamic viscosity, $\dot{\epsilon}$ is the strain rate tensor, u is the velocity vector, k is the thermal conductivity, ρ is the density, C_P is the thermal heat capacity, H is the internal heat production, P the deviatoric pressure, g the gravity and T the temperature.

In our model, the upper crust, lower crust, mantle lithosphere, crustal scar and mantle scar are represented by five distinct compositional fields that are advected with the computed flow velocity. For each field c_i, this formulation introduces an additional advection equation to the systems of equations:

$$\frac{\partial c_i}{\partial t} + \boldsymbol{u} \times \nabla c_i = 0 \quad (3.4)$$

The brittle (plastic) behaviour of the model follows a Drucker-Prager yield criterion in which the yield stress is calculated using the following function of cohesion (C), angle of internal friction (ϕ), and pressure (P):

$$\sigma'_{eff} = C cos\phi + P sin\phi \quad (3.5)$$

Equations (3.1 - 3.5) are solved using the finite element method, where the model is discretized into finite elements and the solution (e.g. velocity, temperature, compositional fields, viscosity) is expanded using Lagrange polynomials as interpolating basis functions (Glerum et al. 2018). Equations 3.1 and 3.2 are solved using an iterative Stokes solver (Kronbichler et al. 2012). The models use a temperature-dependent density in all governing equations, but no pressure dependence, since the model is incompressible. We solve the temperature and composition equations (Equations 3.3 and 3.4, respectively), once at the beginning of each time step and then iterate out the solution of the Stokes' equations to a solver.

3.2.2 Model setup and boundary conditions

The numerical simulations are conducted in a 2D box 800 km (x-axis) wide by 200 km (y-axis) deep which fits the dimensions and scale of the North China rift systems. The computational grid is spaced in 10 km elements initially which is locally reduced to 0.625 km^2 elements based on thermal energy and density contrasts. Resolution tests show no significant differences to the model results at higher resolutions.

The model lithosphere is composed of 5 different compositional fields representing the upper and lower crust, a crustal and mantle scar as well as the mantle lithosphere (Fig. 3.2a). The model extends beyond the base of the lithosphere and the lowermost part represents the asthenosphere. However, the mantle lithosphere and asthenosphere have the same rheological and density parameters in this model and their deformation behaviour entirely depends on the temperature. The rheological parameters assigned to each compositional field are summarised in Table 2. The initial upper crust and lower crustal thicknesses do not vary in our model and are 30 km and 15km thick, respectively, based on current estimates of crustal thickness under the undeformed Ordos block (Chen et al., 2021). We use a wet quartzite flow law for the upper crust (Rutter and Brodie, 2004) and a wet anorthite flow law for the lower crust (Rybacki et al., 2006), while the mantle lithosphere has a dry olivine rheology (Hirth and Kohlstedt, 2004). Values used for each compositional field are found in Table 2 and are scaled to plane strain from uniaxial experiments (Ranalli, 1995).

We implement two different inherited heterogeneities, one at the crustal level and one at the lithosphere level. The crustal heterogeneity is a 110 km wide field (about the width of the TNCO) while the mantle scar is a 10 km thick discrete structure dipping at 45° to mimic the geometry of a relict slab or suture. We computed models with different combinations of crustal and mantle heterogeneities (with both, only one and without any) to test the relative importance of each on the behaviour of the model

(see supplementary material Fig. S3.4-7). The mantle scars have the same rheological parameters as their surrounding material, apart from a lower angle of internal friction

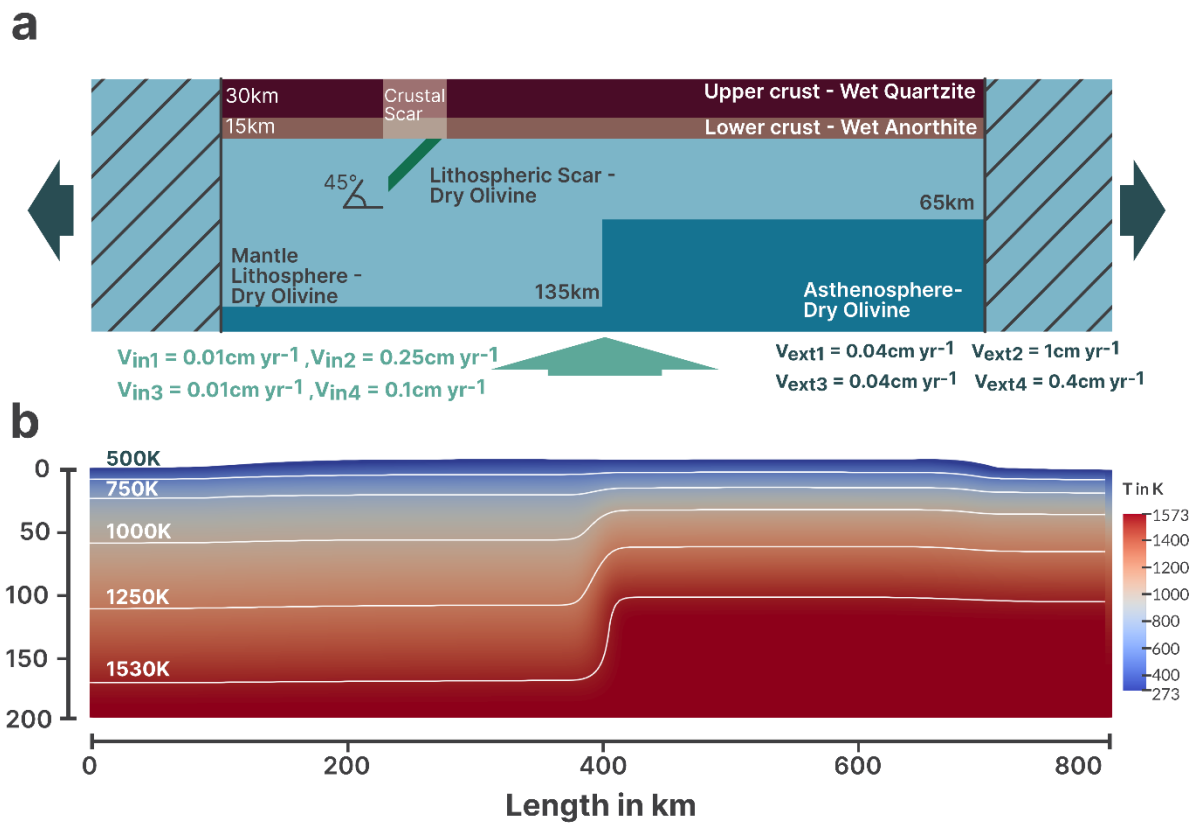

set at 2° for the initial model (compared to 20° for the surrounding material) to mimic their rheologically weaker behaviour (Heron et al., 2019, 2016). The angle of internal friction of the mantle scar is varied for different models to test its influence on deformation.

Figure 3.2 Thermal and Compositional Model Setup

a) showing the thickness of the different compositional fields, the material used, and the velocities imposed at the boundaries. At the edges, we impose two 100 km wide fields of reference material to avoid edge effects. b) thermal model – shows the thermal state of the model after the initial period of isostatic re-equilibration. 1573K is denoted as the base of the lithosphere.

Table 2 -Physical Parameters of the Model

Table 2

Physical Parameters of the Models

Property	Unit	UC	LC	ML	A	CS	LS
Density	**kg/m^3**	2700	2850	3300	3300	2700	3300
Thermal diffusivity[1]	**$m^2 s^{-1}$**	$1.48x10^{-6}$	$1.40x10^{-6}$	$1.33x10^{-6}$	$1.33x10^{-6}$	$1.48x10^{-6}$	$1.33x10^{-6}$
Flow law		WQtzt	WAnth	DryOl	DryOl	WQtzt	DryOl
Dislocation Creep	**$Pa^{-n} s^{-1}$**	$8.57x10^{-28}$	$7.13x10^{-18}$	$6.52x10^{-16}$	$6.52x10^{-16}$	$8.57x10^{-28}$	$6.52x10^{-16}$
Power law exponent[1]		4	3	3.5	3.5	4	3.5
Activation energy[2]	**$J\ mol^{-1}$**	$2.23x10^5$	$3.45x10^5$	$5.30x10^5$	$5.30x10^5$	$2.23x10^5$	$5.30x10^5$
Activation volume[2]	**$m^3\ mol^{-1}$**	0	0	$1.80x10^{-5}$	$1.80x10^{-5}$	0	$1.80x10^{-5}$
Thermal expansivity[1]	**K^{-1}**	$2.00x10^{-5}$	$2.00x10^{-5}$	$2.00x10^{-5}$	$2.00x10^{-5}$	$2.00x10^{-5}$	$2.00x10^{-5}$
Specific heat[1]	**$J\ kg^{-1} K^{-1}$**	750	750	750	750	750	750
Heat production[3]	**W/m^3**	$1.50x10^{-6}$	0	0	0	$1.50x10^{-6}$	0
Angle of internal friction[3]	**degrees**	20	20	20	20	2	2
Cohesion[3]	**Pa**	$2.00x10^7$	$2.00x10^7$	$2.00x10^7$	$2.00x10^7$	$2.00x10^7$	$2.00x10^7$

Flow law references Wet Quartzite (Rutter and Brodie, 2004); Wet Anorthite (Rybacki et al., 2006); Dry Olivine (Hirth and Kohlstedt, 2003). Other physical parameters from 1 – Gouiza and Naliboff (2021); 2 – Naliboff and Buiter (2015); 3 – Heron et al., (2019)

The initial thermal structure is consistent with the applied boundary conditions, i.e. the thermal properties, heat flow and heat production are consistent with a basal mantle potential temperature of 1300°C = 1573K and a surface temperature of 0°C = 273K.

The initial thermal structure is described using the following equations:

$$T(z) = T_t + \left(\frac{q_t}{k}\right) z - \frac{A\, z^2}{2\, k} \quad (3.6)$$

$$q_t = q_b + (A\Delta z) \quad (3.7)$$

where the temperature T is solved for a given depth z. T_t is the temperature at the layer surface (top), q_t is the heat flow at the top of the layer while q_b is the heat flow at the base of the layer, k is the thermal conductivity, and A is the radiogenic heat production with Δz being the thickness of the layer. We use these equations to calculate the temperature for each compositional layer using the layer-specific thermal values from Table 2 ensuring continuity across the layers.

In our model, we specify two blocks with distinct variations in lithospheric thickness and geotherms based on two different surface heat flow rates. The thickness of the lithosphere in this model is largely based on the geotherm. The base of the lithosphere is fixed to 1573K (1300°C); therefore, we model a steeper geotherm for the hotter, eastern lithosphere than for the colder and thicker western lithosphere. In all our models the base of the western lithosphere is kept at a constant depth of 180 km with a surface heat flow of 67mW/m^2. The thickness of the eastern lithosphere varies throughout different model runs and the thermal properties and surface heat flow vary from 67mW/m^2 to 92mW/m^2 however values for heat production, specific heat, thermal expansivity and conduction are kept constant (Tabel 2). The heat flow values for computing the geotherms across a range of lithospheric thicknesses can be found in the supplementary material (Table 3). The values for surface heat flow agree with present-day measured values in North China (He and Zhang, 2018). Figure 3.2b shows the thermal profile of an example model (M21) where the eastern lithosphere is 110 km thick.

We prescribe different velocities during the 60-million-year runtime of the models, based on published data about the kinematics of the North China Rift systems. At the

start there is a period of negligible extension of 0.1mm/year, aimed at re-equilibrating the model that has initially stark temperature and compositional difference, this also broadly coincides with a period of slow tectonic movements in North China in the Early Eocene to Oligocene. While the Bohai Basin has a protracted history of rifting which started in the Early Paleogene, the period of fast subsidence evidenced by the distribution of syn-rift sediments is remarkably short. Ren et al. (2002) found that subsidence rates were highest during the deposition of the Shahejie Formation in the Middle to Late Eocene. While late members of the Shahejie Formation formed in the Oligocene the subsidence rate decreased significantly towards the end of the Oligocene (Ren et al., 2002). Therefore, the period of fast rifting and subsidence was from approximately 45-32.8 Ma (Fu et al., 2022). This fast-rifting period was only about 10-15 Myr for the initial rifting of the Bohai Basin. Therefore, we model the initial period of rifting to be 15 myrs long in our model from 10 to 25 Myr imposing a velocity of 5mm/yr on each side, giving a total extension rate of 10 mm/yr. Towards the late Eocene extension rate and overall tectonic rates in North China slowed down again until the opening of the Shanxi Rift. The initiation of the Shanxi Rift is well constrained to the late Miocene (~10 Ma) by recent studies (Su et al., 2023; Xu et al., 1993). Based on this we impose a 25 million-year period of very slow extension of 0.1mm/yr, followed by 10 million years of slow rifting (2mm/yr on each side; 4mm/yr total extension) which represents the initiation of the Shanxi Rift. Extension rates in Shanxi range from about 1-6mm/yr (Shen et al., 2000; Middleton et al. 2017; Su et al. 2023) and 4mm/yr agrees well with extension rates found by Shen et al. (2000) for the northern Shanxi basin and Su et al. (2023) measurement for the Linfen basin.

We set the minimum viscosity of the models to 10^{18} Pa s and the maximum viscosity to 10^{25} Pa s, as at maximum viscosities above that we found the models can become numerically unstable. However, during test runs at viscosities of 10^{24} Pa s, 10^{25} Pa s

and 10^{26} Pa s, we found little difference in the overall behaviour of the different models.

3. 3 Results

For this study, we computed over a hundred different models to recreate the spatio-temporal rifting behaviour observed in North China. We test our models against four conditions that are key features of the rift spatiotemporal history in North China:

- Extensive (wide) rifting forms in the eastern block forming a wide rift (equivalent to the Bohai Basin) during initial deformation.
- Little to no strain was accommodated in the western block during the initial rifting.
- A switch in rift locus from the eastern to the western block occurs after a period of tectonic quiescence and the start of the second rifting episode.
- Little strain accommodated in the eastern block during the second rift episode.

We found a limited range of model parameters produced results that fit the key features above satisfactorily. Here we present a representative of these 'successful' models in detail in the following. After presenting this example, we will present examples of models that do not meet the key features of rifting North China and analyse the parameters that caused them to fail.

3.3.1 Representative model that matches the key features

Model 21 shows stark differences between the two blocks which govern the behaviour of the two blocks throughout their evolution. These differences are mainly differences in temperature and viscosity. After an initial rapid phase of isostatic adjustment, the model starts with a setup that shows a drastic temperature difference. At 60 km depth, which is in the uppermost lithosphere just below the crust, the western block

reaches a temperature of about 980 K, while the eastern block (on the right side of the model) is at 1180 K, i.e. a difference of 200 K (Fig. 3.2a).

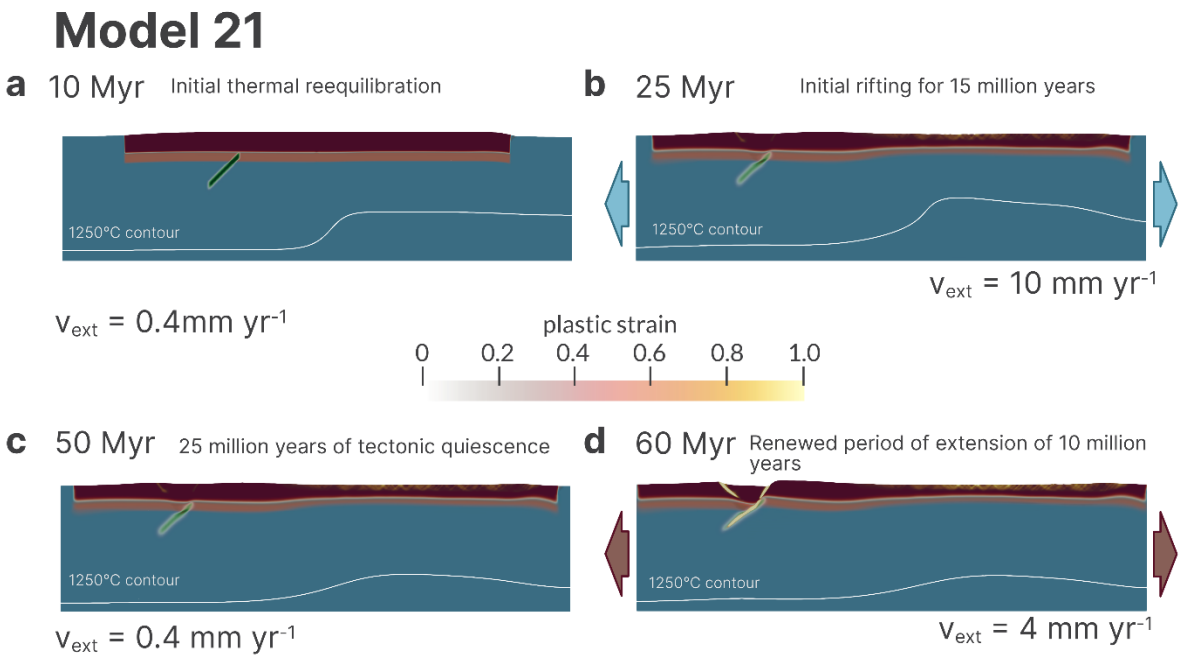

Figure 3.3 Model 21 at Different Evolutionary Stages

Model 21 matches the key features of the time protracted rifting in North China. Background colours are the same as for the compositional model set up in Fig. 3.2a (Upper crust – dark brown, lower crust – light brown, mantle – light blue, mantle scar – dark green), while accumulated plastic strain is plotted on top. The white line denotes the 1250°C isotherm, which can be used as a proxy for the base of the lithosphere. Initial extension at 10 mm yr-1 sees most strain accommodated in the eastern block (b). After a break in extension (c), the model is extended again for 10 million years at 4 mm yr 1(d). Now rifting is accommodated in the western block

exploiting the pre-imposed mantle scar.

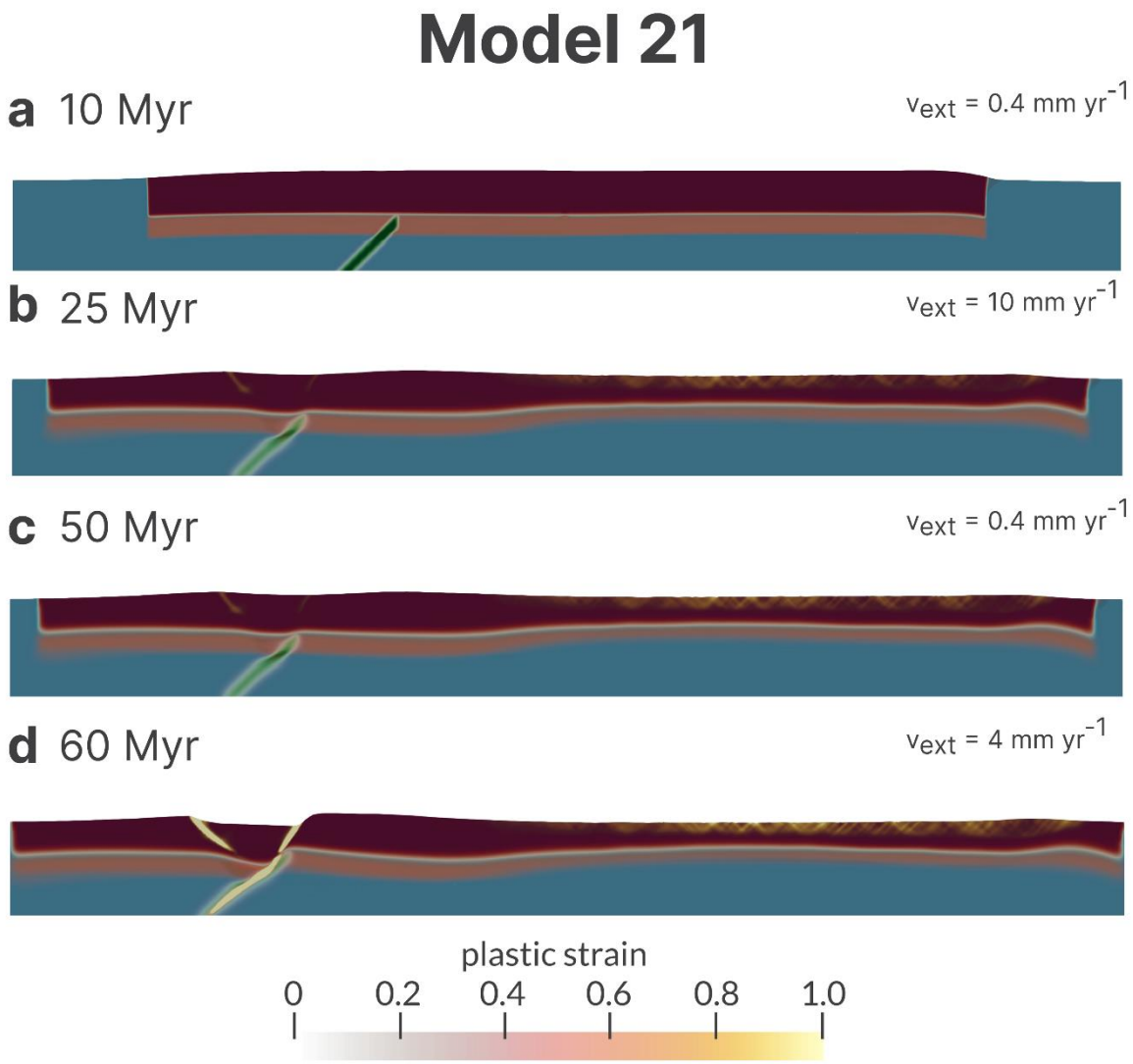

Figure 3.4 Close-up of Model 21 – Focusing on the Crustal Deformation

Focusing on the upper part of the lithosphere only – see Fig. 3.3

During the first period of rifting from 10 Myr to 25 Myr there is a significant amount of plastic strain accommodated in the eastern block (Fig. 3.3b; 3.4b) from 400-700 km. There is some plastic strain accumulating in the western block, but it is minor in comparison to the broad deformation zone in the eastern block (see Fig. S3.3 for details). While strain distribution in the east is broad almost spanning the whole region, in the West the small amount of strain that is accommodated on a small number of

localised fault systems sits above the shallowest part of the mantle scar and the deepest part of the mantle scar. The strain rate in the east is much higher at this point and reaches up to 10^{-14} s^{-1} and is high over a much wider region than in the West, where the strain rate reaches 10^{-16} s^{-1} to 10^{-15} s^{-1} in isolated regions where the inherited weaknesses are located (Fig. 3.5b). However, there is little plastic strain accommodated overall in the west and the faulting is limited to small superficial amounts.

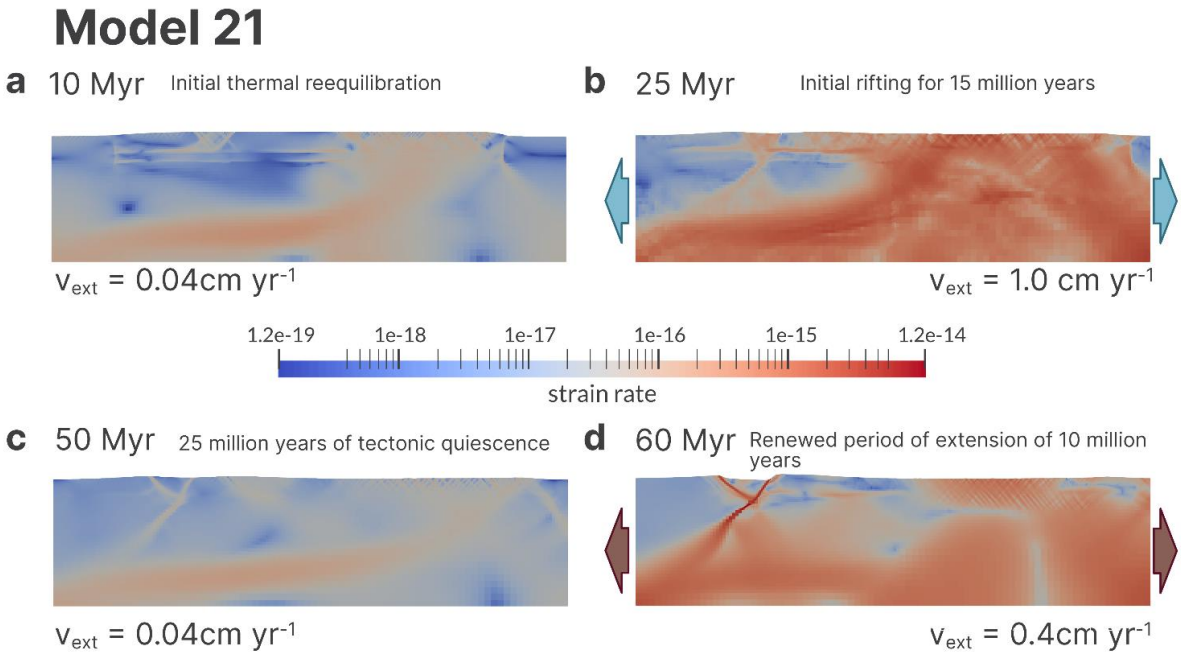

Figure 3.5 Strainrate of Model 21

Showing the strain rate (logarithmic scale) for the working model. The strain rate is low across the whole model with slightly elevated strain rates in the East. During the first phase of extension, the strain rate is very high but diffuse across the eastern block but low in the west, except for slightly elevated strain rates in the weakened area. This is followed by low strain rates across most of the model in the 25 million years of negligible extension. When extension speeds up again, the high strain rates are localised in a narrow region above the lithospheric weakness in the west,

however, there still are areas in the east with elevated strain rates, possibly due to reactivation of previously formed faults.

During the phase of tectonic quiescence, there is, as expected, a lot less strain accommodated (Fig. 3.5c). This allows the temperature of the two blocks to start re-equilibrating. The eastern block now rapidly cools, visible as the 1530 K contour (used as a proxy for the base of the lithosphere) flattens and increases in depth over the quiescent period, which thickens the lithosphere again (Fig. 3.3c; 3.4c) after the rifting phase. The viscosity increases across the whole model but most significantly under the thinned eastern block (Fig. 3.6). Initially, there is a large difference in maximum viscosity across the eastern and western blocks with specifically the upper mantle lithosphere reaching a value of 10^{23} Pa s while the Western block exceeds the maximum viscosity of 10^{25} Pa s. However, at the start of the second rift period at 50 million years (t = 49 Myrs – just before the velocity increase) the eastern block has drastically increased in viscosity (and therefore strength) and is reaching 10^{25} Pa s. It also shows how the crust has thinned as the strongest point of the eastern block – equating to the uppermost part of the lithosphere - is at about 40 km while in the west it is at about 45-60 km. Therefore, the large strength contrast between the two blocks from the start of the model (t = 10 Myrs) has now almost balanced out.

After the quiescent period, the strain rate is much higher in the west than it is in the east and plastic strain rapidly accumulates above the mantle scar in the western block. Strain immediately localises onto two zones of high plastic strain forming a graben-like zone with uplift on either side (Fig. 3.3d; 3.4d). The mantle scar is now involved in the deformation and shows high strain rates and accumulates significant amounts of plastic strain. There is barely any new plastic strain accumulated across the faults in the eastern block which are now largely dormant. This is also seen in the strain rate (Fig. 3.5d) where the strain rate is highly localised in the west onto distinct

structures while it remains lower and more distributed in the east.

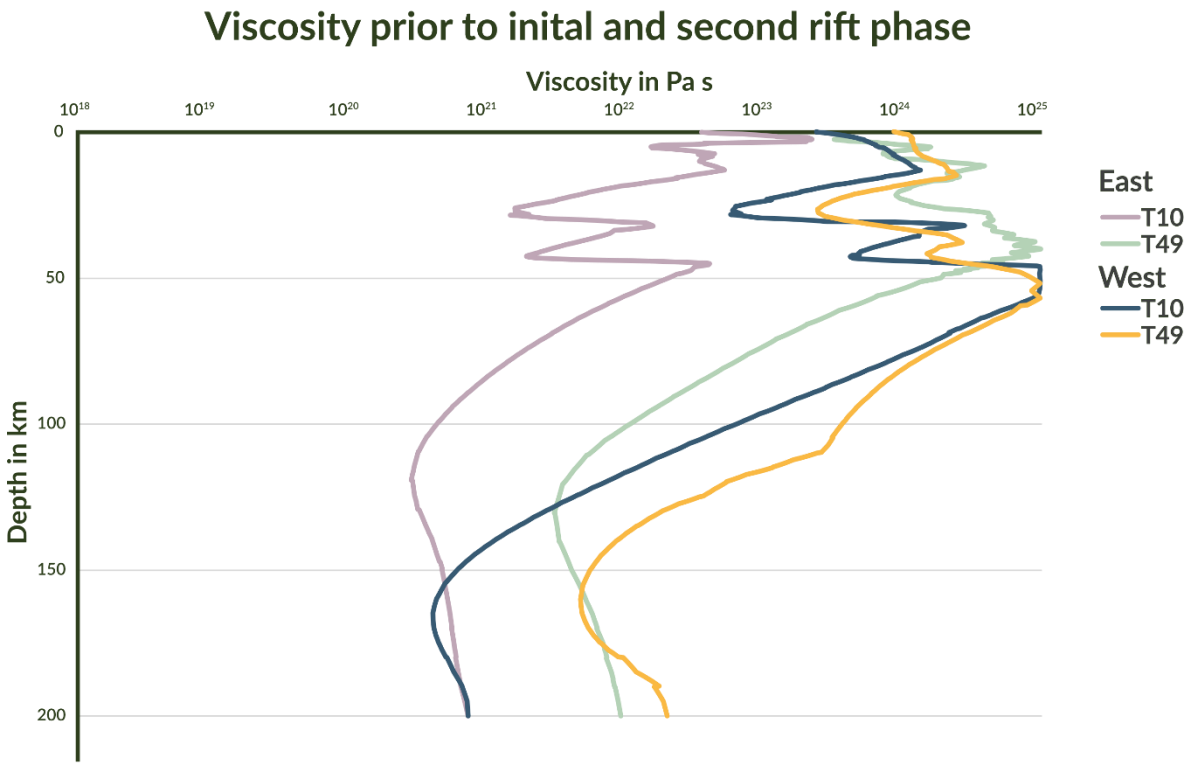

Figure 3.6 Viscosity Plot of Model 21

Viscosity plot showing the difference in viscosity between eastern and western blocks at timestep T10 (start of the first rifting period) and T49 (start of the second rifting period), notice how the viscosity of the two blocks is more similar at T49.

3.3.2 Parameter Space Exploration

To better understand what influences the rifting behaviour of North China and rift migration in general we explored a range of different parameters such as initial and subsequent extension velocity, presence of crustal heterogeneities, length of rift paucity, dislocation creep pre-factors of the mantle scar as well as different scar geometries. While all of these had subtle effects on the model and the overall rift geometry, we found the rifting migration pattern is mostly governed by two parameters: The relative difference in initial lithospheric thickness between the western and eastern parts of the model and the strength of the mantle scar (using the

angle of internal friction as a proxy). The western lithosphere was fixed to the value of 180 km during the parameter space exploration, this value is sensible considering the low amount of modification of the cratonic lithosphere underneath the western part of the North China Craton. The initial thickness of the eastern lithosphere was varied from 60-180 km. Constraints of the initial lithospheric thickness of the eastern block are uncertain and estimates vary, and whether the lithosphere underneath the eastern NCC was completely detached (which would imply a thin lithosphere) or was thermally eroded (which would imply a slightly thicker lithosphere) is a matter of debate (Wu et al., 2019). Varying the angle of internal friction for the mantle scar can be a proxy for the varying rheological weakness of these features. Mantle scars have reduced grain size, as they represent ancient deformation and subduction zones which led to a reduction of grain size (Berovici and Ricard, 2014). The presence of fluids within the mantle scar and potential high hydrostatic pressures could also further weaken these inherited structures in the lithospheric mantle. The exact cause of their low rheological strength is beyond the scope of this study; however, the angle of internal friction can serve as a proxy for the rheological strength of the mantle scar. Changing these parameters leads to vastly different behaviours in rift morphology and rift migration patterns most of which do not match the key features for NCC rifting outlined above.

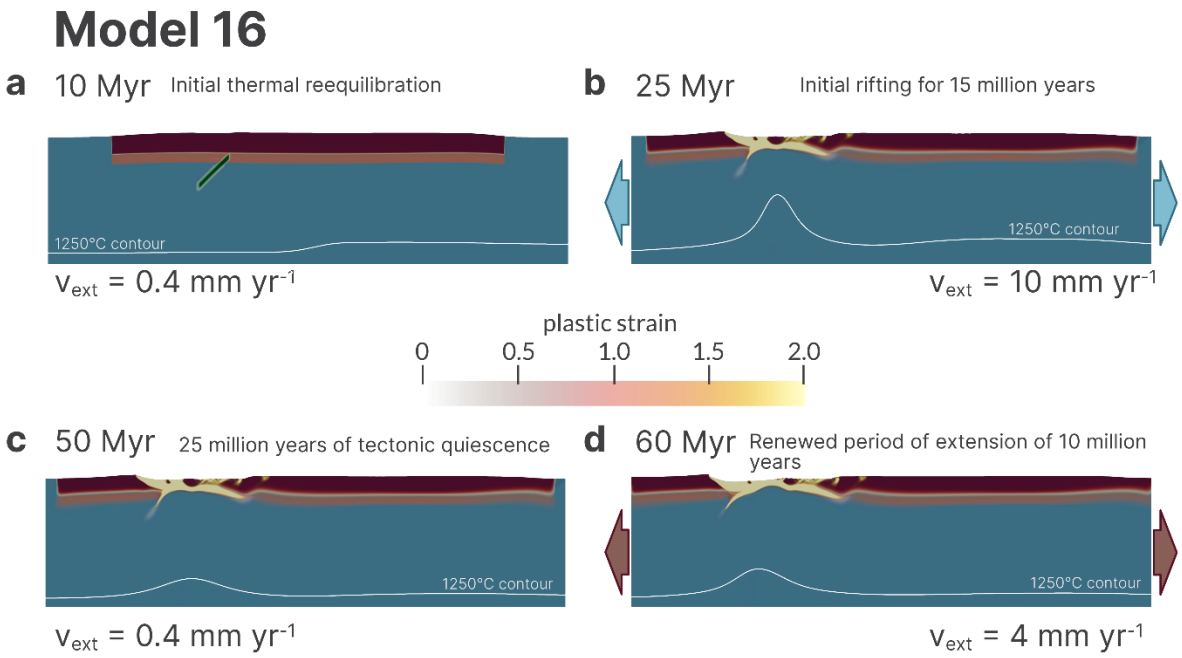

Figure 3.7 Model 16 at Different Evolutionary Stages

Model 16 shows the behaviour of the model if the Eastern and Western lithosphere are too similar in thickness for a given angle of internal friction (in this case 2°). The Eastern lithosphere here is 170 km thick, as opposed to 110 km in the working model. Colours are the same as for the compositional model set up in Fig. 3.2b (upper crust – dark brown, lower crust – light brown, mantle – light blue, lithospheric weakness – dark green) A white line denotes the 1530 K which can be used as a proxy for the base of the lithosphere. During the first 15 million years of rifting instead of rifting in the east as in the previous model, it now exploits the weakest part of the model which is the lithospheric weak zone as the difference in thickness between the two blocks is not significant enough. Therefore, a rift establishes in the west rapidly. During the period of quiescence, the lithosphere underneath the rift in the west cools slightly but during the renewed period of extension, the rift in the west reactivates and forms a broader zone of deformation.

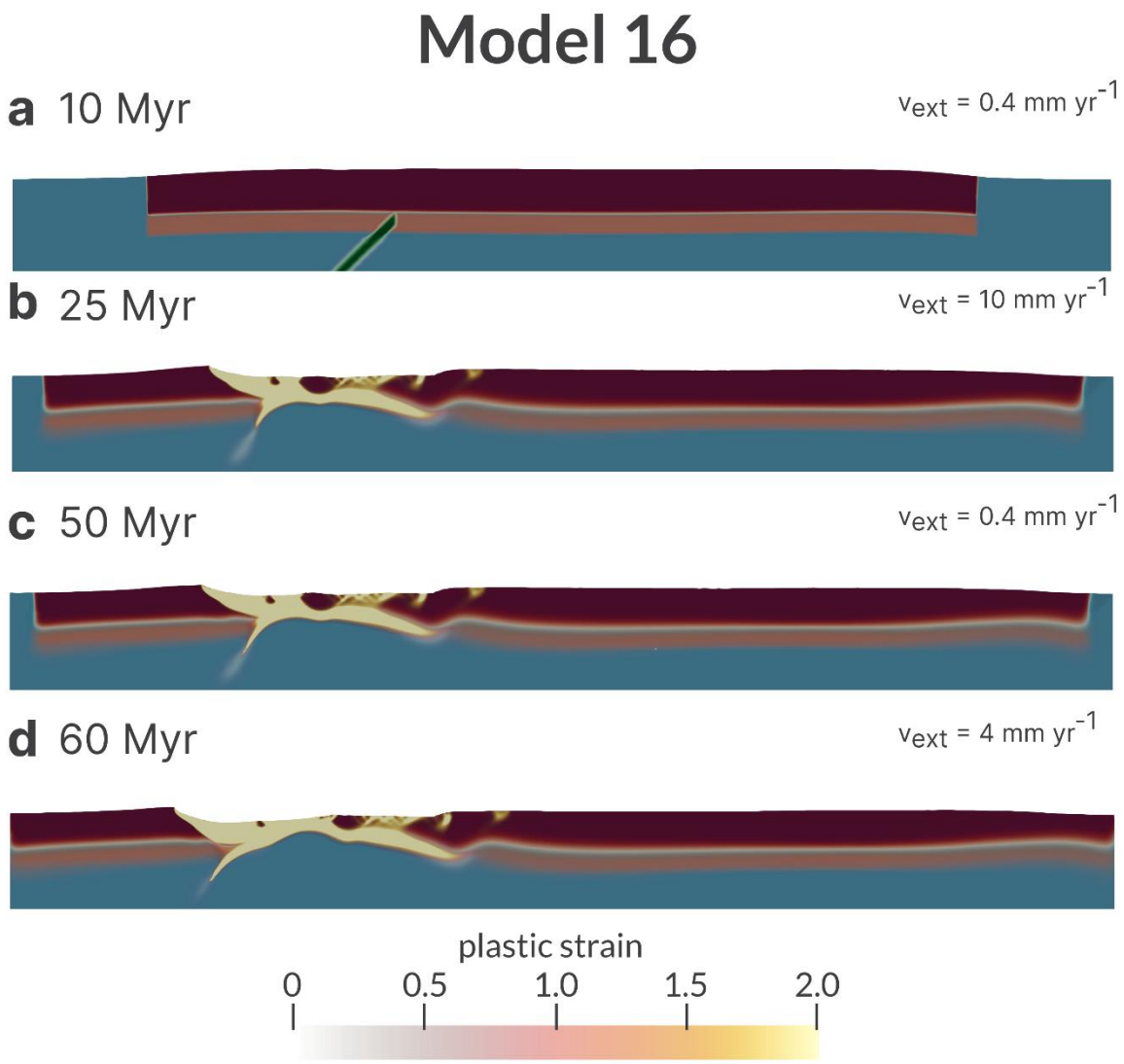

Figure 3.8 Close-up of Model 16 – Focusing on the Crustal Deformation

Focusing on the upper part of the lithosphere only – see Fig. 3.7

Models 16 and 34 show two examples of models that illustrate the importance of these parameters. Model 16 (Fig. 3.7 and 3.8) has a much thicker eastern lithosphere compared to the reference model at 160 km, while the other parameters are the same as for the reference model. At the start of the rifting, the strain rate is evenly distributed across the eastern and western blocks if slightly more localised onto discrete structures in the west. Over the first 10 million years of rifting, however, the

strain quickly localises onto the lithospheric weak zone and the faults above with a narrow rift establishing in the western part of the model and little plastic strain accumulating in the east. Hotter mantle material underneath the rift in the west starts to rise. During the period of quiescence, the strain rate across the whole model is low as expected and the model thermally re-equilibrates. After the quiescent period the rifting restarts in the west. High strain rates immediately localise over the previously formed rift and there is no strain accommodated in the east. Therefore, the distinct migration of rifting from east to west is not observed for a given angle of internal friction (here ϕ = 2°) if the lithospheric thickness of the two blocks is too similar.

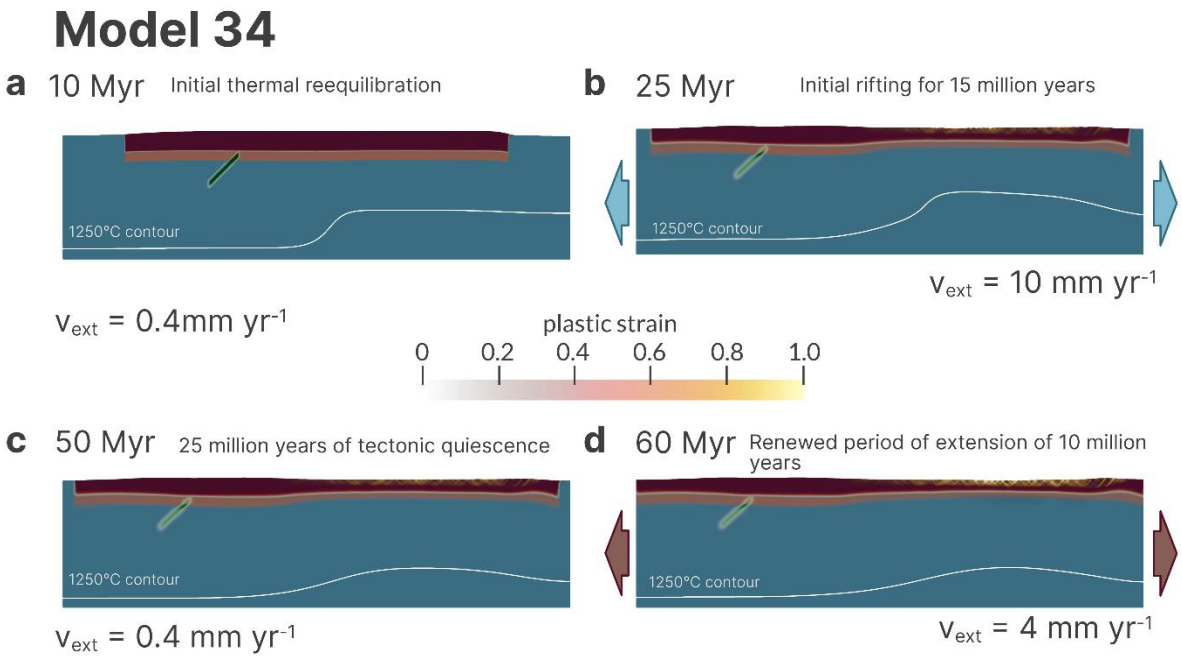

Figure 3.9 Model 34 at Different Evolutionary Stages

Model 34 shows the behaviour of the model if the eastern lithosphere is too thin or the angle of internal friction is too high (in this case 5°). Colours are the same as for the compositional model set up in Fig. 3.2b (Upper crust – dark brown, lower crust – light brown, mantle – light blue, lithospheric weakness – dark green) A white line denotes the 1530 K which can be used as a proxy for the base of the lithosphere.

During the first 15 million years of extension a wide rift is formed in the eastern block similar to M21 (Fig. 3.3). However, this time after the period of quiescence, the rifting does not migrate to the west. The lithospheric weakness, this time with a higher angle of internal friction, is not weak enough to localise rifting, therefore instead rifting continues in the east.

Model 34 (Fig. 3.9 and 3.10) shows an example of where the angle of internal friction of the weak zones has been increased to 5° instead of 2° as for the original model, thus making the suture slightly stronger. The thickness of the lithosphere however remains the same as the reference model. At the start of the model, it behaves similarly to the reference model (Model 21). The rifting starts as expected in the east within the thinner lithosphere. In the first 3-4 million years of the initial extension phase (Fig. 3.9b) there is a small amount of strain accommodated in the west above the weakness but soon all strain localises completely in the east. During the quiescence in the viscosity and temperature field, the lithosphere thickens and strengthens as it re-equilibrates but there remains a stark strength contrast between both blocks. As the rifting restarts most, plastic strain is again accommodated in the east and the rifting starts to localise further in the east, but very little strain is accommodated in the west. Strain accumulates mostly above the weak zone but also along the edge between the eastern and western lithosphere. While the lithospheric architecture is similar to the original model where the rift migration was observed, here the lithospheric weak zone is not weak enough to facilitate the migration of the locus of rifting to the west and the rifting remains confined to the eastern block.

Naturally, the resulting behaviour of rifting behaviour and dynamics does not just fall into these three idealised cases and exists on a spectrum. The results of over 100 simulations are summarised in Figure 3.11 with Models 16 and 34 identified. Broadly the trend shows that as the lithospheric thickness of the eastern block increases so

must the angle of internal friction to make the rift migration work, otherwise the mantle scar will be too weak and focus all deformation from the start. However, if the mantle scar is not weak enough and the angle of internal friction is too high for a given lithospheric thickness contrast the migration will equally not occur as the mantle scar is now “too weak”. This forms a “Goldilocks zone” narrowing as the angle of internal friction increases. No model with a mantle scar that had a value of 7° or higher was found to fulfil all the conditions necessary to be considered an actualist model. Therefore, the mantle scar must at least be 65% weaker than the surrounding lithosphere to focus on the locus of rifting after tectonic quiescence.

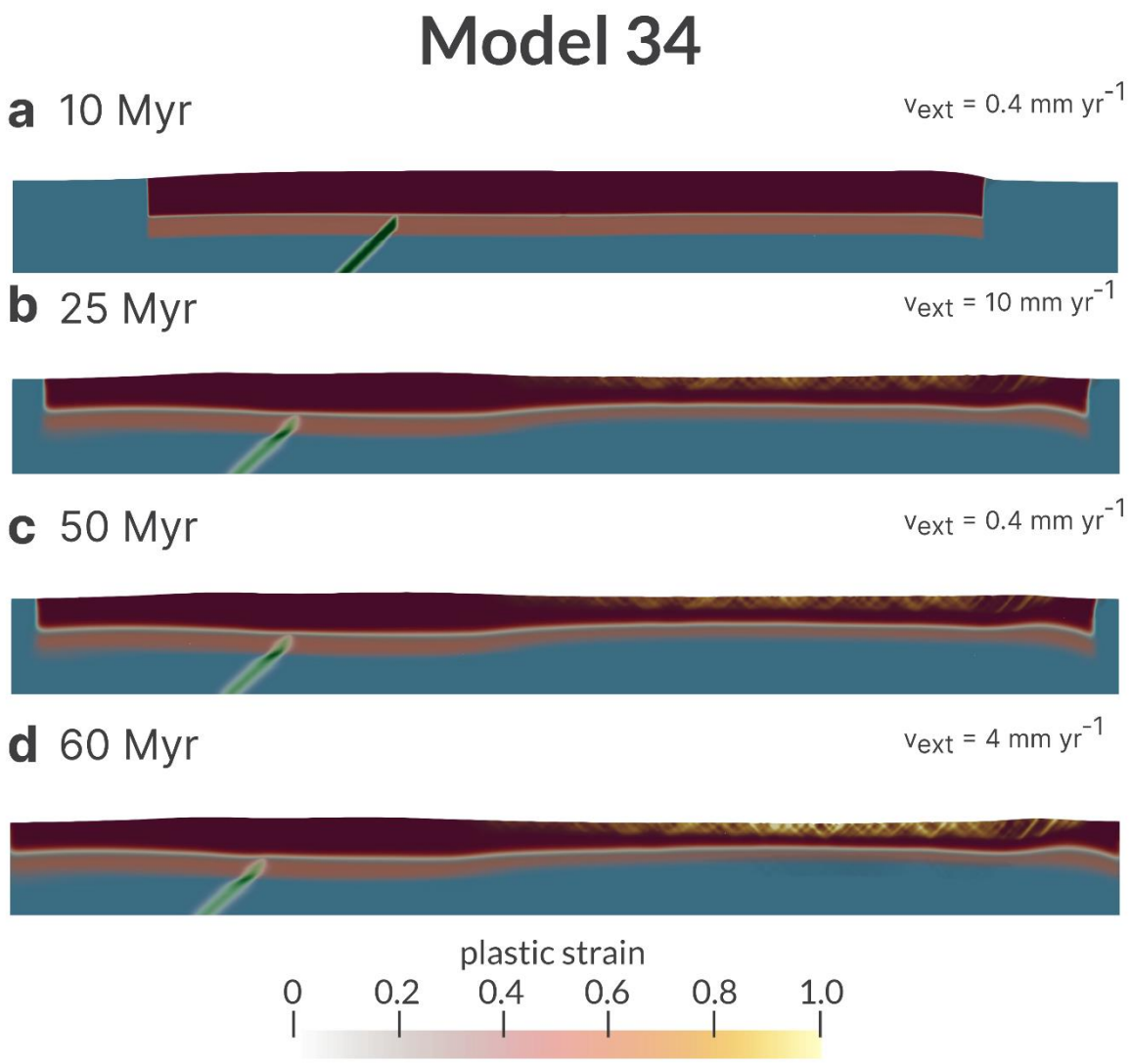

Figure 3.10 Close-up of Model 34 – Focusing on the Crustal Deformation

Focusing on the upper part of the lithosphere only – see Fig. 3.9

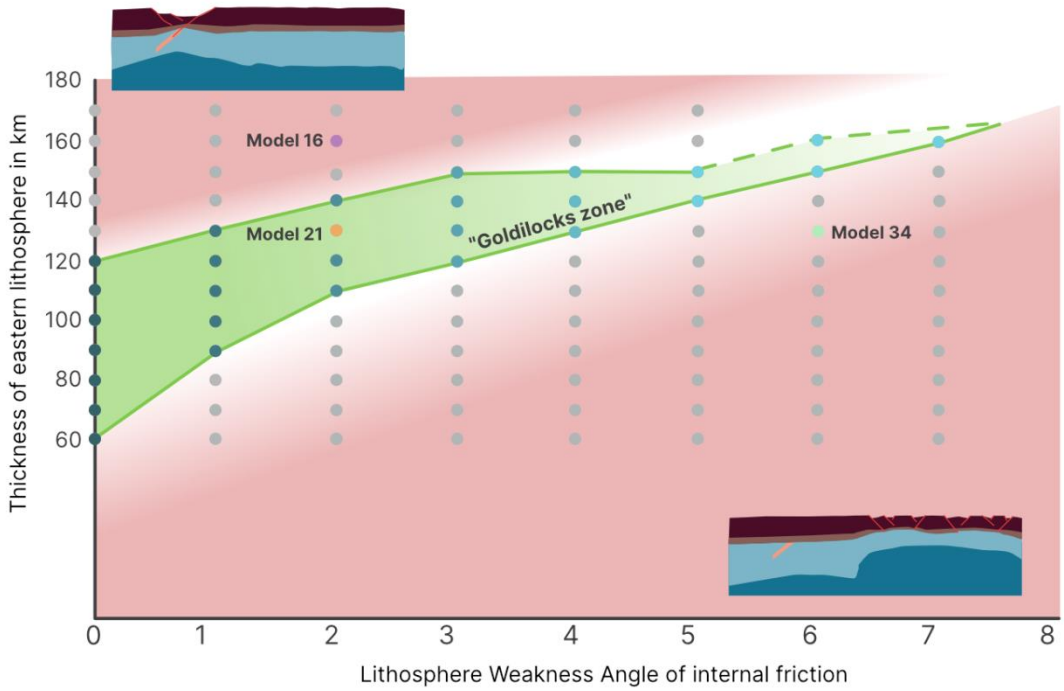

Figure 3.11 Balance of Lithospheric Thickness Variation and Mantle Suture Weakness

Diagram showing the zone where models "work", i.e. the deformation migration pattern observed in North China is reproduced. Over 100 different models were tested with variations in the initial lithospheric thickness and the angle of internal friction of the lithospheric weak zone (Table 4). We found a region where the two are in balance to facilitate the rifting behaviour as it is observed – termed the "Goldilocks zone". In these bounds rifting will start within the eastern block at the onset of extension at 10 Myr and then migrate to the western block after a period of quiescence at 50 Myr. Outside of these bounds, the rifting will either start in the west and not affect the east, as seen for Model 16 (see Fig. 3.7) or rifting will initiate in the east but not migrate to the west, as seen for Model 34 (see Fig. 3.9)

3.4 Discussion

3.4.1 Comparison with Previous Numerical Modelling

In this study, we present a series of 2D thermo-mechanical models examining the influence of lithospheric architecture and discrete lithosphere scale weakness on rift migration. The models presented all require a period of tectonic quiescence during which the eastern lithosphere can thicken and strengthen, between the rift periods to recreate the rift migration pattern of North China (see Fig. S3.4 for a model run without a break in extension). Healing and strengthening of the lithosphere post-extension or during periods of slow extension was modelled by Braun (1992) and van Wijk and Cloetingh (2002). These studies showed that periods of quiescence or slow rifting are conducive to rift migration and may explain rift migration observed in areas such as the Canning Basin, Australia or the Norwegian Margin. Previous modelling work by Naliboff and Buiter (2015) tried to quantify this behaviour further and showed that the duration of cooling and quiescence is essential in determining whether a rift migrates. The duration of quiescence in our model overall agrees well with the range of cooling times required for migration found in their study which is 20 – 60 Myr depending on a range of other factors such as rheology and extension velocity. This modelling study expands on the earlier studies by varying the pre-rift lithospheric architecture to see the effect this has on migration behaviour. We found that a quiescent period is important in the rift migration as it strengthens the eastern part of the lithosphere, the inherited factors contributed to that and facilitated the migration behaviour further. However, the exact duration of the quiescent period was of secondary relevance, as the migration behaviour occurred also when this period was shorter or longer. Only when significantly reducing the length of the quiescent period (<15 Myr) would we see reactivation in the east rather than migration, although this also depends on the “weakness” of the mantle scar. This adds to the findings of

Naliboff and Buiter (2015) who used a three-layer model with no thickness variations and inherited structures and found that the duration of the quiescent period dictated if rift reactivation or migration occurs. Our models show that the pre-existing lithospheric architecture and the presence of a lithospheric weak zone also significantly impact the migration behaviour and may be more important than the duration of the quiescent period. Inheritance not only influences the spatio-temporal patterns of rifting but also the style of rifting. The eastern and western blocks show different rheologies in their pre-rift configuration due to their different lithospheric thickness, resulting in a wide rift in the eastern block and a narrow one in the western block. Gouiza and Naliboff (2021) show in numerical models the impact of rheology and lithospheric architecture on the formation and segmentation of rifted margins. They show that not only does the reactivation of discrete inherited weaknesses impact the evolution of rifted margins but also the general pre-rift rheology and architecture will govern which processes act during rifting. In our models, the cold and thick lithosphere of the western block likely favours the formation of a narrow rift (Brun, 1999), possibly located by the re-activation of a discrete structure, i.e. the inherited (lithospheric) structure. The importance of lithospheric architecture and strength was also shown by Brune et al. (2017) where thinned crust underlain by strong mantle lithosphere of the Turkana depression, results in the segmentation of the Kenya and Ethiopia rift. The influence of inheritance on rifting has seen much attention in recent years, however, most studies focus on crustal-scale inheritance. However, our models show that for migration of rifting a deeper-seated inherited structure in the mantle is needed in the example of North China with a thick (cratonic) lithosphere. Fig. 3.6 shows that the bulk strength of the western lithosphere is situated in the upper mantle, therefore a reduction in the strength of the crust above will not significantly affect the localisation of rifting. Only with a mantle weak zone (“mantle scar”) does

rifting migrate to the west (compare with Fig. S3.5 and S3.6 which do not contain any inherited structures or just a crustal one). Reducing the angle of internal friction is the most efficient way of making this scar weak in the models and Heron et al. (2016, 2019) showed how a mantle scar can segment a rift and control the rifting process. This matches well with our observations as we found the presence of a mantle scar and its angle of internal friction (as a proxy of the rheological strength of the scar) was the most important factor in guiding the migration of rifting to the west. Without a mantle scar, we did not observe migration to the west. The presence of a crustal scar in addition to a mantle scar (such as shown in Fig. 3.3) aids the overall strain localisation and leads to more realistic rift architectures, but model runs without a crustal scar still recreate the overall migration pattern (Fig. S3.7). Therefore, we can show not only that the rift migration in North China is a combination of numerous factors but also how inherited parameters can influence migration behaviour.

While the Shanxi Rift and the Circum-Ordos rifts have been extensively researched in the field (Xu and Ma, 1992; Shi et al. 2015a), only recently has it seen attention in numerical modelling studies. Wang et al. (2020) showed in a model how the thermal state of the lithosphere of North China can explain the difference in rifting style between Shanxi and the North China Plain. This compares well with our results as we also show that the lithospheric architecture and the initial thermal state determine if rifting will be more distributed or localised. They also showed how lithospheric heterogeneity is important in creating the Shanxi Rift, which matches well with our results. However, their study does not include the period of quiescence between the rifting of Bohai and the Circum-Ordos-Rifts and the time difference between the initiation of the two rift events because they use a constant extension velocity, leading to two rifts (one in the eastern and one in the western block) forming simultaneously. They also model a broader rheological weak zone instead of the thinner dipping ‘scar’

used in this model, which may be a less realistic shape for the weak zone if these sutures are relict subduction interfaces. Lin and Liu (2019) use a similar broad geometry for their lithospheric weak zone which extends to the bottom of the lithosphere, to show the importance of an inherited weakness in the formation of the Shanxi Rift. Their models also do not reproduce the time-progressive migration of deformation across North China in the Cenozoic. He et al. (2003, 2004) showed how a crustal weakness combined with topography-induced gravitational stress can create a rift in the Shanxi region. Their model only considers the upper 40 km of the lithosphere, therefore their inherited weakness is only present in the crust. While crustal weaknesses may be important in the segmentation and local architecture of a rift, our models show that the location of a rift is more influenced by weaknesses in the strongest layer of the lithosphere which is often (especially in cases of the cold lithosphere as for North China) the upper mantle (Fig. 3.6). Within our models, topography is generated which creates a downward gravitational force that may further drive rifting in the western block, nonetheless, the imposed extension at the sides of the model are the bigger drivers on the extension in our models, but we can't discount the gravitational force as a factor that contributed to the rifting of the region. While all the previous models on rifting in North China and the Shanxi Rift, in particular, have highlighted how pre-existing thermal and rheology differences between the two blocks and inherited weaknesses can generate two different rift systems in the east and west, our model is the first to show a combination of pre-rift rheology, rift kinematics and a discrete inherited mantle weakness can generate the rift migration pattern observed in North China.

3.4.2 Comparison to the natural system

Despite the simplifications inherent to any numerical modelling approach, our model successfully recreates key features of the geological evolution of North China and

shows that ad-hoc changes in tectonic drivers are not necessary to achieve the overall pattern of deformation. Our results suggest that the initial lithospheric architecture and the presence of a sufficiently weak mantle scar may have led to the observed migration of rifting from east to west. Many of our models compare well to the geology of North China and recreate the same time-dependent strain migration pattern. They display a wide rift forming in the eastern block, due to the thinner and therefore hotter lithosphere. In nature the width of Bohai Basin is most likely a combination of the pre-rift rheology and the transtensional deformation which results in a wider rift basin (Allen et al., 1997; Farangitakis et al., 2021), the latter cannot be recreated or tested by our model however due it being two-dimensional. The initial thickness of the lithosphere of the eastern part of North China before rifting in the Eocene is poorly constrained. Data on the destruction of the NCC suggest 100 km or more of mantle lithosphere were removed through delamination or erosion in the Cretaceous. However, before the formation of the Bohai Basin in the Eocene the mantle beneath the eastern NCC was replaced successively by upwelling asthenosphere which re-equilibrated to mantle lithosphere, but the rate of this is hard to constrain. Present-day values for total lithospheric thickness range from 70-110 km (Fig. 3.1), this suggests that a value in that range or slightly lower is sensible to assume for the Eocene thickness of the eastern NCC. Our model is robust enough to account for uncertainties in our knowledge of the initial state of the North China lithosphere before rifting in the Cenozoic and models with lithospheric thickness between 70-130 km before the onset of rifting can recreate the migration pattern of North China (Fig. 3.11). We also assume that crustal thickness was roughly uniform across the region before rifting, as there is evidence of the Yanshanian orogeny affecting both the western and eastern parts of North China. It is possible that the eastern part of the NCC experienced more compression and further thickening, which

would have further increased the crust-to-mantle ratio and weakened the eastern block more. Rifting migrates to the west after a pre-imposed phase of tectonic quiescence during which the eastern lithosphere thickens. This rifting creates a narrow rift in the cold lithosphere of the western block, equivalent to the Shanxi Rift and other Circum-Ordos rifts which are often bounded by one or two main faults (Zhang et al., 1998; Shi et al., 2020). This rift is separated from the wide rift in the eastern block by a 150-200 km wide rift shoulder, which matches well with the actual geometry of North China. The width of that zone in nature varies along the strike of Shanxi, but there is an unfaulted, uplifted zone separating the Bohai and circum-Ordos rift which makes up the Taihangshan mountains. This region is mainly formed due to the TNCO suture being situated further west than the limit of the thinned cratonic lithosphere of the eastern block (see Fig. 3.1). Models by Naliboff and Buiter (2015), also show a 100-200 km wide rift shoulder separating the new and abandoned rift, the width of that depends on the width of the initial rift, however in our model the separation is chiefly influenced by the position of the crustal and lithosphere heterogeneity and therefore is determined by inheritance. We have shown that the lithospheric thickness difference and the angle of internal friction of the lithosphere scar are the governing factors in the behaviour of the model.

Most studies agree that the formation of the Shanxi Rift was initiated in the Miocene. While Su et al. (2021) show an earlier uplift event in the Eocene for the Shanxi Rift in their thermochronological studies, this may be the result of an uplift of the Taihangshan mountains (which flank the Shanxi Rift system) acting as the rift flank to the Bohai Basin. Therefore, the early uplift recorded in these thermochronological results may not be due to the onset of rifting in the Shanxi Graben but an uplift event due to the formation of adjacent basins. The second rapid uplift that both Su et al. (2021) and Clinkscales et al. (2021) show in the Late Miocene is more likely to be the

onset of rifting in the Shanxi Rift. Other studies show well-dated syn-rift sediments cover the pre-rift basement in the Linfen basin (Su et al. 2023) or other parts of the Shanxi Rift that constrain the rift initiation to the Late Miocene. Our model shows small amounts of strain accommodated at the initial Eocene rift phase (10-25 Myr) but there is no distinct rift basin forming – which agrees with data from Shanxi. However timing of the other Circum-Ordos Rifts (Yinchuan, Weihe and Hetao) is often invoked to have occurred in the Eocene-Oligocene, yet for these rifts and the Shanxi Rift, the same geodynamic driver (India-Asia collision) is often invoked. Early rifting in the Weihe and Hetao-Juncheng Grabens, the early initiation of these systems is disputed (Yin, 2010). Ye et al. (1987) set the age of rift initiation in these basins to be Oligocene due to the presence of Oligocene-dated red beds which is compatible with a brief onset of rifting in the West at the start of the model. However, like the Shanxi Rift, the Weihe, Hetao and Yinchuan Rifts all show a recent sudden uplift event 10 million years ago (Zhao et al., 2007; Liu et al., 2013; Chen et al., 2015), which may be the onset of rifting for all of these rifts. Many of these rifts formed superimposed on Palaeoproterozoic orogens (Fig. 3.1) and our modelling results suggest that mantle scars from these orogens were important during rift localisation. Therefore, despite our model being a 2D study, the general result may apply to all of the circum-Ordos rifts where lithospheric sutures may govern their location rather than a switch in the geodynamic drivers from the Eocene to the Miocene.

Our models show that both a zone of weaker crust and a deeper seated lithospheric weak zone beneath it may have been important for localising deformation in the western block and forming the Shanxi Rift. In the case of North China, several studies show heterogeneity in the upper mantle or the crust that mirrors the geometry of a suture zone or a relict subduction zone (Chen et al., 2014; Wan et al., 2020; Zheng et al., 2009). However, the rheological properties of these zones remain uncertain.

Lowering the angle of internal friction is a simple and effective way to make these zones frictionally weak as shown by Heron et al. (2016, 2019). This low angle of internal friction may be due to an abundance of hydrated and foliated minerals and lithologies, which represent easily reactivated weaknesses, all of these rocks are present at the surface of the Shanxi Rift and are manifestations of the TNCO (Trap et al., 2009; Trap et al., 2012). Alternatively, they may represent zones of reduced grain size in the form of mantle lithosphere peridotite mylonites (Heron et al., 2016; Linckens et al., 2015; Warren and Hirth, 2006). Therefore, imposing a low angle of internal friction is an appropriate and effective simplification of the different processes that make inherited weak zones frictionally weak. Based on recent seismic data, Su et al. (2023) also proposed the possibility of a lower seated lithospheric suture zone which has influenced the localisation of the Shanxi Rift. All of the above shows that both at the surface and on geophysical data a major suture zone is present which is most likely weaker compared to the surrounding cratonic material – thus representing a crustal and mantle scar.

3.4.3 Implications for other natural systems

Rift migration is a common feature in rift basins and rifted margins around the world. Similar migration patterns have often been observed in other parts of the world such as the North Sea, Canning Basin (Braun, 1992) or the North Atlantic margin (Schiffer et al. 2020). Braun (1992) states that for the Canning Basin, discrete heterogeneities such as thrust faults formed in the thickened crust during earlier Proterozoic collisions may have aided strain localisation during the migration of rifting in the Devonian. This may be another factor in the Shanxi Rift migration, as a thicker crust may further weaken the lithosphere by increasing the crust-to-lithosphere ratio, thus making the lithosphere weaker. Constraints on the initial crustal thickness of the western and

eastern parts of the North China Craton prior to rifting are poor. The area of the Bohai Basin has been affected by compressional deformation in the Jurassic to Early Cretaceous. Therefore, it is likely that the crust in the Eastern Block was thickened before the extension (Wu et al. 2019). However, due to the uncertainty in the crustal thickness estimation we assumed a constant crustal thickness in these models. It seems likely that a thickened crust/mantle ratio in the east of the model would have a further weakening effect on the initial rifting and further focus on initial rifting in the east.

Inherited structures in the lithosphere may also influence the later rift axis or break-up position of a rifted margin. The North Atlantic went through an episodic period of rifting starting in the Carboniferous and lasting until the Paleogene (Skogseid et al., 2000; Peron-Pinvidic et al., 2013). While at present day it might not share many commonalities with the continental rift systems of North China, it might have had more in common during its earlier rifting history. There is an apparent offset between the Palaeozoic-Mesozoic early rift basins like the Møre, Vøring, Hatton and Rockall Basins that follow Caledonian trends (Doré et al., 1997; Kimbell et al., 2005) and the eventual breakup axis in the Paleogene, that is oblique to and offset from these basins (Schiffer et al. 2020). Schiffer et al. (2020) further argue that the break-up oblique to the early former basins is due to deeper seated late Caledonian mantle shear fabric, oblique to the shallow Caledonian trends, that was activated later when the principal stress axis rotated (Doré et al., 1999) to be perpendicular to that fabric. While our model does not integrate a change in the extension direction as envisioned here, analogue models by Zwaan et al. (2022) show that deeper seated lithospheric fabrics can influence a rift even if they are oblique to the principal extension direction. The migration of rifting in the North Atlantic was likely helped by the long break between initial rifting in the Mid-Cretaceous and breakup in the Paleogene (~60 Ma) which allowed strengthening of

the lithosphere and therefore made the deeper-seated proposed mantle suture the weakest point, favouring breakup along this structure. The influence of inherited structures on the migration of the rift axis has also been proposed for the North Sea (Fazlikhani et al., 2021; Phillips et al., 2019). While early extension during Permo-Triassic rifting focused extension on the Stord basin, the rifting here was later abandoned during a second phase of rifting that focused on the westwards-lying axis of the present-day Viking Graben. The pause between the rift phases was approximately 50 million years in the North Sea. However, in contrast to North China, structural inheritance has been important in localising the early extension in the North Sea with diminishing effects of inherited structures on migration (Phillips et al., 2019). Later focus of rifting during the second rift phase along the Viking Graben may be more related to thermal factors, noticeably the upwelling of the asthenosphere to the west and the strengthening of the lithosphere in the East (Bell et al., 2014; Phillips et al., 2019). This highlights that while, initial composition, rheology, and nature of inherited structures are important in determining the evolution and migration patterns of rift systems, later rift-induced factors such as asthenospheric upwelling can also affect migration.

Similar patterns of the migration of the rift locus in a multiphase protracted rifting history have also been observed for the West Antarctic Rift System (WARS). During an early stage of extension in the Cretaceous, rifting was distributed over a relatively large area, from the Victoria Land Basin to the Eastern Basin (Behrendt, 1999; Cooper and Davey, 1985; Luyendyk et al., 1996). This accommodated rifting over a wide region of up to 1000 km (Behrendt et al., 1991). In contrast, a later stage of rifting in the Paleogene was primarily focused on the Victoria Land Basin adjacent to the Trans-Antarctic Mountains which have a much thicker lithosphere (Huerta and Harry, 2007; Wilson, 1995). This rift migration is probably facilitated by a relatively weak initial

lithosphere across the entire WARS, which readily stretched in a distributed way (Huerta and Harry, 2007), similar to the Bohai Basin in this study. The later, focused rifting may have occurred over stretched but comparatively stronger lithosphere than before, due to a change in the mantle-to-crust ratio. This stiffer crust was coupled to the lithosphere. It therefore may have exploited pre-existing lithospheric structures (Wilson, 1995) such as the Ross Orogen (Jordan et al., 2019), or simply focused on the largest contrast of strength and lithospheric thickness – the Victoria Land Basin adjacent to the Transantarctic Mountains with thicker lithosphere (Huerta and Harry, 2007). In the case of the Circum Ordos rifts we see that the Shanxi Rift formed in the middle of the Taihangshan Mountains due to the large anisotropy and heterogeneity created by the former TNCO scar rather than where the thickness contrast between the Western and Eastern block is the largest.

Comparisons with other natural examples, however, also highlight the special case of the Shanxi Rift and the other Circum Ordos Rifts: while in most rift systems, the rift locus migrates from one area of pre-stretched lithosphere to another area of already rifted lithosphere, in North China the rift locus switches from the diffuse rift in the East to the thick relatively undeformed region in the West. This unique migration case probably arises due to the architecture of the North China Craton and the Shanxi Rift as it is situated in a partially modified cratonic lithosphere which has a large lateral thickness contrast. In contrast to other cratonic rifts, or craton-adjacent rifts, where deformation localised at the margin of the craton like the Baikal rift or the East African Rift segments, Shanxi formed further inland due to the TNCO suture being located further west than the edge of the mostly unmodified thick western part of the NCC (Fig. 3.1), which broadly coincides with the north-south trending gravity lineament running through North China (Xu, 2007; Deng et al., 2021).

3.4.4 Implications for Cenozoic Tectonics of East Asia

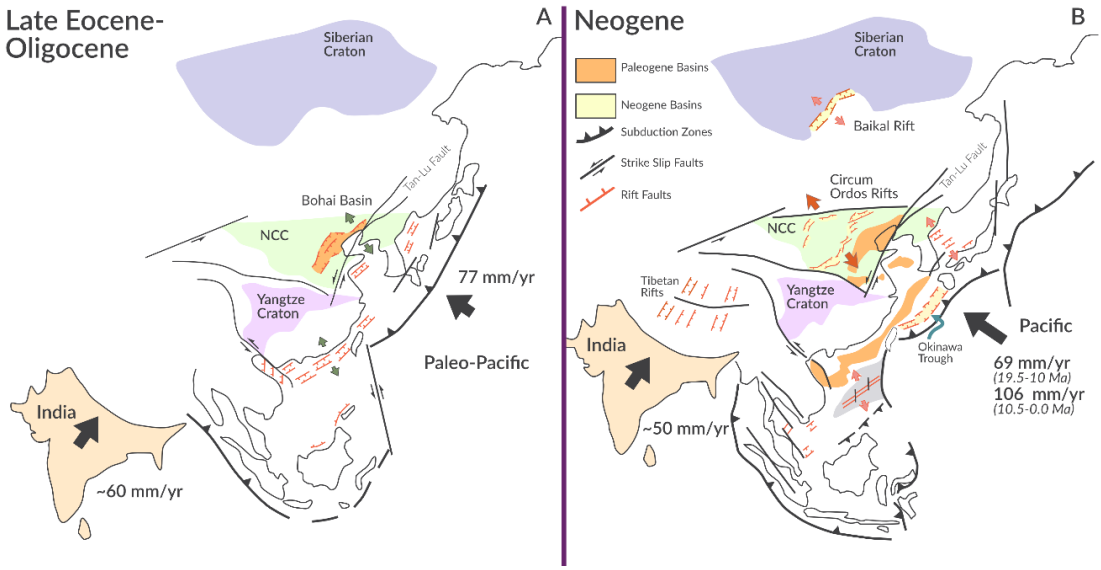

Figure 3.12 Schematic Map of the Cenozoic Tectonic Evolution of East Asia

Schematic map of East Asian tectonics in the Cenozoic (modified from Ren et al. 2002) showing when extensional basins across East Asia formed. It also indicates the convergence velocities of the two main geodynamic drivers, the Indian Plate colliding with Asia (from Ren et al. 2002) and the Pacific subduction (from Northrup et al. 1995). In conventional models, Eocene rifting in the eastern part of North China are formed due to the Paleo-Pacific subduction while the Neogene rifts in the western part form due to the India-Asia Collision.

Since the first seminal paper by Molnar and Tapponier (1975), suggested that the Circum Ordos Rifts (and other Cenozoic rifts in East Asia) formed due to extrusion tectonics chiefly related to the collision of India and Asia, there has been a multitude of papers debating the relative importance of Pacific margin subduction and the India-Asia collision. Northrup et al. (1995) related the Paleogene to mid-Miocene widespread extension across Asia (which formed the Bohai Basin, equivalent to the eastern part of this study) to changes in Pacific convergence rate, with low convergence rates correlating with extension in East Asia. Ren et al. (2002)

emphasised the importance of both Pacific subduction and the India-Asia Collision, in forming an NW-SE extensional strain field to create the Cenozoic basins of East Asia (Fig. 3.12a). They interpret the later Neogene rifts (Circum-Ordos and Baikal) as being by-products of the India-Asia collision when the Pacific convergence rate increased again. However, the Shanxi Graben did not initiate rifting until the Late Miocene (~10 Ma) (Xu and Ma, 1992; Su et al., 2023), at a time when the India-Asia collision rate was lower than during the Paleogne (~50 mm/year; Ren et al. 2002) (Fig. 3.12a). In the case of the Bohai Basin, the onset of extension preceded the onset of the India-Asia collision in the Eocene (Northrup et al., 1995; Ren et al., 2002), therefore it is unlikely that the India-Asia collision caused the Eocene extension. Therefore, the difference in timing and style of the Bohai Basin and the Circum-Ordos Rifts is often attributed to a change in the geodynamic driver from the Pacific subduction to the India-Asia collision. In many analogue models of the Cenozoic tectonics of East Asia, the India-Asia Collision was modelled as the product of an Indian plate rigid indenter (Tapponier et al., 1982; Fournier et al., 2004) while the Pacific subduction to the east was modelled as a passive subduction zone that did not contribute to deformation. Geodynamic models incorporating a subduction zone that actively participates in deformation, show the important role of subduction in the Cenozoic deformation of East Asia (Schellart and Lister, 2005; Schellart et al., 2019). Yin (2000) argued that the Tibetan, Siberian and North China rifts all share a common origin, and their formation may require a 1000s km scale long boundary force such as a subduction margin actively involved in the deformation. The impact of the India-Asia collision on contractional deformation and mountain building in Tibet and the Himalayas is clear; the role in extensional deformation in North China remains speculative. This study does not attempt to recreate the complex subduction and collision dynamics that shaped East Asia but does show that inherited structures can localise rifting far from

plate boundaries without a change in geodynamic drivers. While many authors relate the two extension events and the evolution of Neogene and Paleogene rifts of North China to different geodynamic drivers (Peltzer et al., 1985; Briais et al., 1993; Ren et al., 2002; Zhang et al., 2018; Su et al., 2021), this study hence offers an alternative that shows a change in driver and extension direction are not necessary to explain the different rifts that formed in North China through the Cenozoic. Here we show that a time-progressive evolution of back-arc rifting can be achieved simply by reactivation of inherited lithospheric heterogeneities and strengthening of the previously rifted lithosphere, during a hiatus that results in rift migration to the West.

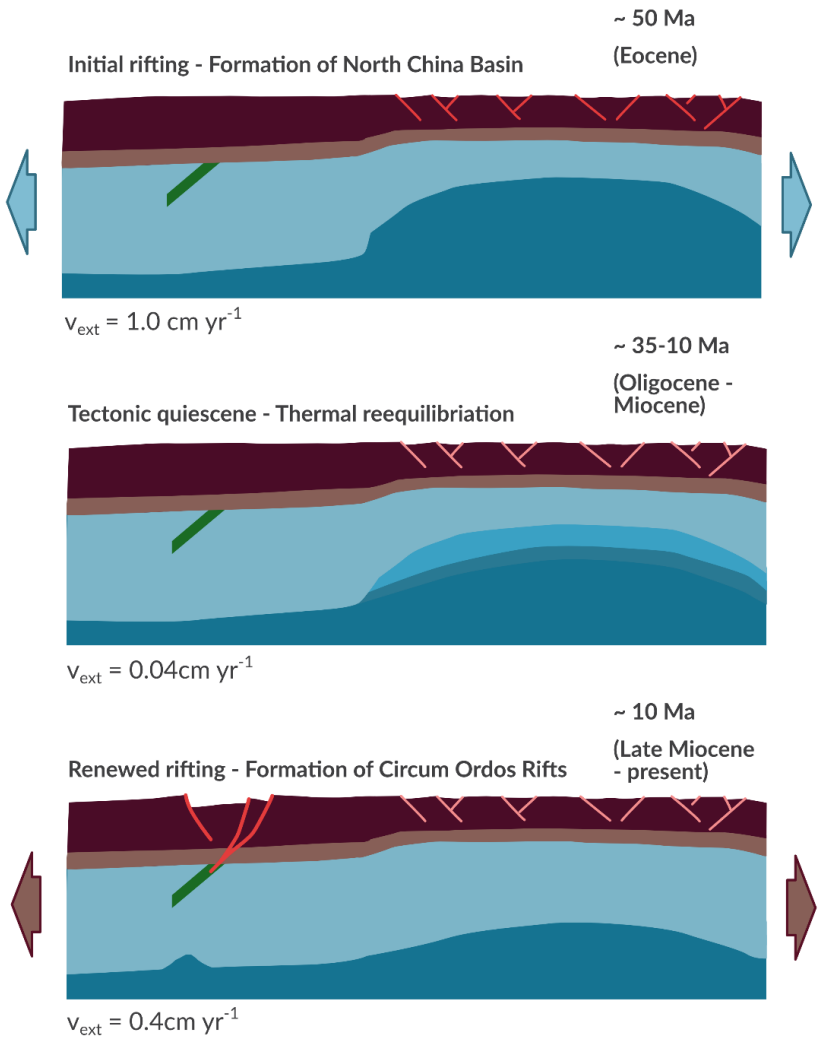

Figure 3.13 Summary of Rifting in North China – Based on 2D Models

Summary diagram of the model explaining rift migration in North China integrating an inherited lithospheric weak zone. Run times of the model converted to geological ages. Rifting started over the thinned modified cratonic lithosphere in the East, while the thicker and less modified Western lithosphere saw little to no deformation. During the quiescent period in the Oligocene to Miocene, the Eastern lithosphere started to thicken up, and strengthened post-rift. When the extension was renewed in the Late Miocene the inherited suture in the Western block was activated and formed narrow localised rifts: The Circum-Ordos Rifts.

3.5 Conclusion

In this study, we used 2D thermo-mechanical models to investigate how lithospheric thickness variations and inherited heterogeneities in the lithosphere can influence the timing and style of rifting. The geometries and temporal evolution of the models closely resemble the natural analogue, the Shanxi Rift, which was the inspiration for this study (Fig. 3.13). We find that:

1. The thinner eastern lithosphere will initially form a broad rift as it is the weakest part of the model, but subsequent conductive cooling changes the lower crust-mantle ratio and strengthens this region after the initial rifting phase.

2. After the quiescent period and the strengthening of the eastern block, the mantle scar becomes the weakest part and localises strain during the renewed period of rifting. As it is situated in a thick, cold and strong lithosphere it forms a narrow, localised rift.

3. Without a rifting hiatus, there is no significant strengthening of the Eastern Part and rift migration will not occur.

4. The main parameters controlling whether migration occurs in this model are the presence of lithospheric heterogeneity that needs to be significantly weaker than the surrounding cratonic lithosphere and the difference in thickness between the Eastern and Western lithosphere.

These results apply to other natural examples where rift migration has occurred such as the North Atlantic, the North Sea or the Western Antarctic Rift System. Due to the nature of the North China lithosphere and the Cenozoic extensional tectonics of North China, it is the interplay of partially destroyed cratonic lithosphere and an ancient suture within the craton that govern the rifting pattern observed. However, the concept may more widely explain the rifting behaviours of the cratonic lithosphere.

These results also question the need for two different geodynamic drivers for the extensional deformation of North China in the Cenozoic. Our model represents an alternative that can explain how the two rift systems (Circum Ordos and Bohai Basin) have evolved due to their different lithospheric architecture without the need for a change in extension dynamics. This opens the possibility that the Shanxi Rift formed due to back-arc rifting related to the Pacific Subduction rather than the India-Asia collision.

3.6 Supplementary Material

Data availability – all input files used to generate these models with ASPECT are available online: https://github.com/MFroemchen/NCC_ASPECT. The 2.3.0 version of ASPECT can be downloaded at: https://github.com/geodynamics/aspect/releases/tag/v2.3.0

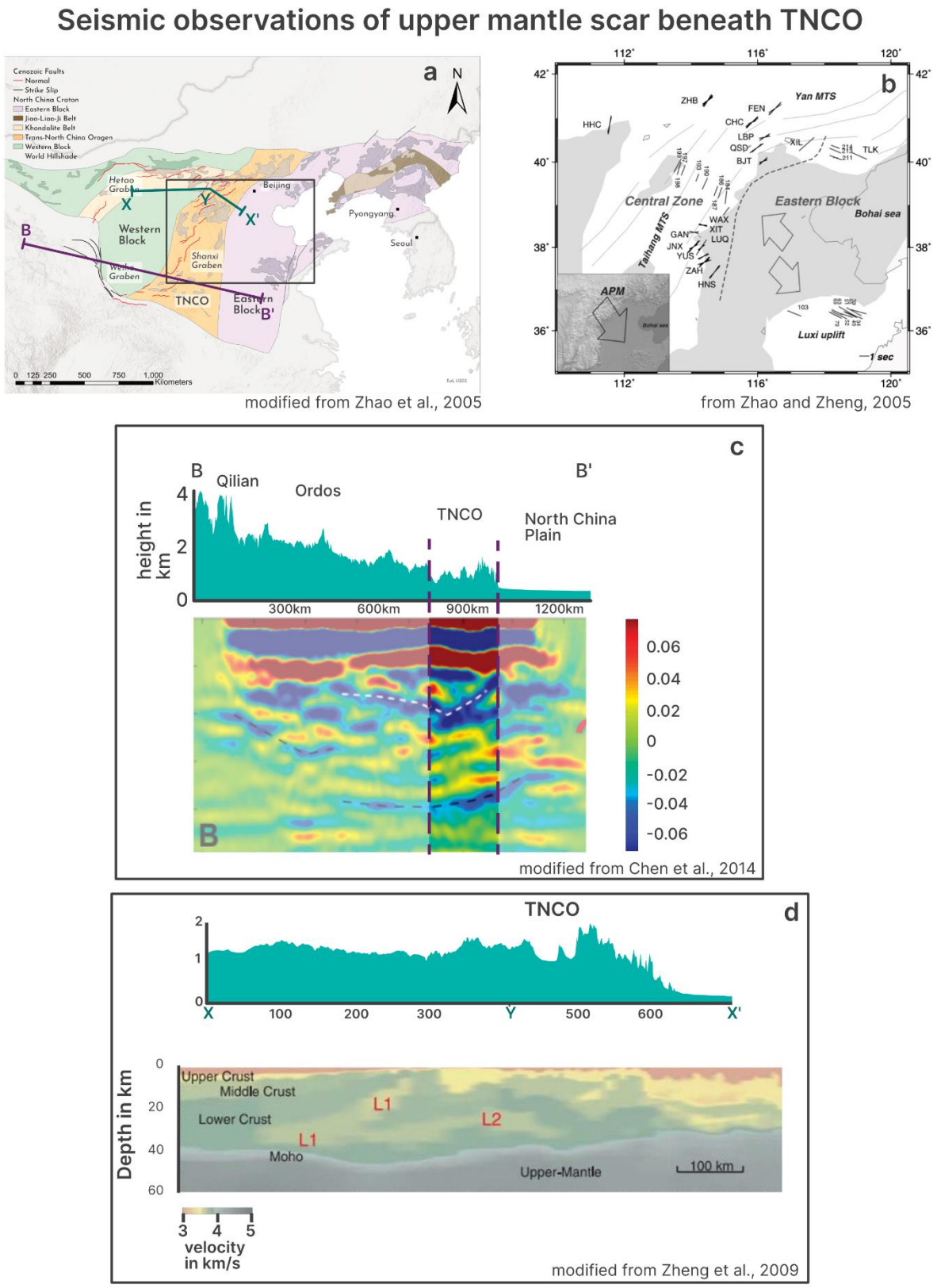

Supplementary Figure S 3.1 – Geophysical evidence for the presence of a crustal and mantle scar beneath the TNCO within the NCC

a) Overview map of the North China Craton based on Zhao et al., (2005) with the seismic lines for c) and d) indicated in purple and turquoise. Black square shows the location for b). b) shows a collection of seismic anisotropy measurements from Shear wave splitting by Zhao and Zheng (2005) which show a possible mantle structure oblique to the main Shanxi Rift. c) show results from seismic receiver function data by Chen et al. (2014) showing a possible upper mantle discontinuity beneath the central and western NCC. The topographic profile in turquoise shows the location of the main geographic regions of Northern China. Purple lines highlight the position of the TNCO. d) shows possible crustal discontinuities beneath NCC and the TNCO based on receiver function data from Zheng et al. (2009). L1 and L2 may represent relic slabs, the data unfortunately does not allow extrapolation into the upper mantle. Topographic profile above with location of the TNCO highlighted.

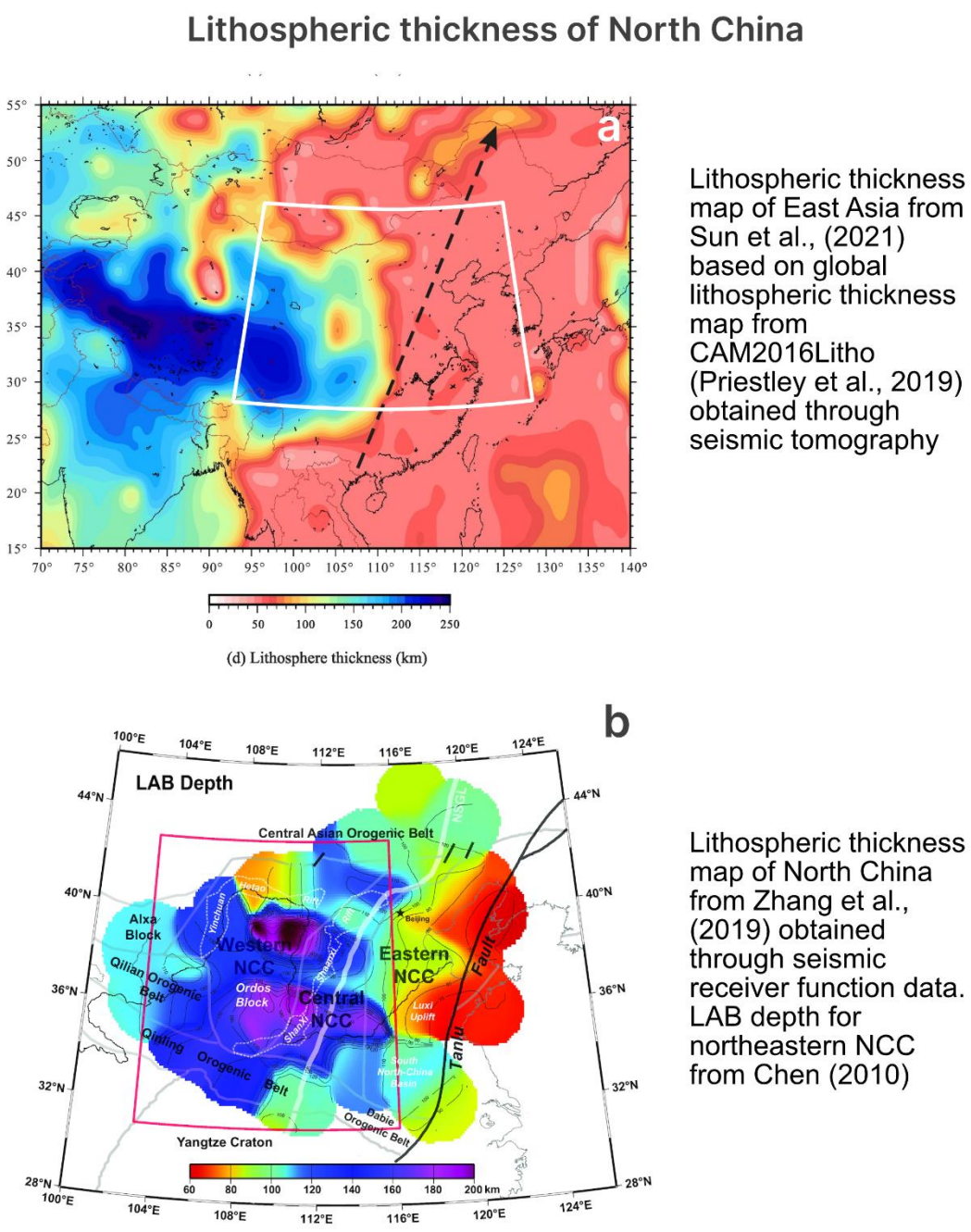

Lithospheric thickness map of East Asia from Sun et al., (2021) based on global lithospheric thickness map from CAM2016Litho (Priestley et al., 2019) obtained through seismic tomography

Lithospheric thickness map of North China from Zhang et al., (2019) obtained through seismic receiver function data. LAB depth for northeastern NCC from Chen (2010)

Supplementary Figure S 3.2 Comparison of lithospheric thickness maps

Comparison of lithospheric thickness maps derived from two different methods: a) shows the lithospheric thickness of East Asia (modified from Sun et al., 2021) based on the CAM2016Litho global lithospheric thickness map by Priestly et al. (2019) obtained from seismic tomography. It shows a stark contrast between east and west with regions in the western part reaching 150-200 km thickness while regions

in the eastern part lie at 50-80 km. White square shows the location of b) which is a lithospheric thickness map by Chen (2010) mapping the LAB depth using seismic receiver function data. This map also shows the contrast with the western NCC showing thickness of up to 200 km, the central NCC lying between 120-180 km and the eastern NCC between 60-100 km. While the two maps may show differences in detail the modelled difference in thickness between the eastern and western block is apparent in both.

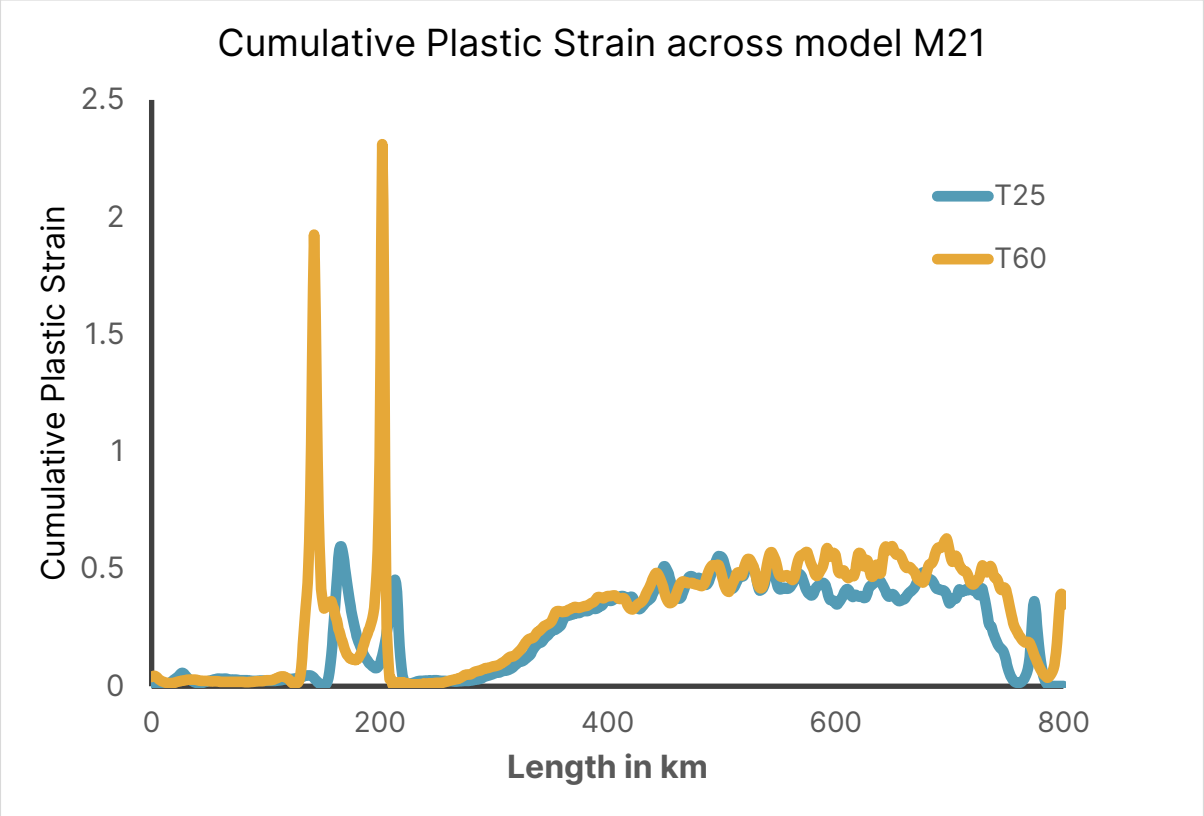

Supplementary Figure S 3.3 Cumulative Plastic Strain for Model 21

Cumulative plastic strain accommodated by model M21 at two different timesteps (T25 – the end of the initial rifting period at t = 25 Myr and T60 – the end of the second rifting period at t = 60 Myr) – the divide between the eastern and western block is at 400 km. Note the more distributed strain accommodation in the East

compared to the very localised one in the West. Little strain is accommodated in the east between the two-time steps.

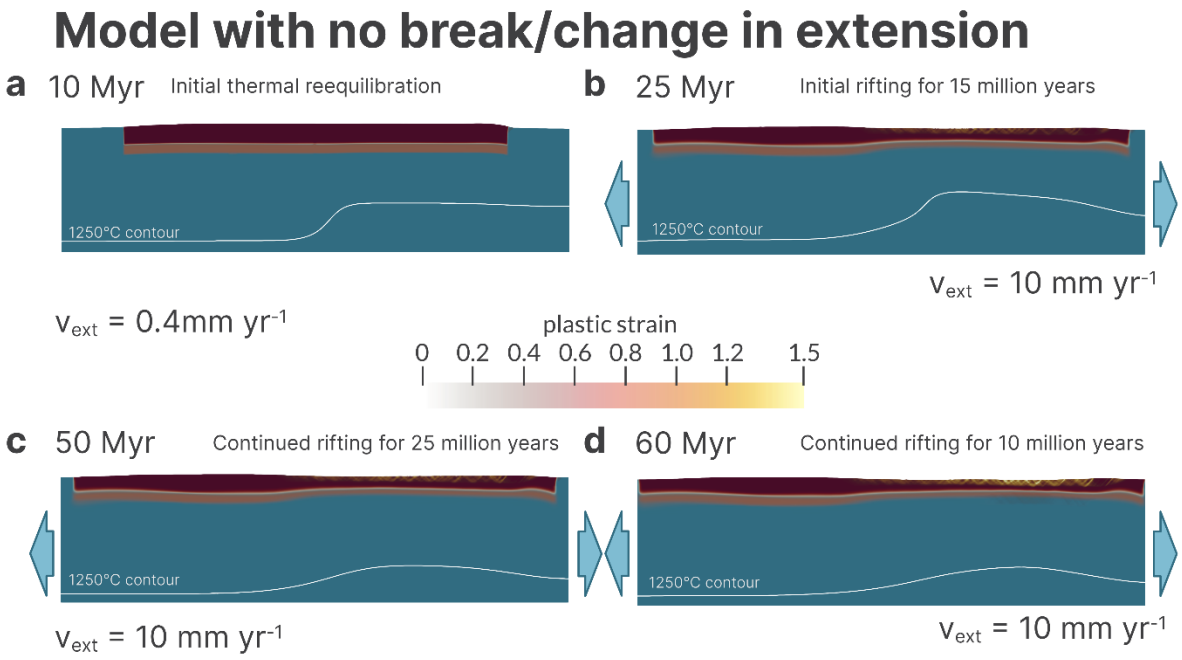

Supplementary Figure S 3.4 Model with no break in extension

Model with no imposed tectonic quiescence and continued extension of 10 mm yr-1 throughout its 60 million year run time. Without the break, the eastern lithosphere cannot strengthen, and rifting does not migrate to the west. Other parameters are the same as M21.

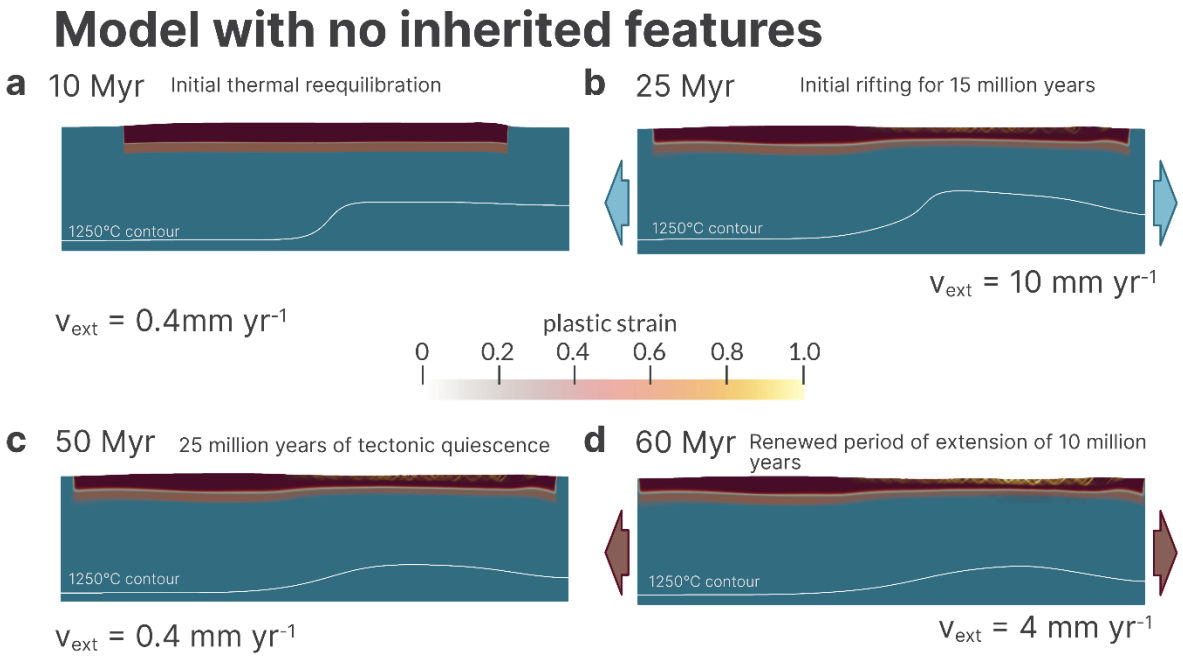

Supplementary Figure S 3.5 Model with no inherited features

Model without any inherited structures in the mantle or crust – while the break can strengthen the lithosphere between the initial and second rifting period without inherited structures the western part of the model remains stronger than the eastern part.

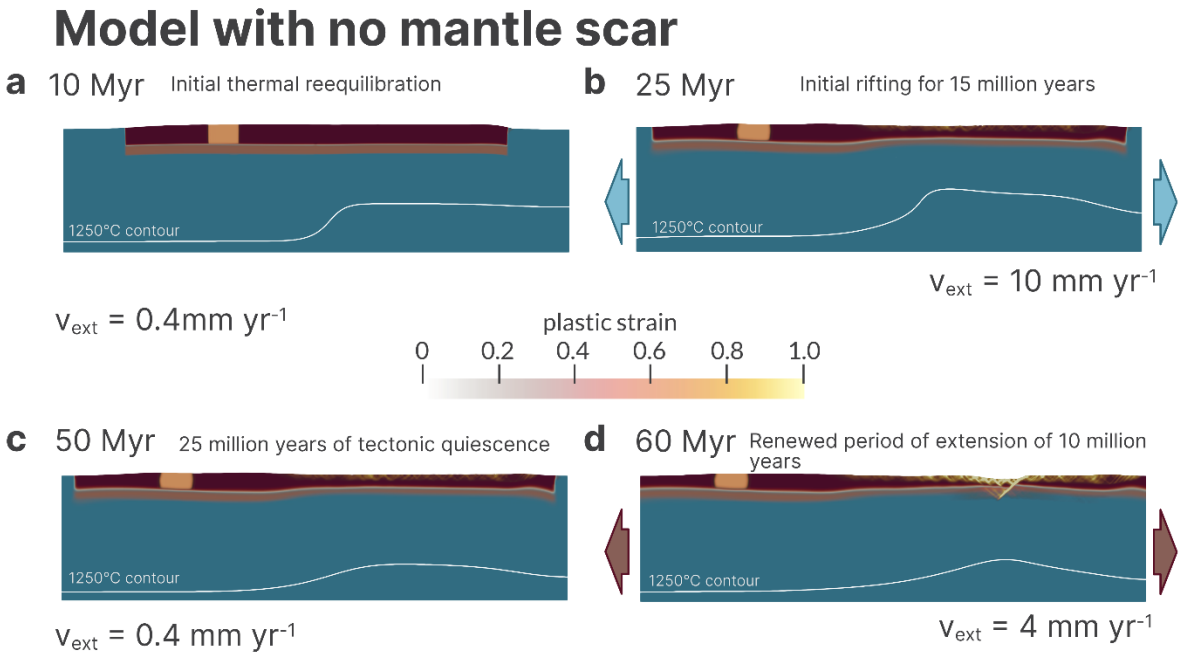

Supplementary Figure S 3.6 Model with no mantle scar

Model with no mantle scar, only the crustal scar (equivalent to the TNCO) is present (highlighted in light brown) and is not sufficiently weak enough to induce the migration of rifting to the west after the break.

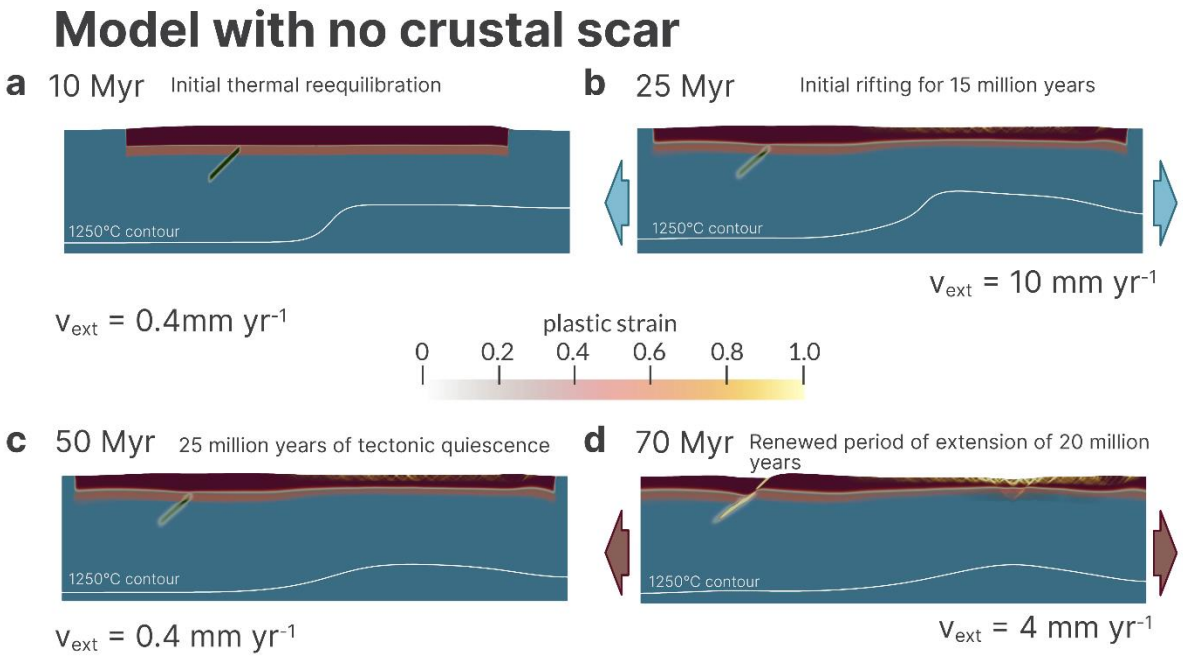

Supplementary Figure S 3.7 Model with no crustal scar

Model without a crustal scar but with a mantle scar. Here the rifting migrates to the west after the break because the inherited structure is within the strongest part of the lithosphere (the upper mantle). However, rifting does not fully switch to the west (rifting still occurs in the east) and takes longer to localise without a crustal scar (thus the longer runtime of 70 million years).

Thermal parameters for lithosphere								
Thickness in km	Surface Heatflow (QS1) in W/m²	Base of UC Heatflow (QS2) in W/m²	Moho Heatflow (QS3) in W/m²	LAB Heatflow (QS4) in W/m²	HeatSurface (TS1) in K	HeatBaseUC (Ts2) in K	HeatMoho(TS3) in K	HeatLAB(TS4) in K
180	0.06696	0.02196	0.01596	0.01596	273	806.52	920.28	1573.19
170	0.06783	0.02283	0.01683	0.01683	273	816.96	935.94	1573.44
160	0.0688	0.0238	0.0178	0.0178	273	828.6	953.4	1573.7
150	0.0699	0.0249	0.0189	0.0189	273	841.8	973.2	1574.56
140	0.0711	0.0261	0.0201	0.0201	273	856.2	994.8	1573.44
130	0.0725	0.0275	0.0215	0.0215	273	873	1020	1573.8
120	0.0741	0.0291	0.0231	0.0231	273	892.2	1048.8	1573.8
110	0.07595	0.03095	0.02495	0.02495	273	914.4	1082.1	1573.54
100	0.0781	0.0331	0.0271	0.0271	273	940.2	1120.8	1572.47
90	0.0807	0.03569999	0.0297	0.0297	273	971.4	1167.6	1572.6
80	0.08386	0.03886	0.03286	0.03286	273	1009.32	1224.48	1573
70	0.08775	0.04275	0.03675	0.03675	273	1056	1294.5	1572.9
60	0.0927	0.0477	0.0417	0.0417	273	1115.4	1383.6	1573.15

Table 3 - Values used for geotherm of the lithosphere.

Parameter space exploration 2D model													
		Thickness Eastern Lithosphere											
		180	170	160	150	140	130	120	110	100	90	80	70	60
Angle of internal friction	0	1	2	3	4	5	6	7	8	9	10	11	12	13
	1	108	109	110	111	112	113	114	115	116	117	118	119	120
	2	14	15	16	17	18	19	20	21	22	23	24	25	26
	3			92	93	94	95	96	97					
	4			99	98	100	101	102	103					
	5	27	28	29	30	31	32	33	34	35	36	37	38	39
	6			104	105	106	107							
	7	40	41	42	43	44	45	56						
	10	53	54	55	56	57	58	59	60	61	62	63	64	65
	20	79	80	81	82	83	84	85	86	87	88	89	90	91

Number equates to Model name - i.e. 21 = Model 21

working model | non working modell | in-between | no run

Table 4 - Parameter space exploration table of 2D model

Input used for Fig. 3.11, showing which model runs were able to reproduce the migration pattern of the North China Craton

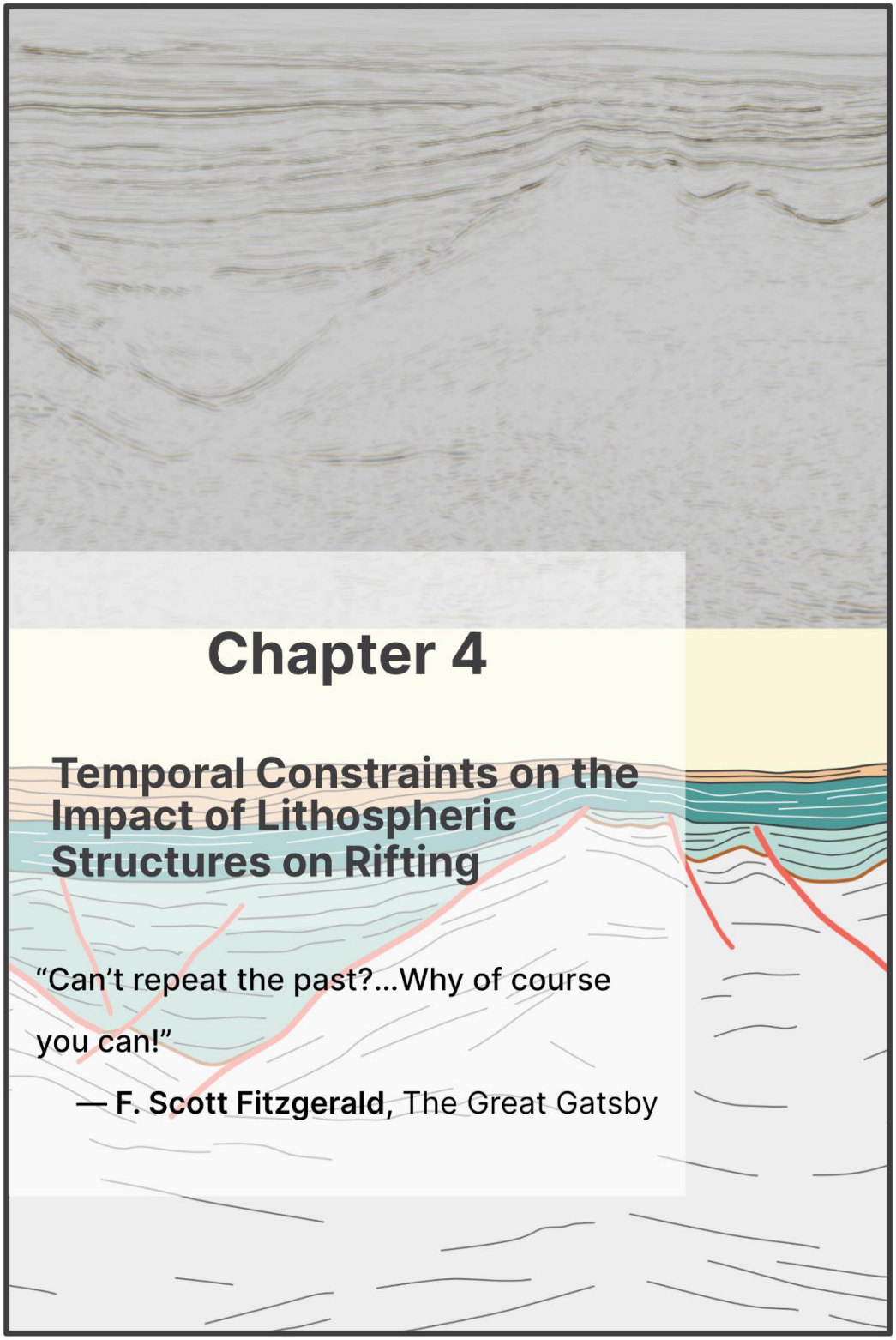

Chapter 4

Temporal Constraints on the Impact of Lithospheric Structures on Rifting

"Can't repeat the past?...Why of course you can!"

— **F. Scott Fitzgerald**, The Great Gatsby

4. Temporal Constraints on the Impact of Lithospheric Structures on Rifting

Abstract - The evolution of continental rifts is influenced by the pre-rift rheology of the lithosphere and the discrete lithospheric structures that it contains. The Great South Basin, offshore New Zealand, is a Cretaceous rift system that developed orthogonal to a series of heterogenous basement terranes. The terrane boundaries influenced the rift architecture and caused faults to locally rotate or splay and segment. The impact of terrane boundaries on rift architecture and the temporal evolution of the rotated faults along them is poorly constrained. Here we use 3D reflection seismic data to investigate the timing and slip rate evolution of the rotated and segmented faults that formed along two of the terrane boundaries. Our results show that the terrane boundaries have a significant but variable impact on rift evolution and architecture: Faults in the Murihiku terrane show asymmetric throw-length profiles and are rotated along the boundary with the Dun Mountain-Maitai (DMM) terrane and they detach into shallow crustal fabrics. Faults in the DMM terrane show less evidence of rotation and more symmetric throw-length profiles but are segmented along the DMM and Caples boundary. The curving faults of the Murihiku terrane likely formed early on but remained as isolated segments only linking up during later stages of rifting when other faults became inactive. These results show that terrane boundaries not only have a first-order effect on the segmentation of a rift during early rifting but also affect the later-stage linkage of misorientated faults. These results may help understand the temporal evolution of lithospheric and crustal inheritance on rift evolution in other regions around the world such as East Africa or North China.

4.1 Introduction

Rifting is commonly influenced by various heterogeneities in the crust and lithosphere. Rifting may be influenced by inherited thermal state, inherited composition, and inherited structures (Manatschal et al., 2015), and in most cases, a combination of all three factors will determine the evolution of a rift. Continental crust and lithosphere are often a highly heterogeneous amalgamation (Thatcher, 1995) of various terranes, igneous intrusions (such as dykes, sills and batholiths) (Fraser and Gawthorpe, 1990; Phillips and McCaffrey, 2019) and inherited structures such as shear zones, metamorphic foliations (Holdsworth et al., 2001b; Morley et al., 2004; Reeve et al., 2015; Phillips et al., 2016; Fazlikhani et al., 2017; Osagiede et al., 2020) and pre-existing fault networks (Henza et al., 2011; Henstra et al., 2015). The boundaries between basement terranes may exert a first-order influence on the location of rifts, as observed for cratonic rifts or craton adjacent rifts such as the Shanxi Rift (Xu and Ma, 1992), the Baikal Rift (Petit et al., 1994), the East African Rift (Rosendahl, 1987; Daly et al., 1989; Ring, 1994) or the Oslo Rift (Pascal and Cloetingh, 2002). These studies show that strain will preferentially localise into the weaker parts, i.e. the mobile belts surrounding the craton, rather than the relatively strong cratonic blocks. Similar observations of rifts nucleating in weaker areas of the crust or lithosphere have also been made in non-cratonic regions (Beniest et al., 2018; Samsu et al., 2021). The influence of terrane boundaries on rift formation is due either to discrete structures between terranes representing the terrane boundary or a result of a large rheological contrast between the terranes. The extension direction during rifting is often oblique or nearly parallel to the existing terrane boundaries and rarely perpendicular to these terrane boundaries (Laó-Dávila et al., 2015; Wright et al., 2020; Phillips et al. 2023). In cases where the extension direction is parallel to the terrane boundaries, all terranes will accommodate some strain and show deformation but the degree of that will vary with strength and rheology (Phillips et al., 2023). Terrane boundaries have therefore

been observed to be important first-order structures that determine the overall rift morphology.

The direct reactivation of inherited structures and their impact on rift basins has been a major focus of study (Holdsworth et al., 2001b), however, in recent years it has been shown that inheritance can impact the evolution of rifts in different ways such as causing fault segmentation, strain partitioning (De Paola et al., 2005), splaying of faults (Daly et al., 1989; Phillips and McCaffrey, 2019) or reorientation of the local extension direction (Morley, 2010; Reeves et al., 2015; Osagiede et al., 2020; Samsu et al. 2023). When interpreting the influence of inheritance, it is important to consider the scale and nature of the inherited structures as they will have varying impacts on rift architecture and evolution, for example, large-scale lithospheric structures such as suture zones and orogenic belts may influence the location and orientation of a rift (Daly et al., 1989; Vauchez et al., 1997), while a zone of pervasive basement fabrics in the upper crust can influence the orientation and segmentation of individual faults (Reeve et al., 2015; Osagiede et al., 2020). Structural inheritance can broadly be defined as hard-linked, i.e., where the fault and inherited structures share a common geometrical orientation (Laó-Dávila et al., 2015; Phillips et al., 2016; Fazlikhani et al., 2017; Kolawole et al., 2018), or soft-linked, i.e. where the orientation of the fault is oblique to both the inherited structure and the extensional strain field (Agostini et al., 2009; Phillipon et al., 2015; Hodge et al., 2018; Samsu et al., 2019). The distinction is most likely related to the behaviour of the inherited structure as reactivation in the frictional domain will generally generate hard-linked structures while viscous deeper-seated deformation may favour soft-linked forms of inheritance (Samsu et al., 2023).

Inheritance in rift basins works across various scales and is possibly influenced by the regime in which the inherited feature is active (Holdsworth et al., 2001a; Samsu et al., 2023) for example it has been suggested that ductile weaknesses in the lower crust or

mantle influence the location and orientation rift segments (Agostini et al., 2009; Corti et al., 2013; Phillipon et al., 2015) and the formation of transfer zones (Acocella et al., 1999; Delvaux et al., 2000) while brittle structures in the upper crust segment individual faults (Reeve et al., 2015; Laó-Dávila et al., 2015; Phillips et al., 2016; Kolawole et al., 2018) and influence fault orientation at a smaller scale. However, there is little constraint on how these differences manifest in the same rift basin at the fault level. Furthermore, there is also little constraint on the temporal evolution of different types of inheritance on rift faults. Sahoo et al. (2020) show that terrane boundaries are important in the early localisation of strain, however, other studies have shown that rheological contrasts and inherited structures may remain active at a later stage of rifting (Muirhead and Kattenhorn, 2018). In this study, we use borehole-constrained 2D and 3D seismic reflection data to analyse the morphology of faults formed along terrane boundaries and their temporal evolution. The Great South Basin (GSB) presents an ideal study area for this as there is good constraint on the nature of the basement from onshore studies (Mortimer, 2004) and the characterisation of offshore geophysical data (Sutherland, 1999; Tulloch et al. 2019) and the rift history is well constrained (Sahoo et al., 2020). The basement structures and terrane boundaries all have a similar trend which is highly oblique to the rift trend, which makes evaluation of their different impact on rift evolution based on scale and rheology possible. Furthermore, high-quality 3D seismic data allows us to get an insight into the temporal evolution of terrane boundaries on rifting. We first examine the first-order differences between rift fault morphology and geometry between the different terranes before using fault analysis to gain a greater understanding of when faults were active and how terrane boundaries and inherited structures have influenced their displacement characteristics.

4.2 Geological Setting

The GSB (Fig. 4.1) contains up to 8.6 km thickness of sedimentary strata, of which 4 km is Late Cretaceous in the age (Sahoo et al., 2014; Morley et al., 2017) and formed during the breakup of Gondwana (Kula et al., 2007). Rifting in the GSB occurred from about 105 Ma to 83 Ma (Strogen et al., 2017) and led to the formation of a series of NE-SW trending grabens. However, several faults are orientated NW-SE that appear to follow basement terrane boundaries (Sahoo et al., 2020; Phillips & McCaffrey, in review). The main rift is however made up of NE trending faults that are significantly longer and have higher displacements than the NW trending faults (Sahoo et al. 2020). After rifting stopped in the GSB at ~83 Ma, seafloor spreading between Zealandia and Australia/Antarctica was established leading to thermal subsidence and a sag basin forming above the rift basins of the GSB (Gaina et al., 1998). The GSB has been relatively unaffected by post-Cretaceous contractional deformation related to subduction in the Tonga-Kermadec region and the formation of the Alpine fault (Sutherland et al., 2000; Sutherland et al., 2010). The remoteness of the GSB from the plate boundary along which this compressive deformation occurred meant only low amplitude and long wavelength folds like the Toroa anticline formed across this region. (Uruski, 2010)

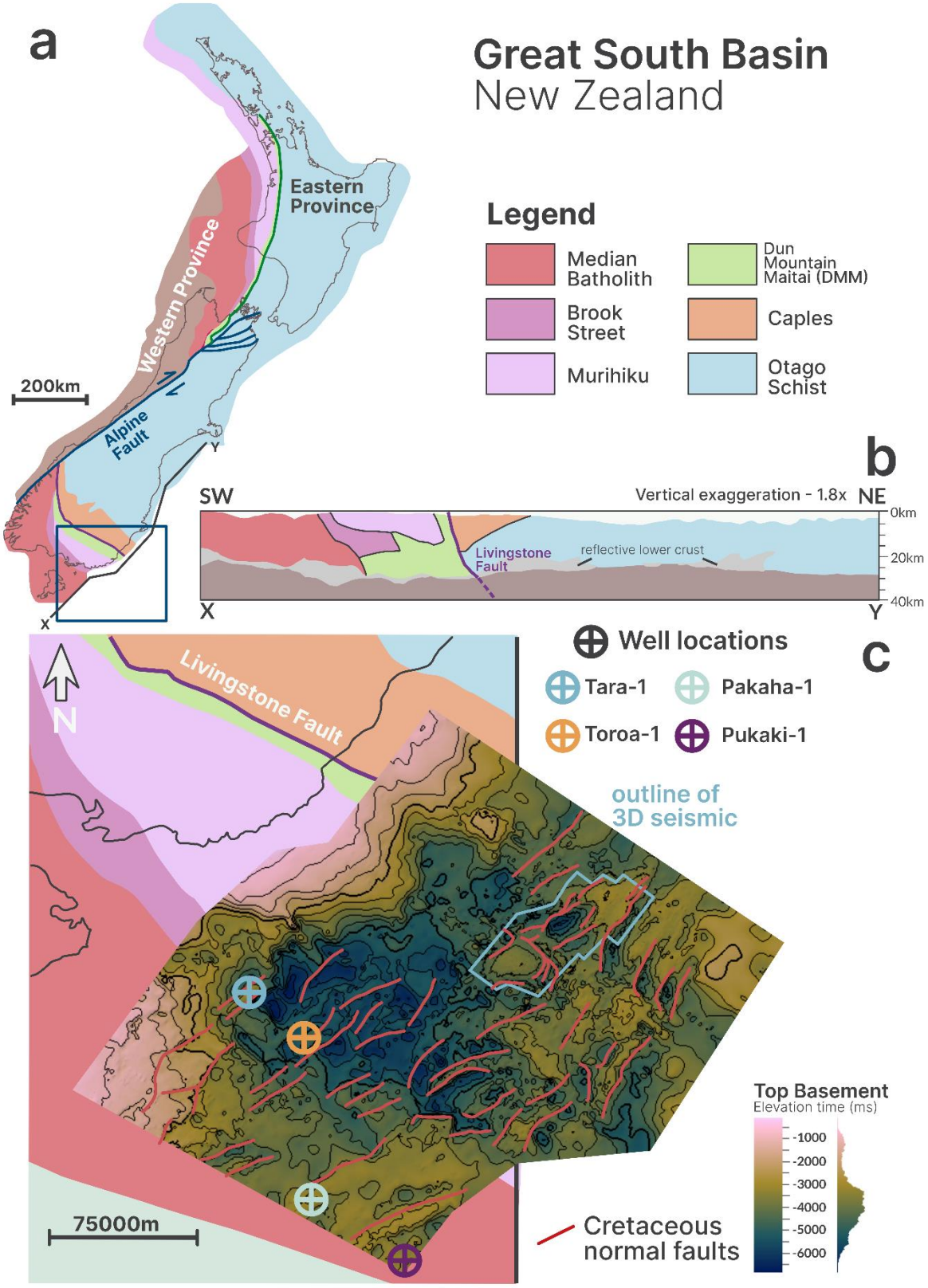
a
Great South Basin
New Zealand
Legend
Median Batholith
Brook Street
Murihiku
Dun Mountain Maitai (DMM)
Caples
Otago Schist
Eastern Province
Western Province
Alpine Fault
200km
X
Y
b
SW
NE
Vertical exaggeration - 1.8x
Livingstone Fault
reflective lower crust
0km
20km
40km
c
Well locations
Tara-1
Pakaha-1
Toroa-1
Pukaki-1
N
Livingstone Fault
outline of 3D seismic
75000m
Top Basement
Elevation time (ms)
-1000
-2000
-3000
-4000
-5000
-6000
Cretaceous normal faults

Figure 4.1 Overview Map of the Great South Basin, NZ

a) Map of New Zealand with the colour-coded basement terranes which have been displaced by dextral motion along the Alpine Fault. b) Cross-section interpreted from the SESI seismic line showing the structural arrangement of the basement terranes (modified from Mortimer et al., 2002) along the southeast coast of New Zealand, colours same as a) – location of SESI profile indicated in a). c) Regional map of the top basement (from Phillips et al. in review) surface of the GSB superimposed on the proposed terrane boundaries along the SE coastline of New Zealand. Major Cretaceous fault of the rift system is indicated in red and well locations used in conjunction with 2D lines to correlate horizons for this survey are indicated with a cross symbol – a generalised stratigraphy of the GSB with references to these wells can be seen in Figure S4.1. The location of the 3D seismic of this study is shown in light blue.

Like many other rift basins, the GSB did not form across homogenous crust and lithosphere but rather on a template of highly heterogeneous basement terranes (Fig. 4.1c). These terranes accreted along the southern margin of Gondwana during Cambrian to Early Cretaceous-aged subduction (Fig. 4.1b) (Bishop et al., 1985; Bradshaw, 1989; Mortimer et al., 2004). The Median Batholith separates the terranes into Eastern and Western Provinces (Mortimer et al. 2014). The Alpine Fault in the Cenozoic (Sutherland et al., 2000) has displaced the terranes and their boundaries so they are also present on the north-western side of New Zealand underneath the Taranaki basin (Muir et al., 2000; Collanega et al., 2019). The GSB is mainly underlain by terranes of the Eastern Province and the Median Batholith. The Eastern Province terranes are a series of volcanic and magmatic arcs and associated sedimentary

basins, derived from the Panthalassa Ocean (Bishop et al., 1985; Mortimer et al., 2002; Mortimer, 2004). In the GSB region, these include the Median Batholith terrane, the Brook Street Terrane, the Murihiku Terrane, the Dun Mountain-Maitai (DMM) terrane, the Caples Terrane and the Otago Schist (Mortimer, 2004). Of those only the Murihiku, the DMM and the Caples terrane are present in our study region. The Murihiku terrane is comprised of Late Permian to Late Jurassic volcaniclastic marine sandstones (Mortimer, 2004). It most likely represents a former fore-arc basin within the accretionary complex and has a low-metamorphic grade (Mortimer, 2004). The DMM terrane is composed of the Early Permian Dun Mountain Ophiolite and the sedimentary Maitai group (Kimbrough et al., 1992). The Livingstone fault, a terrane bounding possibly lithospheric-scale structure separates the DMM complex from the Caples terrane. The Livingstone fault is a major fault structure that is well exposed onshore (Tarling et al., 2019) as an, up to 480 m wide, serpentinite-dominated shear zone (Tarling et al., 2019). The Caples terrane is mainly a quartz-feldspathic volcaniclastic sedimentary terrane. It is weakly metamorphosed and tectonically imbricated, the schistosity of the Caples terrane increases towards the NE where it is overprinted by the Otago Schist (Mortimer, 2004).

4.3 Methods and Data

4.3.1 Data and Seismic Interpretation

In this study, we analyse 3D and 2D seismic datasets from the GSB with a primary focus on the 3D RIGEL dataset, which provides good spatial coverage and resolution of the GSB rift basins and enables us to analyse the influence of terrane boundaries of the Murihiku, DMM and Caples terranes on the rift morphology. The terrane boundaries were based on the onshore boundaries by Mortimer et al., (2002) and were extended offshore helped by aeromagnetic data (EMAG2v3 – Meyer et al., 2017) which can be found in the supplementary material (Fig. S4.2) In addition, we use DUN

2D and OMV 2D seismic surveys to cross-correlate the interpreted reflectors with wells and to analyse the larger structure of the GSB.

We interpret 4 seismic horizons across the area, including the seabed. We mapped the most prominent reflectors that showed major changes in the tectonic history of the area and then used 2D seismic lines to tie these wells outside of the 3D survey area. The mapped horizons are as follows: i) top Basement; ii) top Coniacian (~85 Ma), iii) top Cretaceous (~66 Ma) and iv) the seabed. We then used the mapped reflectors to create surfaces for these horizons and calculate thickness maps of the top Basement to top Coniacian interval and the top Coniacian to top Cretaceous interval.

4.3.2 Quantitative Fault Analyses

We used throw-length plots (Cartwright et al., 1995; Walsh et al. 2003) of key faults along the terrane boundaries to assess the difference in fault behaviour between faults that are influenced by terrane boundaries (those with curving geometries or NW-SE trends) and those that mostly follow the regional NE-SW trend. Throw is calculated by measuring the hanging wall and footwall cutoff across faults of the top-Basement horizon. For the NW-SE trending faults we measured the throw of the top-Coniacian horizon instead as it records the majority of the throw history for these faults.

4.4 Results

4.4.1 General Rift Morphology

Rift morphology shows substantial changes along the strike of the rift system that are most pronounced when crossing terrane boundaries.

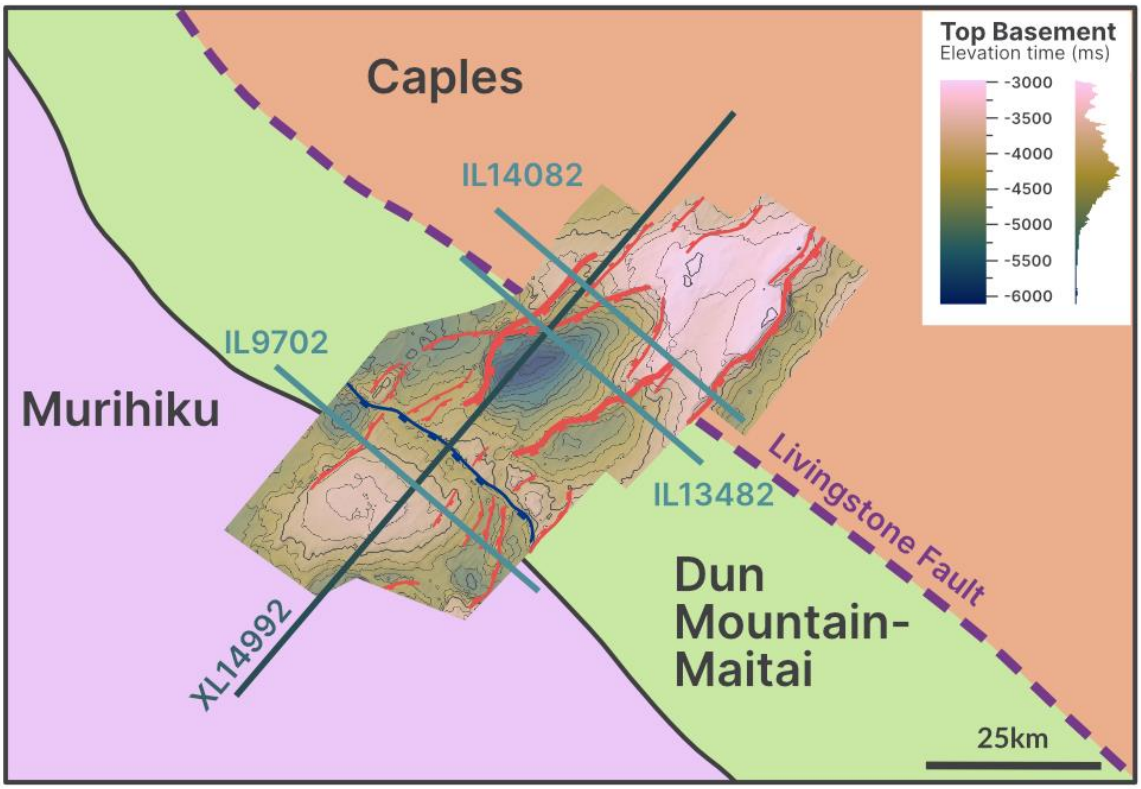

Figure 4.2 Top Basement of the 3D Survey Superimposed on Terrane Boundaries

Top basement of the 3D survey with faults superimposed on the projected terrane boundaries. Faults broadly trending NE-SW in red while the fault trending NW-SE is indicated in dark blue. Seismic lines discussed in 4.1.1 – 4.1.4 are indicated. A version without the overlain seismic lines can be found in the supplementary material (Fig. S.4.2)

The top basement surface with superimposed faults (Fig. 4.2) shows the main structural architecture of this part of the GSB. Most faults trend NE-SW and create large downthrown fault basins on their hanging wall sides. There are two prominent basement highs in the region one to the SW which is within the Murihiku terrane and one in the NE which is within the Caples terrane. Both basement highs represent regions that are less faulted. The Murihiku basement high shows various small-scale faults with small offsets that match the regional trend (NE-SW) while the Caples

basement high shows a small downwarping in the central part of its western margin. While the faults flanking the Caples basement high dip in opposite directions, i.e. faults on the northern side dip to the NW while faults on the southern side dip to the southeast, faults on either side of the Murihiku basement high dip to the northwest. These faults are locally deflected along the terrane boundary between the Murihiku and the DMM. A large structure that trends perpendicular to the regional fault trend is located on the terrane boundary. This NW-SE trending fault (in blue) represents a major ridge line with an elevated footwall that separates the Murihiku faults from the faults within the DMM terrane. Across this structure the fault polarity switches and while the faults mostly still follow the regional NE-SW trend they now dip to the SE. There are smaller faults in the footwall of the NW-SE trending faults that seem to terminate as they approach the fault separating the Murihiku and DMM rather than rotate into the terrane boundary as the faults do in the hanging wall. The DMM terrane also hosts the largest faults which create the largest fault bound basins and extend for up to 25 km in length. These large faults splay and segment into smaller fault segments as they approach the Caples and DMM boundary. There is no large fault separating the two terranes as observed with the Murihiku/DMM boundary and the deformation is partitioned across multiple fault strands and splays. The NE-SW trending faults in the Caples terrane dip in either direction and terminate on the western edge of the basement high or continue along either side of it. There is a major fault-bounded basin on the south side of the Caples basement high while the northern side is more elevated and only shows smaller fault basins. The basement surface map reveals that the terranes host fault systems that vary in geometry and displacement and the two boundaries between the terranes separate areas of contrasting basement morphology.

To best demonstrate and capture the changes in rift morphology across the basement terranes, we discuss four characteristic seismic profiles taken across the rift, one from each basement terrane (Murihiku, DMM and Caples) and one along the prominent boundary of the DMM and Caples Terranes. We also discuss one profile taken along the strike that shows best the morphology of the rotated fault along the DMM and Murihiku boundary. Figure 4.2 shows the location of the respective profiles.

Murihiku – IL 9702

The Murihiku basement terrane in the SW of the study area is characterised by abundant strong intra-basement reflectivity (Fig. 4.3). The shallower part of this intrabasement reflectivity within the main basement high is characterised by gently inclined continuous reflectors which are cut by faults and locally rotate parallel to the dip of the top basement, while lower down, below 5500 ms TWT the reflectors are inclined by long wavelength folds. Below that at about 7500 – 8000 ms TWT the reflector strength increases, and they are horizontal and discontinuous. The fault geometry varies, with faults closer to the southeast displaying a listric geometry that suggests they detach into the basement reflectivity. Further to the northwest, away from the boundary to the DMM terrane, the faults are mostly planar and do not show detachment into the basement reflectivity. Most faults, apart from minor antithetic faults in the basement high, dip to the northwest and accommodate between 500-2000 ms of throw in TWT. The basement high itself shows little deformation in the form of faults with minor offsets. The faults to the NW and SE of the basement high show the highest amount of rotation of the footwall as they accommodate the largest amount of throw and appear to detach into the intrabasement reflectivity. Meanwhile, the faults within the basement high show little vertical displacement and do not appear to detach and therefore exhibit little to no footwall rotation. The fault bounding

the basement high to the NW accommodates the largest amount of displacement in this profile equating to about 1200 ms TWT.

The main syn-rift fill in this section formed between rift initiation (~105 Ma) and the end of the Coniacian stage. The faults do not displace the Top Coniacian reflector therefore rift activity ceased before the end of the Coniacian. The Coniacian synrift fill shows classic wedging geometries and differs in thickness from about 500 – 1000 ms TWT which equates to about 875 to 1750 m of thickness, assuming an average seismic velocity of 3000 m/s for the siliclastic sedimentary infill. The early post-rift fill from the top Coniacian to the top Cretaceous drapes over the topography left behind by earlier rifting (Fig. 4.3) resulted in slight thickness differences due to the underlying relief. It generally thickens towards the northwest from about 200 ms to 600 ms equating to about 300-900 m of thickness.

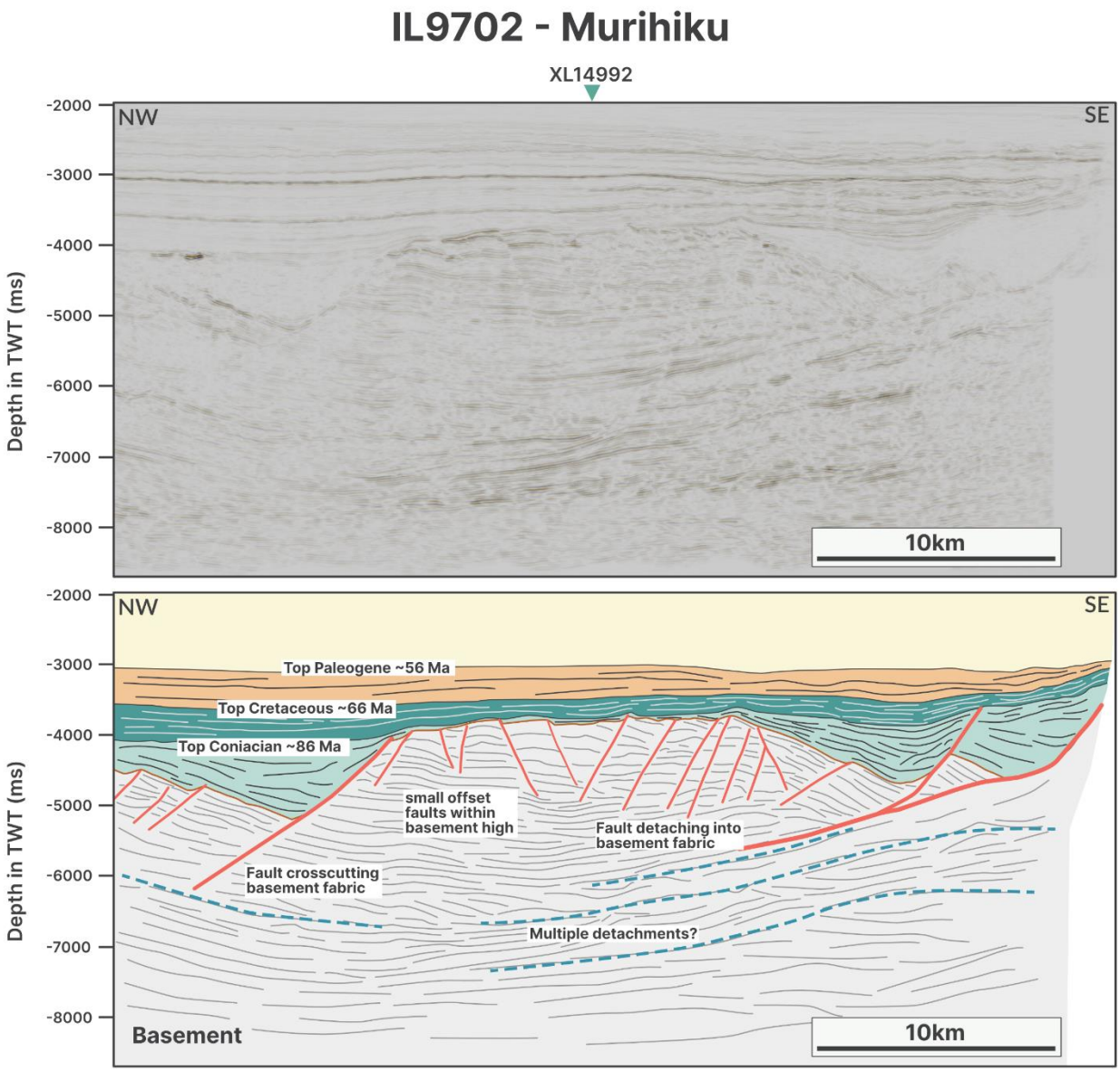

Figure 4.3 Seismic Images of Section through the Murihiku Terrane

Uninterpreted (top) and interpreted (bottom) seismic section across the Murihiku terrane showing the general fault morphology of faults within the Murihiku terrane. Not the normal faults to the SE of the prominent basement high which are detaching in the basement reflectivity. See Fig. 4.2 for location.

Dun Mountain – Maitai IL13482

The Dun Mountain Maitai terrane is characterised by the deepest fault basins and formed by faults with the highest displacements (Fig. 4.4). These faults dip in the opposite direction to those in the Murihiku terrane and deformation is localised on two major faults that dip to the SE. The faults show listric geometries as their dip decreases with depth. The faults show offsets of between 2000-3000 ms of throw in TWT. The basement reflectivity in the DMM terrane is much less pronounced than in the Murihiku. Reflectors are more discontinuous and of lower reflector strength. There are reflectors along the faults and in their immediate vicinity which may reflect the wider damage zone of the major faults. There is a deeper level of basement reflectivity at 7.5-8 s TWT which is characterised by higher reflector strength but discontinuous reflectors which show gentle folding. Similar to the Murihiku terrane, none of the faults in the DMM terrane displace the top Coniacian reflector. The Coniacian synrift shows classic wedge-shaped geometries characteristic for synrift strata and shows maximum thicknesses of 1000 ms and 2000 ms for the two respective fault basins. The Late Cretaceous strata drape over the fault blocks and basins and show little variation in thickness. Therefore, these faults were active up to the Coniacian and experienced major displacement.

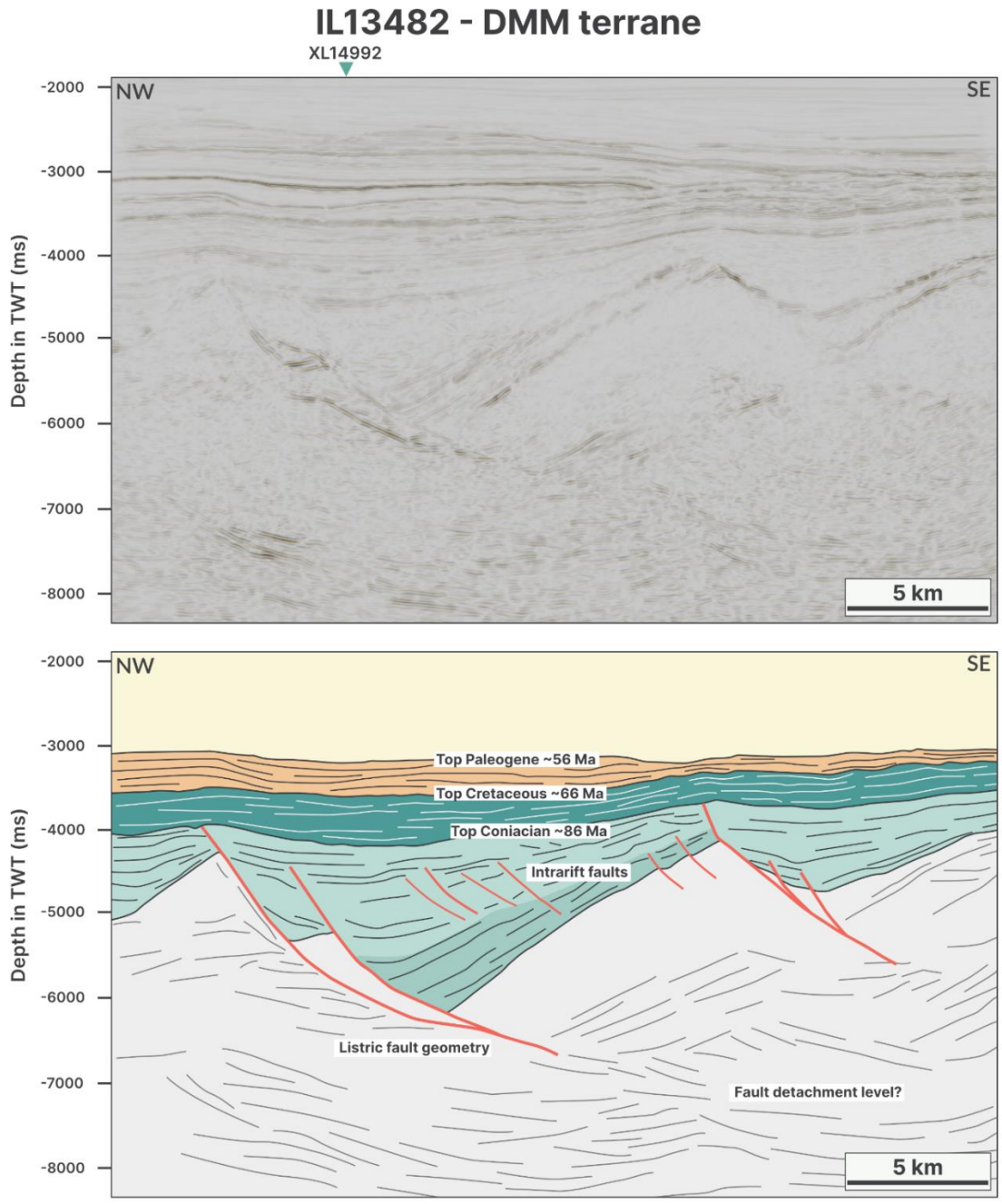

Figure 4.4 Seismic images of Section through the DMM Terrane

Uninterpreted (top) and interpreted (bottom) seismic section across the DMM terrane showing the general fault morphology of faults within the DMM terrane. The DMM terrane is characterised by large displacement southeast dipping half grabens – note the change in fault polarity compared to the Murihiku terrane. See Fig. 4.2 for location.

Caples Dun Mountain-Matai Boundary

Moving from the DMM into the Caples terrane and crossing the Caples-DMM terrane boundary the fault geometry changes again (Fig. 4.5). Instead of the high displacement half graben structures mostly observed in the DMM terrane, faults dip in opposite directions producing horst and graben structures. The graben faults are also much more distributed than in the DMM terrane where the strain was localised onto a few large faults, while at the boundary of the Caples and DMM terrane, the strain is accommodated by multiple faults with varying amounts of displacement dipping both to the NW and SE. There are also different generations of faults visible as some faults are basement rooted while other faults must have formed later and only occur within the Coniacian syn-rift fill (Fig. 4.5). The large border faults that bound the graben were active at a similar time as the large faults in the DMM, they generally do not displace the top Coniacian reflector or any post-Coniacian strata, therefore these faults have likely been active into the Santonian (Fig. 4.5). The intra-rift faults within the Coniacian strata have likely formed later than the larger bounding faults, as they do not displace the basal part of the graben fill sequence. However, these faults may have been more active at a later stage as they bound a smaller graben of later synrift fill, indicated in a lighter shade of green in Figure 4.5. The basement reflectivity is less prominent than in the DMM or Murihiku terranes. Largely the Caples terrane is transparent with only minor traces of basement reflectivity which is seemingly unconnected to the faults and has no impact on these. At greater depths, there are some horizontal reflections similar to the other sections.

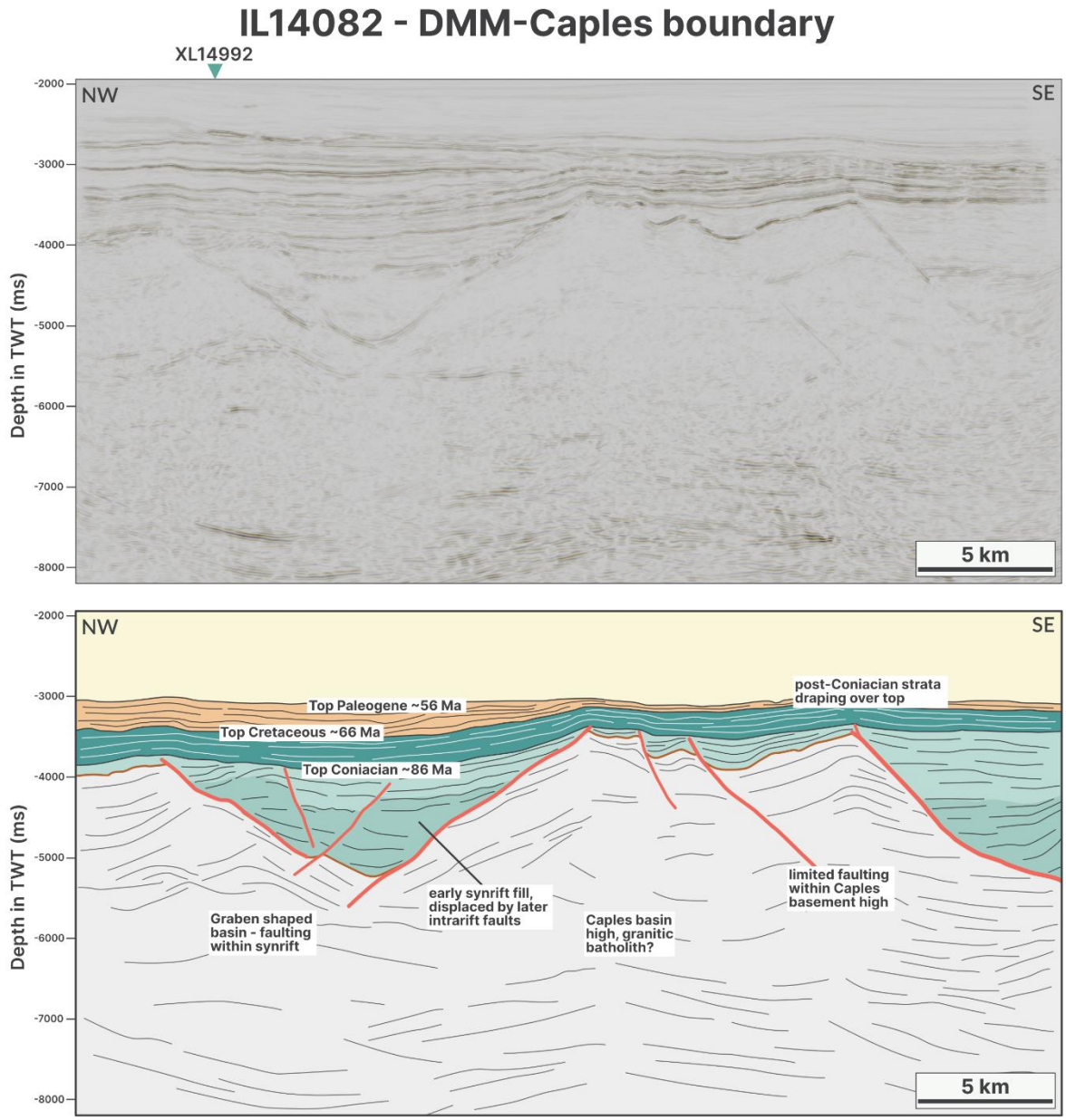

Figure 4.5 Seismic images of Section near the DMM-Caples Boundary

Uninterpreted (top) and interpreted (bottom) seismic section across the Caples terrane showing the general fault morphology of faults near the boundary of the DMM and Caples terrane. Note the change in fault morphology from the DMM (Fig. 4.4) where large SE dipping half grabens have been replaced by grabens with more complex and distributed fault patterns, characteristic of accommodation zones. See Fig. 4.2 for location.

Crossline

The Crossline (Fig. 4.6) is orientated subparallel to the predominant fault trend as opposed to the Inline sections which were orthogonal to the NE-SW trending faults. However, while the major NE-SW trending faults are mostly apparent as large trough-shaped depressions without obvious faults, there is a prominent fault near the DMM and Murihiku terrane boundary. This fault shows both a thin wedge-shaped basin in the Coniacian but also a larger wedge-shaped basin in the Coniacian-Cretaceous strata. The fault displaces both the top Basement and the top Coniacian. Both the Murihiku and Caples form apparent basement highs which flank the larger depressions at the centre of the DMM terrane.

The basement shows the clear differences between the three different basement terranes. Notably, the Murihiku terrane is characterized by strong folded basement reflectivity. Meanwhile, the Caples terrane is more transparent and shows little basement reflectivity. Differentiating the DMM from the Caples is more difficult since both do not have obvious continuous basement reflectivity. However, at depth, the DMM shows more reflectivity which is seemingly truncated by the more transparent Caples which may be a seismic expression of the Livingstone Fault at depth.

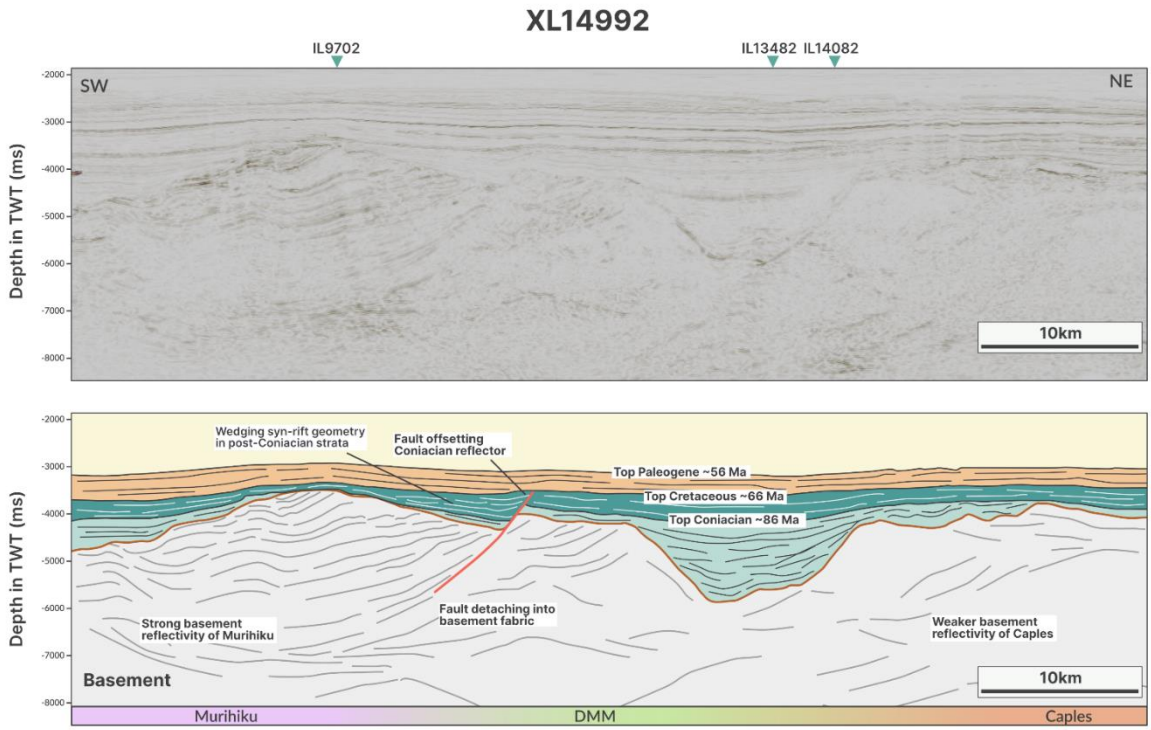

Figure 4.6 Cross-sectional Seismic Line across the Three Terranes.

Uninterpreted (above) and interpreted (below) seismic section across the different terranes, parallel to the predominant NE-SW fault trend. Note the change in basement reflectivity from the well-developed folded basement reflectivity in the Murihiku (left) to the more transparent basement of the Caples (right). The NW-SE trending fault along the Murihiku-DMM terrane boundary displaces both the top basement and top Coniacian reflector, signalling protracted activity along this terrane boundary. See Fig. 4.2 for location.

4.4.2 Surfaces and Thickness Distribution

The top basement surface shows the general morphology of the rift illustrating that the main rift faults of this area of the GSB trend roughly NE-SW except for a major fault parallel to the DMM-Murihiku terrane boundary that trends NW-SE (Fig. 4.2). The previous seismic sections showed that these faults have varying levels of temporal

activity with the NW-SE trending structure active for a longer time period than the NE-SW trending faults as it displaces the Coniacian reflector and is active until later in the Cretaceous. Therefore, it is important to look at the morphology of the syn-rift (with regards to the NW-SE trending fault) and post-rift surfaces, as well as the thickness map of the syn-rift strata to detect the spatial variability of the syn-rift, fill across different time stages. Shifting patterns of syn-rift deposition can reveal patterns of fault activity across the survey area.

Syn- and Post-rift surfaces

The top Coniacian surface (Fig. 4.7a) shows a basement high in the southwest (within the Murihiku terrane) and in the northeast (within the Caples terrane) of the survey, with the basement high in the Caples more elevated than the Murihiku high. Generally, the elevation of the surface increases from the west to the east, where the Caples High is located. However, a major change from the top basement surface is an absence of most of the topography created by the NE-SW trending faults which were prominent features in the top Basement. These basins are now mostly infilled and there a no apparent depression on the Coniacian surface, apart from the area to the southwest of the Caples basement high where a large basin appears underfilled as seen on the seismic lines (Fig. 4.5). However, the northwest trending fault parallel to the Murihiku-DMM terrane boundary is now more apparent and shows a large relief. This ridge extends to the southeast where it starts to curve into the Murihiku terrane, forming a prominent J-shaped curved line. The elevation difference increases towards the SE with a local maximum at the inflexion point. Towards the northern end of the Murihiku high the connection between the northeast trending fault and the northwest trending fault is less defined than in the south.

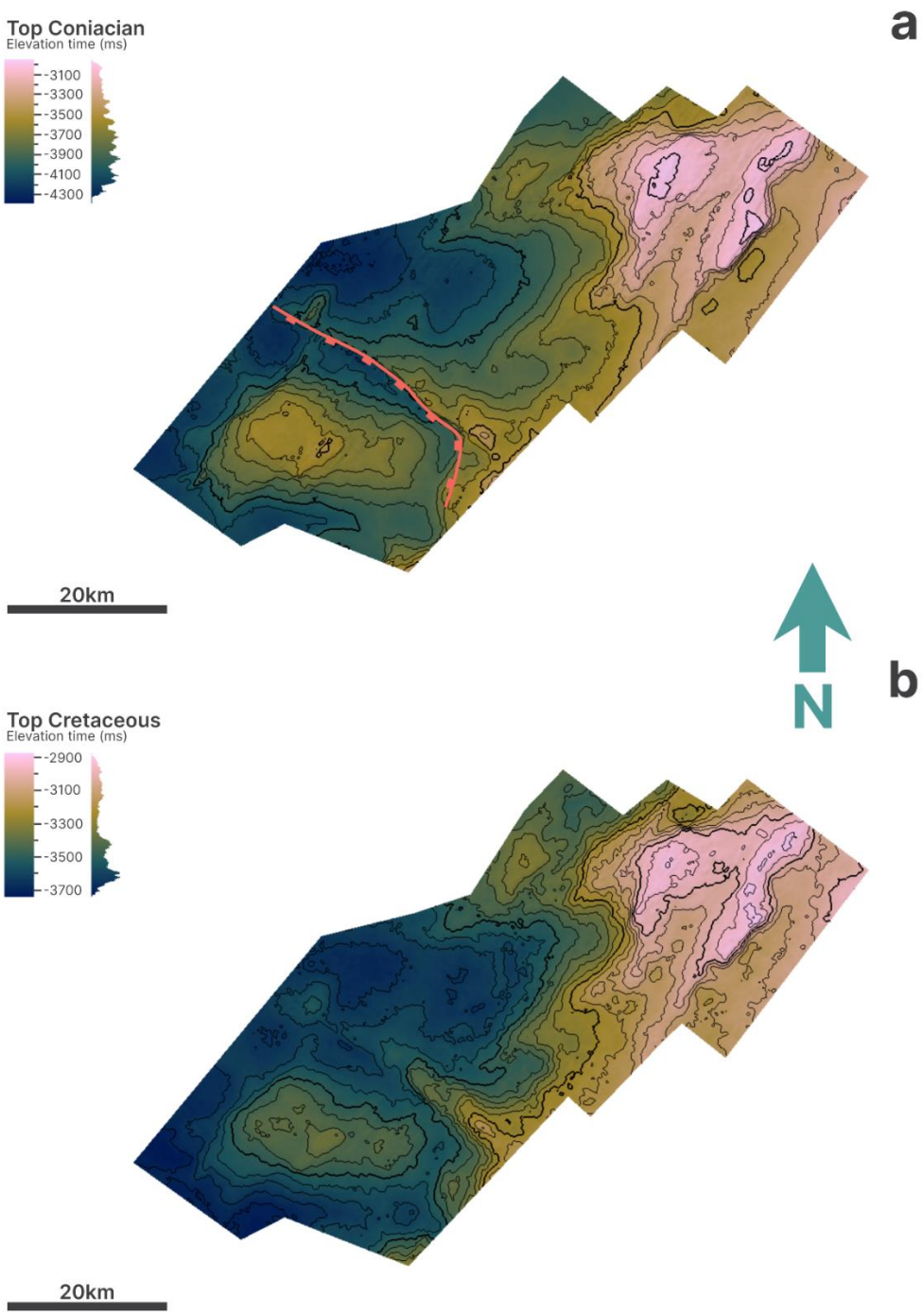

Figure 4.7 Surface Maps of the Top Coniacian and Cretaceous

Surfaces of top Coniacian and top Cretaceous reflectors. Most NE-SW trending faults have been infilled and show no surface expression on either surface, however, the NW-SE trending fault along the DMM-Murihiku boundary shows

prominent surface expression on the Coniacian surface manifesting in a J-shaped ridge. Note also the change of scales with the top Cretaceous only showing a difference of 800 ms across the surface while the Coniacian ranges from -3000 ms TWT to -4300 ms TWT.

The top Cretaceous now marks the point where all fault activity has ceased as apparent on all the selected seismic lines (Fig. 4.3-6) which show no displacement of the top Cretaceous reflector by faults and no obvious fault-generated topography. There is a large elevation difference between the basement high in the Caples and the more low-lying areas in the northwest of the area with the Caples basement high still showing the highest elevation, however, the difference in elevation across the surface is now a mere 800 ms, as opposed to the 1300 ms on the top Coniacian or over 3000 ms difference on the top basement surface. There are some higher-standing topographic features in the Murihiku and the DMM terranes which have been blanketed by Late Cretaceous strata, but they are less apparent.

Thickness Maps

A thickness map of the main syn-rift strata is shown in Figure 4.8. It shows the thickness of the sedimentary strata deposited and preserved from the onset of rifting to the end of the Coniacian. It shows major centres of deposition in the centre which are trending NE–SW. At the eastern edge, there is another major depocenter approximately trending NE-SW. Surrounding these are large areas of no deposition which correspond to the main basement highs which are visible on the top basement surface. In the southwestern part of the thickness map, there is an isolated approximately 900 ms deep depression at the intersection of the NW-SE and NE-SW trending faults. In the southeastern region portion, there are smaller NE-SW trending

basins whose thicknesses increase away from the NW-SE trending fault from 600 ms to about 1400 ms.

The thickness map for the syn-rift strata from the top Coniacian to the top Cretaceous reflectors (Fig. 4.8b) varies significantly from the syn-rift strata (Fig. 4.8a) and is less dominated by large areas of little to no thickness. The scale has also changed, while the thickest basins in the early syn-rift phase were up to 2000 ms thick, now the maximum thicknesses found are 600-700 ms. On top of the larger east-trending basins which were clear in the Basement-Coniacian thickness map, there are now circular patches which may reflect general thermal post-rift subsidence as they do not appear to be fault-controlled. The overall thickness of the Coniacian-Cretaceous strata increases towards the NW and is thickest at the NW edge of the outlined surface. The regions corresponding to basement highs in the top Basement surface received little sedimentary deposition with only up to 100-200 ms thickness recorded in places. The main feature is an NW-SE trending basin running parallel to the Murihiku-DMM terrane boundary which corresponds to the anomalous NW-SE trending fault, here sedimentary fill up to 500 ms is observed. Further to the NW-SE where it intersects with the NE-SW trending fill there is a local maximum of about 600 ms which is broadly superimposed on the circular-shaped depression from the Basement-Coniacian thickness map. At the southern intersection with the NE-SW trending fault the basin curves around and reaches up to 300 ms. Coniacian-Cretaceous synrift fill is more focused and localised on the NW-SE trending fault.

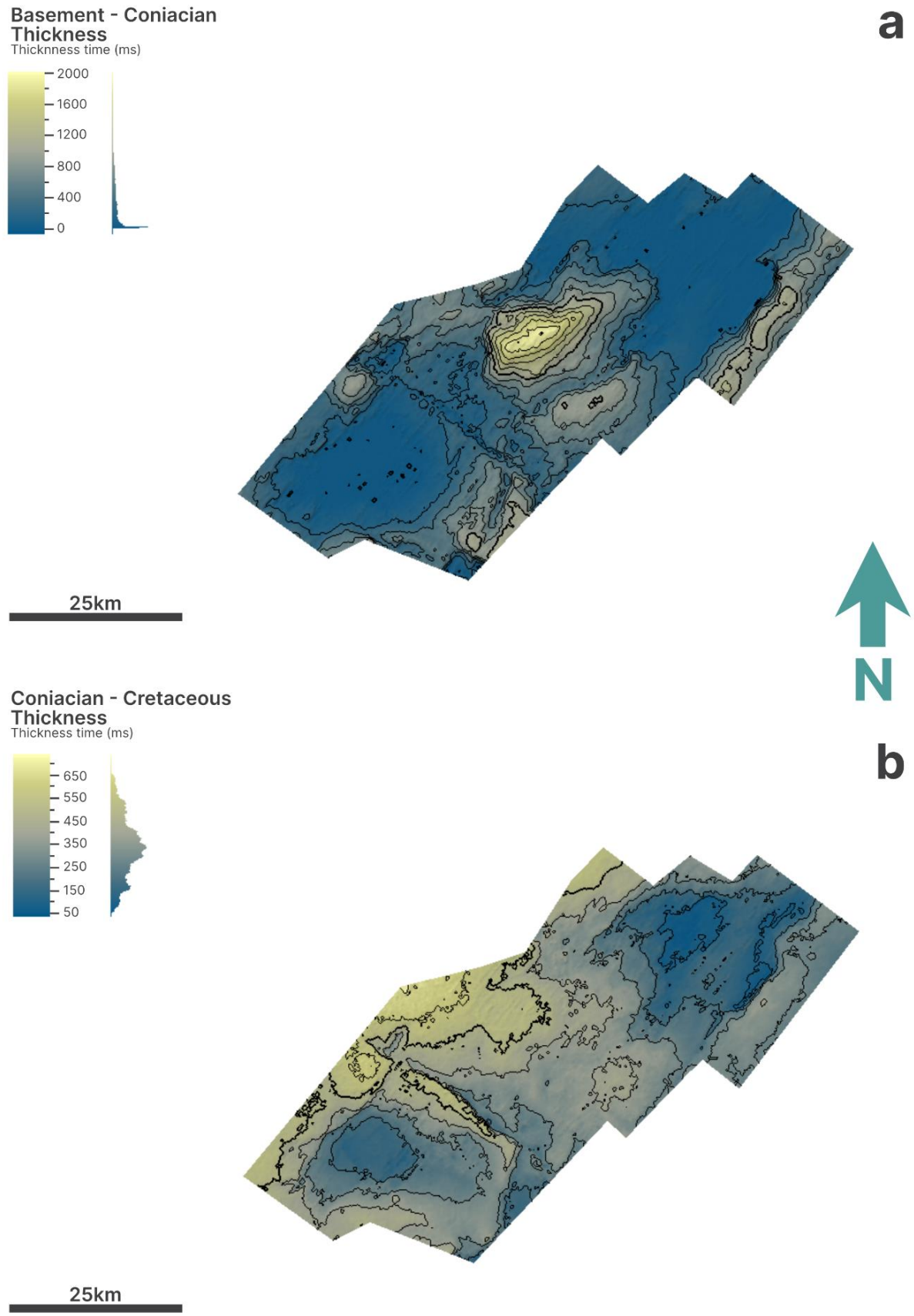
Basement - Coniacian
Thickness
Thicknness time (ms)
2000
1600
1200
800
400
0
a
25km
N
Coniacian - Cretaceous
Thickness
Thickness time (ms)
650
550
450
350
250
150
50
b
25km

Figure 4.8 Thickness Maps

Thickness surfaces of the two syn-rift intervals (Top Basement- Top Coniacian and Top Coniacian- Top Cretaceous). The Early syn-rift fill is much thicker (up to 2000 ms TWT) and focused on the NE-SW trending faults. The NW-SE trending fault saw little syn-rift fill during that period. The second syn-rift period is focused on the NW-SE fault with the NE-SW trending faults being inactive during this period.

4.4.3 Displacement-Length Plots

To further investigate the rift evolution and throw characteristics of faults we selected the main rift faults and analysed their throw variation along fault length. For this, we picked faults from the Murihiku, Caples and the DMM terranes. We also analysed the throw profile of the NW-SE trending fault itself which both offsets the basement and the top Coniacian to further understand its throw evolution. For a further discussion of the displacement-length of the faults in the global context see supplementary figure S4.5

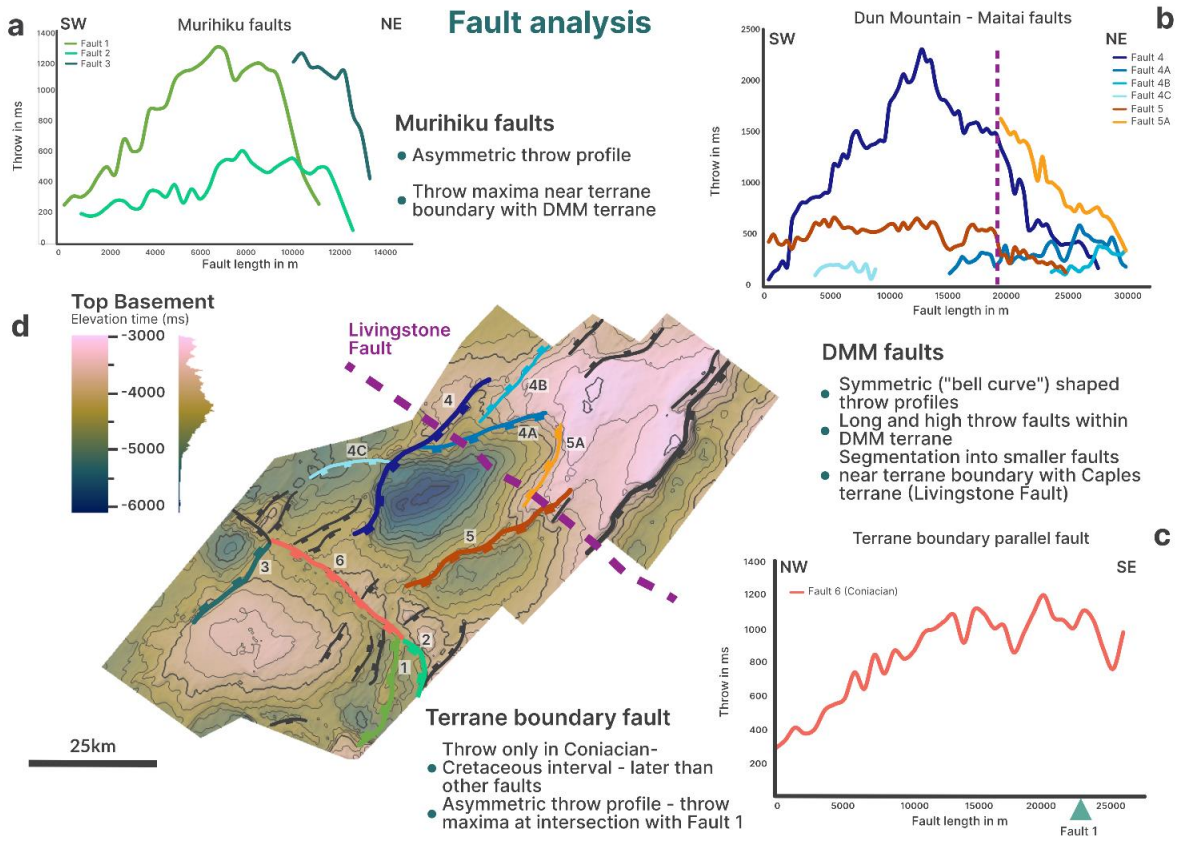

Figure 4.9 Displacement–Length Plots

Displacement-length plots of the major faults within the different basement terranes, faults colour-coded, and the position shown on the top basement surface. a – Faults in the Murihiku terrane showing a highly asymmetrical throw profile with the maximum throw close to the terrane boundary; b – mostly symmetric profiles of the faults in the DMM and Caples terrane. Segmentation into smaller faults and splaying coincide with the projected Caples-DMM boundary (in purple dashed line) c – Terrane boundary parallel fault between Murihiku and DMM terrane shows only displacement in the post-Coniacian period, displacement is highest near the intersections with the NE-SW trending Fault 1, broadly increases from northwest to southeast towards Fault 1. d – Top basement surface showing the location of the colour coded faults, Livingstone Fault (terrane boundary between DMM and Caples) indicated as dashed purple line.

Murihiku terrane

The faults in the Murihiku terrane (Fault 1, 2 and 3) are mostly NE trending and appear to locally curve into the northwest trending terrane boundary as they meet the misorientated fault along it (Fig. 4.9a). All three faults show a highly asymmetrical and remarkably similar throw profile (Fig. 4.9a). Both Fault 1 and 3 have a high displacement of 1200-1300 ms near the terrane boundary with the DMM terrane. Fault 2 has a smaller throw maximum of just 600 ms. However, all faults show the fault throw decaying away from the Murihiku-DMM terrane boundary, therefore the maximum displacement of these faults is not in the centre but close to their inflexion point. Fault 2 is cut off by the end of the 3D survey data, therefore the throw profile is not complete, however, it is likely to be similar to Faults 1 and 3.

Dun Mountain-Maitai terrane

The Dun Mountain-Maitai terrane exhibits two major faults with minor splays towards the Caples terrane boundary. The two major faults are Fault 4 (in dark blue) and Fault 5 (in orange) in Figure 4.9d. Both are major basin bounding faults as shown in the previous sections (compare thickness map, surfaces and seismic expression). Of those two Fault 4 has the highest throw which reaches up to 2500 ms in TWT (Fig. 4.9b), equating to about 3750 m of throw assuming an average seismic velocity of 3000 m/s for the basin fill.

Fault 4 (Fig. 4.9b) shows a broadly bell-shaped displacement profile with the highest displacement of 2500 ms TWT in the centre of the fault at ~ 15000 m. However, it also shows a rapid loss of displacement at around 19000 m where the fault throw drops

from about 1500 ms to 500 ms. This drop in displacement broadly coincides with the terrane boundary between the Dun Mountain-Maitai and the Caples terrane, indicated by a purple line in Figure 4.9b. Around this line, the fault also splays into different smaller fault segments, namely Fault 4A which is a synthetic splay with a slight change in orientation to ENE-WSW and Fault 4B which is an antithetic splay that is broadly the same orientation as Fault 4. On the other side, there is another fault splay towards the Murihiku terrane boundary named Fault 4C, which is similar in orientation to Fault 4A and meets Fault 4 at the same point as Fault 4A.

Fault 5 (Fig. 4.9b) bounds the smaller basin to the south of Fault 4. It reaches a maximum fault throw of 700 ms which drops to about 300 ms at 20000 m. It has again a bell curve-shaped throw profile. At 20000 m Fault 5A starts to develop which has a highly asymmetric throw profile and is antithetic to Fault 5. Closer to the terrane boundary of DMM and Caples it has a fault throw of 1600 ms which then rapidly decays away from it to just 300 ms. Fault 5A is antithetic to Fault 5 and they both bound a high-standing ridge of the Caples terrane. Major changes in fault throw are observed at about 20000 m, coinciding with the Caples DMM terrane boundary.

Terrane boundary parallel fault (Fault 6)

Fault 2 is distinct from the other faults as it is a NW-SE trending fault that has developed parallel to the Murihiku-DMM terrane boundary and is nearly parallel to the extension direction (Fig. 4.9c). It displaces both the top basement reflector and the top Coniacian reflector. It broadly displays a gradual increase of throw towards the southwest. Towards the northwest it reaches Fault 3, against which it terminates, therefore the plot shows the throw of Fault 6 between the intersection points with Fault 3 and Fault 1. It has the lowest throw adjacent to Fault 3 and then gradually rises

to about 1200 ms of throw where it intersects Fault 1. Thus, the maximum displacement is reached at the intersection point with Fault 1.

4.5 Discussion

4.5.1 Differential Impact of Terrane Boundaries on Rift Evolution

Within the study area, we observed the impact of two terrane boundaries (DMM and Murihiku/Caples and DMM) on rift morphology and throw distribution. These two terrane boundaries vary in their scale. While the Murihiku and DMM boundary is most likely a mainly upper crustal inherited feature, the Livingstone fault has been shown to be a much larger fault zone that is up to 400 m in width onshore (Tarling et al., 2019). On the SESI deep-seismic line (Mortimer et al., 2002) the Livingstone Fault appears to extend deep into the lower crust and is likely to be a larger lithospheric scale fault, which may be active in the viscous regime. Based on our observations from 3D seismic data the expression of these two types of inheritance on rift morphology is as variable as their scale and nature. Both structures are highly oblique to the main NE-SW rift axial trend which would make them generally unsuitable for reactivation (Ranalli and Yin, 1990; Leclère and Fabbri, 2013; Williams et al., 2019) and yet their impact on structuring the rift is apparent in the results presented above, in the following we evaluate why their influence has been so different.

The boundary between Murihiku and DMM is directly reactivated by a fault that exploits the abundant upper crustal foliation planes which can be seen on seismic data (Fig. 4.3). These cause the fault to rotate to a direction nearly parallel to the extension direction and terrane boundary. While this may indicate, following classic models of fault mechanics, that this fault is a strike-slip fault (Ranalli and Yin, 1990), based on the seismic data there is no evidence to indicate that this is the case as there has been no lateral offset observed along the fault. Indeed, in cross-section, the fault shows a clear wedging syn-rift infill by Coniacian to Late Cretaceous strata indicating

dip-slip kinematics during evolution. However, strike-slip displacement remains hard to recognise on seismic data alone, therefore oblique-slip on this fault is a distinct possibility. The temporal evolution of this fault is also different to the on-axis trending faults. While most extension direction perpendicular faults are active until the the late Coniacian and are passively infilled by Coniacian-Cretaceous strata, this misorientated fault actively displaces Coniacian strata indicating activity into the Late Cretaceous. That both inheritance-controlled and regional strain field-controlled faults can be active at the same time matches observations by Reeve et al. (2015), from the Maloy Slope in the Northern North Sea. However, they speculate that during the rift evolution, N-S faults controlled by the regional extension direction became dominant over the NE-SW inheritance-controlled structures. Examples from the East African Rift show that inheritance can control fault evolution much later in the rift evolution as well: A transverse fault system develops after the development of rift parallel faults above a transverse basement structure (Muirhead and Kattenhorn, 2018). Faults from the Murihiku appear to rotate into the DMM-Murihiku terrane boundary as they approach it, while faults from the Dun Mountain Maitai terrane are terminated as they approach the DMM-Murihiku terrane boundary from the northwest. This is seen in the J-shaped syn-rift basins developing in the Coniacian along the terrane boundary (see Fig. S4.4 for a variance slice showing the curving of the fault). During the Coniacian to Late Cretaceous, these curved basins are reactivated as there is a small amount of offset observed along the NE-trending faults, however, most activity is now concentrated in the zone separating the curved basins (Fig. 4.9c). This suggests that the terrane boundary actively shaped syn-rift basins during the Coniacian causing faults in the Murihiku to rotate, these remained isolated initially. Similar observations of curving basins aligning along a pre-existing structure oblique to the extensional strain field were made in Thailand by Morley et al. (2004). However, in that study, the temporal

activity of the oblique linkage fault compared to the individual basins which are perpendicular to the extensional strain field is unclear. Here, we see that when the Late Cretaceous activity on the extension perpendicular faults waned, the terrane boundary between Murihiku and the DMM terrane aided linkage resulting in a fault parallel to the extension direction and terrane boundary, connecting the initially curved basins in the Murihiku terrane (Fig. 4.10). The fault has higher displacement towards the southeast (Fig. 4.9c) which may be due to preferential geometric orientation: the curved basins south of the basement high curve towards the basins north of it, therefore it may be easier for linkage to progress from south to north. While the Murihiku-DMM boundary has actively segmented the rift and impacted the geometry of faults approaching it in the Coniacian, easy slip horizons along it were able to accumulate strain for longer during the rift evolution as is seen by the activity along it continuing until the Late Cretaceous (Fig. 4.6).

The boundary between DMM and Caples defined by the Livingstone Fault does not show evidence for direct reactivation but possibly contributed to the segmentation and splaying observed along it (Fig. 4.9b). As observed on the top basement surface (Fig. 4.2) and on the displacement-length plots (Fig. 4.9b) a change in fault geometry and displacement is roughly coincident with the terrane boundary. As the major faults (Fault 4 and 5) experience a drop in displacement, smaller scale faults that are minor fault splays, have accommodated the strain (Fig. 4.9b). Lithospheric structures segmenting rifts are commonly observed or proposed in other rifts such as the North Sea (Fossen et al., 2016), the Taupo Rift (Rowland and Sibson, 2004) or the East African Rift Zone (Ebinger et al., 1989; Corti et al., 2022) and have been modelled in various analogue and numerical modelling experiments (Acocella et al. 1999; Agostini, 2009; Zwaan et al., 2016). In all these examples the lithospheric suture sees no direct reactivation but segments and influences the orientation of rift faults. It is possible the

observed splaying and segmentation could also be explained by a strength contrast as has been observed on a more regional scale in the Western GSB at the boundary to the Median batholith (Phillips and McCaffrey 2019) or in the UK Carboniferous rift systems where granitic bodies form less deformed “stronger” areas surrounded by faults (Fraser and Gawthorpe, 1990; Howell et al., 2020). A granitic body emplaced within the Caples terrane could explain the absence of seismic reflectivity in the basement which might make it much stronger compared to the ophiolitic lithologies of the DMM terrane. Therefore, the DMM-Caples boundary may be a combined effect of a rheological discontinuity and an inherited lithospheric scale feature that causes faults to segment and splay along its boundary, but it does not promote direct reactivation (Fig. 4.11).

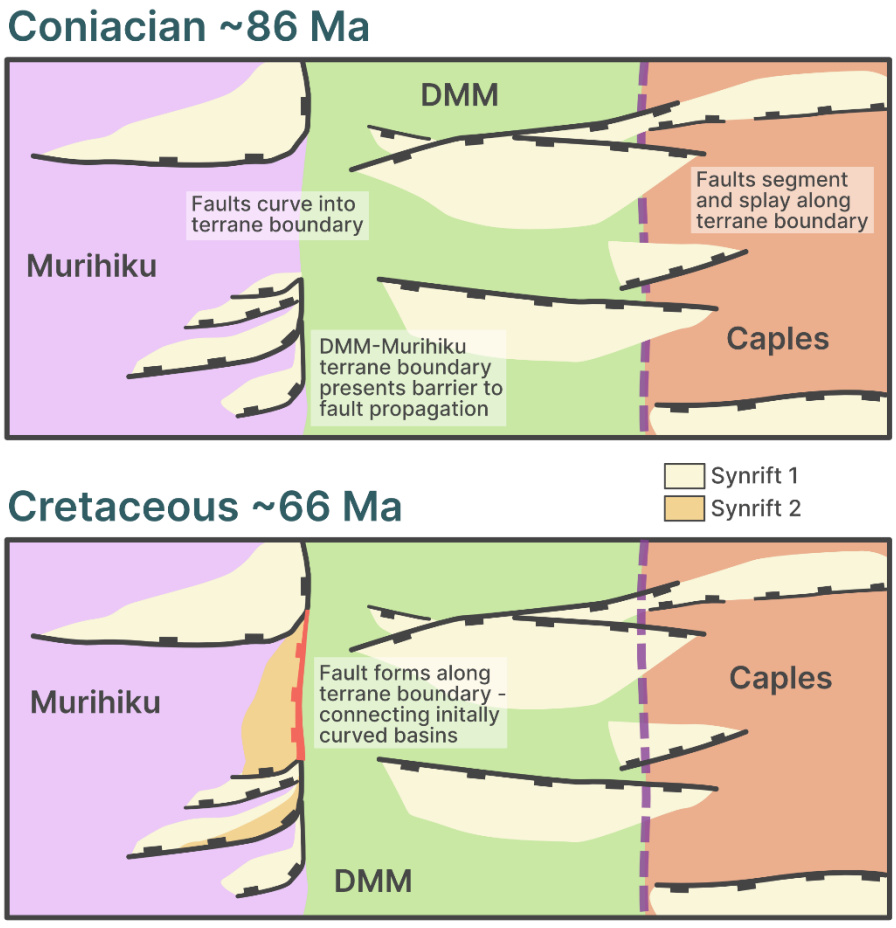

Figure 4.10 Summary Diagram of the Formation of J-shaped Faults

Schematic diagram showing the differential effects of the two terrane boundaries and their influence over time on the rift geometry and kinematics. The lithospheric scale Livingstone fault between the DMM and Caples terrane mostly reactivates in a viscous manner and manifests in the creation of splays and accommodation zones along it. Meanwhile, the frictionally weak fabrics of the Murihiku terrane boundary are directly reactivated and form curved isolated basins in the Coniacian. In the later evolution of the rift basin, the larger rift faults are inactive and only the NW-SE trending linkage fault of these curved basins is active aided by the inherited structure along the DMM-Murihiku terrane boundary.

While the Livingstone fault is the larger structure and presents a clear boundary between the DMM and Caples terranes it is not directly reactivated as opposed to the Murihiku-DMM terrane boundary. Onshore studies of the Murihiku terrane show a large variability in lithologies with interbedded conglomerate, mud-siltstones and sandstones which were ultimately folded into the Southland syncline (Campbell and Coombs, 1966; Noda et al. 2004), which is exposed onshore and runs roughly parallel to the boundary of the DMM and Murihiku terrane. The boundary between the Murihiku and the DMM terrane is unclear, the Hillfoot fault has been traced onshore (Bishop and Turnbull et al., 1996) and is a reverse fault running parallel to the suspected boundary of the Murihiku and DMM terrane (Bishop and Turnbull et al., 1996). This is further complicated by the unit known as the Kaka Structural Belt (Campbell et al., 2020) which sits between the Murihiku and DMM terrane and has been interpreted as a part of the Murihiku (Roser and Coombs, 2005), the DMM (Campbell et al., 2003) or its fragmented terrane (Jeans et al., 2003; Campbell et al., 2003). Therefore, the fault zone separating the Murihiku and DMM terrane most likely contains a heterogeneous mixture of siliclastic units which are further weakened

through faulting and brittle deformation. Onshore studies (Cawood, 1986; Edbrooke et al., 2015; Robertson et al., 2019) show complex slithers of DMM and Murihiku at the boundary with various faults in between, therefore the terrane boundary is probably characterised by an intensely faulted and fractured zone of different lithological units (sandstones, siltstones, conglomerates). This makes the terrane boundary between the DMM and Murihiku likely to be prone to frictional reactivation due to their inherent heterogeneity (Samsu et al. 2023) and the presence of phyllosilicates, graphite or clays that could potentially further frictionally weaken this zone (Colletini et al. 2009; Healy, 2009; Massironi et al. 2011; Marín et al., 2023). Thus, this severely misorientated structure could be frictionally weak enough to reactivate without increased fluid pressure. Meanwhile, the DMM-Caples terrane boundary, the Livingstone Fault, may be represented by a wide fault zone which traverses a larger part of the lithosphere. The lack of any geometrically similar faults to this terrane boundary shows that it has not been directly reactivated but may have reorientated the strain as seen by the occurrence of accommodation zones and rift segmentation along it (Fig. 4.2; Fig. 4.9b). As it is a larger lithospheric scale heterogeneity, it may have been active at depth in the ductile domain of the lithosphere and therefore influenced segmentation along it rather than being directly reactivated (Fig. 4.11) – an example of soft linked inheritance where the structure is not directly reactivated but reorientates the strain (Samsu et al. 2023).

Inherited structures are often invoked to control the strain distribution during the early phases of rifting (Collanega et al., 2019; Heilman et al., 2019; Kolawole et al., 2021b; Corti et al., 2022) and have the most impact on the formation of the large border faults. Later their influence wanes and faults align perpendicular to the regional extension direction (Agostini et al., 2011; Phillips et al., 2019). In the early stage of rifting in the GSB the largest influence is the strength contrasts of the terranes that

dictate the wider rift geometry (Phillips et al., 2023) and determine the locations of accommodation zones and segmentation (Fig. 4.2; Fig. 4.8). The Murihiku-DMM boundary had both an early passive effect on the rift geometry causing faults to terminate against it and rotate into it, possibly due to the strength contrast between the two terranes, however, it was also actively reactivated during later rifting. During the Coniacian-Cretaceous when the extension perpendicular NE-SW trending faults show no evidence of further activity, the larger linkage fault between the initial curved Murihiku faults becomes active (Fig. 4.9c). Extensional strain was likely low at this point as there was little activity elsewhere in the GSB during this time (Sahoo et al., 2020). A combination of low frictional strength and strain concentration by the surrounding curved rift faults may have led to the eventual formation of a fault along this zone which took advantage of the pre-existing structures along this terrane boundary and reactivated crustal detachment horizons (Fig. 4.6). The fault may have had a small amount of activity and displacement in the earlier stage of rifting, on the seismic data it is however difficult to determine if the sediment in the hangingwall between top Basement and top Coniacian is a syn-rift wedge or just onlapping sediment that was later displaced by this fault (Fig. 4.6). The top Coniacian – top Cretaceous strata shows a more convincing wedging geometry, and the thickness map shows little thickness variation along Fault 6 up to the Coniacian (Fig. 4.8), therefore we argue for the structure to have chiefly formed in the Coniacian-Cretaceous period. Examples from the East African Rift show that inheritance can control fault evolution much later in the rift evolution similar to these observations from the GSB: In the Magadi Basin of the East Africa Rift, a transverse fault system develops after the development of rift parallel faults above a transverse basement structure (Muirhead and Kattenhorn, 2018). This illustrates that inheritance control of

faults and reactivation not only occurs during early rifting stages but sufficiently weak fault rocks and terrane boundaries can lead to late-stage inheritance in rift basins.

4.5.2 Implications for Seismic Hazard and Resources

The observations made in this study have major implications for seismic hazards in more actively deforming rift basins. Here we show that within the same rift system, different terrane boundaries can have a major influence on the style of deformation. While larger lithospheric style structures along terrane boundaries influence the deformation on a large scale and impact the first-order geometry and arrangement of rift interaction zones, shallower crustal features may reactivate more directly due to increased heterogeneity making them more prone to frictional reactivation. This could have major consequences for the spatial and temporal distribution of seismic hazards and the formation of resources.

Faults that reactivate inherited structures or accommodation zones formed above lithospheric structures have considerable economic significance for the subsurface energy industries. Basement-influenced faults that are more prone to reactivation can for example compartmentalise the reservoir and break the top seal (Lyon et al. 2007), which could be for example case for the NW-SE trending fault along the DMM-Murihiku boundary, especially considering it has a more protracted activity than the major NE-SW striking faults. Complex fault patterns with different orientations that are controlled by inheritance can also influence migration pathways (Wang et al. 2021). Therefore, faults such as the NW-SE trending fault in our study, which is strongly controlled by oblique crustal fabrics could be beneficial for migration pathways but also compartmentalise potential reservoir rocks. Whereas the accommodation zones which form preferentially along inherited lithospheric fabrics such as the Livingstone fault may be areas of preferred hydrocarbon accumulation (Morley et al., 1990). As

found for other examples in New Zealand such as the Taupo Volcanic zone, deep-seated basement structures control the segmentation of a rift and the formation of rift accommodation zones that then can be sites of increased hydrothermal activity with the potential to be harnessed for geothermal energy (Rowland and Sibson, 2004). In the Taupo Volcanic zone, the proposed basement lineaments are highly oblique to the rift zone which is similar to the case of the GSB where inherited structures strike nearly at 90° to the rift axis. Accommodation zones can serve as the vertical up flow zones with the established rift segments surrounding it channelling horizontal flow and therefore serving as recharge areas for the hydrothermal system. The differential impact of inheritance observed in this segment of the GSB can reveal complexities crucial to the evaluation of the viability of analogue hydrothermal systems. The lithospheric scale structures (Livingstone Fault), mainly acting in a viscous manner, may aid the development of accommodation zones which preserve the vertical permeability necessary for the formation of a hydrothermal system. This vertical permeability may be inhibited by the curving faults and directly reactivated frictionally weak fabrics (DMM-Murihiku boundary). Therefore, evaluating the presence of inherited structures and their potential effects on fault geometry and development is important for the assessment of hydrothermal systems. Accommodation zones do not necessarily have to form along inherited lithospheric structures (Schlische and Withjack, 2009; Nixon et al. 2016), but it is a common feature in rift basins (Fossen et al. 2016; Zwaan and Schreurs, 2017; Peace et al. 2018) and inherited structures may further aid fluid flow as well as the connection between deeper and shallower sections (Rowland and Simmons, 2012). The implications may also apply to other resources such as mineral resources or water which are heavily impacted by fluid flow; however, this is beyond the scope of this paper. The differential effect of inherited structures on the rift basin may also affect the economic potential of rift zones.

Results from the GSB present new constraints on the temporal activity of linkage across shallow crustal fabrics, as can be seen in the case of the fault along the DMM-Murihiku terrane boundary. The fact that linkage along this boundary exploiting shallow crustal fabrics may have considerable connotations for seismic risk in actively deforming areas. While the seismic risk of the GSB is generally low due to it being a dormant rift far away from major civilisation centres, findings from the GSB are widely applicable to other rift systems that form across varying basement terranes. The ability of faults to generate large earthquakes is proportionally related to the fault length (Scholz, 1990; Wells and Coopersmith, 1994), therefore longer faults can generate larger earthquakes. The influence of crustal fabrics on linking initially isolated fault segments into a single fault, as observed in the GSB, may mean that this linked fault can generate more devastating earthquakes. This phenomenon has been observed in Malawi, where multiple segments may detach into a common structure at depth such as for the Bilila-Mtakataka Fault (Hodge et al. 2018). Knowledge about the connectivity of individual fault segments can therefore significantly impact seismic hazard assessments as individual fault segments may only be long enough to generate Magnitude 4 or 5 earthquakes, but if these are connected at depth and rupture together the fault could host magnitude 6 or 7 earthquakes. This study not only highlights how crustal fabrics can aid the linkage of off-axis trending fault segments in a rift zone and connect rupturing segments but also shows that crustal fabrics may be active at the late stages of a rift's evolution, as linkage in the GSB only progressed during the latest stage of rifting when the other on-axis trending faults were already dormant. This highlights the potential danger of faults influenced by terrane boundaries. Faults that are severely misorientated by crustal inherited fabrics may be active longer than other structures of the rift and be connected at depth through the crustal inheritance making them potential sites of larger earthquakes. On the contrary

lithospheric deep-seated inherited structures highly oblique to the main rift trend, such as the Livingstone fault, may limit the potential to generate large earthquakes as they are prone to segment faults and promote the formation of accommodation zones as observed in this study. Here faults become shorter but also more numerous as the total accommodated strain is divided over a larger number of active structures. This may lead to smaller but more frequent earthquakes. The inherent structural complexity of these zones may also lead to a more complex earthquake cycle as the faults interacting will severely impact the loading-release cycle of faults (Cowie et al., 2012; Walters et al., 2018).

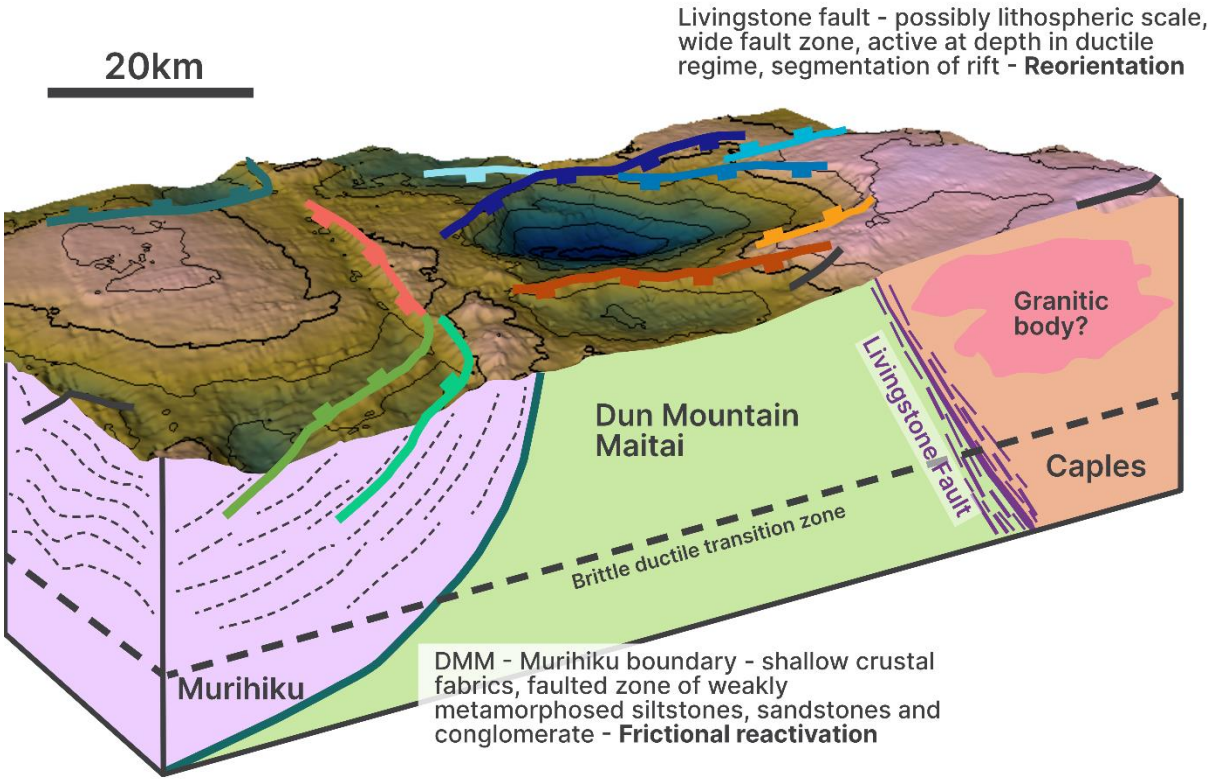

Figure 4.11 3D Diagram of the Great South Basin

3D diagram summarising the 3D relationship between the inherited structures along the major terrane boundaries and the rift geometry. Both terrane boundaries have a varying effect on the rift, with the Livingstone fault reorientating the strain

and dictating the location of segmentation while the DMM-Murihiku boundary was actively reactivated by a fault trending parallel to it. This differing behaviour may be explained by their contrasting rheology.

4.6 Conclusion

In this study, we present a detailed examination of the impact of two different terrane boundaries on the evolution of rifting in the GSB using high-resolution 3D seismic data. We evaluate how the different fault patterns observed at either terrane boundary could be directly related to the nature of the terrane boundary which varies in scale and rheology.

Through detailed mapping of three key horizons for the evolution of the GSB – the pre-rift basement, the Coniacian syn-rift and the Late Cretaceous post-rift horizon – as well as analysing the fault displacement patterns, we show that:

1. Both active (frictional reactivation) and passive (reorientation) inheritance can occur in the same system

2. Crustal structures that are nearly parallel to the extension direction can still influence rift fault orientation and development. Basins that strike along the principal rift axis may align along them and curve into the weak crustal fabrics forming J-shaped basins. These may later link up along the weak crustal fabrics which can be active after the main rift faults have become dormant.

3. Larger deeper deeper-seated lithospheric structures may be active in the ductile regime and reorientate the strain, leading to the formation of transfer and accommodation zones.

4. The rheology and scale of the inherited structure affect the likelihood of reactivation even if the inherited structures are not orientated favourably with

regard to the extensional strain field. While generally favourably orientated structures are more likely to reactivate, here we show that even severely misorientated structures can be reactivated if they are frictionally weak enough.

While these observations are made on a small part of the larger GSB rift system the results and findings are perhaps widely applicable and are comparable to observations of other rift systems around the world. We highlight that depending on the nature of the inherited structure affecting the rift fault this can have severe impacts on the temporal activity of the connected rift fault which may have major implications for seismic hazard assessment as faults that are severely misorientated by crustal fabrics can be active longer.

4.7 Supplementary Material

Data availability – 3D seismic volume freely available for download from https://geodata.nzpam.govt.nz/

Raw data used to generate D-L plots of Figure 4.9 available online: https://github.com/MFroemchen/GSB_FaultAnalysis

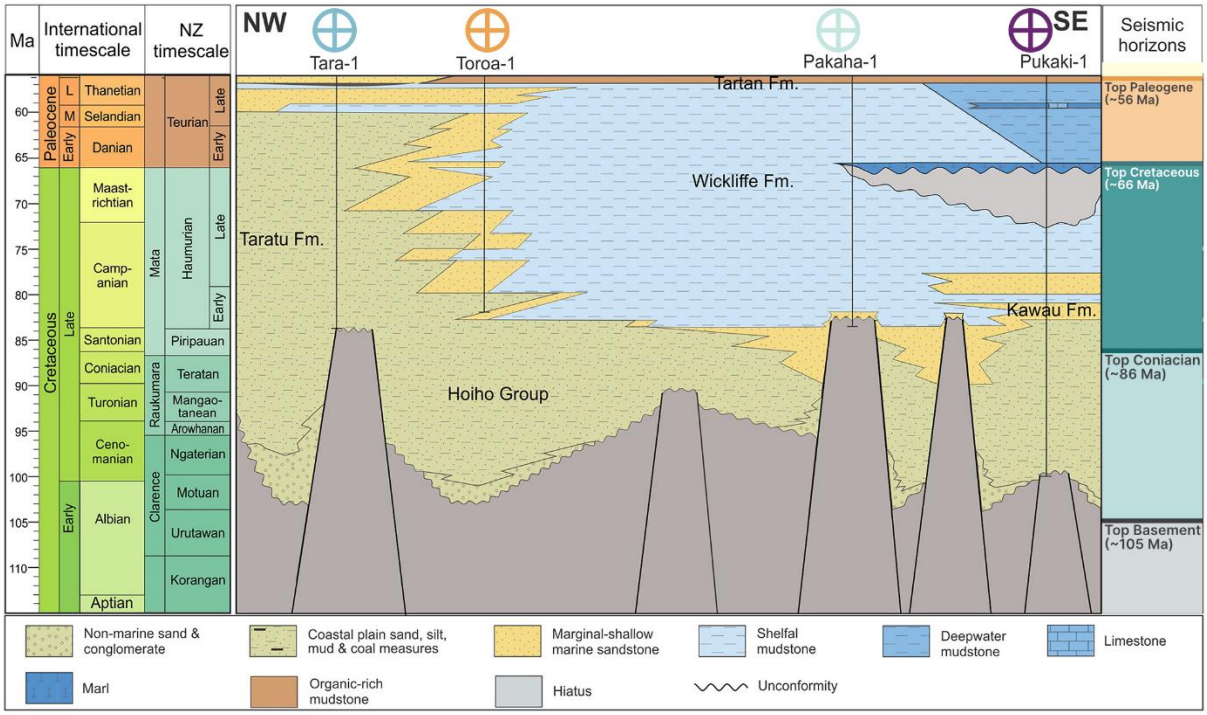

Supplementary Figure S 4.1 Generalised chronostratigraphic chart of the GSB

Chronostratigraphic chart of the GSB (modifed from Sahoo et al., 2020) showing the position of the four wells from Fig. 4.1 and the interpreted seismic horizons on the right. Most sedimentary rocks were originally deposited as a mixture of siliclastic sediments such as sandstones, mudstones, siltstones and conglomerate. Only minor amounts of marls of limestone are found in the wells.

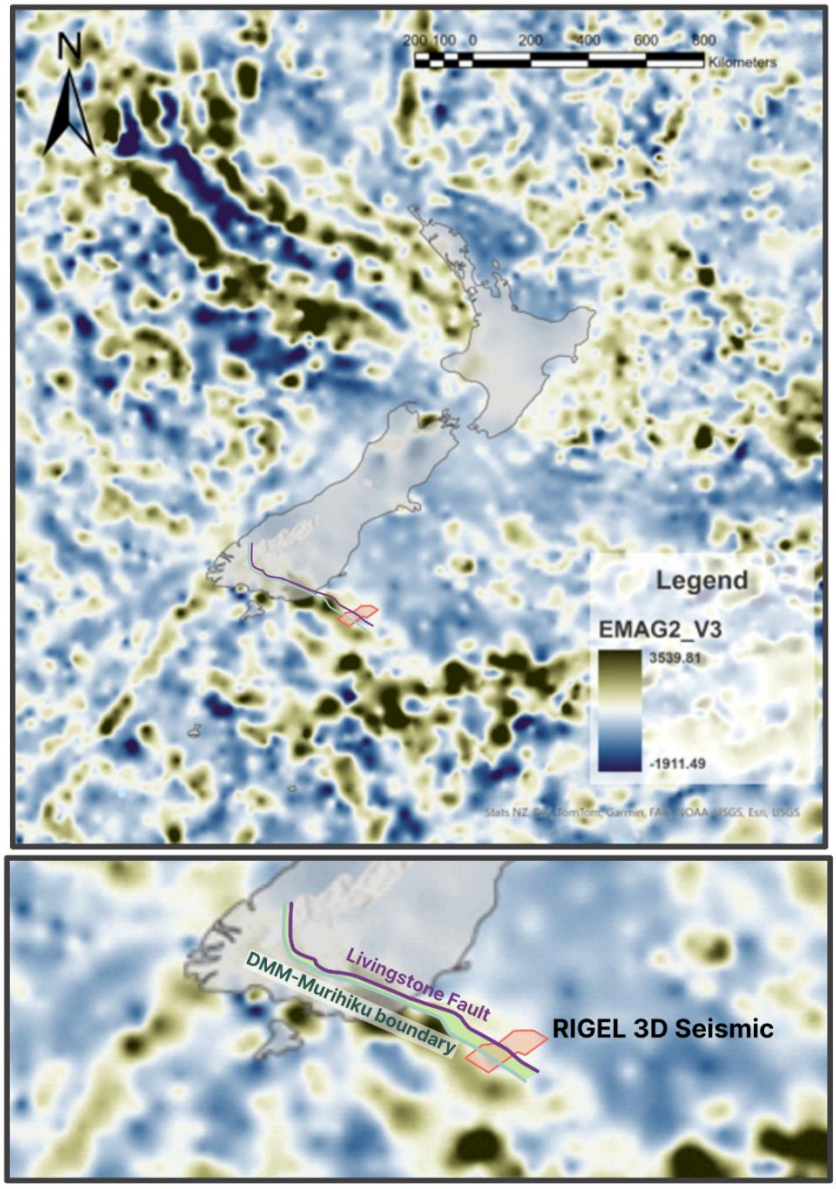

Supplementary Figure S 4.2 Aeromagnetic Anomaly Map of New Zealand

Showing the EMAG2v3 aeromagnetic survey (Meyer et al., 2017) around New Zealand that was used to constrain the terrane boundary. Large positive aeromagnetic anomaly extends offshore parallel to the proposed boundaries

onshore, used to constrain the location of terrane boundaries offshore. A large positive anomaly likely corresponds to the mafic rocks of the ophiolitic DMM terrane (Sutherland et al., 1999)

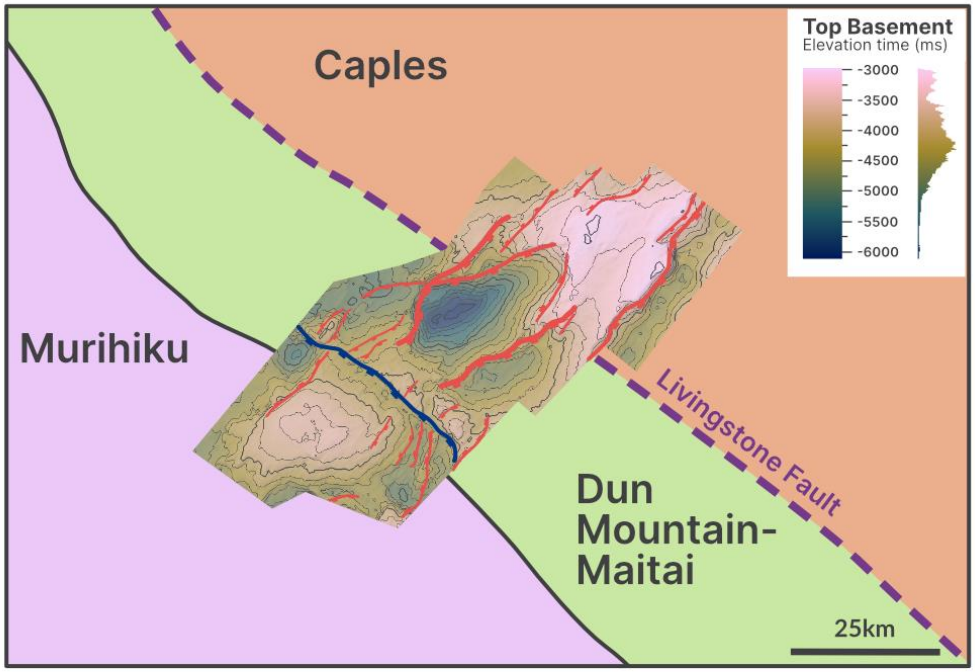

Supplementary Figure S 4.3 Top Basement Map

A clean version (without seismic location lines) of the top Basement map (compare with Fig. 4.2) of the interpreted 3D dataset overlain on the projected terrane boundaries. Faults broadly trending NE-SW in red while the fault trending NW-SE is indicated in dark blue.

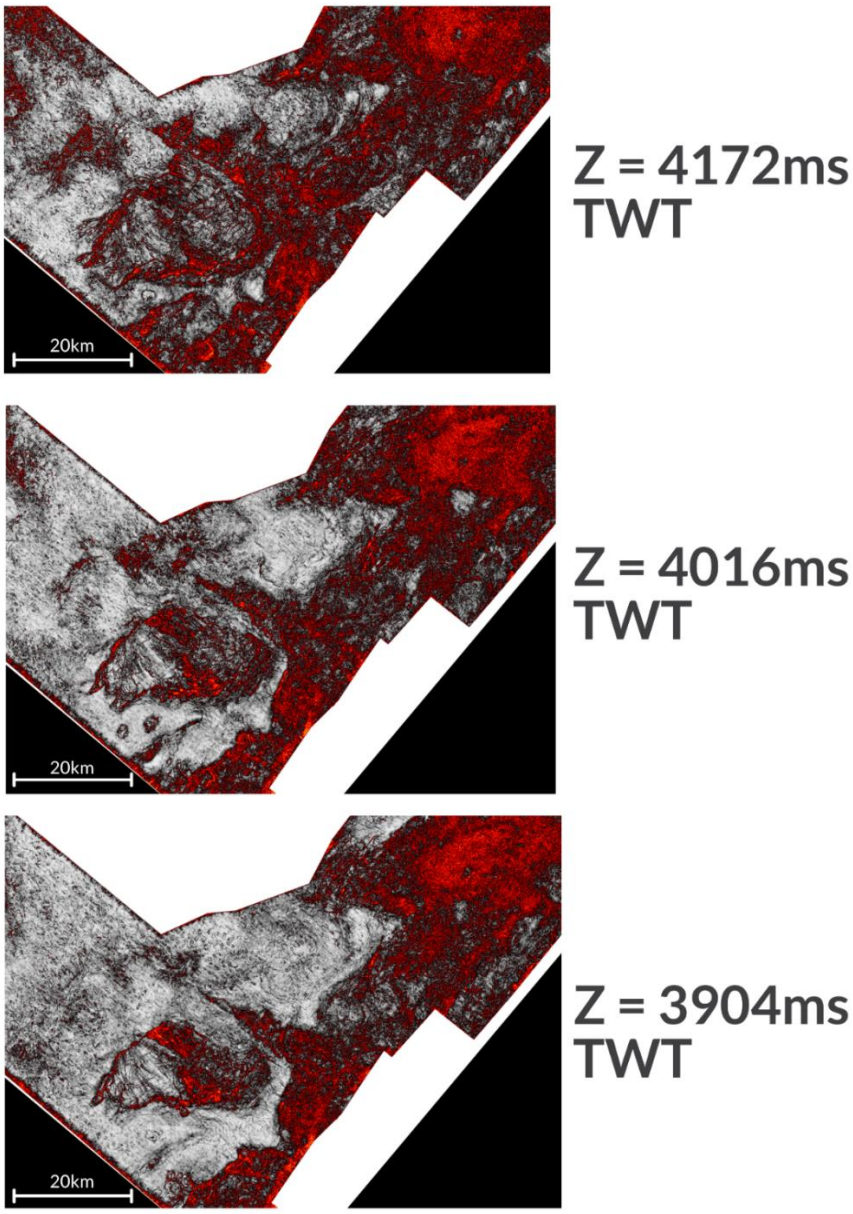

Supplementary Figure S 4.4 Variance Slices of 3D Seismic through Syn-Rift Strata

Showing the calculated variance attribute of the timeslices of the survey to highlight the evolution of fault basins along the Murihiku-DMM terrane boundary from the isolated curved basin in the Coniacian (4172ms) into a larger J-shaped basin (4016 and 3904ms)

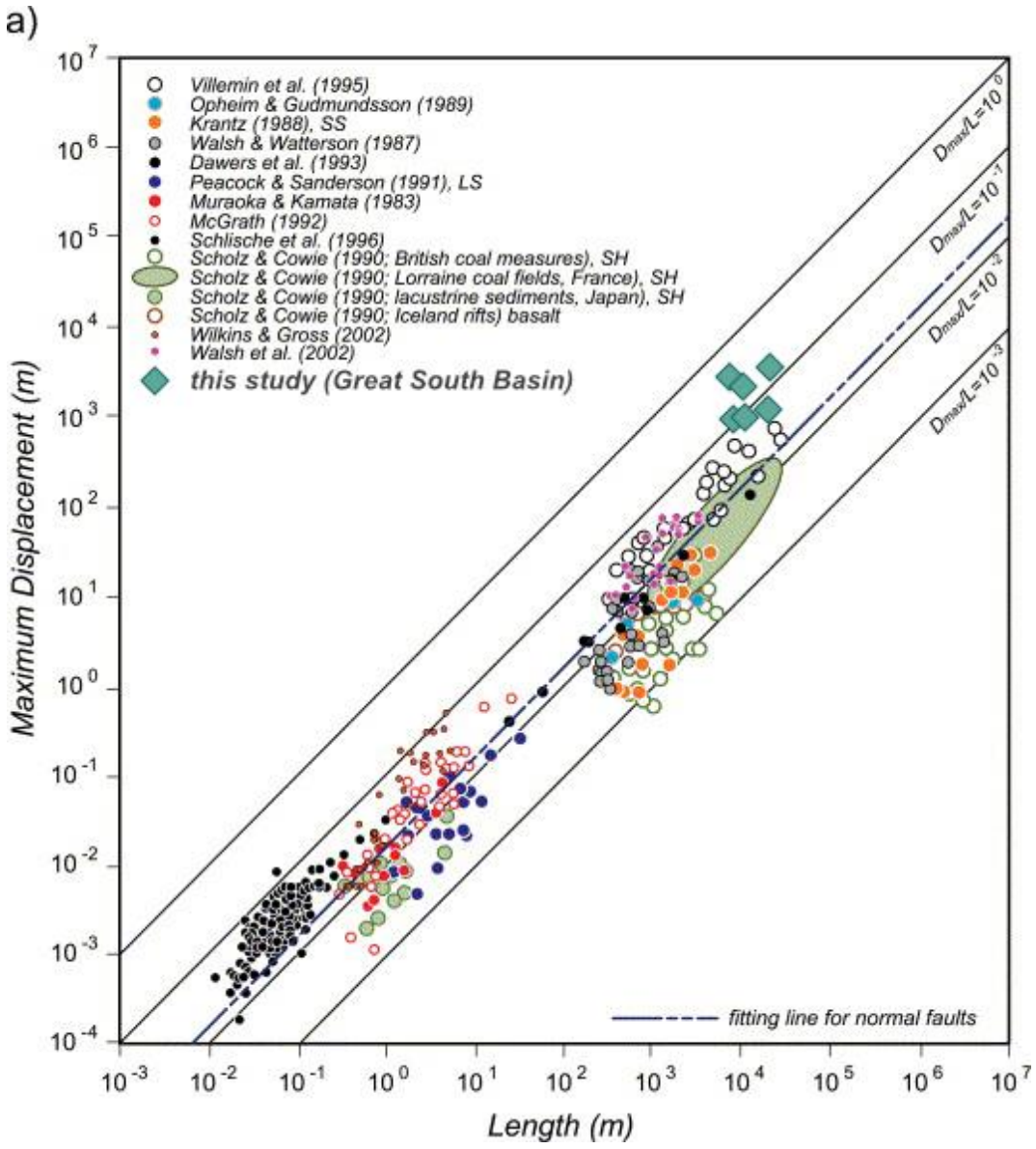

Supplementary Figure S 4.5 Comparison of GSB faults with global data base

The main rift faults of the GSB (green diamonds) compared to a global data base of length-displacement of normal faults (from Kim and Sanderson, 2005). The GSB faults show generally slightly elevated displacement for their lengths. Plotting between the D_{max}/L ratios of 10^0 and 10^{-1}. Lithology might have an effect as 4 of the 6 plotted faults are within the DMM terrane which is comparatively weaker (see Phillips et al. 2022) and may promote higher displacements during fault growth.

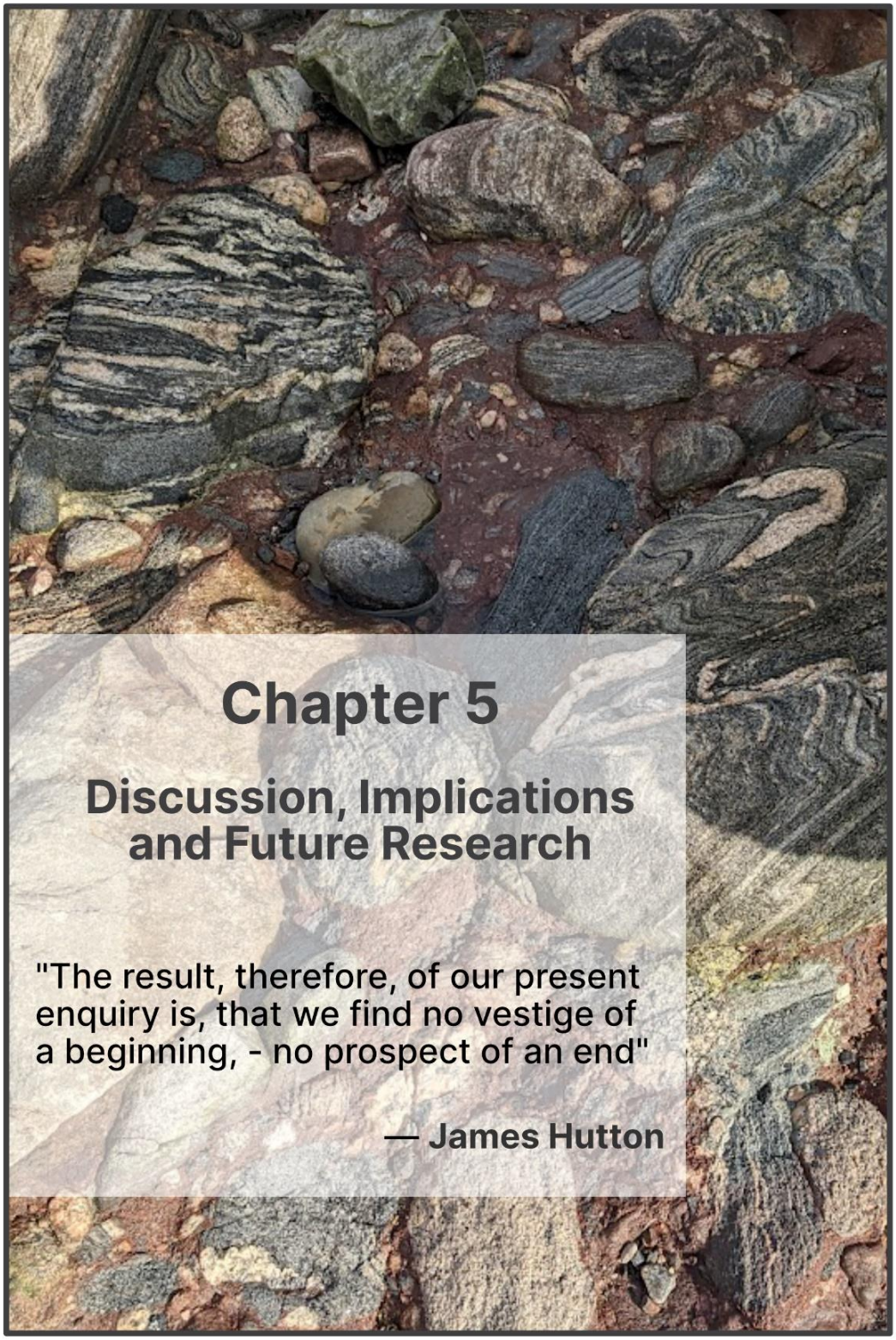
Chapter 5
Discussion, Implications and Future Research
"The result, therefore, of our present enquiry is, that we find no vestige of a beginning, - no prospect of an end"
— James Hutton

5. Discussion, Conclusions, and Suggestions for Future Research

5.1 Discussion

The three preceding chapters examined different expressions of inherited structures influencing rift evolution in two different geological settings. While some pre-existing structures appear to be directly reactivated, others show more diffuse reorientation of the extensional strain. However, a common thread connecting the three studies is the importance of scale and rheology of the pre-existing structures in determining the impact of it on rift evolution. All chapters observed and modelled inheritance at different scales: from the large plate tectonic scale, modelling the influence of lithospheric structures on the nucleation of the Shanxi Rift, to the individual fault scale, examining how terrane boundaries rotate faults in rift basins of the Great South Basin. I have found that both large-scale lithospheric and shallow crustal structures act together to segment the Shanxi Rift and the Great South Basin (GSB). In the following, I will explore how these results fit into the existing knowledge of the scale dependence of inheritance and the temporal evolution of inheritance in rift basins. Furthermore, it will be discussed how geomorphology can be helpful for studying inheritance in rift basins and the seismic hazard implications of our work. Finally, this chapter and thesis are finished with a brief discussion of future avenues of research.

5.1.1 Inheritance – active reactivation or passive reorientation

In the previous three chapters, we have found multiple examples of how inheritance has influenced rifting in two different regions. One key takeaway from this work is that the influence of inheritance may be subtle and does not need to be manifest in obvious faults that are oblique to the proposed extension direction and geometrical parallel to basement fabrics. Not all inherited structures influence rift evolution by reactivation and the mechanism by which inherited structures control rift evolution may be related to rheology and scale (Holdsworth et al., 2001a; Samsu et al., 2023).

In the Shanxi Rift, pre-existing fabrics aligned perpendicular to the later extension direction may have helped the early establishment of faults and contributed to the formation of long faults such as Zhongtiaoshan, Xizhoushan and Wutai which reach up to 100 km in length (Fig. 2.5). Thus, reactivation of basement fabrics, in the Shanxi Rift is mostly likely to be the inheritance mechanism responsible for modifying individual fault geometries at the local fault scale. Similar observations were made in East Greenland by Rotevatn et al. (2018), who proposed that inherited structures led to the establishment of long faults. Without clear control of the depth and the total throw of the faults in the Shanxi Rift, it is not possible to establish if these faults have acquired length and throw simultaneously or first lengthened, as discussed in different models of fault evolution (Rotevatn et al., 2019; Walsh et al., 2002), but it seems likely that reactivation of inherited structures aided the rapid lengthening of these faults relative to their displacement. Furthermore, the inherited structures influenced the trend of the rift faults (Phillips et al., 2016), causing them to strike parallel to the inherited structure and slightly oblique to the regional strain field (see Zhongtiaoshan, Hengshan or Wutai faults in Chapter 2). Reactivation is also a factor in the formation of non-colinear fault systems observed in the previous chapters. The “zig-zag” faulting in the RIZs of the Shanxi Rift and the “J-shaped” basins in the GSB near the terrane boundary are a result of fault segments following the inherited structures connecting to other segments that form perpendicular to the regional or perturbated strain field, oblique to the inherited structures (Corti, 2009; Hodge et al., 2018; Peace et al., 2018; Corti et al., 2022). Previously these non-colinear fault networks have often been proposed to have formed during multiple phases of extension (Bonini et al., 1997; Henza et al., 2011; Henstra et al., 2015). The non-colinear faults in Chapters 2 and 4 are unlikely to be the result of a change in extension direction, but more likely caused by selective reactivation of basement structures, similar to observations in the North Sea by Reeve

et al., (2015) and Osagiede et al., (2020). Other examples of similar zig-zag faults influenced by inheritance are documented in West Greenland (Peace et al., 2019) or East Africa (Corti, 2009; Corti et al., 2022). At the map scale, it remains hard to prove reactivation as there is no direct evidence of a hard link between the inherited structure and the rift fault (Holdsworth et al., 1997). However, by setting out diagnostic criteria such as the geometric similarity of the rift faults and the pre-existing structures and any obliquity between the rift fault to the extension direction, it is possible to make a reasonable assessment of which structures have experienced reactivation. In the case where pre-existing structures are nearly perpendicular to the rift extension direction is hard to distinguish if these structures are indeed reactivating basement fabrics or just simply formed perpendicular to the extension direction without reactivation.

The orientation of the inherited structure with regards to the overall extension direction may be of secondary importance, provided the inherited structure is frictionally weak as shown by the DMM-Murihiku terrane boundary which is nearly parallel to the extension direction or by Utsira Shear Zone in the North Sea, which is severely misorientated but still was reactivated during rifting (Fossen et al., 2016; Osagiede et al., 2020). In all cases, the structure that was reactivated was at shallow levels in the upper crust. Inherited structures that are shallow and frictionally weak will more likely reactivate (Samsu et al., 2023). In these cases, reactivation may be a combination of frictionally weak structures, due to the presence of weak lithologies and intense deformation fabrics.

Reactivation is accepted as an important mechanism by which inheritance influences rifting (Morley et al., 2004; Laó-Dávila et al., 2015; Phillips et al., 2016; Fazlikhani et al., 2017) and the terms inheritance and reactivation have often been used interchangeably. A more subtle mechanism of inheritance may also affect rifting:

Reorientation (Morley, 2010; Samsu et al., 2023). Reorientation of rift faults occurs without any direct reactivation of the underlying pre-existing structure in an exploitative sense (Phillips et al., 2016) this can result in rift faults parallel to inherited structures that do not reactivate but merge, bound or crosscut the inherited structure or rift faults that are both oblique to the extension direction and the inherited structures as the local strain field is re-orientated (Samsu et al., 2023). In the previous chapters, reorientation was mostly recognisable at the larger map scale and manifested itself at the basin scale. Both Chapter 2 and Chapter 4 have shown that deeper seated structures (TNCO trend and Livingstone fault) affect the location of accommodation zones or at a larger scale RIZs as well as control the overall orientation of the rift. There does not need to be a connection between the inherited structure and the rift fault for reorientation to occur as for example strength contrasts in the viscous lower crust (but also in the brittle crust; Morley, 2010) can reorientate the strain above. Due to the common decoupling of the upper mantle and upper crust by a ductile lower crust, large-scale lithospheric structures in the mantle may often reorientate rather than reactivate, which is shown by various modelling studies (Agostini et al., 2009; Molnar et al., 2020; Zwaan et al., 2022). The importance of upper mantle structures on the localisation of rifts was shown for the Shanxi Rift in Chapter 3, and several other studies have highlighted similar influences (Vauchez et al., 1997; Molnar et al., 2020). Heron et al. (2019) show the importance of an upper mantle structure in the formation of the Davis Strait, a large-scale transfer zone of the North Atlantic spreading system, revealing the importance of strain reorientation by lithospheric structure on the large-scale architecture of rift basins – similar to our findings of the Shanxi Rift and the GSB. Similarly, Fossen et al. (2016), show that the large-scale segmentation of the North Sea Rift coincides with regional scale Caledonian shear zones, even though they suggest these structures were partially

reactivated, reorientation, caused by the strength contrasts of these shear zones, was important in the first order segmentation of the North Sea Rift. The impact of upper mantle structures most likely depends on the lithospheric architecture (Heron et al., 2016), as in cold, thick areas of the lithosphere, the mantle is a considerable contributor to the overall strength of the lithosphere (Burov, 2011) and therefore weak zones in the mantle are important in the localisation of deformation (Brune et al., 2023). For back-arc basins and orogens with a hot thin lithosphere the mantle most likely has diminished control. Deeper seated structures active in the viscous domain therefore more likely to have a broader impact on rift orientation and the larger basin scale architecture. This highlights the scale dependency of inheritance, as observation scale can significantly influence how we recognise the influence of inheritance on rift basins., but also the effect of inheritance on rift basins is dependent on the scale (Laó-Dávila et al., 2015; Corti et al., 2022). Large-scale lithospheric structures may determine the larger rift architecture through reorientation of the strain field and discrete inherited structures influencing fault geometry through reactivation. It must be noted that reorientation is not confined to the large scale as it has also been observed at the smaller fault-level scale (Samsu et al., 2019; Phillips et al., 2022). The rift pattern in the RIZs of the Shanxi Rift also shows signs of reorientation by the deeper-seated upper mantle structure. Both reorientation and reactivation can occur in the same rift and affect segmentation across the scales as shown by the examples from the Shanxi Rift and the GSB.

5.1.2 Temporal Evolution of Inheritance Influenced Rifting

Inheritance has been suggested to influence the entire duration of the rifting process but is generally considered to be especially important during the early stages of continental rifting and border fault formation (Agostini et al., 2011; Phillips et al., 2019; Kolawole et al., 2021b). However, the preceding chapters have shown this is not

always the case. While early nucleation and propagation of faults were likely inheritance controlled in the Shanxi Rift, in the case of the GSB, linkage along the extension direction parallel terrane boundary, only occurred during the later stages of rifting when other rift faults were inactive and strain rates were low. The earlier rift faults in the GSB that formed up to the Coniacian show no direct effect of inheritance, except for segmentation along larger lithospheric scale terrane boundaries. In the Shanxi Rift, while early border fault orientation and nucleation were affected by inherited crustal fabrics, the effect is also noticeable later during linkage across the RIZs where crustal fabrics likely play a role in the fault segmentation. A similar effect was observed by Muirhead and Kattenhorn (2018) in the Magadi Basin of the Kenya Rift, where transversal fabrics only influenced the later formation of intra-rift faults which postdate the rift parallel border faults. The later localisation along these transverse structures may be magma-assisted, as magmatic fluids may have further weakened these. While none of our study regions show significant magmatic contribution, general fluid flow along faults which is often focused on transfer or accommodation zones (Rowland and Sibson, 2004; Rowland and Simmons, 2012) may have contributed to the weakening of the inherited structures both in the Great South Basin and in the RIZs of Shanxi. Late Cretaceous to Eocene hydrothermal and minor volcanic activity in the Great South Basin has been documented by Phillips and Magee (2020), and Cao et al. (2023) and was potentially focused along terrane boundaries. Furthermore, in the Shanxi Rift hydrothermal circulation, in the form of hot springs and aquifers, has been observed near active faults (Qiao et al., 2011; Zhou et al., 2022), but their relation would need further study to make concrete assessments on the fluid flow along active faults in the Shanxi Rift. In both cases increased fluid flow may have contributed towards weakening of the inherited structures and their reactivation during linkage. Analogue models of the effect of lithospheric weaknesses on rifting

show, after basins initially align in an en-echelon pattern along a deeper-seated weak zone, that late-stage intrarift faults trend parallel to the weak zone and oblique to the imposed extension direction (Corti, 2008; Agostini et al., 2009; Zwaan et al., 2022). In these cases, the lithospheric weakness likely has a renewed effect on the later fault population due to crustal thinning removing the ductile lower crust. In the case of the Shanxi Rift receiver function data indicates that the crust remains 30 km thick at the present day (Chen et al. 2021) and the projected lithospheric weak zone is likely located in the upper mantle, therefore the proposed mantle scar is decoupled from the rift faults through ductile layers in the crust. Therefore, the weak zone parallel segments of faults in the RIZs are more likely a consequence of an earlier established en-echelon arrangement and the perturbation of the strain field by the surrounding faults. In most continental rifts the crustal thickness likely remains too thick (Camelbeeck and Iranga, 1996; Meier and Eisbacher, 1991) for structures in the upper mantle to influence the intra-rift fault orientation and it is more likely that structures at deeper levels in the upper crust gain importance. Yet, as rifting matures and evolves towards hyperextension and breakup, upper mantle structures might then become important as the drastic thinning of the crust during the necking stage and the removal of the middle crust (Mohn et al., 2012) leads to coupling of the crust and mantle and the deeper-seated structures could influence morphology and location of necking (Manatschal et al., 2015). While this is speculative, studies from the Norwegian margin (Muñoz-Barrera et al., 2020) highlight the role of structural inheritance in this late stage of rift evolution, therefore the effect of inheritance on necking may demand further study. In both Shanxi and the GSB, lithospheric structures had their largest effect during the early localisation and affected the large-scale architecture of the rift, while crustal structures mainly affected faults during propagation and linkage.

Nonetheless, lithospheric structures mainly being active at the localisation stage and crustal structures during propagation and linkage may be too simplistic since a clear hierarchy cannot be established. The scale of the feature may also influence its rheology and effect on rifting as discussed in Section 5.1.1 – lithospheric structures may be more active in the viscous domain and reorientate the stress without being directly reactivated, this behaviour may affect rifts early in their evolution, while frictional reactivation of crustal fabrics may dictate fault behaviour during continued rifting. Possibly increased fluid circulation after rift initiation may contribute to the frictional weakening of basement fabrics and favour their reactivation. While lithospheric architecture and structures (TNCO suture and Livingstone Fault) govern the orientation and segmentation of the rift during the early localisation stage, during this early localisation stage individual faults also nucleated along preferentially aligned shallow crustal fabrics that locally influence the fault orientation (see Fig. 2.5) and were most likely influenced by both lithospheric and crustal structures. It appears lithospheric structures had less of an impact during the later stages of rifting and segmentation was mainly accommodated by shallow crustal fabrics. Basement fabrics that both influence the early nucleation of faulting and cause later fault linkage have been observed for the East African Rift (Heilman et al., 2019) and for Thailand (Morley et al., 2004). Lithospheric structures may still influence the intra-rift fault population as noted by analogue models, however, in the Shanxi Rift there is little constraint on the location or the orientation of the intra-rift faults due to the absence of detailed seismic imagery and poor exposure of intra-rift faults at the surface. While there appears to be no simple hierarchy, generally the scale and rheology of an inherited feature may influence which stage of continental rift evolution it has its largest impact. Figure 5.1 shows a summary sketch of the scale dependence of inherited structures during their temporal evolution of influencing rift basins.

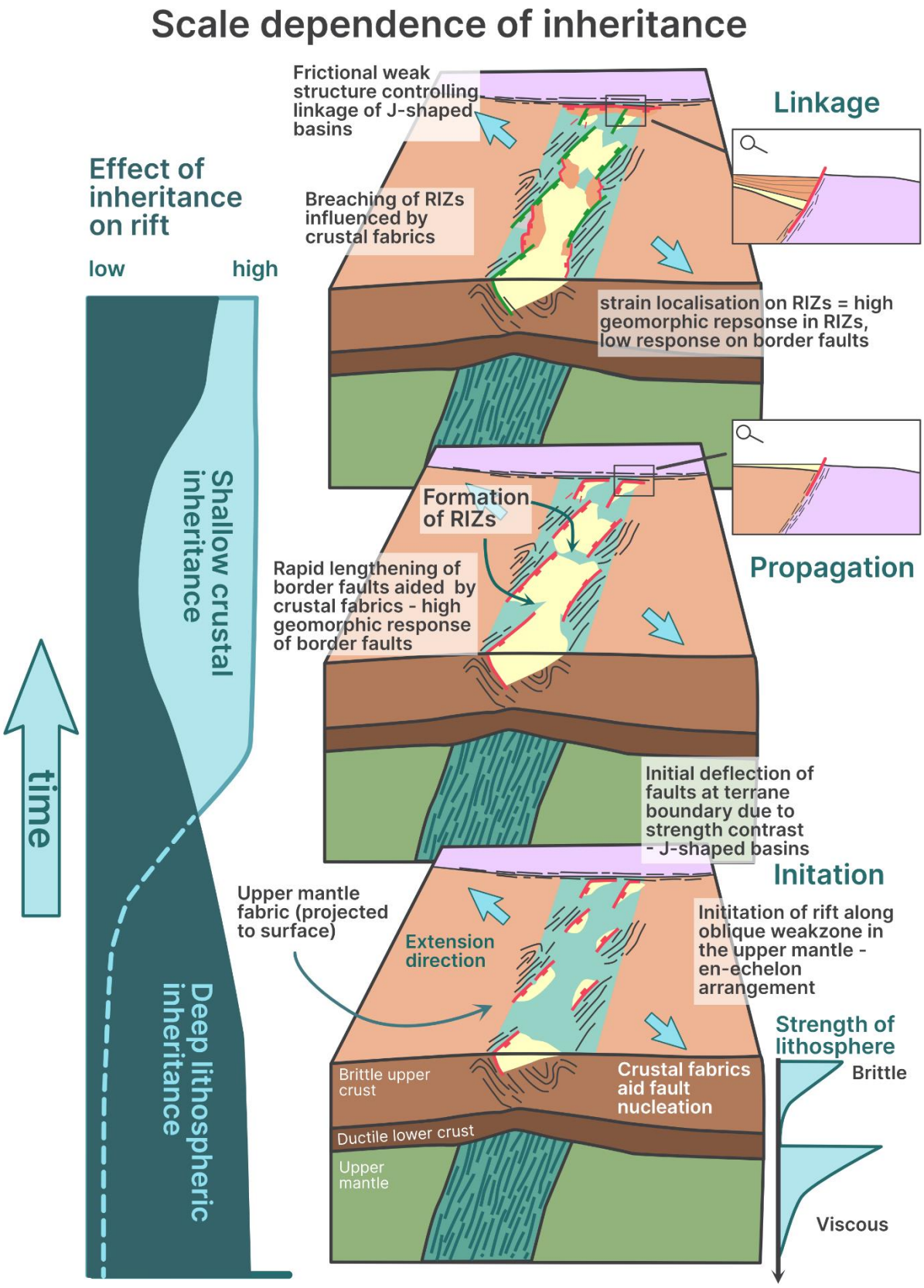

Figure 5.1 Summary Sketch of Scale and Rheology Dependence of Inheritance

Summary figure showing how scale and rheology of an inherited structure determine the effect on rifting across the rift evolution. During rift initiation, an extension oblique deeper seated lithospheric weak zone in the viscous regime is important in the overall orientation of the rift and the first-order segmentation. Shallow crustal structures may help nucleate individual faults. During propagation and later linkage, these shallow crustal structures are increasingly important during fault lengthening and later linkage across the RIZs and accommodation zones, resulting in non-colinear fault patterns. During this linkage the faults along the terrane boundary also show increased activity as they link the early established curved basins. This is shown in schematic "zoomed-in" panels similar to observations from the GSB (chapter 4).

5.1.3 Geomorphology – an Underutilised Method for Decoding Rift Basins and Their Inherited History

The influence of inheritance cannot always be readily detected particularly in the case of more subtle expressions of inheritance such as strain reorientation or where the pre-existing structures and faults are perpendicular to the strain field (5.1.1), as it can be hard to decipher if inheritance has influenced the faults at all, as would be the case with misorientated faults relative to the strainfield. Furthermore, many continental rifts are subaerially exposed and only have limited coverage of seismic data which limits the clear identification of pre-existing structures in the crust and lithosphere. Geomorphological investigations of active rift basins rarely consider the effect that inherited structures have. Geomorphology cannot directly reveal inherited structures and how they influenced the rift evolution, but my work has shown how geomorphic indices can be used to better constrain the evolution of a rift which then can be related back to inheritance. Especially in low strain rate regions such as Shanxi, there is often a lack of reliable data to constrain the rift evolution such as geodetic data or fault slip rates, in these cases quantitative geomorphology can provide new constraints on the activity of faults (van der Wal et al., 2021). In recent years there has been an increase in studies that have employed geomorphic techniques to

characterise rifts (Whittaker et al., 2008; Pérez-Peña et al., 2009; Kolawole et al., 2018; Geurts et al., 2020; Erbello et al., 2022). Quantitative geomorphic indices can be used to provide relative assessments of the activity of faults and to identify areas of higher activity in slowly deforming regions such as the Shanxi Rift. Combined with an assessment of the influence of inheritance to explain the heightened level of activity (as we have done in Chapter 2), geomorphology indices can build a comprehensive model of how a rift evolved and what the most active zones in a rift basin are at the present day. For example, in the Shanxi Rift, the geomorphic indices have highlighted areas of more recent uplift and that likely coincides with higher fault activity in the RIZs, which can improve our understanding of the evolution of the Shanxi Rift. Using geomorphology to characterise RIZ has not only been successfully employed by this study (Section 2.5.2), but also by Kolawole et al., (2021b) and Dulanya et al., (2021), and can possibly be extended to other rifts as well, which can improve our understanding of the complex deformation within RIZs. RIZs are zones of active linkage with possibly increased seismicity and are therefore important to our understanding of seismic risk in rift basins. Especially the relationship between RIZs and inherited structures remains poorly constrained, however, this study shows examples of how deeper seated structures may govern their location and initial geometry, while crustal structures influence the linkage across RIZs.

However, while geomorphology can be a powerful tool to decode rift evolution, It also comes with many assumptions and limitations which need to be taken into consideration when assessing the activity of rift faults. Lithology and climate have significant effects on the geomorphic response (Masek et al., 1994; Whittaker, 2012), I have tried to circumvent the effect of lithology by comparing faults with similar footwall geology, however, it remains a broad generalisation and there is considerable variation within the footwall lithologies of the Shanxi Rift. Methods like channel

steepness are based on the assumption that uplift will change the steepness of the river channel in an attempt to return to base level, yet, other adjustments of the river channel such as bed state and channel morphology may also be part of this adjustment (Wobus et al., 2006). HI may account for this as it measures the shape of the entire drainage basin rather than just focusing on the river channel but comes with its own pitfalls, as there is debate on the scale dependency of HI (Lifton and Chase, 1992; Masek et al., 1994; Hurtrez et al., 1999). Combining different indices may be the best way to circumvent these limitations of each individual geomorphic index, however, one is faced with a choice of dozens of different indices developed over the years. In Chapter 2 I chose HI, k_{sn} and local relief as they were the most discerning at identifying areas of higher geomorphic response. A lot of different factors influence the geomorphology of an area therefore it can be difficult to isolate the tectonic contribution from factors such as lithology, and climate but also glacial or even human factors (hydroelectric dams, terracing). For the Shanxi Rift, certain factors can be ignored, for example, the region was unaffected by large-scale glaciation in the Pleistocene, however during this time period thick Loess deposits blanketed part of the Shanxi Rift and surrounding areas, the effect of which has been discussed in section 2.5.1. There is also a scale element to the study of tectonics from geomorphology, with certain geomorphic indices being better at picking up smaller features and faults, while other indices are better at evaluating the regional relative tectonics across a larger area. HI was often successfully employed to evaluate tectonics at larger regional scales (Lifton and Chase, 1992; Chen et al., 2003; Walcott and Summerfield, 2006) and therefore is most likely appropriate to evaluate the tectonics of the Shanxi Rift. The fault locations were mostly known mapped as large scarps along mountain faces and the quantitative geomorphology was mainly used to characterise the recent uplift patterns of the footwalls. At smaller scales, HI may not

have the resolution required for the identification of faults and stream-long profiles or knickpoints may be more appropriate. Diercks et al. (2023) successfully employed terrain ruggedness and basin asymmetry to identify individual faults within the karstic landscape at the border of Slovenia and Italy, but noted other geomorphic indices were less helpful at identifying faults (e.g. local relief, HI). Many faults in Diercks et al. (2023) study show mainly strike-slip motion, therefore they note that HI was less effective at identifying strike-slip faults, than for example terrain ruggedness. Strike-slip faults often do not generate a significant amount of uplift and therefore do not significantly affect the distribution of elevation within drainage basins and will show only little difference in the HI values. Geomorphic studies in rift basins, dominated by dip-slip faulting, have been generally successful in decoding tectonics using HI (Pérez-Peña et al., 2009; Erbello et al., 2022). It does however show that possible strike-slip faulting may not show up in the geomorphic analysis of the Shanxi Rift based on the indices used in Chapter 2. Nonetheless, based on aerial imagery, I was not able to identify significant lateral displacement along the Shanxi Rift border faults as suggested by Zhang et al. (1998), Li et al. (1998) and Luo et al., (2022). There may be no one size fits all approach when it comes to the assessment of tectonics from geomorphology and the choice of geomorphic indices depends on the scale of observation.

5.1.4 Seismic Hazard – Should Inheritance be Featured More Prominently in Seismic Hazard Assessments?

The findings of this thesis may have considerable implications for seismic hazards. Structural inheritance remains underappreciated in assessing seismic hazards, but a growing body of work shows how the occurrence of earthquakes in rift basins is significantly influenced by inherited structures (Kolawole et al., 2018). Furthermore, in “stable” continental regions, inherited structures may be the nucleation site of infrequent ‘intraplate’ earthquakes (Rimando and Peace, 2021; Muir et al., 2023) which

are generally poorly understood. Integrating inheritance into models of seismic risk is important not only due to inherited structures being able to significantly affect the seismic risk of a rift but also because inheritance-controlled rift evolution and therefore seismic risk is the norm, rather than the exception.

The rheology of inherited structures may affect the mechanism of how they influence rifting across the spatial and temporal scales (section 5.1.2), which presents significant implications for seismic hazard analysis. Deeper seated inherited structures that reorientate strain may affect seismic hazard in various ways. Through their large-scale impact on rift architecture and segmentation, deep-seated pre-existing structures govern where accommodation, transfer zones or RIZs form zones of more distributed deformation and more complex records of seismicity. Within the RIZs and accommodation zones, faulting may be more complex as faults show highly segmented “zig-zag” patterns which can generate smaller magnitude but more frequent earthquakes. With increasing breaching status, faults in the RIZs may link up along deeper-seated structures which reorientate the strain, similar to the Bilila-Mtakataka Fault in Malawi (Hodge et al., 2018) causing multiple segments to rupture together, potentially leading to larger magnitude earthquakes. Reorientation of the strain field by deep-seated lithospheric weaknesses such as suggested for the Luangwa Rift (Wedmore et al., 2022) or at a shallower level for the Rukwa Rift (Morley, 2010) causes faults in these rifts to exhibit dip-slip kinematics rather than oblique slip kinematics (Phillipon et al., 2015) even though faults may form oblique to the regional strain field (Williams et al., 2019). Therefore, faults that are oblique to the extension direction, such as the Huoshan fault in the Shanxi Rift, may only display dip-slip kinematics and only generate dip-slip earthquakes as they are reorientated at depth. Indeed, it was shown by Xu et al. (2018), that the Huoshan fault exhibits dip-slip kinematics, therefore the potential for oblique-slip or pure strike-slip mechanism

earthquakes on reorientated faults may be limited. Shallower structures in the frictional domain are prone to reactivation and may segment faults or aid their linkage, crucially we have shown in Chapter 4, that frictionally weak structures such as the DMM-Murihiku terrane boundary can aid linkage much later in the rift evolution and lead to more protracted fault activity than faults not influenced by inherited structures. Faults that frictionally reactivate pre-existing structures potentially release stored seismic energy more easily. Williams et al. (2022) show that limited fracturing and other fault-induced damage occurred on the Bilila-Mtakataka Fault that based on geomorphic evidence generated large magnitude (M_w 7.5-8) earthquakes in the Quaternary. The Bilila-Mtakataka Fault likely reactivates low frictional planes of weakness and therefore less earthquake energy is consumed by dissipation and fracturing processes. This may also explain the narrow fault zones observed in the Zomba Graben by Carpenter et al. (2022). Overall, this just shows a few examples of how based on our observations, reorientation and reactivation mechanism of inherited structures may affect the seismic risk of a rift basin, but an increasing amount of work has shown how crucial gaining an understanding of inherited structures is on earthquake dynamics.

5.2 Conclusions

The aim of this study was to further understand the impact of structural inheritance in rift basins, particularly how scale and rheology influence their impact on rift architecture and the temporal evolution of rift structures. I utilised a variety of approaches to investigate this, which enabled me to adopt a multi-scale view. While there remain many questions and unsolved puzzles about inheritance in rift basins, based on this work several conclusions can be made that further constrain the impact of inheritance:

1. Structural Inheritance is a common feature in rift basins and can act in two main ways: Reorientation and Reactivation.
2. Scale and rheology of the inherited structure determine the mechanism by which it will affect the rift evolution.
3. Lithospheric scale structures, that are commonly active in the viscous domain, reorientate the strain rather than being directly reactivated. This mechanism of inheritance can be harder to identify in rift basins as it will often result in rift faults neither parallel to surface-level inherited structures nor perpendicular to the extension direction. Most commonly they determine the overall orientation of the rift or segment the rift at the basin scale and determine the location of accommodation and rift interaction zones (RIZs).
4. Crustal scale structures, that are commonly active in the frictional domain, are more commonly directly reactivated, resulting in geometrically similar structures. They more commonly affect rift evolution at the fault scale level either by localising faults oblique to the extension direction or segmenting faults causing variable fault scarp trends along strike. Frictional reactivation may occur even if the inherited structure is severely oblique to the extension direction, provided it is frictionally weak enough.
5. Both levels of inheritance combine to segment a rift across the scales. For example, lithospheric scale inheritance may dictate the location of large-scale RIZs, while crustal scale inheritance will influence the local fault geometry within these.
6. Broadly speaking, lithospheric inheritance will dominate during the early stages of rift nucleation, as it most effectively weakens the strong continental lithosphere, while crustal inheritance gains greater importance during later propagation and linkage of rift basins. Nonetheless, crustal inheritance may also influence the orientation and length of faults during early nucleation, while lithospheric inheritance may gain further importance during later stages of rifting and necking.
7. Sufficiently frictional weak crustal inheritance can cause faults to remain active longer than faults not influenced by inheritance, even at low strain rates. This is potentially

related to less seismic energy needed to fracture the fault rocks – encouraging continued slip along the reactivated surface.

8. Geomorphology is a powerful tool to understand the evolution of rift basins and can be used in conjunction with the analysis of exposed inherited structures to better understand how the rift was segmented.

These conclusions are based on two study areas with different lithospheric configurations to show that these ideas apply across various systems. Naturally, these concepts can be expanded to numerous further rift settings (e.g. Rhine Graben, Eger Rift, Bresse Graben, East Irish Sea, Asunción Rift) and it is likely that in many of these basins, the role of inheritance has so far been underestimated.

5.3 Suggestions for Future Research

This study confirms suggestions by earlier research on the influence of inheritance on rift basins and shows new insights into the scale dependency of inheritance influence, there are many outstanding questions which open up a plethora of new research avenues.

Chapter 2 highlighted the importance of structural inheritance in the segmentation of the Shanxi Rift, but mostly utilised a regional map scale view. Assertions of inherited structures segmenting the rift can best be tested through fieldwork that would look for evidence of faults reactivating basement fabrics through direct field observations (Dawson et al., 2018; Hodge et al., 2018) and establish through detailed field maps the relation of basement fabrics and present-day faults at smaller scales. Within the Shanxi Rift especially the RIZs would be of great interest as we have shown that these zones are the most active zones in the Shanxi Rift at present day and basement fabrics likely impacted their geometry. Here the hypothesis that the regional strain field is perturbated by the surrounding border faults, could be tested through the collection of structural data and kinematic analysis of this data. The different

segments of the “zig-zag” faults could be measured to test if the kinematics match the imposed overall extension direction or show evidence of a perturbated strain field. Studies by Xu et al. (2018) have shown dip slip kinematics for the Huoshan fault which would rule out that this region has seen transtension as suggested by other authors (Shi et al., 2015; Assie et al., 2021), this could be extended to the Shilingguan fault with evidence on N-S and NE-SW trending segments to see if they have contrasting fault kinematics. Furthermore, to obtain a better regional picture of trends in the basement especially in regions covered by sediments would be utilising aeromagnetic data as was successfully done in the East African Rift by Láo-Dávila et al. (2015), Kolawole et al. (2018), and Heilman et al. (2019). The high-resolution aeromagnetic data needed for this is currently not accessible and thus has not been utilised in this study. Lastly while recently great advances in thermochronology of the Shanxi Rift were made (Su et al., 2021; Clinkscales et al., 2021) this could be expanded to further fault blocks to get better temporal constraints on the uplift rate of different fault footwalls that would complement the geomorphology work to establish a model for the Shanxi Rift evolution and understand relative timing of rift initiation and linkage.

To further expand on the modelling work, better integration of the 2D geodynamic model with the geomorphological and seismic work could be achieved through comprehensive 3D models which combine different levels of inherited structures. For Shanxi initial attempts at a 3D model with a zone of crustal inheritance oblique to a broader mantle suture were conducted but were ultimately cut short due to the computing demands of 3D models and the time constraints. However, it would be a fruitful avenue for further research to develop this model further and compare it to similar analogue models by Zwaan et al., (2022) and Molnar et al., (2020). Different geometries and rheological properties of the initial inherited crustal and mantle features could be further tested to get better constraints on their impact on rifting and

how the two mechanisms of reorientation and reactivation vary through time. While lowering the angle of internal friction was a useful proxy to make the mantle scar weak in our models, there are further avenues to tie this closer to physical observations for example by lowering the grain size or exploring other avenues of weakening the mantle scar. The 3D model could also be coupled with the landscape evolution model "FastScape", which was done successfully by Neuharth et al., (2022), allowing an even tighter link to the geomorphic analysis of the Shanxi Rift. Another 3D model inspired by the GSB could be focused on trying to better replicate the reactivation/reorientation relationships of the two terrane boundaries by varying the rheological properties and scale of the two terrane boundaries to further investigate what influences the different effects of the terrane boundaries have on the GSB. Ultimately both models would feed into a more generalist model of reorientation, reactivation, and its scale dependency across rift basins.

References

Aanyu, K., Koehn, D., 2011. Influence of pre-existing fabrics on fault kinematics and rift geometry of interacting segments: Analogue models based on the Albertine Rift (Uganda), Western Branch-East African Rift System. Journal of African Earth Sciences 59, 168–184. https://doi.org/10.1016/j.jafrearsci.2010.10.003

Acocella, V., Faccenna, C., Funiciello, R., Rosetti, F., 1999. Sand-box modelling of basement-controlled transfer zones in extensional domains. Terra Nova 11, 149–156. https://doi.org/10.1046/j.1365-3121.1999.00238.x

Agostini, A., Bonini, M., Corti, G., Sani, F., Mazzarini, F., 2011. Fault architecture in the Main Ethiopian Rift and comparison with experimental models: Implications for rift evolution and Nubia–Somalia kinematics. Earth and Planetary Science Letters 301, 479–492. https://doi.org/10.1016/j.epsl.2010.11.024

Agostini, A., Corti, G., Zeoli, A., Mulugeta, G., 2009. Evolution, pattern, and partitioning of deformation during oblique continental rifting: Inferences from lithospheric-scale centrifuge models. Geochemistry, Geophysics, Geosystems 10, Q11015. https://doi.org/10.1029/2009GC002676

Ahnert, F., 1970. Functional relationships between denudation, relief, and uplift in large, mid-latitude drainage basins. American Jornal of Science 268, 243–263. https://doi.org/10.2475/ajs.268.3.243

Ai, S., Zheng, Y., He, L., Song, M., 2019. Joint inversion of ambient noise and earthquake data in the Trans-North China Orogen: On-going lithospheric modification and its impact on the Cenozoic continental rifting. Tectonophysics 763, 73–85. https://doi.org/10.1016/j.tecto.2019.05.003

Allen, M.B., Macdonald, D.I.M., Xun, Z., Vincent, S.J., Brouet-Menzies, C., 1997. Early Cenozoic two-phase extension and late Cenozoic thermal subsidence and inversion of the Bohai Basin, northern China. Marine and Petroleum Geology 14, 951–972. https://doi.org/10.1016/S0264-8172(97)00027-5

Assie, K.R., Wang, Y., Tranos, M.D., Ma, H., Kouamelan, K.S., Brantson, E.T., Zhou, L., Ketchaya, Y.B., 2022. Late Cenozoic faulting deformation of the Fanshi Basin (northern Shanxi rift, China), inferred from palaeostress analysis of mesoscale fault-slip data. Geological Magazine 1–17. https://doi.org/10.1017/S0016756822000085

Bailey, G., Manighetti, I., King, G., 2000. Tectonics, volcanism, landscape structure and human evolution in the African Rift, in: Bailey, G., Charles, R., Winder, N. (Eds.), . Oxbow Books, pp. 31–46.

Bailey, G.N., Reynolds, S.C., King, G.C.P., 2011. Landscapes of human evolution: models and methods of tectonic geomorphology and the reconstruction of hominin landscapes. Journal of Human Evolution 60, 257–280. https://doi.org/10.1016/j.jhevol.2010.01.004

Bangerth, W., Dannberg, J., Fraters, M., Gassmoeller, R., Glerum, A., Heister, T., Myhill, R., Naliboff, J., 2018. ASPECT: Advanced Solver for Problems in Earth's ConvecTion, User Manual. https://doi.org/10.6084/m9.figshare.4865333.v10

Behrendt, J.C., 1999. Crustal and lithospheric structure of the West Antarctic Rift System from geophysical investigations — a review.

Behrendt, J.C., LeMasurier, W.E., Cooper, A.K., Tessensohn, F., Tréhu, A., Damaske, D., 1991. Geophysical studies of the West Antarctic Rift System. Tectonics 10, 1257–1273. https://doi.org/10.1029/91TC00868

Bell, R.E., Jackson, C.A.-L., Whipp, P.S., Clements, B., 2014. Strain migration during multiphase extension: Observations from the northern North Sea. Tectonics 33, 1936–1963. https://doi.org/10.1002/2014TC003551
Bellahsen, N., Faccenna, C., Funiciello, F., Daniel, J.M., Jolivet, L., 2003. Why did Arabia separate from Africa? Insights from 3-D laboratory experiments. Earth and Planetary Science Letters 216, 365–381. https://doi.org/10.1016/S0012-821X(03)00516-8
Beniest, A., Willingshofer, E., Sokoutis, D., Sassi, W., 2018. Extending Continental Lithosphere With Lateral Strength Variations: Effects on Deformation Localization and Margin Geometries. Front. Earth Sci. 6. https://doi.org/10.3389/feart.2018.00148
Bercovici, D., Ricard, Y., 2014. Plate tectonics, damage and inheritance. Nature 508, 513–516. https://doi.org/10.1038/nature13072
Bialas, R.W., Buck, W.R., Qin, R., 2010. How much magma is required to rift a continent? Earth and Planetary Science Letters 292, 68–78. https://doi.org/10.1016/j.epsl.2010.01.021
Biggs, J., Ayele, A., Fischer, T.P., Fontijn, K., Hutchison, W., Kazimoto, E., Whaler, K., Wright, T.J., 2021. Volcanic activity and hazard in the East African Rift Zone. Nat Commun 12, 6881. https://doi.org/10.1038/s41467-021-27166-y
Bishop, D.G., Bradshaw, J.D., Landis, C.A., 1985. Provisional Terrane Map of South Island, New Zealand.
Bishop, D.G., Turnbull, I.M., 1996. Geology of the Dunedin area.
Blumenschine, R.J., Peters, C.R., Masao, F.T., Clarke, R.J., Deino, A.L., Hay, R.L., Swisher, C.C., Stanistreet, I.G., Ashley, G.M., McHenry, L.J., Sikes, N.E., van der Merwe, N.J., Tactikos, J.C., Cushing, A.E., Deocampo, D.M., Njau, J.K., Ebert, J.I., 2003. Late Pliocene Homo and Hominid Land Use from Western Olduvai Gorge, Tanzania. Science 299, 1217–1221. https://doi.org/10.1126/science.1075374
Boccaletti, M., Bonini, M., Mazzuoli, R., Abebe, B., Piccardi, L., Tortorici, L., 1998. Quaternary oblique extensional tectonics in the Ethiopian Rift (Horn of Africa). Tectonophysics 287, 97–116.
Bonini, M., Souriot, T., Boccaletti, M., Brun, J.P., 1997. Successive orthogonal and oblique extension episodes in a rift zone: Laboratory experiments with application to the Ethiopian Rift. Tectonics 16, 347–362. https://doi.org/10.1029/96TC03935
Bosworth, W., 1985. Geometry of propagating continental rifts. Nature 316, 625–627. https://doi.org/10.1038/316625a0
Bott, M.H.P., 1992. The stress regime associated with continental break-up. Geological Society, London, Special Publications 68, 125–136. https://doi.org/10.1144/GSL.SP.1992.068.01.08
Bradshaw, J.D., 1993. A review of the Median Tectonic Zone: Terrane boundaries and terrane amalgamation near the Median Tectonic Line. New Zealand Journal of Geology and Geophysics 36, 117–125. https://doi.org/10.1080/00288306.1993.9514559
Braun, J., 1992. Postextensional mantle healing and episodic extension in the Canning Basin. Journal of Geophysical Research: Solid Earth 97, 8927–8936. https://doi.org/10.1029/92JB00584
Briais, A., Patriat, P., Tapponnier, P., 1993. Updated interpretation of magnetic anomalies and seafloor spreading stages in the south China Sea: Implications for the Tertiary tectonics of Southeast Asia. Journal of Geophysical Research: Solid Earth 98, 6299–6328. https://doi.org/10.1029/92JB02280
Brun, J.P., 1999. Narrow rifts versus wide rifts: inferences for the mechanics of rifting from laboratory experiments. Philosophical Transactions of the Royal Society of London. Series A: Mathematical, Physical and Engineering Sciences. https://doi.org/10.1098/rsta.1999.0349

Brune, S., Corti, G., Ranalli, G., 2017. Controls of inherited lithospheric heterogeneity on rift linkage: Numerical and analog models of interaction between the Kenyan and Ethiopian rifts across the Turkana depression. Tectonics 36, 1767–1786. https://doi.org/10.1002/2017TC004739

Brune, S., Kolawole, F., Olive, J.-A., Stamps, D.S., Buck, W.R., Buiter, S.J.H., Furman, T., Shillington, D.J., 2023. Geodynamics of continental rift initiation and evolution. Nat Rev Earth Environ 4, 235–253. https://doi.org/10.1038/s43017-023-00391-3

Bull, W.B., McFadden, L.D., 1980. Tectonic Geomorphology North and South of the Garlock Fault, California, in: Geomorphology in Arid Regions. Routledge.

Burov, E.B., 2011. Rheology and strength of the lithosphere. Marine and Petroleum Geology 28, 1402–1443. https://doi.org/10.1016/j.marpetgeo.2011.05.008

Burov, E.B., 2010. The equivalent elastic thickness (Te), seismicity and the long-term rheology of continental lithosphere: Time to burn-out "crème brûlée"? Tectonophysics, Quantitative modelling of geological processes 484, 4–26. https://doi.org/10.1016/j.tecto.2009.06.013

Burov, E.B., Watts, A.B., 2006. The long-term strength of continental lithosphere: "jelly sandwich" or "crème brûlée"? Gsa Today 16, 4. https://doi.org/10.1130/1052-5173(2006)016<4:TLTSOC>2.0.CO;2

Butler, R.W., Tavarnelli, E., Grasso, M., 2006. Structural inheritance in mountain belts: an Alpine–Apennine perspective. Journal of Structural geology 28, 1893–1908.

Butler, R.W.H., 1989. The influence of pre-existing basin structure on thrust system evolution in the Western Alps. SP 44, 105–122. https://doi.org/10.1144/GSL.SP.1989.044.01.07

Butler, R.W.H., Tavarnelli, E., Grasso, M., 2006. Structural inheritance in mountain belts: An Alpine–Apennine perspective. Journal of Structural Geology, Tectonic inversion and structural inheritance in mountain belts 28, 1893–1908. https://doi.org/10.1016/j.jsg.2006.09.006

Byerlee, J., 1978. Friction of rocks. PAGEOPH 116, 615–626. https://doi.org/10.1007/BF00876528

Calvert, A.J., Sawyer, E.W., Davis, W.J., Ludden, J.N., 1995. Archaean subduction inferred from seismic images of a mantle suture in the Superior Province. Nature 375, 670–674. https://doi.org/10.1038/375670a0

Camelbeeck, T., Iranga, M.D., 1996. Deep crustal earthquakes and active faults along the Rukwa trough, eastern Africa. Geophysical Journal International 124, 612–630. https://doi.org/10.1111/j.1365-246X.1996.tb07040.x

Campbell, J.D., Coombs, D.S., 1966. Murihiku Supergroup (Triassic—Jurassic) of Southland and South Otago. New Zealand Journal of Geology and Geophysics 9, 393–398. https://doi.org/10.1080/00288306.1966.10422483

Campbell, J.D., Coombs, D.S., Grebneff, A., 2003. Willsher Group and geology of the Triassic Kaka Point coastal section, south-east Otago, New Zealand. Journal of the Royal Society of New Zealand 33, 7–38. https://doi.org/10.1080/03014223.2003.9517719

Campbell, M.J., Rosenbaum, G., Allen, C.M., Mortimer, N., 2020. Origin of dispersed Permian–Triassic fore-arc basin terranes in New Zealand: Insights from zircon petrochronology. Gondwana Research 78, 210–227. https://doi.org/10.1016/j.gr.2019.08.010

Cao, L., Sun, Q., Magee, C., 2023. Reutilization of fluid flow pathways over 54 million years, offshore New Zealand. Basin Research 35, 2349–2363. https://doi.org/10.1111/bre.12801

Carpenter, M., Williams, J.N., Fagereng, Å., Wedmore, L.N.J., Biggs, J., Mphepo, F., Mdala, H., Dulanya, Z., Manda, B., 2022. Comparing intrarift and border fault structure in the

Malawi Rift: Implications for normal fault growth. Journal of Structural Geology 165, 104761. https://doi.org/10.1016/j.jsg.2022.104761
Cartwright, J.A., Trudgill, B.D., Mansfield, C.S., 1995. Fault growth by segment linkage: an explanation for scatter in maximum displacement and trace length data from the Canyonlands Grabens of SE Utah. Journal of Structural Geology 17, 1319–1326. https://doi.org/10.1016/0191-8141(95)00033-A
Cawood, P.A., 1986. Stratigraphic and structural relations of the southern Dun Mountain Ophiolite Belt and enclosing strata, northwestern Southland, New Zealand. New Zealand Journal of Geology and Geophysics 29, 179–203. https://doi.org/10.1080/00288306.1986.10427534
Chang, L., Wang, C.-Y., Ding, Z., 2012. Upper mantle anisotropy beneath North China from shear wave splitting measurements. Tectonophysics 522–523, 235–242. https://doi.org/10.1016/j.tecto.2011.12.009
Chen, G., 1987. On the geotectonic nature of the Fen-Wei rift system. Tectonophysics, Continental Rifts-Principal and Regional Characteristics 143, 217–223. https://doi.org/10.1016/0040-1951(87)90091-6
Chen, H., Hu, J., Wu, G., Shi, W., Geng, Y., Qu, H., 2015. Apatite fission-track thermochronological constraints on the pattern of late Mesozoic–Cenozoic uplift and exhumation of the Qinling Orogen, central China. Journal of Asian Earth Sciences, Mesozoic Lithospheric Structures and Tectonic Development of East Asia 114, 649–673. https://doi.org/10.1016/j.jseaes.2014.10.004
Chen, L., 2010. Concordant structural variations from the surface to the base of the upper mantle in the North China Craton and its tectonic implications. Lithos, The lithosphere/asthenosphere boundary: Nature, formation and evolution 120, 96–115. https://doi.org/10.1016/j.lithos.2009.12.007
Chen, L., Jiang, M., Yang, J., Wei, Z., Liu, C., Ling, Y., 2014. Presence of an intralithospheric discontinuity in the central and western North China Craton: Implications for destruction of the craton. Geology 42, 223–226. https://doi.org/10.1130/G35010.1
Chen, L., Tao, W., Zhao, L., Zheng, T., 2008. Distinct lateral variation of lithospheric thickness in the Northeastern North China Craton. Earth and Planetary Science Letters 267, 56–68. https://doi.org/10.1016/j.epsl.2007.11.024
Chen, W.-P., Nábelek, J., 1988. Seismogenic strike-slip faulting and the development of the North China Basin. Tectonics 7, 975–989. https://doi.org/10.1029/TC007i005p00975
Chen, Y., Chen, J., Li, S., Yu, Z., Liu, X., Shen, X., 2021. Variations of crustal thickness and average Vp/Vs ratio beneath the Shanxi Rift, North China, from receiver functions. Earth, Planets and Space 73, 200. https://doi.org/10.1186/s40623-021-01528-8
Chen, Y.-C., Sung, Q., Cheng, K.-Y., 2003. Along-strike variations of morphotectonic features in the Western Foothills of Taiwan: tectonic implications based on stream-gradient and hypsometric analysis. Geomorphology 56, 109–137. https://doi.org/10.1016/S0169-555X(03)00059-X
Chiarabba, C., Amato, A., Anselmi, M., Baccheschi, P., Bianchi, I., Cattaneo, M., Cecere, G., Chiaraluce, L., Ciaccio, M.G., De Gori, P., De Luca, G., Di Bona, M., Di Stefano, R., Faenza, L., Govoni, A., Improta, L., Lucente, F.P., Marchetti, A., Margheriti, L., Mele, F., Michelini, A., Monachesi, G., Moretti, M., Pastori, M., Piana Agostinetti, N., Piccinini, D., Roselli, P., Seccia, D., Valoroso, L., 2009. The 2009 L'Aquila (central Italy) MW6.3 earthquake: Main shock and aftershocks. Geophysical Research Letters 36. https://doi.org/10.1029/2009GL039627

Claringbould, J.S., Bell, R.E., Jackson, C.A.-L., Gawthorpe, R.L., Odinsen, T., 2017. Pre-existing normal faults have limited control on the rift geometry of the northern North Sea. Earth and Planetary Science Letters 475, 190–206. https://doi.org/10.1016/j.epsl.2017.07.014

Clinkscales, C., Kapp, P., 2019. Structural style and kinematics of the Taihang-Luliangshan fold belt, North China: Implications for the Yanshanian orogeny. Lithosphere 11, 767–783. https://doi.org/10.1130/L1096.1

Clinkscales, C., Kapp, P., Thomson, S., Wang, H., Laskowski, A., Orme, D.A., Pullen, A., 2021. Regional exhumation and tectonic history of the Shanxi Rift and Taihangshan, North China. Tectonics 40, e2020TC006416.

Coblentz, D.D., Richardson, R.M., Sandiford, M., 1994. On the gravitational potential of the Earth's lithosphere. Tectonics 13, 929–945. https://doi.org/10.1029/94TC01033

Collanega, L., Siuda, K., A.-L. Jackson, C., Bell, R.E., Coleman, A.J., Lenhart, A., Magee, C., Breda, A., 2019. Normal fault growth influenced by basement fabrics: The importance of preferential nucleation from pre-existing structures. Basin Research 31, 659–687. https://doi.org/10.1111/bre.12327

Collettini, C., Viti, C., Smith, S.A.F., Holdsworth, R.E., 2009. Development of interconnected talc networks and weakening of continental low-angle normal faults. Geology 37, 567–570. https://doi.org/10.1130/G25645A.1

Cooper, A.K., Davey, F.J., 1985. Episodic Rifting of Phanerozoic Rocks in the Victoria Land Basin, Western Ross Sea, Antarctica. Science 229, 1085–1087. https://doi.org/10.1126/science.229.4718.1085

Corti, G., 2012. Evolution and characteristics of continental rifting: Analog modeling-inspired view and comparison with examples from the East African Rift System. Tectonophysics 522–523, 1–33. https://doi.org/10.1016/j.tecto.2011.06.010

Corti, G., 2009. Continental rift evolution: From rift initiation to incipient break-up in the Main Ethiopian Rift, East Africa. Earth-Science Reviews 96, 1–53. https://doi.org/10.1016/j.earscirev.2009.06.005

Corti, G., 2008. Control of rift obliquity on the evolution and segmentation of the main Ethiopian rift. Nature Geosci 1, 258–262. https://doi.org/10.1038/ngeo160

Corti, G., Iandelli, I., Cerca, M., 2013a. Experimental modeling of rifting at craton margins. Geosphere 9, 138–154. https://doi.org/10.1130/GES00863.1

Corti, G., Maestrelli, D., Sani, F., 2022. Large-to Local-Scale Control of Pre-Existing Structures on Continental Rifting: Examples From the Main Ethiopian Rift, East Africa. Frontiers in Earth Science 10.

Corti, G., Philippon, M., Sani, F., Keir, D., Kidane, T., 2013b. Re-orientation of the extension direction and pure extensional faulting at oblique rift margins: comparison between the Main Ethiopian Rift and laboratory experiments. Terra Nova 25, 396–404. https://doi.org/10.1111/ter.12049

Cowie, P.A., Roberts, G.P., Bull, J.M., Visini, F., 2012. Relationships between fault geometry, slip rate variability and earthquake recurrence in extensional settings. Geophysical Journal International 189, 143–160. https://doi.org/10.1111/j.1365-246X.2012.05378.x

Cowie, P.A., Underhill, J.R., Behn, M.D., Lin, J., Gill, C.E., 2005. Spatio-temporal evolution of strain accumulation derived from multi-scale observations of Late Jurassic rifting in the northern North Sea: A critical test of models for lithospheric extension. Earth and Planetary Science Letters 234, 401–419. https://doi.org/10.1016/j.epsl.2005.01.039

Cox, R.T., 1994. Analysis of drainage-basin symmetry as a rapid technique to identify areas of possible Quaternary tilt-block tectonics: An example from the Mississippi Embayment. GSA Bulletin 106, 571–581. https://doi.org/10.1130/0016-7606(1994)106<0571:AODBSA>2.3.CO;2

Crider, J.G., Pollard, D.D., 1998. Fault linkage: Three-dimensional mechanical interaction between echelon normal faults. Journal of Geophysical Research: Solid Earth 103, 24373–24391. https://doi.org/10.1029/98JB01353
Dall'Asta, N., Manatschal, G., Hoareau, G., 2024. Linking mineral deposits to crustal necking: insights from the Western Alps. Miner Deposita 59, 773–793. https://doi.org/10.1007/s00126-023-01226-3
Daly, M.C., Chorowicz, J., Fairhead, J.D., 1989. Rift basin evolution in Africa: the influence of reactivated steep basement shear zones. Geological Society, London, Special Publications 44, 309–334. https://doi.org/10.1144/GSL.SP.1989.044.01.17
Davies, T.C., 2008. Environmental health impacts of East African Rift volcanism. Environ Geochem Health 30, 325–338. https://doi.org/10.1007/s10653-008-9168-7
Davis, G., Zheng, Y., Cong, W., Darby, B., Zhang, C., Gehrels, G., 2001. Mesozoic tectonic evolution of the Yanshan fold and thrust belt, with emphasis on Hebei and Liaoning provinces, northern China, in: Geol. Soc. Am. Mem. pp. 171–197. https://doi.org/10.1130/0-8137-1194-0.171
Dawson, S.M., Laó-Dávila, D.A., Atekwana, E.A., Abdelsalam, M.G., 2018. The influence of the Precambrian Mughese Shear Zone structures on strain accommodation in the northern Malawi Rift. Tectonophysics 722, 53–68. https://doi.org/10.1016/j.tecto.2017.10.010
de Boer, J.Z., Sanders, D.T., 2004. Earthquakes in Human History: The Far-Reaching Effects of Seismic Disruptions, in: Earthquakes in Human History. Princeton University Press. https://doi.org/10.1515/9780691234205
De Paola, N., Holdsworth, R.E., McCaffrey, K.J.W., Barchi, M.R., 2005. Partitioned transtension: an alternative to basin inversion models. Journal of Structural Geology 27, 607–625. https://doi.org/10.1016/j.jsg.2005.01.006
Delvaux, D., Fronhoffs, A., Hus, R., Poort, J., 2000. Normal fault splays, relay ramps and transfer zones in the central part of the Baikal rift basin: Insight from digital topography and bathymetry. 22.
Delvaux, D., Kervyn, F., Macheyeki, A.S., Temu, E.B., 2012. Geodynamic significance of the TRM segment in the East African Rift (W-Tanzania): Active tectonics and paleostress in the Ufipa plateau and Rukwa basin. Journal of Structural Geology 37, 161–180. https://doi.org/10.1016/j.jsg.2012.01.008
Deng, C., Fossen, H., Gawthorpe, R.L., Rotevatn, A., Jackson, C.A.-L., FazliKhani, H., 2017a. Influence of fault reactivation during multiphase rifting: The Oseberg area, northern North Sea rift. Marine and Petroleum Geology 86, 1252–1272. https://doi.org/10.1016/j.marpetgeo.2017.07.025
Deng, C., Gawthorpe, R.L., Finch, E., Fossen, H., 2017b. Influence of a pre-existing basement weakness on normal fault growth during oblique extension: Insights from discrete element modeling. Journal of Structural Geology 105, 44–61. https://doi.org/10.1016/j.jsg.2017.11.005
Deng, H., McClay, K., Bilal, A., 2020. 3D structure and evolution of an extensional fault network of the eastern Dampier Sub-basin, North West Shelf of Australia. Journal of Structural Geology 132, 103972. https://doi.org/10.1016/j.jsg.2019.103972
Deng, Q., Ran, Y., Yang, X., Min, W., Chu, Q., 2007. Map of Active tectonics in China.
Deng, Y., Xu, Y.-G., Chen, Y., 2021. Formation mechanism of the North–South Gravity Lineament in eastern China. Tectonophysics 818, 229074. https://doi.org/10.1016/j.tecto.2021.229074
Densmore, A.L., Dawers, N.H., Gupta, S., Allen, P.A., Gilpin, R., 2003. Landscape evolution at extensional relay zones. Journal of Geophysical Research: Solid Earth 108. https://doi.org/10.1029/2001JB001741

Densmore, A.L., Dawers, N.H., Gupta, S., Guidon, R., Goldin, T., 2004. Footwall topographic development during continental extension. Journal of Geophysical Research: Earth Surface 109, F03001. https://doi.org/10.1029/2003JF000115
Dewitte, O., Dille, A., Depicker, A., Kubwimana, D., Maki Mateso, J.-C., Mugaruka Bibentyo, T., Uwihirwe, J., Monsieurs, E., 2021. Constraining landslide timing in a data-scarce context: from recent to very old processes in the tropical environment of the North Tanganyika-Kivu Rift region. Landslides 18, 161–177. https://doi.org/10.1007/s10346-020-01452-0
Di Giacomo, D., Engdahl, E.R., Storchak, D.A., 2018. The ISC-GEM Earthquake Catalogue (1904–2014): status after the Extension Project. Earth Syst. Sci. Data 10, 1877–1899. https://doi.org/10.5194/essd-10-1877-2018
DiBiase, R.A., Whipple, K.X., Heimsath, A.M., Ouimet, W.B., 2010. Landscape form and millennial erosion rates in the San Gabriel Mountains, CA. Earth and Planetary Science Letters 289, 134–144. https://doi.org/10.1016/j.epsl.2009.10.036
Dichiarante, A.M., Holdsworth, R.E., Dempsey, E.D., Selby, D., McCaffrey, K.J.W., Michie, U.McL., Morgan, G., Bonniface, J., 2016. New structural and Re–Os geochronological evidence constraining the age of faulting and associated mineralization in the Devonian Orcadian Basin, Scotland. Journal of the Geological Society 173, 457–473. https://doi.org/10.1144/jgs2015-118
Diercks, M.-L., Grützner, C., Welte, J., Ustaszewski, K., 2023. Challenges of geomorphologic analysis of active tectonics in a slowly deforming karst landscape (W Slovenia and NE Italy). Geomorphology 440, 108894. https://doi.org/10.1016/j.geomorph.2023.108894
Dong, S., Zhang, Y., Zhang, F., Cui, J., Chen, X., Zhang, S., Miao, L., Li, J., Shi, W., Li, Z., Huang, S., Li, H., 2015. Late Jurassic–Early Cretaceous continental convergence and intracontinental orogenesis in East Asia: A synthesis of the Yanshan Revolution. Journal of Asian Earth Sciences, Mesozoic Lithospheric Structures and Tectonic Development of East Asia 114, 750–770. https://doi.org/10.1016/j.jseaes.2015.08.011
Doré, A.G., Lundin, E.R., Fichler, C., Olesen, O., 1997. Patterns of basement structure and reactivation along the NE Atlantic margin. Journal of the Geological Society 154, 85–92. https://doi.org/10.1144/gsjgs.154.1.0085
Doré, A.G., Lundin, E.R., Jensen, L.N., Birkeland, Ø., Eliassen, P.E., Fichler, C., 1999. Principal tectonic events in the evolution of the northwest European Atlantic margin. Geological Society, London, Petroleum Geology Conference Series 5, 41–61. https://doi.org/10.1144/0050041
Duffy, O.B., Bell, R.E., Jackson, C.A.-L., Gawthorpe, R.L., Whipp, P.S., 2015. Fault growth and interactions in a multiphase rift fault network: Horda Platform, Norwegian North Sea. Journal of Structural Geology 80, 99–119. https://doi.org/10.1016/j.jsg.2015.08.015
Dulanya, Z., Gallen, S.F., Kolawole, F., Williams, J.N., Wedmore, L.N.J., Biggs, J., Fagereng, Å., 2022. Knickpoint morphotectonics of the Middle Shire River basin: Implications for the evolution of rift interaction zones. Basin Research 34, 1839–1858. https://doi.org/10.1111/bre.12687
Dunbar, J.A., Sawyer, D.S., 1988. Continental rifting at pre-existing lithospheric weaknesses. Nature 333, 450–452. https://doi.org/10.1038/333450a0
Ebinger, C.J., 1989. Geometric and kinematic development of border faults and accommodation zones, Kivu-Rusizi Rift, Africa. Tectonics 8, 117–133. https://doi.org/10.1029/TC008i001p00117
Ebinger, C.J., Reiss, M.C., Bastow, I., Karanja, M.M., 2024. Shallow sources of upper mantle seismic anisotropy in East Africa. Earth and Planetary Science Letters 625, 118488. https://doi.org/10.1016/j.epsl.2023.118488

Ebinger, C.J., Rosendahl, B.R., Reynolds, D.J., 1987. Tectonic model of the Malaŵi rift, Africa. Tectonophysics, Sedimentary basins within the Dead Sea and other rift zones 141, 215–235. https://doi.org/10.1016/0040-1951(87)90187-9

Edbrooke, S.W., Heron, D.W., Forsyth, P.J., Jongens, R., 2015. Geological Map of New Zealand 1:1 000 000.

Erbello, A., Melnick, D., Zeilinger, G., Bookhagen, B., Pingel, H., Strecker, M.R., 2022. Geomorphic expression of a tectonically active rift-transfer zone in southern Ethiopia. Geomorphology 403, 108162. https://doi.org/10.1016/j.geomorph.2022.108162

Færseth, R.B., 1996. Interaction of Permo-Triassic and Jurassic extensional fault-blocks during the development of the northern North Sea. Journal of the Geological Society 153, 931–944. https://doi.org/10.1144/gsjgs.153.6.0931

Farangitakis, G.P., Heron, P.J., McCaffrey, K.J.W., van Hunen, J., Kalnins, L.M., 2020. The impact of oblique inheritance and changes in relative plate motion on the development of rift-transform systems. Earth and Planetary Science Letters 541, 116277. https://doi.org/10.1016/j.epsl.2020.116277

Faulds, J.E., Varga, R.J., 1998. The role of accommodation zones and transfer zones in the regional segmentation of extended terranes, in: Faulds, J.E., Stewart, J.H. (Eds.), Accommodation Zones and Transfer Zones; the Regional Segmentation of the Basin and Range Province. Geological Society of America, p. 0. https://doi.org/10.1130/0-8137-2323-X.1

Faulkner, D.R., Jackson, C.A.L., Lunn, R.J., Schlische, R.W., Shipton, Z.K., Wibberley, C.A.J., Withjack, M.O., 2010. A review of recent developments concerning the structure, mechanics and fluid flow properties of fault zones. Journal of Structural Geology, Fault Zones 32, 1557–1575. https://doi.org/10.1016/j.jsg.2010.06.009

Faure, M., Trap, P., Lin, W., Monié, P., Bruguier, O., 2007. Polyorogenic evolution of the Paleoproterozoic Trans-North China Belt—New insights from the Lüliangshan-Hengshan-Wutaishan and Fuping massifs. Episodes Journal of International Geoscience 30, 96–107.

Fazlikhani, H., Aagotnes, S.S., Refvem, M.A., Hamilton-Wright, J., Bell, R.E., Fossen, H., Gawthorpe, R.L., Jackson, C.A.-L., Rotevatn, A., 2021. Strain migration during multiphase extension, Stord Basin, northern North Sea rift. Basin Research 33, 1474–1496. https://doi.org/10.1111/bre.12522

Fazlikhani, H., Fossen, H., Gawthorpe, R.L., Faleide, J.I., Bell, R.E., 2017. Basement structure and its influence on the structural configuration of the northern North Sea rift. Tectonics 36, 1151–1177. https://doi.org/10.1002/2017TC004514

Fernández-Blanco, D., de Gelder, G., Lacassin, R., Armijo, R., 2020. Geometry of Flexural Uplift by Continental Rifting in Corinth, Greece. Tectonics 39, e2019TC005685. https://doi.org/10.1029/2019TC005685

Fick, S.E., Hijmans, R.J., 2017. WorldClim 2: new 1-km spatial resolution climate surfaces for global land areas. International Journal of Climatology 37, 4302–4315. https://doi.org/10.1002/joc.5086

Fisher, J.A., Pazzaglia, F.J., Anastasio, D.J., Gallen, S.F., 2022. Linear Inversion of Fluvial Topography in the Northern Apennines: Comparison of Base-Level Fall to Crustal Shortening. Tectonics 41, e2022TC007379. https://doi.org/10.1029/2022TC007379

Flack, C., Warner, M., 1990. Three-dimensional mapping of Seismic reflections from the crust and upper mantle, northwest of Scotland. Tectonophysics, Siesmic Probing of Continents and their Margins 173, 469–481. https://doi.org/10.1016/0040-1951(90)90239-5

Flint, J.-J., 1974. Stream gradient as a function of order, magnitude, and discharge. Water Resources Research 10, 969–973.
Foley, S.F., Fischer, T.P., 2017. An essential role for continental rifts and lithosphere in the deep carbon cycle. Nature Geosci 10, 897–902. https://doi.org/10.1038/s41561-017-0002-7
Ford, M., Rohais, S., Williams, E.A., Bourlange, S., Jousselin, D., Backert, N., Malartre, F., 2013. Tectono-sedimentary evolution of the western Corinth rift (Central Greece). Basin Research 25, 3–25. https://doi.org/10.1111/j.1365-2117.2012.00550.x
Fossen, H., Khani, H.F., Faleide, J.I., Ksienzyk, A.K., Dunlap, W.J., 2017. Post-Caledonian extension in the West Norway–northern North Sea region: the role of structural inheritance. Geological Society, London, Special Publications 439, 465–486. https://doi.org/10.1144/SP439.6
Fossen, H., Rotevatn, A., 2016. Fault linkage and relay structures in extensional settings—A review. Earth-Science Reviews 154, 14–28. https://doi.org/10.1016/j.earscirev.2015.11.014
Fournier, M., Jolivet, L., Davy, P., Thomas, J.-C., 2004. Backarc extension and collision: an experimental approach to the tectonics of Asia. Geophysical Journal International 157, 871–889. https://doi.org/10.1111/j.1365-246X.2004.02223.x
Fraser, A.J., Gawthorpe, R.L., 1990. Tectono-stratigraphic development and hydrocarbon habitat of the Carboniferous in northern England. Geological Society, London, Special Publications 55, 49–86. https://doi.org/10.1144/GSL.SP.1990.055.01.03
Friedmann, S.J., Burbank, D.W., 1995. Rift basins and supradetachment basins: intracontinental extensional end-members. Basin Research 7, 109–127. https://doi.org/10.1111/j.1365-2117.1995.tb00099.x
Fu, C., Li, Shengli, Li, Shunli, Xu, J., 2022. Tectonostratigraphic evolution of a rift basin and corresponding source-to-sink systems: Implications for the western Bohai Bay Basin, North China. Marine and Petroleum Geology 139, 105587. https://doi.org/10.1016/j.marpetgeo.2022.105587
Gaina, C., Müller, D.R., Royer, J.-Y., Stock, J., Hardebeck, J., Symonds, P., 1998. The tectonic history of the Tasman Sea: A puzzle with 13 pieces. Journal of Geophysical Research: Solid Earth 103, 12413–12433. https://doi.org/10.1029/98JB00386
Gallen, S.F., Fernández-Blanco, D., 2021. A New Data-Driven Bayesian Inversion of Fluvial Topography Clarifies the Tectonic History of the Corinth Rift and Reveals a Channel Steepness Threshold. Journal of Geophysical Research: Earth Surface 126, e2020JF005651. https://doi.org/10.1029/2020JF005651
Gao, M., Zeilinger, G., Xu, X., Tan, X., Wang, Q., Hao, M., 2016. Active tectonics evaluation from geomorphic indices for the central and the southern Longmenshan range on the Eastern Tibetan Plateau, China. Tectonics 35, 1812–1826. https://doi.org/10.1002/2015TC004080
Gao, S., Davis, P.M., Liu, H., Slack, P.D., Rigor, A.W., Zorin, Y.A., Mordvinova, V.V., Kozhevnikov, V.M., Logatchev, N.A., 1997. SKS splitting beneath continental rift zones. Journal of Geophysical Research: Solid Earth 102, 22781–22797. https://doi.org/10.1029/97JB01858
Gao, S., Rudnick, R.L., Carlson, R.W., McDonough, W.F., Liu, Y.-S., 2002. Re–Os evidence for replacement of ancient mantle lithosphere beneath the North China craton. Earth and Planetary Science Letters 198, 307–322. https://doi.org/10.1016/S0012-821X(02)00489-2
Gao, S., Rudnick, R.L., Yuan, H.-L., Liu, X.-M., Liu, Y.-S., Xu, W.-L., Ling, W.-L., Ayers, J., Wang, X.-C., Wang, Q.-H., 2004. Recycling lower continental crust in the North China craton. Nature 432, 892–897. https://doi.org/10.1038/nature03162

Gardner, T.W., 1975. The History of Part of the Colorado River and Its Tributaries: An Experimental Study 87–95.
Gavel, M.M., Amato, J.M., Ricketts, J.W., Kelley, S., Biddle, J.M., Delfin, R.A., 2021. Thermochronological transect across the Basin and Range/Rio Grande rift transition: Contrasting cooling histories in contiguous extensional provinces. Geosphere 17, 1807–1839. https://doi.org/10.1130/GES02381.1
Gawthorpe, R.L., Hurst, J.M., 1993. Transfer zones in extensional basins: their structural style and influence on drainage development and stratigraphy. Journal of the Geological Society 150, 1137–1152. https://doi.org/10.1144/gsjgs.150.6.1137
Gawthorpe, R.L., Leeder, M.R., 2000. Tectono-sedimentary evolution of active extensional basins. Basin Research 12, 195–218. https://doi.org/10.1111/j.1365-2117.2000.00121.x
Gawthorpe, R.L., Leeder, M.R., Kranis, H., Skourtsos, E., Andrews, J.E., Henstra, G.A., Mack, G.H., Muravchik, M., Turner, J.A., Stamatakis, M., 2018. Tectono‐sedimentary evolution of the Plio‐Pleistocene Corinth rift, Greece. Basin Research 30, 448–479. https://doi.org/10.1111/bre.12260
Geological Survey Bureau of Shanxi Province (GSBSX), 2008. Regional Geology of Linfen (1:250000).
Geological Survey Bureau of Shanxi Province (GSBSX), 2007. Regional Geology of Houma (1:250000).
Geological Survey Bureau of Shanxi Province (GSBSX), 2002. Regional Geology of Yingxian (1:250000).
Geurts, A.H., Whittaker, A.C., Gawthorpe, R.L., Cowie, P.A., 2020. Transient landscape and stratigraphic responses to drainage integration in the actively extending central Italian Apennines. Geomorphology 353, 107013. https://doi.org/10.1016/j.geomorph.2019.107013
Giba, M., Walsh, J.J., Nicol, A., 2012. Segmentation and growth of an obliquely reactivated normal fault. Journal of Structural Geology 39, 253–267. https://doi.org/10.1016/j.jsg.2012.01.004
Glerum, A., Thieulot, C., Fraters, M., Blom, C., Spakman, W., 2018. Nonlinear viscoplasticity in ASPECT: benchmarking and applications to subduction. Solid Earth 9, 267–294. https://doi.org/10.5194/se-9-267-2018
Goldsworthy, M., Jackson, J., 2000. Active normal fault evolution in Greece revealed by geomorphology and drainage patterns. Journal of the Geological Society 157, 967–981. https://doi.org/10.1144/jgs.157.5.967
Gouiza, M., Naliboff, J., 2021. Rheological inheritance controls the formation of segmented rifted margins in cratonic lithosphere. Nat Commun 12, 4653. https://doi.org/10.1038/s41467-021-24945-5
Griffin, B., Andi, Z., O'Reilly, S., Ryan, C., 1998. Phanerozoic evolution of the lithosphere beneath the Sino-Korean craton: Conference on Mantle Dynamics and Plate Interactions in East Asia. Mantle dynamics and plate interactions in east Asia, Geodynamics Series 107–126.
Griffin, W.L., Andi, Z., O'Reilly, S.Y., Ryan, C.G., 1998. Phanerozoic Evolution of the Lithosphere Beneath the Sino-Korean Craton, in: Mantle Dynamics and Plate Interactions in East Asia. American Geophysical Union (AGU), pp. 107–126. https://doi.org/10.1029/GD027p0107

Groves, K., Saville, C., Hurst, M.D., Jones, S.J., Song, S., Allen, M.B., 2020. Geomorphic expressions of collisional tectonics in the Qilian Shan, north eastern Tibetan Plateau. Tectonophysics 788, 228503. https://doi.org/10.1016/j.tecto.2020.228503
Hack, J.T., 1957. Studies of longitudinal stream profiles in Virginia and Maryland. US Government Printing Office.
Hamdouni, R., Irigaray, C., Castillo, T., Chacón, J., Keller, E., 2008. Assessment of relative active tectonics, southwest border of the Sierra Nevada (southern Spain). Geomorphology 150–173. https://doi.org/10.1016/j.geomorph.2007.08.004
Hao, P., 2023. Several strong historical earthquakes during Ming and Qing Dynasties and their effects to local reconstruction at Southern Shanxi Province, North China: Insight from the Chinese literature. Natural Hazards Research 3, 598–607. https://doi.org/10.1016/j.nhres.2023.11.009
Harden, D.R., 1990. Controlling factors in the distribution and development of incised meanders in the central Colorado Plateau. GSA Bulletin 102, 233–242. https://doi.org/10.1130/0016-7606(1990)102<0233:CFITDA>2.3.CO;2
Harkins, N.W., Anastasio, D.J., Pazzaglia, F.J., 2005. Tectonic geomorphology of the Red Rock fault, insights into segmentation and landscape evolution of a developing range front normal fault. Journal of Structural Geology 27, 1925–1939. https://doi.org/10.1016/j.jsg.2005.07.005
Havlin, C., Parmentier, E.M., Hirth, G., 2013. Dike propagation driven by melt accumulation at the lithosphere–asthenosphere boundary. Earth and Planetary Science Letters 376, 20–28. https://doi.org/10.1016/j.epsl.2013.06.010
He, J., Cai, D., Li, Y., Gong, Z., 2004. Active extension of the Shanxi rift, north China: does it result from anticlockwise block rotations? Terra Nova 16, 38–42. https://doi.org/10.1046/j.1365-3121.2003.00523.x
He, J., Liu, M., Li, Y., 2003. Is the Shanxi rift of northern China extending? Geophysical research letters 30.
He, L., Zhang, L., 2018. Thermal evolution of cratons in China. Journal of Asian Earth Sciences 164, 237–247. https://doi.org/10.1016/j.jseaes.2018.06.028
Healy, D., 2009. Anisotropy, pore fluid pressure and low angle normal faults. Journal of Structural Geology 31, 561–574. https://doi.org/10.1016/j.jsg.2009.03.001
Heilman, E., Kolawole, F., Atekwana, E.A., Mayle, M., 2019. Controls of Basement Fabric on the Linkage of Rift Segments. Tectonics 38, 1337–1366. https://doi.org/10.1029/2018TC005362
Heister, T., Dannberg, J., Gassmöller, R., Bangerth, W., 2017. High accuracy mantle convection simulation through modern numerical methods – II: realistic models and problems. Geophysical Journal International 210, 833–851. https://doi.org/10.1093/gji/ggx195
Henstra, G.A., Rotevatn, A., Gawthorpe, R.L., Ravnås, R., 2015. Evolution of a major segmented normal fault during multiphase rifting: The origin of plan-view zigzag geometry. Journal of Structural Geology 74, 45–63. https://doi.org/10.1016/j.jsg.2015.02.005
Henza, A.A., Withjack, M.O., Schlische, R.W., 2011. How do the properties of a pre-existing normal-fault population influence fault development during a subsequent phase of extension? Journal of Structural Geology 33, 1312–1324. https://doi.org/10.1016/j.jsg.2011.06.010
Heron, P.J., Peace, A.L., McCaffrey, K.J.W., Welford, J.K., Wilson, R., van Hunen, J., Pysklywec, R.N., 2019. Segmentation of Rifts Through Structural Inheritance: Creation of the Davis Strait. Tectonics 38, 2411–2430. https://doi.org/10.1029/2019TC005578
Heron, P.J., Pysklywec, R.N., Stephenson, R., 2016. Lasting mantle scars lead to perennial plate tectonics. Nat Commun 7, 11834. https://doi.org/10.1038/ncomms11834

Hirth, G., Kohlstedt, D., 2004. Rheology of the Upper Mantle and the Mantle Wedge: A View from the Experimentalists, in: Inside the Subduction Factory. American Geophysical Union (AGU), pp. 83–105. https://doi.org/10.1029/138GM06
Hodge, M., Biggs, J., Goda, K., Aspinall, W., 2015. Assessing infrequent large earthquakes using geomorphology and geodesy: the Malawi Rift. Nat Hazards 76, 1781–1806. https://doi.org/10.1007/s11069-014-1572-y
Hodge, M., Fagereng, Å., Biggs, J., 2018a. The Role of Coseismic Coulomb Stress Changes in Shaping the Hard Link Between Normal Fault Segments. Journal of Geophysical Research: Solid Earth 123, 797–814. https://doi.org/10.1002/2017JB014927
Hodge, M., Fagereng, Å., Biggs, J., Mdala, H., 2018b. Controls on early-rift geometry: New perspectives from the Bilila-Mtakataka Fault, Malawi. Geophysical Research Letters 45, 3896–3905.
Holdsworth, R.E., Butler, C.A., Roberts, A.M., 1997. The recognition of reactivation during continental deformation. Journal of the Geological Society 154, 73–78. https://doi.org/10.1144/gsjgs.154.1.0073
Holdsworth, R.E., Hand, M., Miller, J.A., Buick, I.S., 2001a. Continental reactivation and reworking: An introduction, in: Miller, J.A., Holdsworth, R.E., Buick, I.S., Hand, M. (Eds.), Continental Reactivation and Reworking. Geological Society of London, p. 0. https://doi.org/10.1144/GSL.SP.2001.184.01.01
Holdsworth, R.E., Selby, D., Dempsey, E., Scott, L., Hardman, K., Fallick, A.E., Bullock, R., 2020. The nature and age of Mesoproterozoic strike-slip faulting based on Re–Os geochronology of syntectonic copper mineralization, Assynt Terrane, NW Scotland. Journal of the Geological Society 177, 686–699. https://doi.org/10.1144/jgs2020-011
Holdsworth, R.E., Stewart, M., Imber, J., Strachan, R.A., 2001b. The structure and rheological evolution of reactivated continental fault zones: a review and case study. Geological Society, London, Special Publications 184, 115–137. https://doi.org/10.1144/GSL.SP.2001.184.01.07
Howell, L., Egan, S., Leslie, G., Clarke, S., Mitten, A., Pringle, J., 2020. The influence of low-density granite bodies on extensional basins. Geology Today 36, 22–26. https://doi.org/10.1111/gto.12297
Hu, X., Li, Y., Yang, J., 2005. Quaternary paleolake development in the Fen River basin, North China. Geomorphology 65, 1–13. https://doi.org/10.1016/j.geomorph.2004.06.008
Huerta, A.D., Harry, D.L., 2007. The transition from diffuse to focused extension: Modeled evolution of the West Antarctic Rift system. Earth and Planetary Science Letters 255, 133–147. https://doi.org/10.1016/j.epsl.2006.12.011
Huismans, R.S., Podladchikov, Y.Y., Cloetingh, S., 2001. Transition from passive to active rifting: Relative importance of asthenospheric doming and passive extension of the lithosphere. Journal of Geophysical Research: Solid Earth 106, 11271–11291. https://doi.org/10.1029/2000JB900424
Hurtrez, J.-E., Sol, C., Lucazeau, F., 1999. Effect of drainage area on hypsometry from an analysis of small-scale drainage basins in the Siwalik Hills (Central Nepal). Earth Surface Processes and Landforms 24, 799–808. https://doi.org/10.1002/(SICI)1096-9837(199908)24:9<799::AID-ESP12>3.0.CO;2-4
Jackson, J., 2002. Strength of the continental lithosphere: Time to abandon the jelly sandwich? Gsa Today 12, 4. https://doi.org/10.1130/1052-5173(2002)012<0004:SOTCLT>2.0.CO;2
Jackson, J., Leeder, M., 1994. Drainage systems and the development of normal faults: an example from Pleasant Valley, Nevada. Journal of Structural Geology 16, 1041–1059. https://doi.org/10.1016/0191-8141(94)90051-5

Jeans, C.V., Fisher, M.J., Raine, J.I., Merriman, R.J., Campbell, H.J., Fallick, A.E., Carr, A.D., Kemp, S.J., 2003. Triassic sediments of the Kaka Point Structural Belt, South Island, New Zealand, and their relationship to the Murihiku Terrane. Journal of the Royal Society of New Zealand 33, 57–84. https://doi.org/10.1080/03014223.2003.9517721

Jolie, E., Scott, S., Faulds, J., Chambefort, I., Axelsson, G., Gutiérrez-Negrín, L.C., Regenspurg, S., Ziegler, M., Ayling, B., Richter, A., Zemedkun, M.T., 2021. Geological controls on geothermal resources for power generation. Nat Rev Earth Environ 2, 324–339. https://doi.org/10.1038/s43017-021-00154-y

Jones, C.H., Unruh, J.R., Sonder, L.J., 1996. The role of gravitational potential energy in active deformation in the southwestern United States. Nature 381, 37–41. https://doi.org/10.1038/381037a0

Jordan, T.A., Riley, T.R., Siddoway, C.S., 2020. The geological history and evolution of West Antarctica. Nat Rev Earth Environ 1, 117–133. https://doi.org/10.1038/s43017-019-0013-6

Kapp, P., Pullen, A., Pelletier, J.D., Russell, J., Goodman, P., Cai, F., 2015. From dust to dust: Quaternary wind erosion of the Mu Us Desert and Loess Plateau, China. Geology 43, 835–838. https://doi.org/10.1130/G36724.1

Karig, D.E., 1971. Origin and development of marginal basins in the western Pacific. Journal of Geophysical Research (1896-1977) 76, 2542–2561. https://doi.org/10.1029/JB076i011p02542

Kattenhorn, S.A., Aydin, A., Pollard, D.D., 2000. Joints at high angles to normal fault strike: an explanation using 3-D numerical models of fault-perturbed stress fields. Journal of Structural Geology 22, 1–23. https://doi.org/10.1016/S0191-8141(99)00130-3

Kendall, J.-M., Pilidou, S., Keir, D., Bastow, I.D., Stuart, G.W., Ayele, A., 2006. Mantle upwellings, melt migration and the rifting of Africa: insights from seismic anisotropy. Geological Society, London, Special Publications 259, 55–72. https://doi.org/10.1144/GSL.SP.2006.259.01.06

Kim, Y.-S., Sanderson, D.J., 2005. The relationship between displacement and length of faults: a review. Earth-Science Reviews 68, 317–334. https://doi.org/10.1016/j.earscirev.2004.06.003

Kimbell, G.S., Ritchie, J.D., Johnson, H., Gatliff, R.W., 2005. Controls on the structure and evolution of the NE Atlantic margin revealed by regional potential field imaging and 3D modelling. Geological Society, London, Petroleum Geology Conference Series 6, 933–945. https://doi.org/10.1144/0060933

Kimbrough, D.L., Mattinson, J.M., Coombs, D.S., Landis, C.A., Johnston, M.R., 1992. Uranium-lead ages from the Dun Mountain ophiolite belt and Brook Street terrane, South Island, New Zealand. GSA Bulletin 104, 429–443. https://doi.org/10.1130/0016-7606(1992)104<0429:ULAFTD>2.3.CO;2

Kinabo, B.D., Hogan, J.P., Atekwana, E.A., Abdelsalam, M.G., Modisi, M.P., 2008. Fault growth and propagation during incipient continental rifting: Insights from a combined aeromagnetic and Shuttle Radar Topography Mission digital elevation model investigation of the Okavango Rift Zone, northwest Botswana. Tectonics 27, TC3013. https://doi.org/10.1029/2007TC002154

Kirby, E., Whipple, K.X., 2012. Expression of active tectonics in erosional landscapes. Journal of Structural Geology 44, 54–75. https://doi.org/10.1016/j.jsg.2012.07.009

Koehn, D., Aanyu, K., Haines, S., Sachau, T., 2008. Rift nucleation, rift propagation and the creation of basement micro-plates within active rifts. Tectonophysics, Geodynamics of Lithospheric Extension 458, 105–116. https://doi.org/10.1016/j.tecto.2007.10.003

Kolawole, F., Atekwana, E.A., Laó-Dávila, D.A., Abdelsalam, M.G., Chindandali, P.R., Salima, J., Kalindekafe, L., 2018. Active Deformation of Malawi Rift's North Basin Hinge Zone Modulated by Reactivation of Preexisting Precambrian Shear Zone Fabric. Tectonics 37, 683–704. https://doi.org/10.1002/2017TC004628

Kolawole, F., Firkins, M.C., Al Wahaibi, T.S., Atekwana, E.A., Soreghan, M.J., 2021a. Rift interaction zones and the stages of rift linkage in active segmented continental rift systems. Basin Research 33, 2984–3020.

Kolawole, F., Phillips, T.B., Atekwana, E.A., Jackson, C.A.-L., 2021b. Structural Inheritance Controls Strain Distribution During Early Continental Rifting, Rukwa Rift. Front. Earth Sci. 9, 707869. https://doi.org/10.3389/feart.2021.707869

Kolawole, F., Vick, T., Atekwana, E.A., Laó-Dávila, D.A., Costa, A.G., Carpenter, B.M., 2022. Strain localization and migration during the pulsed lateral propagation of the Shire Rift Zone, East Africa. Tectonophysics 839, 229499. https://doi.org/10.1016/j.tecto.2022.229499

Kolawole, F., Xue, L., Dulanya, Z., 2024. Rapid Versus Delayed Linkage and Coalescence of Propagating Rift Tips. https://doi.org/10.22541/essoar.168167202.29986035/v2

Krabbendam, M., 2001. When the Wilson Cycle breaks down: how orogens can produce strong lithosphere and inhibit their future reworking. Geological Society, London, Special Publications 184, 57–75. https://doi.org/10.1144/GSL.SP.2001.184.01.04

Krabbendam, M., Barr, T.D., 2000. Proterozoic orogens and the break-up of Gondwana: why did some orogens not rift? Journal of African Earth Sciences 31, 35–49. https://doi.org/10.1016/S0899-5362(00)00071-3

Kronbichler, M., Heister, T., Bangerth, W., 2012. High accuracy mantle convection simulation through modern numerical methods. Geophysical Journal International 191, 12–29. https://doi.org/10.1111/j.1365-246X.2012.05609.x

Kula, J., Tulloch, A., Spell, T.L., Wells, M.L., 2007. Two-stage rifting of Zealandia-Australia-Antarctica: Evidence from 40Ar/39Ar thermochronometry of the Sisters shear zone, Stewart Island, New Zealand. Geology 35, 411–414. https://doi.org/10.1130/G23432A.1

Kusky, T., Li, J., Santosh, M., 2007. The Paleoproterozoic North Hebei Orogen: North China craton's collisional suture with the Columbia supercontinent. Gondwana Research, Tectonic evolution of China and adjacent crustal fragments 12, 4–28. https://doi.org/10.1016/j.gr.2006.11.012

Kusky, T.M., Li, J., 2003. Paleoproterozoic tectonic evolution of the North China Craton. Journal of Asian Earth Sciences 22, 383–397. https://doi.org/10.1016/S1367-9120(03)00071-3

Kusky, T.M., Polat, A., Windley, B.F., Burke, K.C., Dewey, J.F., Kidd, W.S.F., Maruyama, S., Wang, J.P., Deng, H., Wang, Z.S., Wang, C., Fu, D., Li, X.W., Peng, H.T., 2016. Insights into the tectonic evolution of the North China Craton through comparative tectonic analysis: A record of outward growth of Precambrian continents. Earth-Science Reviews 162, 387–432. https://doi.org/10.1016/j.earscirev.2016.09.002

Lambiase, J.J., Bosworth, W., 1995. Structural controls on sedimentation in continental rifts. Geological Society, London, Special Publications 80, 117–144. https://doi.org/10.1144/GSL.SP.1995.080.01.06

Laó-Dávila, D.A., Al-Salmi, H.S., Abdelsalam, M.G., Atekwana, E.A., 2015. Hierarchical segmentation of the Malawi Rift: The influence of inherited lithospheric heterogeneity and kinematics in the evolution of continental rifts. Tectonics 34, 2399–2417. https://doi.org/10.1002/2015TC003953

Larsen, P.-H., 1988. Relay structures in a Lower Permian basement-involved extension system, East Greenland. Journal of Structural Geology 10, 3–8. https://doi.org/10.1016/0191-8141(88)90122-8
Lawley, C.J.M., McCafferty, A.E., Graham, G.E., Huston, D.L., Kelley, K.D., Czarnota, K., Paradis, S., Peter, J.M., Hayward, N., Barlow, M., Emsbo, P., Coyan, J., San Juan, C.A., Gadd, M.G., 2022. Data–driven prospectivity modelling of sediment–hosted Zn–Pb mineral systems and their critical raw materials. Ore Geology Reviews 141, 104635. https://doi.org/10.1016/j.oregeorev.2021.104635
Leclère, H., Fabbri, O., 2013. A new three-dimensional method of fault reactivation analysis. Journal of Structural Geology 48, 153–161. https://doi.org/10.1016/j.jsg.2012.11.004
Lee, H., Muirhead, J.D., Fischer, T.P., Ebinger, C.J., Kattenhorn, S.A., Sharp, Z.D., Kianji, G., 2016. Massive and prolonged deep carbon emissions associated with continental rifting. Nature Geosci 9, 145–149. https://doi.org/10.1038/ngeo2622
Leeder, M.R., Jackson, J.A., 1993. The interaction between normal faulting and drainage in active extensional basins, with examples from the western United States and central Greece. Basin Research 5, 79–102. https://doi.org/10.1111/j.1365-2117.1993.tb00059.x
Lemoine, M., Bas, T., Arnaud-Vanneau, A., Arnaud, H., Dumont, T., Gidon, M., Bourbon, M., de Graciansky, P.-C., Rudkiewicz, J.-L., Megard-Galli, J., Tricart, P., 1986. The continental margin of the Mesozoic Tethys in the Western Alps. Marine and Petroleum Geology 3, 179–199. https://doi.org/10.1016/0264-8172(86)90044-9
Leonard, M., 2010. Earthquake Fault Scaling: Self-Consistent Relating of Rupture Length, Width, Average Displacement, and Moment Release. Bulletin of the Seismological Society of America 100, 1971–1988. https://doi.org/10.1785/0120090189
Lezzar, K.E., Tiercelin, J.-J., Le Turdu, C., Cohen, Andrew.S., Reynolds, D.J., Le Gall, B., Scholz, C.A., 2002. Control of Normal Fault Interaction on the Distribution of Major Neogene Sedimentary Depocenters, Lake Tanganyika, East African Rift. AAPG Bulletin 86, 1027–1059. https://doi.org/10.1306/61EEDC1A-173E-11D7-8645000102C1865D
Li, B., Atakan, K., Sørensen, M.B., Havskov, J., 2015. Stress pattern of the Shanxi rift system, North China, inferred from the inversion of new focal mechanisms. Geophysical Journal International 201, 505–527. https://doi.org/10.1093/gji/ggv025
Li, S., Zhao, G., Wilde, S.A., Zhang, J., Sun, M., Zhang, G., Dai, L., 2010. Deformation history of the Hengshan–Wutai–Fuping Complexes: Implications for the evolution of the Trans-North China Orogen. Gondwana Research 18, 611–631. https://doi.org/10.1016/j.gr.2010.03.003
Li, Y., Yang, J., Xia, Z., Mo, D., 1998. Tectonic geomorphology in the Shanxi Graben System, northern China. Geomorphology 23, 77–89. https://doi.org/10.1016/S0169-555X(97)00092-5
Lifton, N.A., Chase, C.G., 1992. Tectonic, climatic and lithologic influences on landscape fractal dimension and hypsometry: implications for landscape evolution in the San Gabriel Mountains, California. Geomorphology 5, 77–114. https://doi.org/10.1016/0169-555X(92)90059-W
Lin, F., Liu, M., 2019. Crustal extension in North China since the Mesozoic: A numerical study. Geodesy and Geodynamics 10, 363–371. https://doi.org/10.1016/j.geog.2018.09.005
Lin, F., Qi, L., Zhang, N., Guo, Z., 2024. An ongoing lithospheric dripping process beneath northeast China and its impact on intraplate volcanism. Geology 52, 435–440. https://doi.org/10.1130/G51861.1

Linckens, J., Herwegh, M., Müntener, O., 2015. Small quantity but large effect — How minor phases control strain localization in upper mantle shear zones. Tectonophysics 643, 26–43. https://doi.org/10.1016/j.tecto.2014.12.008

Liu, J., Zhang, P., Lease, R.O., Zheng, D., Wan, J., Wang, W., Zhang, H., 2013. Eocene onset and late Miocene acceleration of Cenozoic intracontinental extension in the North Qinling range–Weihe graben: Insights from apatite fission track thermochronology. Tectonophysics, Active Tectonic Deformation of the Tibetan Plateau and Great Earthquakes 584, 281–296. https://doi.org/10.1016/j.tecto.2012.01.025

Liu, S., Shen, Z.-K., Bürgmann, R., Jónsson, S., 2020. Thin crème brûlée rheological structure for the Eastern California Shear Zone. Geology 49, 216–221. https://doi.org/10.1130/G47729.1

Luo, Q., Li, Y., Schoenbohm, L., Rimando, J., Hu, X., Guo, A., Zhao, J., Li, X., Liu, Q., Jiang, S., Li, C., Sun, K., 2022. Direct Evidence for Dextral Shearing in the Shanxi Graben System: Geologic and Geomorphologic Constraints From the North Liulengshan Fault. Tectonics 41, e2022TC007490. https://doi.org/10.1029/2022TC007490

Luyendyk, B., Cisowski, S., Smith, C., Richard, S., Kimbrough, D., 1996. Paleomagnetic study of the northern Ford Ranges, western Marie Byrd Land, West Antarctica: Motion between West and East Antarctica. Tectonics 15, 122–141. https://doi.org/10.1029/95TC02524

Lyon, P.J., Boult, P.J., Hillis, R.R., Bierbrauer, K., 2007. Basement controls on fault development in the Penola Trough, Otway Basin, and implications for fault-bounded hydrocarbon traps. Australian Journal of Earth Sciences 54, 675–689. https://doi.org/10.1080/08120090701305228

Ma, J., Feng, X.J., Li, G.Y., Li, X.N., 2020. New insights from analysis of historical texts on the 1568 Northeast Xi'an earthquake, Shaanxi, China. International Journal of Disaster Risk Reduction 44, 101417. https://doi.org/10.1016/j.ijdrr.2019.101417

Maerten, L., 2000. Variation in slip on intersecting normal faults: Implications for paleostress inversion. Journal of Geophysical Research: Solid Earth 105, 25553–25565. https://doi.org/10.1029/2000JB900264

Makrari, S., Sharma, G., Taloor, A.K., Singh, M.S., Sarma, K.K., Aggarwal, S.P., 2022. Assessment of the geomorphic indices in relation to tectonics along selected sectors of Borpani River Basin, Assam using Cartosat DEM data. Geosystems and Geoenvironment 1, 100068. https://doi.org/10.1016/j.geogeo.2022.100068

Manatschal, G., 2004. New models for evolution of magma-poor rifted margins based on a review of data and concepts from West Iberia and the Alps. Int J Earth Sci (Geol Rundsch) 93, 432–466. https://doi.org/10.1007/s00531-004-0394-7

Manatschal, G., Lavier, L., Chenin, P., 2015. The role of inheritance in structuring hyperextended rift systems: Some considerations based on observations and numerical modeling. Gondwana Research 27, 140–164. https://doi.org/10.1016/j.gr.2014.08.006

Marín, M., Roca, E., Baqués, V., Cantarero, I., Cabrera, L., Ferrer, O., Travé, A., 2023. Fluid-rock interaction control on fault reactivation: A review of the Montmell-Vallès Fault System, central Catalan Coastal Ranges (NE Iberia). Global and Planetary Change 220, 104011. https://doi.org/10.1016/j.gloplacha.2022.104011

Masek, J.G., Isacks, B.L., Gubbels, T.L., Fielding, E.J., 1994. Erosion and tectonics at the margins of continental plateaus. Journal of Geophysical Research: Solid Earth 99, 13941–13956. https://doi.org/10.1029/94JB00461

Massironi, M., Bistacchi, A., Menegon, L., 2011. Misoriented faults in exhumed metamorphic complexes: Rule or exception? Earth and Planetary Science Letters 307, 233–239. https://doi.org/10.1016/j.epsl.2011.04.041

McCaffrey, K.J.W., 1997. Controls on reactivation of a major fault zone: the Fair Head–Clew Bay line in Ireland. Journal of the Geological Society 154, 129–133. https://doi.org/10.1144/gsjgs.154.1.0129
McKenzie, D., 1978. Some remarks on the development of sedimentary basins. Earth and Planetary Science Letters 40, 25–32. https://doi.org/10.1016/0012-821X(78)90071-7
McKenzie, D., Bickle, M.J., 1988. The Volume and Composition of Melt Generated by Extension of the Lithosphere. Journal of Petrology 29, 625–679. https://doi.org/10.1093/petrology/29.3.625
Meier, L., Eisbacher, G.H., 1991. Crustal kinematics and deep structure of the northern Rhine Graben, Germany. Tectonics 10, 621–630. https://doi.org/10.1029/91TC00142
Menzies, M., Xu, Y., Zhang, H., Fan, W., 2007. Integration of geology, geophysics and geochemistry: A key to understanding the North China Craton. Lithos, The Origin, Evolution and Present State of Continental Lithosphere 96, 1–21. https://doi.org/10.1016/j.lithos.2006.09.008
Menzies, M.A., Fan, W., Zhang, M., 1993. Palaeozoic and Cenozoic lithoprobes and the loss of >120 km of Archaean lithosphere, Sino-Korean craton, China. Geological Society, London, Special Publications 76, 71–81. https://doi.org/10.1144/GSL.SP.1993.076.01.04
Menzies, M.A., Xu, Y., 1998. Geodynamics of the North China Craton, in: Mantle Dynamics and Plate Interactions in East Asia. American Geophysical Union (AGU), pp. 155–165. https://doi.org/10.1029/GD027p0155
Meyer, B., Chulliat, A., Saltus, R., 2017. Derivation and Error Analysis of the Earth Magnetic Anomaly Grid at 2 arc min Resolution Version 3 (EMAG2v3). Geochemistry, Geophysics, Geosystems 18, 4522–4537. https://doi.org/10.1002/2017GC007280
Middleton, T.A., Elliott, J.R., Rhodes, E.J., Sherlock, S., Walker, R.T., Wang, W., Yu, J., Zhou, Y., 2017. Extension rates across the northern Shanxi Grabens, China, from Quaternary geology, seismicity and geodesy. Geophysical Journal International 209, 535–558.
Middleton, T.A., Parsons, B., Walker, R.T., 2018. Comparison of seismic and geodetic strain rates at the margins of the Ordos Plateau, northern China. Geophysical Journal International 212, 988–1009. https://doi.org/10.1093/gji/ggx446
Mohn, G., Manatschal, G., Beltrando, M., Haupert, I., 2014. The role of rift-inherited hyper-extension in Alpine-type orogens. Terra Nova 26, 347–353. https://doi.org/10.1111/ter.12104
Mohn, G., Manatschal, G., Beltrando, M., Masini, E., Kusznir, N., 2012. Necking of continental crust in magma-poor rifted margins: Evidence from the fossil Alpine Tethys margins. Tectonics 31. https://doi.org/10.1029/2011TC002961
Molnar, N., Cruden, A., Betts, P., 2020. The role of inherited crustal and lithospheric architecture during the evolution of the Red Sea: Insights from three dimensional analogue experiments. Earth and Planetary Science Letters 544, 116377. https://doi.org/10.1016/j.epsl.2020.116377
Molnar, P., England, P.C., Jones, C.H., 2015. Mantle dynamics, isostasy, and the support of high terrain. Journal of Geophysical Research: Solid Earth 120, 1932–1957. https://doi.org/10.1002/2014JB011724
Molnar, P., Tapponnier, P., 1975. Cenozoic Tectonics of Asia: Effects of a Continental Collision. Science 189, 419–426. https://doi.org/10.1126/science.189.4201.419
Moore, J.M., Davidson, A., 1978. Rift structure in southern Ethiopia. Tectonophysics 46, 159–173. https://doi.org/10.1016/0040-1951(78)90111-7
Morgan, W.J., 1972. Deep Mantle Convection Plumes and Plate Motions. AAPG Bulletin 56, 203–213.

Morley, C.K., 2010. Stress re-orientation along zones of weak fabrics in rifts: An explanation for pure extension in 'oblique' rift segments? Earth and Planetary Science Letters 297, 667–673. https://doi.org/10.1016/j.epsl.2010.07.022
Morley, C.K., 1988. Variable extension in Lake Tanganyika. Tectonics 7, 785–801. https://doi.org/10.1029/TC007i004p00785
Morley, C.K., Haranya, C., Phoosongsee, W., Pongwapee, S., Kornsawan, A., Wonganan, N., 2004. Activation of rift oblique and rift parallel pre-existing fabrics during extension and their effect on deformation style: examples from the rifts of Thailand. Journal of Structural Geology 26, 1803–1829. https://doi.org/10.1016/j.jsg.2004.02.014
Morley, C.K., Maczak, A., Rungprom, T., Ghosh, J., Cartwright, J.A., Bertoni, C., Panpichityota, N., 2017. New style of honeycomb structures revealed on 3D seismic data indicate widespread diagenesis offshore Great South Basin, New Zealand. Marine and Petroleum Geology 86, 140–154. https://doi.org/10.1016/j.marpetgeo.2017.05.035
Morley, C.K., Nelson, R.A., Patton, T.L., Munn, S.G., 1990. Transfer Zones in the East African Rift System and Their Relevance to Hydrocarbon Exploration in Rifts1. AAPG Bulletin 74, 1234–1253. https://doi.org/10.1306/0C9B2475-1710-11D7-8645000102C1865D
Mortimer, N., 2004. New Zealand's Geological Foundations. Gondwana Research 7, 261–272. https://doi.org/10.1016/S1342-937X(05)70324-5
Mortimer, N., Campbell, H.J., Tulloch, A.J., King, P.R., Stagpoole, V.M., Wood, R.A., Rattenbury, M.S., Sutherland, R., Adams, C.J., Collot, J., Seton, M., 2017. Zealandia: Earth's Hidden Continent. GSAT 27–35. https://doi.org/10.1130/GSATG321A.1
Mortimer, N., Davey, F.J., Melhuish, A., Yu, J., Godfrey, N.J., 2002. Geological interpretation of a deep seismic reflection profile across the Eastern Province and Median Batholith, New Zealand: Crustal architecture of an extended Phanerozoic convergent orogen. New Zealand Journal of Geology and Geophysics 45, 349–363. https://doi.org/10.1080/00288306.2002.9514978
Mortimer, N., Rattenbury, M., King, P., Bland, K., Barrell, D., Bache, F., Begg, J., Campbell, H., Cox, S., Crampton, J., Edbrooke, S., Forsyth, P., Johnston, M., Jongens, R., Lee, J., Leonard, G., Raine, J., Skinner, D., Timm, C., Townsend, D., Tulloch, A., Turnbull, I., Turnbull, R., 2014. High-level stratigraphic scheme for New Zealand rocks. New Zealand Journal of Geology and Geophysics 57, 402–419. https://doi.org/10.1080/00288306.2014.946062
Muir, R.A., Whitehead, B.A., New, T., Stevens, V., Macey, P.H., Groenewald, C.A., Salomon, G., Kahle, B., Hollingsworth, J., Sloan, R.A., 2023. Exceptional Scarp Preservation in SW Namibia Reveals Geological Controls on Large Magnitude Intraplate Seismicity in Southern Africa. Tectonics 42, e2022TC007693. https://doi.org/10.1029/2022TC007693
Muir, R.J., Bradshaw, J.D., Weaver, S.D., Laird, M.G., 2000. The influence of basement structure on the evolution of the Taranaki Basin, New Zealand. Journal of the Geological Society 157, 1179–1185. https://doi.org/10.1144/jgs.157.6.1179
Muirhead, J.D., Fischer, T.P., Oliva, S.J., Laizer, A., van Wijk, J., Currie, C.A., Lee, H., Judd, E.J., Kazimoto, E., Sano, Y., Takahata, N., Tiberi, C., Foley, S.F., Dufek, J., Reiss, M.C., Ebinger, C.J., 2020. Displaced cratonic mantle concentrates deep carbon during continental rifting. Nature 582, 67–72. https://doi.org/10.1038/s41586-020-2328-3
Muirhead, J.D., Kattenhorn, S.A., 2018. Activation of preexisting transverse structures in an evolving magmatic rift in East Africa. Journal of Structural Geology 106, 1–18. https://doi.org/10.1016/j.jsg.2017.11.004
Mulaya, E., Gluyas, J., McCaffrey, K., Phillips, T., Ballentine, C., 2022. Structural geometry and evolution of the Rukwa Rift Basin, Tanzania: Implications for helium potential. Basin Research 34, 938–960. https://doi.org/10.1111/bre.12646

Muñoz-Barrera, J.M., Rotevatn, A., Gawthorpe, R.L., Henstra, G.A., Kristensen, T.B., 2020. The role of structural inheritance in the development of high-displacement crustal faults in the necking domain of rifted margins: The Klakk Fault Complex, Frøya High, offshore mid-Norway. Journal of Structural Geology 140, 104163. https://doi.org/10.1016/j.jsg.2020.104163

Musila, M., Ebinger, C.J., Bastow, I.D., Sullivan, G., Oliva, S.J., Knappe, E., Perry, M., Kounoudis, R., Ogden, C.S., Bendick, R., Mwangi, S., Mariita, N., Kianji, G., Kraus, E., Illsley-Kemp, F., 2023. Active Deformation Constraints on the Nubia-Somalia Plate Boundary Through Heterogenous Lithosphere of the Turkana Depression. Geochemistry, Geophysics, Geosystems 24, e2023GC010982. https://doi.org/10.1029/2023GC010982

Naliboff, J., Buiter, S.J.H., 2015. Rift reactivation and migration during multiphase extension. Earth and Planetary Science Letters 421, 58–67. https://doi.org/10.1016/j.epsl.2015.03.050

Nelson, R.A., Patton, T.L., Morley, C.K., 1992a. Rift-Segment Interaction and Its Relation to Hydrocarbon Exploration in Continental Rift Systems1. AAPG Bulletin 76, 1153–1169. https://doi.org/10.1306/BDFF898E-1718-11D7-8645000102C1865D

Nelson, R.A., Patton, T.L., Morley, C.K., 1992b. Rift-Segment Interaction and Its Relation to Hydrocarbon Exploration in Continental Rift Systems (1). AAPG Bulletin 76, 1153–1169.

Neuharth, D., Brune, S., Wrona, T., Glerum, A., Braun, J., Yuan, X., 2022. Evolution of Rift Systems and Their Fault Networks in Response to Surface Processes. Tectonics 41, e2021TC007166. https://doi.org/10.1029/2021TC007166

Nixon, C.W., McNeill, L.C., Bull, J.M., Bell, R.E., Gawthorpe, R.L., Henstock, T.J., Christodoulou, D., Ford, M., Taylor, B., Sakellariou, D., Ferentinos, G., Papatheodorou, G., Leeder, M.R., Collier, R.E.LI., Goodliffe, A.M., Sachpazi, M., Kranis, H., 2016. Rapid spatiotemporal variations in rift structure during development of the Corinth Rift, central Greece. Tectonics 35, 1225–1248. https://doi.org/10.1002/2015TC004026

Noda, A., Takeuchi, M., Adachi, M., 2004. Provenance of the Murihiku Terrane, New Zealand: evidence from the Jurassic conglomerates and sandstones in Southland. Sedimentary Geology 164, 203–222. https://doi.org/10.1016/j.sedgeo.2003.10.003

Northrup, C.J., Royden, L.H., Burchfiel, B.C., 1995. Motion of the Pacific plate relative to Eurasia and its potential relation to Cenozoic extension along the eastern margin of Eurasia. Geology 23, 719–722. https://doi.org/10.1130/0091-7613(1995)023<0719:MOTPPR>2.3.CO;2

Obaid, A.K., Allen, M.B., 2019. Landscape expressions of tectonics in the Zagros fold-and-thrust belt. Tectonophysics 766, 20–30. https://doi.org/10.1016/j.tecto.2019.05.024

Osagiede, E.E., Rotevatn, A., Gawthorpe, R., Kristensen, T.B., Jackson, C.A.-L., Marsh, N., 2020. Pre-existing intra-basement shear zones influence growth and geometry of non-colinear normal faults, western Utsira High–Heimdal Terrace, North Sea. Journal of Structural Geology 130, 103908. https://doi.org/10.1016/j.jsg.2019.103908

Pascal, C., Cloetingh, S. a. P.L., 2002. Rifting in heterogeneous lithosphere: Inferences from numerical modeling of the northern North Sea and the Oslo Graben. Tectonics 21, 10-1-10–15. https://doi.org/10.1029/2001TC901044

Pavlides, S.B., Zouros, N.C., Zhongjing, F., Shaoping, C., Tranos, M.D., Chatzipetros, A.A., 1999. Geometry, kinematics and morphotectonics of the Yanqing–Huailai active faults (northern China). Tectonophysics 308, 99–118. https://doi.org/10.1016/S0040-1951(99)00074-8

Peace, A., McCaffrey, K., Imber, J., Hunen, J. van, Hobbs, R., Wilson, R., 2018. The role of pre-existing structures during rifting, continental breakup and transform system

development, offshore West Greenland. Basin Research 30, 373–394. https://doi.org/10.1111/bre.12257
Peacock, D.C.P., Sanderson, D.J., 1991. Displacements, segment linkage and relay ramps in normal fault zones. Journal of Structural Geology 13, 721–733. https://doi.org/10.1016/0191-8141(91)90033-F
Peltzer, G., Tapponnier, P., Zhitao, Z., Qin, X.Z., 1985. Neogene and Quaternary faulting in and along the Qinling Shan. Nature 317, 500–505. https://doi.org/10.1038/317500a0
Pérez-Peña, J.V., Azañón, J.M., Booth-Rea, G., Azor, A., Delgado, J., 2009. Differentiating geology and tectonics using a spatial autocorrelation technique for the hypsometric integral. Journal of Geophysical Research: Earth Surface 114. https://doi.org/10.1029/2008JF001092
Peron-Pinvidic, G., Manatschal, G., Osmundsen, P.T., 2013. Structural comparison of archetypal Atlantic rifted margins: A review of observations and concepts. Marine and Petroleum Geology 43, 21–47. https://doi.org/10.1016/j.marpetgeo.2013.02.002
Perron, J.T., Royden, L., 2013. An integral approach to bedrock river profile analysis. Earth Surface Processes and Landforms 38, 570–576. https://doi.org/10.1002/esp.3302
Petit, C., Déverchère, J., 2006. Structure and evolution of the Baikal rift: A synthesis. Geochemistry, Geophysics, Geosystems 7. https://doi.org/10.1029/2006GC001265
Petit, C., Deverchere, J., Houdry, F., Sankov, V.A., Melnikova, V.I., Delvaux, D., 1996. Present-day stress field changes along the Baikal rift and tectonic implications. Tectonics 15, 1171–1191.
Philippon, M., Willingshofer, E., Sokoutis, D., Corti, G., Sani, F., Bonini, M., Cloetingh, S., 2015. Slip re-orientation in oblique rifts. Geology 43, 147–150.
Phillips, T.B., Fazlikhani, H., Gawthorpe, R.L., Fossen, H., Jackson, C.A.-L., Bell, R.E., Faleide, J.I., Rotevatn, A., 2019. The Influence of Structural Inheritance and Multiphase Extension on Rift Development, the NorthernNorth Sea. Tectonics 38, 4099–4126. https://doi.org/10.1029/2019TC005756
Phillips, T.B., Jackson, C.A., Bell, R.E., Duffy, O.B., Fossen, H., 2016. Reactivation of intrabasement structures during rifting: A case study from offshore southern Norway. Journal of Structural Geology 91, 54–73.
Phillips, T.B., Magee, C., 2020. Structural controls on the location, geometry and longevity of an intraplate volcanic system: the Tuatara Volcanic Field, Great South Basin, New Zealand. Journal of the Geological Society 177, 1039–1056. https://doi.org/10.1144/jgs2020-050
Phillips, T.B., McCaffrey, K., 2023. Rifting a crustal mosaic – The influence of basement rheology and lithology on rift physiography in the Great South Basin, New Zealand.
Phillips, T.B., McCaffrey, K., Magarinos, L., 2022. Influence of variable decoupling between vertically separated fault populations on structural inheritance – The Laminaria High, NW Shelf of Australia. Basin Research 34, 440–456. https://doi.org/10.1111/bre.12626
Phillips, T.B., McCaffrey, K.J.W., 2019. Terrane Boundary Reactivation, Barriers to Lateral Fault Propagation and Reactivated Fabrics: Rifting Across the Median Batholith Zone, Great South Basin, New Zealand. Tectonics 38, 4027–4053. https://doi.org/10.1029/2019TC005772
Phillips, T.B., Naliboff, J.B., McCaffrey, K.J.W., Pan, S., van Hunen, J., Froemchen, M., 2023. The influence of crustal strength on rift geometry and development – insights from 3D numerical modelling. Solid Earth 14, 369–388. https://doi.org/10.5194/se-14-369-2023
Priestley, K., McKenzie, D., Ho, T., 2018. A Lithosphere–Asthenosphere Boundary—a Global Model Derived from Multimode Surface-Wave Tomography and Petrology, in:

Lithospheric Discontinuities. American Geophysical Union (AGU), pp. 111–123. https://doi.org/10.1002/9781119249740.ch6
Qi, J., Yang, Q., 2010. Cenozoic structural deformation and dynamic processes of the Bohai Bay basin province, China. Marine and Petroleum Geology 27, 757–771. https://doi.org/10.1016/j.marpetgeo.2009.08.012
Qiao, X., Li, G., Li, M., Zhou, J., Du, J., Du, C., Sun, Z., 2011. Influence of coal mining on regional karst groundwater system: a case study in West Mountain area of Taiyuan City, northern China. Environ Earth Sci 64, 1525–1535. https://doi.org/10.1007/s12665-010-0586-3
Rajaonarison, T.A., Stamps, D.S., Naliboff, J., 2021. Role of Lithospheric Buoyancy Forces in Driving Deformation in East Africa From 3D Geodynamic Modeling. Geophysical Research Letters 48, e2020GL090483. https://doi.org/10.1029/2020GL090483
Ramos, G.V., Vasconcelos, D.L., Marques, F.O., de Castro, D.L., Nogueira, F.C.C., Bezerra, F.H.R., Perez, Y.A.R., Souza, J.A.B., Medeiros, V.C., 2022. Relations between inherited basement fabric and fault nucleation in a continental setting: The Rio do Peixe Basin, NE Brazil. Marine and Petroleum Geology 139, 105635. https://doi.org/10.1016/j.marpetgeo.2022.105635
Ranalli, G., 1995. Rheology of the Earth. Springer Science & Business Media.
Ranalli, G., Yin, Z.-M., 1990. Critical stress difference and orientation of faults in rocks with strength anisotropies: the two-dimensional case. Journal of Structural Geology 12, 1067–1071. https://doi.org/10.1016/0191-8141(90)90102-5
Reeve, M.T., Bell, R.E., Duffy, O.B., Jackson, C.A.-L., Sansom, E., 2015. The growth of non-colinear normal fault systems; What can we learn from 3D seismic reflection data? Journal of Structural Geology 70, 141–155.
Regional Geology of Linfen (1:250000), n.d.
Ren, J., Tamaki, K., Li, S., Junxia, Z., 2002. Late Mesozoic and Cenozoic rifting and its dynamic setting in Eastern China and adjacent areas. Tectonophysics 344, 175–205. https://doi.org/10.1016/S0040-1951(01)00271-2
Richter, F., McKenzie, D., 1977. Simple plate models of mantle convection. J Geophys 44, 441–471.
Rimando, J.M., Peace, A.L., 2021. Reactivation Potential of Intraplate Faults in the Western Quebec Seismic Zone, Eastern Canada. Earth and Space Science 8, e2021EA001825. https://doi.org/10.1029/2021EA001825
Ring, U., 1994. The influence of preexisting structure on the evolution of the Cenozoic Malawi rift (East African rift system). Tectonics 13, 313–326. https://doi.org/10.1029/93TC03188
Roberts, G.G., Wani, O., 2024. A theory of stochastic fluvial landscape evolution. Proceedings of the Royal Society A: Mathematical, Physical and Engineering Sciences 480, 20230456. https://doi.org/10.1098/rspa.2023.0456
Robertson, A.H.F., Palamakumbura, R., Campbell, H.J., 2019. Chapter 13 Permian–Triassic felsic tuffs in South Island, New Zealand: significance for oceanic and active continental margin subduction. Geological Society, London, Memoirs 49, 293–321. https://doi.org/10.1144/M49.15
Rose, I., Buffett, B., Heister, T., 2017. Stability and accuracy of free surface time integration in viscous flows. Physics of the Earth and Planetary Interiors 262, 90–100. https://doi.org/10.1016/j.pepi.2016.11.007
Rosendahl, B.R., 1987. Architecture of Continental Rifts with Special Reference to East Africa. Annual Review of Earth and Planetary Sciences 15, 445–503. https://doi.org/10.1146/annurev.ea.15.050187.002305

Roser, B.P., Coombs, D.S., 2005. Geochemistry of the Willsher Group, southeast Otago, New Zealand, and comparison with the Murihiku and Dun Mountain-Maitai Terranes. New Zealand Journal of Geology and Geophysics 48, 415–434. https://doi.org/10.1080/00288306.2005.9515123
Rotevatn, A., Jackson, C.A.-L., Tvedt, A.B., Bell, R.E., Blækkan, I., 2019. How do normal faults grow? Journal of Structural Geology 125, 174–184.
Rotevatn, A., Kristensen, T.B., Ksienzyk, A.K., Wemmer, K., Henstra, G.A., Midtkandal, I., Grundvåg, S.-A., Andresen, A., 2018. Structural Inheritance and Rapid Rift-Length Establishment in a Multiphase Rift: The East Greenland Rift System and its Caledonian Orogenic Ancestry. Tectonics 37, 1858–1875. https://doi.org/10.1029/2018TC005018
Rowland, J.V., Sibson, R.H., 2004. Structural controls on hydrothermal flow in a segmented rift system, Taupo Volcanic Zone, New Zealand. Geofluids 4, 259–283. https://doi.org/10.1111/j.1468-8123.2004.00091.x
Rowland, J.V., Simmons, S.F., 2012. Hydrologic, Magmatic, and Tectonic Controls on Hydrothermal Flow, Taupo Volcanic Zone, New Zealand: Implications for the Formation of Epithermal Vein Deposits. Economic Geology 107, 427–457. https://doi.org/10.2113/econgeo.107.3.427
Rutter, E.H., Brodie, K.H., 2004. Experimental grain size-sensitive flow of hot-pressed Brazilian quartz aggregates. Journal of Structural Geology 26, 2011–2023. https://doi.org/10.1016/j.jsg.2004.04.006
Rybacki, E., Gottschalk, M., Wirth, R., Dresen, G., 2006. Influence of water fugacity and activation volume on the flow properties of fine-grained anorthite aggregates. Journal of Geophysical Research: Solid Earth 111. https://doi.org/10.1029/2005JB003663
Sachau, T., Koehn, D., Stamps, D.S., Lindenfeld, M., 2016. Fault kinematics and stress fields in the Rwenzori Mountains, Uganda. Int J Earth Sci (Geol Rundsch) 105, 1729–1740. https://doi.org/10.1007/s00531-015-1162-6
Sahoo, T., King, P., Bland, K., Strogen, D., Sykes, R., Bache, F., 2014. Tectono-sedimentary evolution and source rock distribution of the mid to Late Cretaceous succession in the Great South Basin, New Zealand. The APPEA Journal 54, 259–274. https://doi.org/10.1071/AJ13026
Sahoo, T.R., Nicol, A., Browne, G.H., Strogen, D.P., 2020. Evolution of a Normal Fault System Along Eastern Gondwana, New Zealand. Tectonics 39, e2020TC006181. https://doi.org/10.1029/2020TC006181
Samsu, A., Cruden, A.R., Hall, M., Micklethwaite, S., Denyszyn, S.W., 2019. The influence of basement faults on local extension directions: Insights from potential field geophysics and field observations. Basin Research 31, 782–807. https://doi.org/10.1111/bre.12344
Samsu, A., Cruden, A.R., Micklethwaite, S., Grose, L., Vollgger, S.A., 2020. Scale matters: The influence of structural inheritance on fracture patterns. Journal of Structural Geology 130, 103896. https://doi.org/10.1016/j.jsg.2019.103896
Samsu, A., Cruden, A.R., Molnar, N.E., Weinberg, R.F., 2021. Inheritance of penetrative basement anisotropies by extension-oblique faults: Insights from analogue experiments. Tectonics 40, e2020TC006596.
Samsu, A., Micklethwaite, S., Williams, J.N., Fagereng, Å., Cruden, A.R., 2023. Structural inheritance in amagmatic rift basins: Manifestations and mechanisms for how pre-existing structures influence rift-related faults. Earth-Science Reviews 246, 104568. https://doi.org/10.1016/j.earscirev.2023.104568

Santosh, M., 2010. Assembling North China Craton within the Columbia supercontinent: The role of double-sided subduction. Precambrian Research 178, 149–167. https://doi.org/10.1016/j.precamres.2010.02.003
Schellart, W.P., Chen, Z., Strak, V., Duarte, J.C., Rosas, F.M., 2019. Pacific subduction control on Asian continental deformation including Tibetan extension and eastward extrusion tectonics. Nat Commun 10, 4480. https://doi.org/10.1038/s41467-019-12337-9
Schellart, W.P., Lister, G.S., 2005. The role of the East Asian active margin in widespread extensional and strike-slip deformation in East Asia. Journal of the Geological Society 162, 959–972. https://doi.org/10.1144/0016-764904-112
Schiffer, C., Doré, A.G., Foulger, G.R., Franke, D., Geoffroy, L., Gernigon, L., Holdsworth, B., Kusznir, N., Lundin, E., McCaffrey, K., Peace, A.L., Petersen, K.D., Phillips, T.B., Stephenson, R., Stoker, M.S., Welford, J.K., 2020. Structural inheritance in the North Atlantic. Earth-Science Reviews, A new paradigm for the North Atlantic Realm 206, 102975. https://doi.org/10.1016/j.earscirev.2019.102975
Schiffer, C., Stephenson, R.A., Petersen, K.D., Nielsen, S.B., Jacobsen, B.H., Balling, N., Macdonald, D.I.M., 2015. A sub-crustal piercing point for North Atlantic reconstructions and tectonic implications. Geology 43, 1087–1090. https://doi.org/10.1130/G37245.1
Schlische, R.W., Withjack, M.O., 2009. Origin of fault domains and fault-domain boundaries (transfer zones and accommodation zones) in extensional provinces: Result of random nucleation and self-organized fault growth. Journal of Structural Geology, Nickelsen–Groshong volume: Low-temperature deformation mechanisms and their interpretation 31, 910–925. https://doi.org/10.1016/j.jsg.2008.09.005
Schmidt, K.M., Montgomery, D.R., 1995. Limits to Relief. Science 270, 617–620. https://doi.org/10.1126/science.270.5236.617
Scholz, C.A., 1995. Deltas of the Lake Malawi Rift, East Africa: Seismic Expression and Exploration Implications 1. AAPG Bulletin 79, 1679–1697. https://doi.org/10.1306/7834DE54-1721-11D7-8645000102C1865D
Scholz, C.H., 2019. The Mechanics of Earthquakes and Faulting. Cambridge University Press.
Scholz, C.H., 1982. Scaling laws for large earthquakes: Consequences for physical models. Bulletin of the Seismological Society of America 72, 1–14. https://doi.org/10.1785/BSSA0720010001
Schrenk, F., Bromage, T.G., Betzler, C.G., Ring, U., Juwayeyi, Y.M., 1993. Oldest Homo and Pliocene biogeography of the Malawi Rift. Nature 365, 833–836. https://doi.org/10.1038/365833a0
Schumacher, M.E., 2002. Upper Rhine Graben: Role of preexisting structures during rift evolution. Tectonics 21, 6-1-6–17. https://doi.org/10.1029/2001TC900022
Schwanghart, W., Scherler, D., 2014. Short Communication: TopoToolbox 2 – MATLAB-based software for topographic analysis and modeling in Earth surface sciences. Earth Surface Dynamics 2, 1–7. https://doi.org/10.5194/esurf-2-1-2014
Sengör, A.M.C., Burke, K., 1978. Relative timing of rifting and volcanism on Earth and its tectonic implications. Geophysical Research Letters 5, 419–421. https://doi.org/10.1029/GL005i006p00419
Şengör, A.M.C., Lom, N., Sağdıç, N.G., 2019. Tectonic inheritance, structure reactivation and lithospheric strength: the relevance of geological history. Geological Society, London, Special Publications 470, 105–136. https://doi.org/10.1144/SP470.8
Seward, T.M., Kerrick, D.M., 1996. Hydrothermal CO2 emission from the Taupo Volcanic Zone, New Zealand. Earth and Planetary Science Letters 139, 105–113. https://doi.org/10.1016/0012-821X(96)00011-8

Shanxi Bureau of Geology and Mineral Resources (SBGMR), 1989. Regional Geology of Shanxi Province.
Shen, Z.-K., Zhao, C., Yin, A., Li, Y., Jackson, D.D., Fang, P., Dong, D., 2000. Contemporary crustal deformation in east Asia constrained by Global Positioning System measurements. Journal of Geophysical Research: Solid Earth 105, 5721–5734. https://doi.org/10.1029/1999JB900391
Shi, W., Cen, M., Chen, L., Wang, Y., Chen, X., Li, J., Chen, P., 2015a. Evolution of the late Cenozoic tectonic stress regime in the Shanxi Rift, central North China Plate inferred from new fault kinematic analysis. Journal of Asian Earth Sciences, Active Tectonics and Meso-Cenozoic Intraplate Deformation in North China Block 114, 54–72. https://doi.org/10.1016/j.jseaes.2015.04.044
Shi, W., Dong, S., Hu, J., 2020. Neotectonics around the Ordos Block, North China: A review and new insights. Earth-Science Reviews 200, 102969.
Shi, W., Dong, S., Liu, Y., Hu, J., Chen, X., Chen, P., 2015b. Cenozoic tectonic evolution of the South Ningxia region, northeastern Tibetan Plateau inferred from new structural investigations and fault kinematic analyses. Tectonophysics 649, 139–164. https://doi.org/10.1016/j.tecto.2015.02.024
Shi, Y.-N., Niu, F., Li, Z.-H., Huangfu, P., 2020. Craton destruction links to the interaction between subduction and mid-lithospheric discontinuity: Implications for the eastern North China Craton. Gondwana Research 83, 49–62. https://doi.org/10.1016/j.gr.2020.01.016
Skogseid, J., Planke, S., Faleide, J.I., Pedersen, T., Eldholm, O., Neverdal, F., 2000. NE Atlantic continental rifting and volcanic margin formation. Geological Society, London, Special Publications 167, 295–326. https://doi.org/10.1144/GSL.SP.2000.167.01.12
Smith, M., Mosley, P., 1993. Crustal heterogeneity and basement influence on the development of the Kenya Rift, East Africa. Tectonics 12, 591–606. https://doi.org/10.1029/92TC01710
Snyder, N.P., Whipple, K.X., Tucker, G.E., Merritts, D.J., 2000. Landscape response to tectonic forcing: Digital elevation model analysis of stream profiles in the Mendocino triple junction region, northern California. Geological Society of America Bulletin 112, 1250–1263.
Steer, D.N., Knapp, J.H., Brown, L.D., 1998. Super-deep reflection profiling: exploring the continental mantle lid. Tectonophysics 286, 111–121. https://doi.org/10.1016/S0040-1951(97)00258-8
Stewart, I.S., Piccardi, L., 2017. Seismic faults and sacred sanctuaries in Aegean antiquity. Proceedings of the Geologists' Association 128, 711–721. https://doi.org/10.1016/j.pgeola.2017.07.009
Storchak, D.A., Di Giacomo, D., Bondar, I., Engdahl, E.R., Harris, J., Lee, W.H.K., Villasenor, A., Bormann, P., 2013. Public Release of the ISC-GEM Global Instrumental Earthquake Catalogue (1900-2009). Seismological Research Letters 84, 810–815. https://doi.org/10.1785/0220130034
Storchak, D.A., Di Giacomo, D., Engdahl, E.R., Harris, J., Bondár, I., Lee, W.H., Bormann, P., Villaseñor, A., 2015. The ISC-GEM global instrumental earthquake catalogue (1900–2009): introduction. Physics of the Earth and Planetary Interiors 239, 48–63.
Strahler, A.N., 1957. Quantitative analysis of watershed geomorphology. Eos, Transactions American Geophysical Union 38, 913–920. https://doi.org/10.1029/TR038i006p00913
Strahler, A.N., 1952. Hypsometirc (area-altitude) Analysis of erosional topography. GSA Bulletin 63, 1117–1142. https://doi.org/10.1130/0016-7606(1952)63[1117:HAAOET]2.0.CO;2

Strogen, D.P., Seebeck, H., Nicol, A., King, P.R., 2017. Two-phase Cretaceous–Paleocene rifting in the Taranaki Basin region, New Zealand; implications for Gondwana break-up. Journal of the Geological Society 174, 929–946. https://doi.org/10.1144/jgs2016-160

Su, P., He, H., Liu, Y., Shi, F., Granger, D.E., Kirby, E., Luo, L., Han, F., Lu, R., 2023. Quantifying the Structure and Extension Rate of the Linfen Basin, Shanxi Rift System Since the Latest Miocene: Implications for Continental Magma-Poor Rifting. Tectonics 42, e2023TC007885. https://doi.org/10.1029/2023TC007885

Su, P., He, H., Tan, X., Liu, Y., Shi, F., Kirby, E., 2021. Initiation and evolution of the Shanxi Rift System in North China: Evidence from low-temperature thermochronology in a plate reconstruction framework. Tectonics 40, e2020TC006298.

Sun, P., Guo, P., Niu, Y., 2021. Eastern China continental lithosphere thinning is a consequence of paleo-Pacific plate subduction: A review and new perspectives. Earth-Science Reviews 218, 103680. https://doi.org/10.1016/j.earscirev.2021.103680

Sutherland, R., 1999. Basement geology and tectonic development of the greater New Zealand region: an interpretation from regional magnetic data. Tectonophysics 308, 341–362. https://doi.org/10.1016/S0040-1951(99)00108-0

Sutherland, R., Collot, J., Lafoy, Y., Logan, G.A., Hackney, R., Stagpoole, V., Uruski, C., Hashimoto, T., Higgins, K., Herzer, R.H., Wood, R., Mortimer, N., Rollet, N., 2010. Lithosphere delamination with foundering of lower crust and mantle caused permanent subsidence of New Caledonia Trough and transient uplift of Lord Howe Rise during Eocene and Oligocene initiation of Tonga-Kermadec subduction, western Pacific. Tectonics 29. https://doi.org/10.1029/2009TC002476

Sutherland, R., Davey, F., Beavan, J., 2000. Plate boundary deformation in South Island, New Zealand, is related to inherited lithospheric structure. Earth and Planetary Science Letters 177, 141–151. https://doi.org/10.1016/S0012-821X(00)00043-1

Tamas, A., Holdsworth, R.E., Underhill, J.R., Tamas, D.M., Dempsey, E.D., Hardman, K., Bird, A., McCarthy, D., McCaffrey, K.J.W., Selby, D., 2022. New onshore insights into the role of structural inheritance during Mesozoic opening of the Inner Moray Firth Basin, Scotland. Journal of the Geological Society 179, jgs2021-066. https://doi.org/10.1144/jgs2021-066

Tang Y.-C., Fen Y.-G., Chen Zhongshun J., Zhou S.-Y., Ning J.-Y., Wei S.-Q., Li P., Chun-Quan Y., Fan W.-Y., Wang H.-Y., 2010. Receiver function analysis at Shanxi Rift. Chinese Journal of Geophysics 53, 2102–2109. https://doi.org/10.3969/j.issn.0001-5733.2010.09.010

Tapponnier, P., Molnar, P., 1977. Active faulting and tectonics in China. Journal of Geophysical Research (1896-1977) 82, 2905–2930. https://doi.org/10.1029/JB082i020p02905

Tapponnier, P., Peltzer, G., Le Dain, A.Y., Armijo, R., Cobbold, P., 1982. Propagating extrusion tectonics in Asia: New insights from simple experiments with plasticine. Geology 10, 611–616. https://doi.org/10.1130/0091-7613(1982)10<611:PETIAN>2.0.CO;2

Tarling, M.S., Smith, S.A.F., Scott, J.M., Rooney, J.S., Viti, C., Gordon, K.C., 2019. The internal structure and composition of a plate-boundary-scale serpentinite shear zone: the Livingstone Fault, New Zealand. Solid Earth 10, 1025–1047. https://doi.org/10.5194/se-10-1025-2019

Tatsumi, Y., Otofuji, Y.-I., Matsuda, T., Nohda, S., 1989. Opening of the Sea of Japan back-arc basin by asthenospheric injection. Tectonophysics 166, 317–329. https://doi.org/10.1016/0040-1951(89)90283-7

Taylor, B., Goodliffe, A.M., Martinez, F., 1999. How continents break up: Insights from Papua New Guinea. Journal of Geophysical Research: Solid Earth 104, 7497–7512. https://doi.org/10.1029/1998JB900115

Taylor, S.K., Bull, J.M., Lamarche, G., Barnes, P.M., 2004. Normal fault growth and linkage in the Whakatane Graben, New Zealand, during the last 1.3 Myr. Journal of Geophysical Research: Solid Earth 109. https://doi.org/10.1029/2003JB002412

Tepp, G., Ebinger, C.J., Zal, H., Gallacher, R., Accardo, N., Shillington, D.J., Gaherty, J., Keir, D., Nyblade, A.A., Mbogoni, G.J., Chindandali, P.R.N., Ferdinand-Wambura, R., Mulibo, G.D., Kamihanda, G., 2018. Seismic Anisotropy of the Upper Mantle Below the Western Rift, East Africa. Journal of Geophysical Research: Solid Earth 123, 5644–5660. https://doi.org/10.1029/2017JB015409

Tett, D., Sawyer, D., 1996. Dynamic models of multiphase continental rifting and their implications for the Newfoundland and Iberia conjugate margins 149. https://doi.org/10.2973/odp.proc.sr.149.247.1996

Thatcher, W., 1995. Microplate versus continuum descriptions of active tectonic deformation. Journal of Geophysical Research: Solid Earth 100, 3885–3894. https://doi.org/10.1029/94JB03064

Theunissen, K., Klerkx, J., Melnikov, A., Mruma, A., 1996. Mechanisms of inheritance of rift faulting in the western branch of the East African Rift, Tanzania. Tectonics 15, 776–790. https://doi.org/10.1029/95TC03685

Tommasi, A., Vauchez, A., 2001. Continental rifting parallel to ancient collisional belts: an effect of the mechanical anisotropy of the lithospheric mantle. Earth and Planetary Science Letters 185, 199–210. https://doi.org/10.1016/S0012-821X(00)00350-2

Tosdal, R.M., Dilles, J.H., Cooke, D.R., 2009. From Source to Sinks in Auriferous Magmatic-Hydrothermal Porphyry and Epithermal Deposits. Elements 5, 289–295. https://doi.org/10.2113/gselements.5.5.289

Trap, P., Faure, M., Lin, W., Bruguier, O., Monié, P., 2008. Contrasted tectonic styles for the Paleoproterozoic evolution of the North China Craton. Evidence for a ~2.1Ga thermal and tectonic event in the Fuping Massif. Journal of Structural Geology 30, 1109–1125. https://doi.org/10.1016/j.jsg.2008.05.001

Trap, P., Faure, M., Lin, W., Le Breton, N., Monié, P., 2012. Paleoproterozoic tectonic evolution of the Trans-North China Orogen: Toward a comprehensive model. Precambrian Research 222–223, 191–211. https://doi.org/10.1016/j.precamres.2011.09.008

Trap, P., Faure, M., Lin, W., Meffre, S., 2009a. The Lüliang Massif: a key area for the understanding of the Palaeoproterozoic Trans-North China Belt, North China Craton. Geological Society, London, Special Publications 323, 99–125.

Trap, P., Faure, M., Lin, W., Monié, P., 2007. Late Paleoproterozoic (1900–1800Ma) nappe stacking and polyphase deformation in the Hengshan–Wutaishan area: Implications for the understanding of the Trans-North-China Belt, North China Craton. Precambrian Research 156, 85–106. https://doi.org/10.1016/j.precamres.2007.03.001

Trap, P., Faure, M., Lin, W., Monié, P., Meffre, S., Melleton, J., 2009b. The Zanhuang Massif, the second and eastern suture zone of the Paleoproterozoic Trans-North China Orogen. Precambrian Research 172, 80–98.

Trauth, M.H., Maslin, M.A., Deino, A.L., Junginger, A., Lesoloyia, M., Odada, E.O., Olago, D.O., Olaka, L.A., Strecker, M.R., Tiedemann, R., 2010. Human evolution in a variable environment: the amplifier lakes of Eastern Africa. Quaternary Science Reviews 29, 2981–2988. https://doi.org/10.1016/j.quascirev.2010.07.007

Tulloch, A.J., Mortimer, N., Ireland, T.R., Waight, T.E., Maas, R., Palin, J.M., Sahoo, T., Seebeck, H., Sagar, M.W., Barrier, A., Turnbull, R.E., 2019. Reconnaissance Basement Geology and Tectonics of South Zealandia. Tectonics 38, 516–551. https://doi.org/10.1029/2018TC005116

Uruski, C.I., 2010. New Zealand's deepwater frontier. Marine and Petroleum Geology 27, 2005–2026. https://doi.org/10.1016/j.marpetgeo.2010.05.010
van der Wal, J.L.N., Nottebaum, V.C., Stauch, G., Binnie, S.A., Batkhishig, O., Lehmkuhl, F., Reicherter, K., 2021. Geomorphological Evidence of Active Faulting in Low Seismicity Regions—Examples From the Valley of Gobi Lakes, Southern Mongolia. Front. Earth Sci. 8. https://doi.org/10.3389/feart.2020.589814
van Wijk, J.W., Cloetingh, S.A.P.L., 2002. Basin migration caused by slow lithospheric extension. Earth and Planetary Science Letters 198, 275–288. https://doi.org/10.1016/S0012-821X(02)00560-5
Vasconcelos, D.L., Bezerra, F.H.R., Medeiros, W.E., de Castro, D.L., Clausen, O.R., Vital, H., Oliveira, R.G., 2019. Basement fabric controls rift nucleation and postrift basin inversion in the continental margin of NE Brazil. Tectonophysics 751, 23–40. https://doi.org/10.1016/j.tecto.2018.12.019
Vauchez, A., Barruol, G., Tommasi, A., 1997. Why do continents break-up parallel to ancient orogenic belts? Terra Nova 9, 62–66. https://doi.org/10.1111/j.1365-3121.1997.tb00003.x
Versfelt, J., Rosendahl, B.R., 1989. Relationships between pre-rift structure and rift architecture in Lakes Tanganyika and Malawi, East Africa. Nature 337, 354–357. https://doi.org/10.1038/337354a0
Vetel, W., Le Gall, B., 2006. Dynamics of prolonged continental extension in magmatic rifts: the Turkana Rift case study (North Kenya). Geological Society, London, Special Publications 259, 209–233. https://doi.org/10.1144/GSL.SP.2006.259.01.17
Walcott, R.C., Summerfield, M.A., 2008. Scale dependence of hypsometric integrals: An analysis of southeast African basins. Geomorphology 96, 174–186. https://doi.org/10.1016/j.geomorph.2007.08.001
Walsh, J.J., Bailey, W.R., Childs, C., Nicol, A., Bonson, C.G., 2003. Formation of segmented normal faults: a 3-D perspective. Journal of Structural Geology 25, 1251–1262. https://doi.org/10.1016/S0191-8141(02)00161-X
Walsh, J.J., Nicol, A., Childs, C., 2002. An alternative model for the growth of faults. Journal of Structural Geology 24, 1669–1675. https://doi.org/10.1016/S0191-8141(01)00165-1
Walters, R.J., Gregory, L.C., Wedmore, L.N.J., Craig, T.J., McCaffrey, K., Wilkinson, M., Chen, J., Li, Z., Elliott, J.R., Goodall, H., Iezzi, F., Livio, F., Michetti, A.M., Roberts, G., Vittori, E., 2018. Dual control of fault intersections on stop-start rupture in the 2016 Central Italy seismic sequence. Earth and Planetary Science Letters 500, 1–14. https://doi.org/10.1016/j.epsl.2018.07.043
Wan, B., Yang, X., Tian, X., Yuan, H., Kirscher, U., Mitchell, R.N., 2020. Seismological evidence for the earliest global subduction network at 2 Ga ago. Science Advances 6, eabc5491. https://doi.org/10.1126/sciadv.abc5491
Wang, D., Wu, Z., Yang, L., Li, W., He, C., 2021. Influence of two-phase extension on the fault network and its impact on hydrocarbon migration in the Linnan sag, Bohai Bay Basin, East China. Journal of Structural Geology 145, 104289. https://doi.org/10.1016/j.jsg.2021.104289
Wang, K., Chen, L., Xiong, X., Yan, Z., Xie, R., 2020. The role of lithospheric heterogeneities in continental rifting: Implications for rift diversity in the North China Craton. Journal of Geodynamics 139, 101765. https://doi.org/10.1016/j.jog.2020.101765
Wang, Q., Li, C., Tian, G., Zhang, W., Liu, C., Ning, L., Yue, J., Cheng, Z., He, C., 2002. Tremendous change of the earth surface system and tectonic setting of salt-lake formation in Yuncheng Basin since 7.1 Ma. Sci. China Ser. D-Earth Sci. 45, 110–122. https://doi.org/10.1007/BF02879788

Warren, J.M., Hirth, G., 2006. Grain size sensitive deformation mechanisms in naturally deformed peridotites. Earth and Planetary Science Letters 248, 438–450. https://doi.org/10.1016/j.epsl.2006.06.006
Wedmore, L.N.J., Turner, T., Biggs, J., Williams, J.N., Sichingabula, H.M., Kabumbu, C., Banda, K., 2022. The Luangwa Rift Active Fault Database and fault reactivation along the southwestern branch of the East African Rift. Solid Earth 13, 1731–1753. https://doi.org/10.5194/se-13-1731-2022
Wedmore, L.N.J., Williams, J.N., Biggs, J., Fagereng, Å., Mphepo, F., Dulanya, Z., Willoughby, J., Mdala, H., Adams, B.A., 2020. Structural inheritance and border fault reactivation during active early-stage rifting along the Thyolo fault, Malawi. Journal of Structural Geology 139, 104097. https://doi.org/10.1016/j.jsg.2020.104097
Weinlich, F.H., Bräuer, K., Kämpf, H., Strauch, G., Tesař, J., Weise, S.M., 1999. An active subcontinental mantle volatile system in the western Eger rift, Central Europe: gas flux, isotopic (He, C, and N) and compositional fingerprints. Geochimica et Cosmochimica Acta 63, 3653–3671. https://doi.org/10.1016/S0016-7037(99)00187-8
Wells, D.L., Coppersmith, K.J., 1994. New empirical relationships among magnitude, rupture length, rupture width, rupture area, and surface displacement. Bulletin of the Seismological Society of America 84, 974–1002. https://doi.org/10.1785/BSSA0840040974
Wheeler, W.H., Karson, J.A., 1989. Structure and kinematics of the Livingstone Mountains border fault zone, Nyasa (Malawi) Rift, southwestern Tanzania. Journal of African Earth Sciences (and the Middle East) 8, 393–413. https://doi.org/10.1016/S0899-5362(89)80034-X
Whipple, K.X., 2004. Bedrock rivers and the geomorphology of active orogens. Annu. Rev. Earth Planet. Sci. 32, 151–185. https://doi.org/10.1146/annurev.earth.32.101802.120356
Whitmarsh, R.B., Manatschal, G., Minshull, T.A., 2001. Evolution of magma-poor continental margins from rifting to seafloor spreading. Nature 413, 150–154. https://doi.org/10.1038/35093085
Whittaker, A.C., 2012. How do landscapes record tectonics and climate? Lithosphere 4, 160–164.
Whittaker, A.C., Attal, M., Cowie, P.A., Tucker, G.E., Roberts, G., 2008. Decoding temporal and spatial patterns of fault uplift using transient river long profiles. Geomorphology 100, 506–526. https://doi.org/10.1016/j.geomorph.2008.01.018
Whittaker, A.C., Walker, A.S., 2015. Geomorphic constraints on fault throw rates and linkage times: Examples from the Northern Gulf of Evia, Greece. Journal of Geophysical Research: Earth Surface 120, 137–158. https://doi.org/10.1002/2014JF003318
Williams, J.N., Fagereng, Å., Wedmore, L.N.J., Biggs, J., Mdala, H., Mphepo, F., Hodge, M., 2022. Low Dissipation of Earthquake Energy Where a Fault Follows Pre-Existing Weaknesses: Field and Microstructural Observations of Malawi's Bilila-Mtakataka Fault. Geophysical Research Letters 49, e2021GL095286. https://doi.org/10.1029/2021GL095286
Williams, J.N., Fagereng, Å., Wedmore, L.N.J., Biggs, J., Mphepo, F., Dulanya, Z., Mdala, H., Blenkinsop, T., 2019. How Do Variably Striking Faults Reactivate During Rifting? Insights From Southern Malawi. Geochemistry, Geophysics, Geosystems 20, 3588–3607. https://doi.org/10.1029/2019GC008219
Wilson, J.T., 1966. Did the Atlantic Close and then Re-Open? Nature 211, 676–681. https://doi.org/10.1038/211676a0
Wilson, R.W., Holdsworth, R.E., Wild, L.E., McCaffrey, K.J.W., England, R.W., Imber, J., Strachan, R.A., 2010. Basement-influenced rifting and basin development: a reappraisal of post-

Caledonian faulting patterns from the North Coast Transfer Zone, Scotland. Geological Society, London, Special Publications 335, 795–826. https://doi.org/10.1144/SP335.32
Wilson, T.J., 1995. Cenozoic transtension along the Transantarctic Mountains-West Antarctic rift boundary, southern Victoria Land, Antarctica. Tectonics 14, 531–545. https://doi.org/10.1029/94TC02441
Wobus, C., Whipple, K.X., Kirby, E., Snyder, N., Johnson, J., Spyropolou, K., Crosby, B., Sheehan, D., 2006. Tectonics from topography: Procedures, promise, and pitfalls, in: Willett, S.D., Hovius, N., Brandon, M.T., Fisher, D.M. (Eds.), Tectonics, Climate, and Landscape Evolution. Geological Society of America, p. 0. https://doi.org/10.1130/2006.2398(04)
Wong, K., Mason, E., Brune, S., East, M., Edmonds, M., Zahirovic, S., 2019. Deep Carbon Cycling Over the Past 200 Million Years: A Review of Fluxes in Different Tectonic Settings. Front. Earth Sci. 7. https://doi.org/10.3389/feart.2019.00263
Wong, W.H., 1927. Crustal Movements and Igneous Activities in Eastern China Since Mesozoic Time.1. Bulletin of the Geological Society of China 6, 9–37. https://doi.org/10.1111/j.1755-6724.1927.mp6001002.x
Wright, L.J.M., Muirhead, J.D., Scholz, C.A., 2020. Spatiotemporal Variations in Upper Crustal Extension Across the Different Basement Terranes of the Lake Tanganyika Rift, East Africa. Tectonics 39, e2019TC006019. https://doi.org/10.1029/2019TC006019
Wu, F.-Y., Lin, J.-Q., Wilde, S.A., Zhang, X., Yang, J.-H., 2005. Nature and significance of the Early Cretaceous giant igneous event in eastern China. Earth and Planetary Science Letters 233, 103–119. https://doi.org/10.1016/j.epsl.2005.02.019
Wu, F.-Y., Yang, J.-H., Xu, Y.-G., Wilde, S.A., Walker, R.J., 2019. Destruction of the North China Craton in the Mesozoic. Annual Review of Earth and Planetary Sciences 47, 173–195. https://doi.org/10.1146/annurev-earth-053018-060342
Xu, X., Ma, X., 1992. Geodynamics of the Shanxi rift system, China. Tectonophysics 208, 325–340.
Xu, X., Ma, X., Deng, Q., 1993. Neotectonic activity along the Shanxi rift system, China. Tectonophysics 219, 305–325.
Xu, Y., He, H., Deng, Q., Allen, M.B., Sun, H., Bi, L., 2018. The CE 1303 Hongdong Earthquake and the Huoshan Piedmont Fault, Shanxi Graben: Implications for Magnitude Limits of Normal Fault Earthquakes. J. Geophys. Res. Solid Earth 123, 3098–3121. https://doi.org/10.1002/2017JB014928
Xu, Y.-G., 2007. Diachronous lithospheric thinning of the North China Craton and formation of the Daxin'anling–Taihangshan gravity lineament. Lithos, The Origin, Evolution and Present State of Continental Lithosphere 96, 281–298. https://doi.org/10.1016/j.lithos.2006.09.013
Ye, H., Zhang, B., Mao, F., 1987. The Cenozoic tectonic evolution of the Great North China: two types of rifting and crustal necking in the Great North China and their tectonic implications. Tectonophysics, Deep Internal Processes and Continental Rifting 133, 217–227. https://doi.org/10.1016/0040-1951(87)90265-4
Yielding, G., Roberts, A., 1992. Footwall uplift during normal faulting — implications for structural geometries in the North Sea, in: Larsen, R.M., Brekke, H., Larsen, B.T., Talleraas, E. (Eds.), Structural and Tectonic Modelling and Its Application to Petroleum Geology, Norwegian Petroleum Society Special Publications. Elsevier, Amsterdam, pp. 289–304. https://doi.org/10.1016/B978-0-444-88607-1.50025-5
Yin, A., 2010. Cenozoic tectonic evolution of Asia: A preliminary synthesis. Tectonophysics 488, 293–325. https://doi.org/10.1016/j.tecto.2009.06.002

Yin, A., 2000. Mode of Cenozoic east-west extension in Tibet suggesting a common origin of rifts in Asia during the Indo-Asian collision. Journal of Geophysical Research: Solid Earth 105, 21745–21759. https://doi.org/10.1029/2000JB900168
Zhai, M., Li, T.-S., Peng, P., Hu, B., Liu, F., Zhang, Y., 2010. Precambrian key tectonic events and evolution of the North China craton. https://doi.org/10.1144/SP338.12
Zhai, M.-G., Santosh, M., 2011. The early Precambrian odyssey of the North China Craton: A synoptic overview. Gondwana Research, Precambrian geology and tectonic evolution of the North China Craton 20, 6–25. https://doi.org/10.1016/j.gr.2011.02.005
Zhang, C., Li, C., Deng, H., Liu, Y., Liu, L., Wei, B., Li, H., Liu, Z., 2011. Mesozoic contraction deformation in the Yanshan and northern Taihang mountains and its implications to the destruction of the North China Craton. Sci. China Earth Sci. 54, 798–822. https://doi.org/10.1007/s11430-011-4180-7
Zhang, Yaoyang, Chen, L., Ai, Y., Jiang, M., 2019. Lithospheric structure beneath the central and western North China Craton and adjacent regions from S-receiver function imaging. Geophysical Journal International 219, 619–632. https://doi.org/10.1093/gji/ggz322
Zhang, Yueqiao, Dong, S., Li, J., 2019. Late Paleogene sinistral strike-slip system along east Qinling and in southern North China: Implications for interaction between collision-related block trans-rotation and subduction-related back-arc extension in East China. Tectonophysics 769, 228181. https://doi.org/10.1016/j.tecto.2019.228181
Zhang, Y., Dong, S., Zhao, Y., Zhang, T., 2008. Jurassic Tectonics of North China: A Synthetic View. Acta Geologica Sinica - English Edition 82, 310–326. https://doi.org/10.1111/j.1755-6724.2008.tb00581.x
Zhang, Y., Ma, Y., Yang, N., Shi, W., Dong, S., 2003. Cenozoic extensional stress evolution in North China. Journal of Geodynamics 36, 591–613. https://doi.org/10.1016/j.jog.2003.08.001
Zhang, Y.G., Zheng, W.J., Wang, Y.J., Zhang, D.L., Tian, Y.T., Wang, M., Zhang, Z.Q., Zhang, P.Z., 2018. Contemporary Deformation of the North China Plain From Global Positioning System Data. Geophysical Research Letters 45, 1851–1859. https://doi.org/10.1002/2017GL076599
Zhang, Y.Q., Mercier, J.L., Vergély, P., 1998. Extension in the graben systems around the Ordos (China), and its contribution to the extrusion tectonics of south China with respect to Gobi-Mongolia. Tectonophysics 285, 41–75. https://doi.org/10.1016/S0040-1951(97)00170-4
Zhao, G., Min, S., Wilde, S.A., Sanzhong, L., 2005. Late Archean to Paleoproterozoic evolution of the North China Craton: key issues revisited. Precambrian Research 136, 177–202. https://doi.org/10.1016/j.precamres.2004.10.002
Zhao, G., Wilde, S.A., Cawood, P.A., Sun, M., 2001. Archean blocks and their boundaries in the North China Craton: lithological, geochemical, structural and P–T path constraints and tectonic evolution. Precambrian Research 107, 45–73. https://doi.org/10.1016/S0301-9268(00)00154-6
Zhao, H., Liu, C., Wang, F., Wang, J., Li, Q., Yao, Y., 2007. Uplift and evolution of Helan Mountain. Sci. China Ser. D-Earth Sci. 50, 217–226. https://doi.org/10.1007/s11430-007-6010-5
Zhao, L., Zheng, T., 2005. Using shear wave splitting measurements to investigate the upper mantle anisotropy beneath the North China Craton: Distinct variation from east to west. Geophysical Research Letters 32, L10309. https://doi.org/10.1029/2005GL022585
Zheng, T., Zhao, L., Zhu, R., 2009. New evidence from seismic imaging for subduction during assembly of the North China craton. Geology 37, 395–398. https://doi.org/10.1130/G25600A.1

Zhou, W., Hu, X., Guo, H., Liu, Shuang, Liu, Sijing, Yang, B., 2022. Three-dimensional magnetotelluric inversion reveals the typical geothermal structure of Yanggao geothermal field in Datong Basin, northern China. Geothermics 105, 102505. https://doi.org/10.1016/j.geothermics.2022.102505

Zhu, R., Xu, Y., Zhu, G., Zhang, H., Xia, Q., Zheng, T., 2012. Destruction of the North China Craton. Sci. China Earth Sci. 55, 1565–1587. https://doi.org/10.1007/s11430-012-4516-y

Ziegler, P.A., 1992. North Sea rift system. Tectonophysics, Geodynamics of rifting, volume 1 Case history studies on rifts: Europe and Asia 208, 55–75. https://doi.org/10.1016/0040-1951(92)90336-5

Ziegler, P.A., 1978. North Sea Rift and Basin Development, in: Ramberg, I.B., Neumann, E.-R. (Eds.), Tectonics and Geophysics of Continental Rifts. Springer Netherlands, Dordrecht, pp. 249–277. https://doi.org/10.1007/978-94-009-9806-3_21

Ziegler, P.A., Cloetingh, S., 2004. Dynamic processes controlling evolution of rifted basins. Earth-Science Reviews 64, 1–50. https://doi.org/10.1016/S0012-8252(03)00041-2

Zwaan, F., Chenin, P., Erratt, D., Manatschal, G., Schreurs, G., 2022. Competition between 3D structural inheritance and kinematics during rifting: Insights from analogue models. Basin Research 34, 824–854. https://doi.org/10.1111/bre.12642

Zwaan, F., Schreurs, G., 2017. How oblique extension and structural inheritance influence rift segment interaction: Insights from 4D analog models. Interpretation 5, SD119–SD138. https://doi.org/10.1190/INT-2016-0063.1

Zwaan, F., Schreurs, G., Naliboff, J., Buiter, S.J.H., 2016. Insights into the effects of oblique extension on continental rift interaction from 3D analogue and numerical models. Tectonophysics, Special issue on Tectonics of oblique plate boundary systems 693, 239–260. https://doi.org/10.1016/j.tecto.2016.02.036